INTERGRATION OF REMOTE SENSING AND METEOROLOGICAL DATA FOR MONITORING AGRICULTURAL DROUGHT

by

Chunming Peng
A Dissertation
Submitted to the
Graduate Faculty
of
George Mason University
in Partial Fulfillment of
The Requirements for the Degree
of
Doctor of Philosophy
Earth Systems and Geoinformation Sciences

Committee:

______________________	Dr. Liping Di, Dissertation Director
______________________	Dr. Arie Croitoru, Committee Member
______________________	Dr. Dan Carr, Committee Member
______________________	Dr. Ruixin Yang, Committee Member
______________________	Dr. Anthony Stefanidis, Department Chairperson
______________________	Dr. Donna M. Fox, Associate Dean, Office of Student Affairs & Special Programs, College of Science
______________________	Dr. Peggy Agouris, Interim Dean, College of Science
Date: 03/18/2014	Spring Semester 2014 George Mason University Fairfax, VA

INTERGRATION OF REMOTE SENSING AND METEOROLOGICAL DATA FOR MONITORING AGRICULTURAL DROUGHT

A Dissertation submitted in partial fulfillment of the requirements for the degree of Doctor of Philosophy at George Mason University

by

Chunming Peng
Master of Science
George Mason University, 2010

Director: Liping Di, Professor
Department of Geography and Geoinformation Science

Spring Semester 2014
George Mason University
Fairfax, VA

DEDICATION

This is dedicated to my loving family and friends.

ACKNOWLEDGEMENTS

Special thanks go to my dissertation committee for their guidance in leading this research. I owe my deepest gratitude to my PhD advisor, Dr. Liping Di, who has always been innovative, encouraging and inspiring, and guided me through all stages of this dissertation with his wisdom and patience. I equally thank Dr. Ruixin Yang, Dr. Dan Carr, and Dr. Arie Croitoru for their invaluable help and support, instructing me towards creative thinking, idea delivery, experiment, and dissertation writing.

Also, Dr. Meixia Deng, Dr. Wenli Yang, Dr. Weiguo Han, and Dr. Genong Yu have generously helped me with their excellent touch in Science and Technology, and guided me so much in multiple projects. Other wonderful colleagues at CSISS deserve my sincere gratitude as well, including Ali Yagci, Ziheng Sun, Dr. Yuanzheng Shao, Bei Zhang, Dr. Zhengwei Yang, Dr. Aijun Chen, Dr. Peisheng Zhao, Dr. Peng Yue, Ronjay Shrestha, Lingjun Kang, Weishu Gong, Xicheng Tan, Gil Heo, Huilin Wang and Xuanang Cheng.

I would like to thank me dearest family and friends who have always stood behind me and given me strengths. My loving parents, Qiaohong Li, and Hongsi Peng, have always been the backbone of my life, and encouraged me to explore the unknown.

Finally, thanks go out to Fenwick Library and University Writing Center for all the support in formatting and revising my dissertation.

This research was partially supported by a grant from NASA Applied Science Program (Grant #: NNX09AO14G, PI: Dr. Liping Di).

TABLE OF CONTENTS

LIST OF TABLES

LIST OF FIGURES

LIST OF EQUATIONS

LIST OF ABBREVIATIONS

National Oceanic and Atmospheric Administration	NOAA
National Aeronautics and Space Administration	NASA
United States Department of Agriculture	USDA
United States Drought Monitor	USDM
Advanced Very High Resolution Radiometer	AVHRR
Moderate Resolution Imaging Spectroradiometer	MODIS
Remote Sensing	RS
Visible	VIS
Optical	OPT
Near-Infrared	NIR
Shortwave-Infrared	SWIR
Thermal-Infrared	TIR
Vegetation Index	VI
Drought Index	DI
Normalized Difference Vegetation Index	NDVI
Normalized Difference Drought Index	NDDI
Normalized Difference Water Index	NDWI
Vegetation Condition Index	VCI
Vegetation Health Index	VHI
Enhanced Vegetation Index	EVI
Growing Degree Days	GDD
Agricultural Drought Knowledge Base	ADKB
Rule-Based System	RBS
Expert System	ES

ABSTRACT

INTERGRATION OF REMOTE SENSING AND METEOROLOGICAL DATA FOR MONITORING AGRICULTURAL DROUGHT

Chunming Peng, Ph.D.

George Mason University, 2014

Dissertation Director: Dr. Liping Di

Affecting more people than other natural hazards, drought may lead to enormous decrease in crop production and also in the amount of poultry and livestock, and thus endangering food security and economy. Developing an appropriate drought indicator and a timely and accurate drought monitoring system has been a motivation for scientists in the last two decades. Vegetation conditions valued via remotely sensed indices have been used as indicators for agricultural drought since the 1980s. However, the anomalies in vegetation performance do not always signify droughts. Wild fire, extreme temperature, flood, pesticides or lack of fertilizers can all cause the vegetation stress. One of the major goals for this dissertation is to evaluate and investigate vegetation drought stress and other vegetation stresses using remote sensing techniques. The other major goal is to estimate the root-zone soil moisture levels beneath various crop canopies using satellite data and ground observations. Since soil moisture is the primary indicator for

agricultural drought, accurate and reliable soil moisture estimates have important implications for drought monitoring.

Recent technological advances in remote sensing have shown that vegetation vigor, land surface temperature (LST), vegetation water level and soil moisture (SM) can be measured by a variety of remote sensing techniques, each with its own strengths and weaknesses. This research is designed to combine the strengths of Moderate Resolution Imaging Spectroradiometer (MODIS) based visible/near-infrared (VIS/NIR), shortwave infrared (SWIR) and thermal infrared remote sensing approaches for detection of vegetation drought stress, and also to integrate VIS/NIR and microwave data from Aavanced Microwave Scanning Radiometer (AMSR-E) of the Earth Observing System (EOS) for soil moisture estimation. A vegetation drought stress estimation algorithm at moderate resolution was developed based on the existing "trapezoid" relation model by using MODIS-based LST as well as Normalized Difference Water Index (NDWI) and Normalized Difference Vegetation Index (NDVI).

A new index, the Combined Condition Index (CCI) was proposed here for monitoring vegetation drought stress from space by interpreting the relationships between LST and Normalized Difference Drought Index (NDDI). Drought Condition maps from the U. S. Drought Monitor (USDM) and other reliable agencies are used to validate the spatial patterns of drought. Also, the feasibility of constructing a library of weighing factors for vegetation overall conditions, water, and temperature for each spatial and temporal unit across the U. S. will be discussed in the dissertation. The CCI will be compared with currently used indices, for example, Vegetation Health Index (VHI), for pros and cons.

Also, the departure from precipitation, Palmer Drought Severity Index (PDSI), and crop yield/progress will be used to validate this index. This new drought indicator is expected to show higher sensitivity to drought occurrences than the existing ones.

Combining the proposed methods in detecting vegetation conditions and estimating soil moisture, we can obtain time-series profiles of vegetation conditions and soil moisture of various crops at different geo-spatial situations, and thus be able to monitor agricultural drought across the whole nation.

Data, information, knowledge, and wisdom are the four basic steps humans use to perceive objects (Ackoff, 1989). Agricultural droughts being considered as objects can also be perceived in these four forms – drought data, information, knowledge, and wisdom. Hence it is necessary to extract drought information out of related data (e.g., remotely sensed data) and discover knowledge from the extracted information. Lastly, this dissertation is to explore advantages of geospatial Web services in providing on-demand agricultural drought analysis and equipping experts, decision-makers and farmers alike with information, knowledge and even wisdom needed in the process of agricultural drought monitoring, assessment and management. Various Web services are established to support drought analysis and decision-making for the general public, which also illustrates the potential of Web services in automating geospatial knowledge discovery and dissemination within the Big Data era.

CHAPTER 1 INTRODUCTION

Droughts can cause devastating impact to a region's agriculture. Lack of proper drought warning and assessment systems may lead to enormous decrease in crop production and also in the amount of poultry and livestock, and thus endangering the security and economy. Early monitoring and detection of drought can help prepare farmers for vegetation drought, and thus mitigate drought impact. Researchers have noticed the importance of drought monitoring ever since the early 1900s, and have contributed many drought indicators, models, and methods to the area. However, accurately monitor drought is still challenging due to these reasons: (1) droughts are developing slowly (over months or years) and they exist before humans realize their occurrences, (2) the severity of a drought varies by precipitation deficit, spatial extent, and duration, and is hardly comparable to another drought, and (3) drought impacts are based on the range of economic, environmental and social resources within a region, and are not operationally capable to be quantified into a single index (Peters et al., 2002).

Section 1.1 Importance of agricultural drought monitoring

For decades, researchers have developed different methods to measure drought, using ground data and/or satellite imageries. Ground observed data alone is not sufficient for drought monitoring of an area, since weather data is usually untimely, sparse, and incomplete (Peters et al., 2002). Utilizing the remote sensing data to provide large area coverage and rapid detection of drought is a trend.

Different from meteorological or hydrological drought, an agricultural drought sets in when the soil moisture availability to plants has dropped to such a level that it affects the crop yield and hence agricultural production in a negative way. Since significant decrease in soil moisture availability and increase in leaf temperature can be seen during drought periods, quantifying these changes in vegetation based on satellite imagery records have proven to be an effective way to monitor agricultural drought.

In the case of agricultural drought, the measurement of its determinant factor (e.g. soil moisture) is difficult, and for most of the time, the related data sets for historic periods are not available. Such droughts could be best studied through a complex regional analysis involving a battery of variables (e.g. soil moisture, crop yield, leaf area index, vegetative growth etc.) rather than a simple point analysis. The complexity is further increased by the intricate relationships that exist between the crop yield and the soil moisture deficit. Because of such multiple reasons, there have been very limited efforts towards evaluating agricultural droughts. It is noted that the impact of drought on agriculture is slower than on stream flows or reservoir levels.

Section 1.2 Advantages and disadvantages of Remote Sensing based drought indicators

The Normalized Difference Vegetation Index (NDVI) measures the amount and condition of vegetation on a per-pixel basis, while the LST calculates the energy balance at the Earth's surface. Kogan (1990, 1995) used the Vegetation Condition Index (VCI) and the Temperature Condition Index (TCI), ratios derived from long-term Advanced

Very High Resolution Radiometer (AVHRR) NDVI and LST data, for 0.5/0.5 addition to measure the status of water- and temperature-related vegetation stress. The resulting index, Vegetation Health Index (VHI), can be used for drought measurement and reference to compare against other vegetation indicators. However, the VHI requires long-term data sets and certain issues complicate the evaluation of the ratio between the VCI and the TCI. One of the reasons is that VCI and TCI are not always positively correlated. It is generally believed that abnormally high temperatures intensifies the plant water demand, yet in some circumstances, especially at the beginning of the growing period, higher-than-normal temperatures can provide optimal environment for the plants to emerge. In this case, decrease in TCI values (caused by the increase of temperatures) is related to increase in VCI values since vegetation conditions at the germination/emerging stage are improved by warmth. The correlation relationship between TCI and VCI is largely determined by the current crop growing stage, soil moisture conditions, and the evapotranspiration of the surface, and changing from season to season.

Five disadvantages observed from traditional NDVI/VCI methods are: (1) the amplitudes and phases of NDVI vary by crop type, but the traditional NDVI calculation ignores the difference of per-pixel crop type across years (VCI has remedied the second part); (2) There is always a lagging period between NDVI and precipitation, and the NDVI fails to pick up the vegetation moisture difference after saturation; (3) Soil type and wetness largely influence the NDVI values, so the NDVI is in fact a combined information of vegetation condition and soil situations; (4) NDVI/VCI is not directly related to the occurrence or the severity of drought. Drought can be due to moisture-stress or thermal-stress. A lower NDVI/VCI could mean that the crop land is suffering from vegetation stress due to many reasons – drought, flood, extreme temperature, wild fire, pesticides or lack of fertilizers; (5) operational drought definitions were developed by fitting an appropriate distribution function to a drought index. Five drought thresholds (ranging from abnormally dry to exceptional drought) were defined based on the percentiles used by the USDM. Using an objective approach for determining drought definitions ensures that droughts are accurately and correctly identified at the local level. It is inappropriate to use a single set of drought definitions for an entire state (especially a state the size of Texas). Overall, no single index can represent all aspects of meteorological or hydrological/water supply drought so it is best to use a multi-index approach for operational drought monitoring. Due to these reasons, choosing the correct drought indicator and severity classification scheme, based on the geospatial and environmental characteristics, is the key to successfully monitoring and forecasting drought.

Adopting a good drought indicator will enable us (1) to detect and monitor drought conditions, (2) to determine the timing and level of drought responses, (3) to characterize and compare drought events, and (4) to tie together levels of drought severity with drought responses thereby forming an operationally workable drought management plan. With a universally usable drought indicator, the next step is to establish a threshold for the drought indicator, which is also important because it aims to assess the change thereby to determine drought risk and vulnerability of an area. Normally, the thresholds should be region specific and are subject to modifications in order to reflect market, climate, environment, public health and socio-economic changes (Nagarajan, 2009).

A more accurate drought monitoring system is proposed here by (1) combining the vegetation conditions, VWC and LST into the detection of vegetation drought stress; (2) integrating microwave measurements and ground observations for estimation of the soil moisture levels; (3) fusing indicators for evaluation of vegetation drought stress and soil moisture levels to form drought condition reports. In practice, the way this system might work is as follows: A web-based GIS platform serves as a central data and information source for users throughout the State. On this server, the necessary historical drought calculations have been performed for all geographical and jurisdictional boundaries likely to be of interest. Users can request raw data at full resolution or aggregated data and products for any requested region. An ideal system would also include options for time series analysis and cross-index comparisons for individual regions, as well as projections of future drought index values based upon high, medium, low, and historical worst case scenarios, with probabilities of each given by medium and long range forecasts. To sum up, this research is designed to combine vegetation condition detected from NIR/SWIR and TIR remote sensing approaches and the soil moisture levels estimated using AMSR-E and ground measurements, to provide refined agricultural drought monitoring, based on a pre-knowledge of the crop type per pixel.

Section 1.3 Statement of Problem

Monitoring drought stress of vegetation is a critical component of proactive drought planning designed to mitigate the impact of this natural hazard. Approaches that characterize the spatial extent, intensity, and duration of drought-related vegetation stress provide essential information for a wide range of management and planning decisions. Among all the operational drought monitoring systems, which use remotely sensed vegetation indices and other information to determine the spatial, temporal extents and severity of vegetation stress, few can provide accurate, timely and comprehensive monitoring results. Either they use single index for the entire process, or they choose an unconvincing standard for drought/non-drought definitions.

Two major challenges exist among all these satellite-based drought indicators (DI) in terms of applying them for drought monitoring. The first challenge is whether the method used can discriminate drought-impacted areas from other locations experiencing vegetation stress due to other causes solely from remotely sensed DI information. A number of environmental factors (e.g., wild fire, flooding, hail, pests, plant disease, and human-induced land cover/use changes) can produce negative DI anomalies (Peters et al., 2002) that mimic a drought stress signal. And the second challenge is how to establish the appropriate threshold(s) that discriminates between drought and non-drought conditions, as well as varying levels of drought stress (e.g., moderate, severe, and extreme).

Generally, lack/excessive of heat, nutrient, and moisture, etc. can all add up to vegetation stress. It is of great importance to identify areas which are suffering from drought stress (mostly moisture or thermal stress) and those suffering from other stresses (e.g. lack of nutrition, extreme weather, wild fire, etc.). In order to understand vegetation drought stress, the first priority should be to interpret the three-dimensional space of LST-NDVI-NDWI, and to see how these indices can reflect the drought impact on crops.

Also, root-zone soil moisture as a primary indictor for agricultural drought, can be used to validate whether the low VI value appears in accordance with low soil moisture (with or without time lag), and thus to indicate a real occurrence of agricultural drought. In all, this research uses temperature, vegetation water content, and soil moisture as facilitating tools in order to rule out the situations of false VI alarms.

Section 1.4 Objectives and Scopes

In general, the objectives of this research are to present remote sensing approaches to detect vegetation drought stress, estimate soil moisture, and thus perform more accurate diagnostics of agricultural drought in the crop lands. The Combined Condition Index (CCI) is a new drought indicator proposed to depict the status of agricultural drought via vegetation conditions at refined level. In particular, the CCI integrates vegetation water status with thermal properties to monitor drought more precisely. It fuses NDVI, NDWI, and LST, which are derived from the VIS, NIR, SWIR and thermal infrared (TIR) bands of the MODIS data, to give an estimation of vegetation vigor that is solely determined by its water and temperature conditions. The specific objectives are proposed below:

i. To estimate vegetation drought stress by combining the strengths of multi-sensor and ground measurements to achieve higher accuracy and spatial resolution.

ii. To investigate the potentials of using a combination of multiple VIS-NIR-SWIR-TIR spectral signatures to estimate vegetation moisture, thermal, and health conditions from space and to find the algorithm that will be best-suited for monitoring vegetation drought stress.

iii. To estimate the soil moisture levels by combining the strengths of multi-sensor and ground measurements in order to get more accurate results at finer spatial scales.

iv. To investigate the relationship between soil moisture and vegetation greenness, particularly when there is drought, and thus rule out the false VI signals when VI is low but soil moisture level is high.

v. To provide an integrated drought condition index and a flexible drought severity standard (D0 to D4 drought levels) as to form an accurate and comprehensive view for agricultural drought monitoring at the national or even global scale.

vi. To facilitate the community with drought information Web Services that will offer drought severity and duration report for state, ASD, county, or user-customized area, so users can have a quantitative understanding of how the drought develops over a specific area.

Section 1.5 Organization of dissertation

The dissertation consists of eight chapters. In order to better understand the study, the background and literature review are presented in the second chapter of the dissertation. The following five chapters give various works related to the objectives of the study and the last chapter concludes with summary and discussion of future directions.

Chapter 1 gives the general introduction, including the background for understanding the importance of using remotely sensed data for drought monitoring, limitations of current methods for assessing drought conditions, research objectives, major data sources and principal results of the study.

Chapter 2 gives the literature review of drought definition, historic droughts in the United States, and factors contributing to vegetation drought stress. The moisture and thermal stress will be explained in detail, as well as the complicated nature of vegetation drought. Chapter 3 describes how to determine crop phenologic stages using growing degree days (GDD), which is a function of surface temperature. In chapter 4, readers can find the performance curve of vegetation vigor change by latitude, climate zone, season, and crop type. Chapter 5 presents a new methodology to estimate the soil moisture by combining multi-sensor and ground measurements.

A new drought index integrating vegetation, water and thermal stress is proposed in chapter 6. A trapezoid relation existing among vegetation condition and LST, and water level is presented in detail, and multi-year satellite measurements and ground observed data have been used to determine this relation. The relation, in conjunction with satellite measurements, is then applied to obtain drought conditions at moderate resolution. The drought condition indicator integrating LST and vegetation water content to vegetation conditions is shown to be correlated to precipitation departure index at a higher degree than a single VI, or VI and temperature integrated. Also from here, readers can see how the LST/NDVI relations change at different time, location or crop type.

In chapter 7, methods to define drought severity thresholds and quantify confidence level of drought scales will be discussed. Various geospatial Web Services are proposed for the general users to extract drought information and knowledge from raw data, to customize their own drought indicators, and validate the drought indicators with selected source of station-based observations. Chapter 8 summarizes the results from the previous chapters and gives limitations and discussions of future directions.

Section 1.6 Data source and study area

Repetitive measurements at the same location day after day, week after week, month after month, and year after year, are one of the most important requirements for operational drought monitoring. Another requirement is for the monitoring tools to provide reliable sources of time-series data at effective spatial and temporal scales for accurate and timely information. As an obvious data source meeting these two requirements, satellite remote sensing supplies synoptic coverage of the land surface with objective, automated data collections for use in spatially specific models.

Among all satellite data products, spectral vegetation indices (VI) are the most commonly used for the monitoring, measurement, and evaluation of vegetation cover, condition, biophysical processes, change, and during the past two decades have been put into operational use in a broad variety of applications, including monitoring of drought effects at regional, national or even global scales. Details for accessing, downloading and handling satellite data can be found in section 1.6.1.

Subsection 1.6.1 Source of remotely sensed data

National Oceanic and Atmospheric Administration (NOAA)'s Advanced Very High Resolution Radiometer (AVHRR) has been the most commonly used remote sensing instrument for large area drought monitoring in its 30-year history, partially due to its sufficiently long time series which enables a relatively reasonable "normal" reference line to be drawn, and hence anomalies to be identified (Brown et al., 2008). The AVHRR data records traces back to June 1979 (when NOAA-6 was launched), and covers the globe at 4 to 8 kilometers resolution (Tucker et al., 2005). The joint initiative of the U. S. Geological Survey (USGS) and the National Aeronautics and Space Administration (NASA) has launched the Landsat 7 Thematic Mapper (TM) and Enhanced Thematic Mapper Plus (ETM+) projects in the 1990s. The spatial resolution of the surface reflectance data collected by Landsat can get as refined as 30 meters.

Similar to the AVHRR, the Moderate Resolution Imaging Spectroradiometer (MODIS) launched by NASA has high temporal resolution and provides reliable drought monitoring data. The two platforms, Terra and Aqua, were launched in 1999 and 2002, respectively, as part of its Earth Observing System (EOS). The morning and afternoon overpasses collected by Terra and Aqua, respectively, combine to form a complementary source of daily global drought data. Its advancement from AVHRR and Landsat is in providing finer spatial resolution at 250-m, 500-m, and 1-km, higher spectral resolutions within the near-infrared and shortwave-infrared spectrums (as shown in Figure 1), more precise geolocation, and improved atmospheric corrections (Brown et al., 2008).

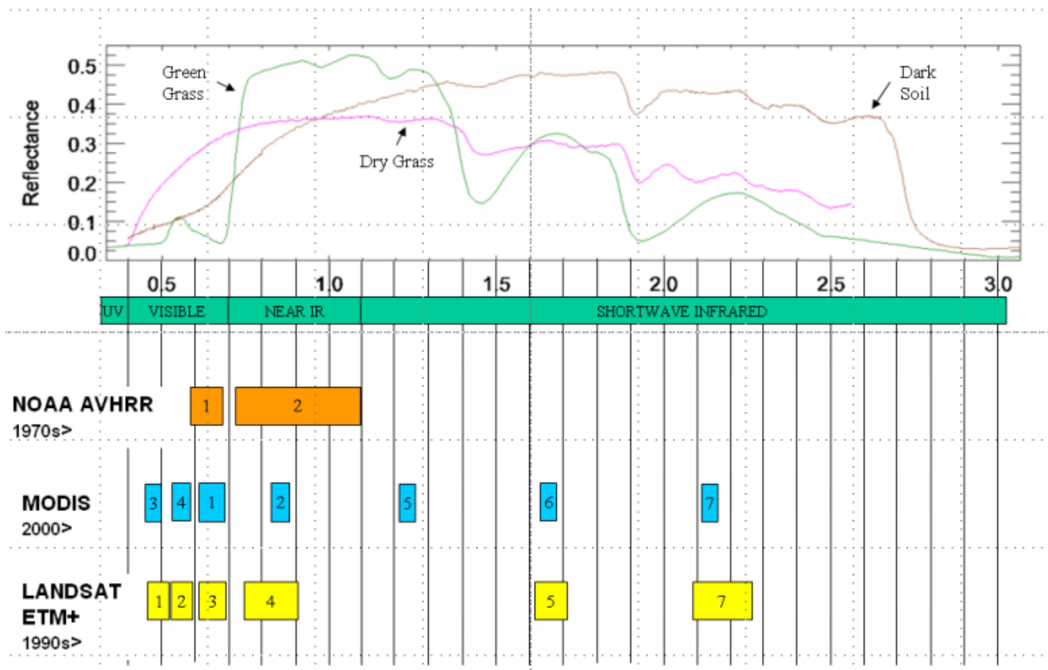

Figure 1 The optical (land) channel band widths for NOAA AVHRR, LANDSAT ETM+, and MODIS instruments (Brown et al., 2008).

A variety of MODIS products are available on-line at the NASA's Land Processes Distributed Active Archive Center (LP DAAC) (LPDAAC, 2006). To capture the agricultural drought occurred in the study region in the growing periods each year three kinds of MODIS products described in table below were employed.

The NDVI and LST were derived from the MODIS data products MOD13Q1 and MOD11A2, respectively. MOD13Q1 provides per pixel NDVI values and Enhanced Vegetation Index (EVI) values (tile, 250m, and per 16 days), and MOD11A2 provides LST and emissivity (tile, 1km, and every 8 days).

The MOD13Q1 is also a level-3 product. Among 11 SDSs of this product, 16-day composite NDVI, quality for each NDVI pixel, and view zenith angle for each NDVI pixel were employed. The NDVI is encoded in 16-bit signed integer, ranging from -2000 to 10000. With the “SCALE” field defined as 10,000 in the metadata for MOD13 products, the pixel values need to be divided by 10000 to obtain NDVI in its original range from -0.2 to 1. In theory, NDVI takes values between -1 and 1, with values larger than 0.1 indicating vegetation, values larger than 0 and less than 0.1 indicating bare soils or cloud (that cloud is always very close to 0, e.g. 0.002), and values less than 0 indicating water, snow and ice. However, because the MODIS products have assigned pixels located in ocean, lakes and other water bodies fill values (e.g. -10000, equivalent to null), the NDVI values lower than -0.2 will not be shown in the dataset, and thus the MODIS products only keep pixels whose values are no less than -0.2 for the sake of memory space.

The quality and view zenith angle were used as criteria for the NDVI data for each pixel to be used in the analyses. The 16-bit VI quality can be used along with the VI dataset to assure the quality of each pixel: bits 0–1, MODLAND_QA; bits 2–5, VI usefulness; bits 6–7, Aerosol quantity; bit 8, Adjacent cloud detected; bit 9, Atmosphere BRDF correction performed; bit 10, Mixed Clouds; bits 11–13, Land/Water Flag, bit 14, Possible snow/ice; bit 15, Possible shadow. The VI usefulness field (bits 2-5) is giving users different levels of recommendation of whether the VI value for this pixel can be used, that “0000” signifying highest quality and “1111” signifying not useful for any other reasons. The same view zenith angle criterion as the LST was used for the NDVI.

The reason for using 16-day-composite VIs in this research since there are numerous products with different temporal resolutions (e.g. daily, 7-day, 10-day, and 14-day) is because the 16-day MODIS products are closest to our goal of fetching cloud-free

VI maps with minimal atmospheric and sun-surface-sensor angular effects (Holben, 1986). The 16-day composited NDVI products take advantage of the maximum value composite (MVC) technique, which is to select, on a pixel-by-pixel basis, the input pixel with the highest NDVI value as output to the composited image, and the process includes cloud screening and data quality assurance (Goward et al., 1994; Eidenshink & Faundeer, 1994). As a result, the maximum composite NDVI value has selected the least cloud- and atmospheric pixels. Also, since the increase in optical path length intensifies the influence of atmospheric contamination and residual cloud cover, choosing maximum NDVI composite values is to select the most near-nadir view and smallest solar zenith angle pixels (that is with least optical path length) (Holben, 1986; Cihlar et al., 1994).

The MOD11A2 product is a level-3 product which consists of 12 Science Data Sets (SDSs), including 8-day composite LST, quality of each LST pixel, and view zenith angle of each LST pixel. The LST values in Kelvin are encoded in 16-bit unsigned integer, ranging from 7500 to 65535. To derive the actual value of temperature these values need to be multiplied with 0.02. With the lower and upper limits of the LST values rescaled to Kelvin degrees and converted to Fahrenheit degrees, the lowest and highest Fahrenheit degrees that can be represented in MOD11A2 product are -189.67 and 1900.4°F. This range has been sufficient for daily temperatures collected from land surfaces; extremely high temperatures (e.g. 3.6 billion degrees Fahrenheit created by Sandia Laboratory) are not taken into consideration in this case.

The quality and view zenith angle were used as criteria for LST pixel data to be included in the analyses. The quality information is represented in 8 bit data, in which each of 2-bit combination (i.e. bit fields) represents different quality information. Only LST pixels with the highest quality (average LST error is less than 1 Kelvin) were used. The view zenith angles are in degrees and encoded in 8-bit unsigned integer. LST pixels within -45 to 45 degrees view zenith angle were employed.

The NDWI is calculated using the reflectance data from the MODIS data product MOD09A1, which estimates surface spectral reflectance at a 500-m resolution in an 8-day gridded level-3 product in the sinusoidal projection. The data used are from March to October of 2000 to 2012 as to provide uniform temporal resolution. Reflectance and LST data is rescaled to the 16-day temporal resolution and to a 500-m spatial resolution. The NDVI, LST and NDWI data sets are all subjected to geometric correction.

Scatter plots were then prepared for each dataset with the LST, NDVI and NDWI and the least squares root method was used to determine the warm edge. The warm edge can be detected along the upper limit of the scatter plots, which are plotted with the maximum and minimum LST assigned the same values as the NDVI, or the Vegetation Dryness Index (VDI), or the NDDI.

Monthly precipitation data obtained by the Tropical Rainfall Measuring Mission (TRMM) satellite precipitation radar (PR) were used to generate a difference precipitation image (DPI) by deducting a drought period precipitation image from a normal period precipitation image. The DPI was then compared to the VTCI, VWTCI and CCI images.

Subsection 1.6.2 Source of Crop Mask

Even being planted in the same soil and climate system, different crops have their own growing patterns. The first step for inspecting how crops respond to agricultural drought stress is to apply a crop mask to the study area and separate the drought image into several crop layers (depending on how many crops the research is concerned). The images below display the spatial distributions of corn and soybeans respectively. We can see that, five largest corn-producing states in the U. S. are Iowa, Illinois, Nebraska, Minnesota, and Indiana, each contributing to 18%, 17%, 12%, 10% and 7% of the nation's total corn yields from 2006 to 2010 respectively. And the growing season for corn starts from end of April and lasts until the mid-November. These five states also are the largest soybeans-producing states, each contributing to 15%, 14%, 8%, 9% and 8% of the nation's total harvested soybeans from 2006 to 2010 respectively. And the growing season for soybeans starts from early May and lasts until the early November.

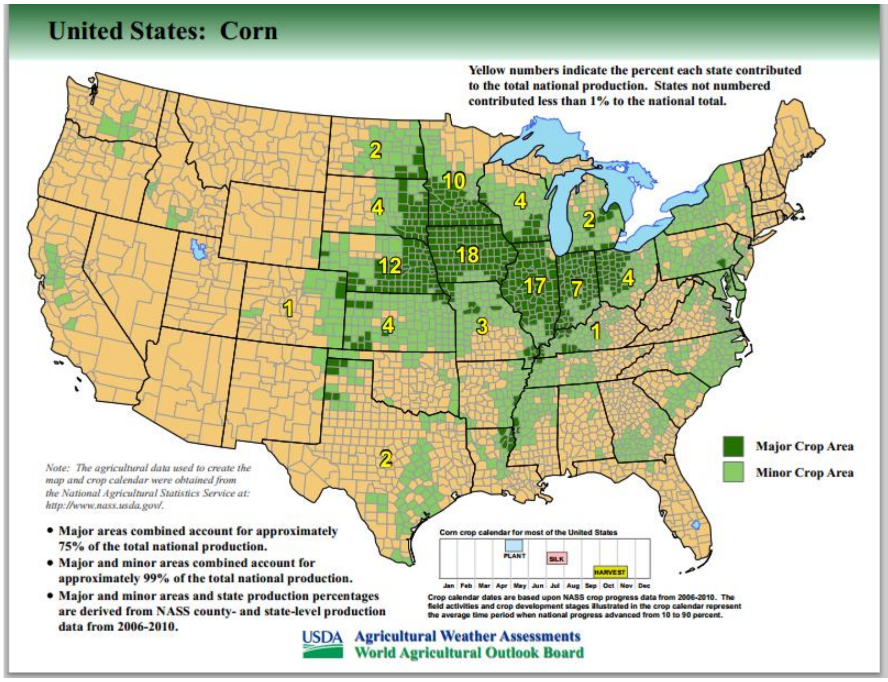

Figure 2 Major and minor corn areas in the U.S. (source: http://www.usda.gov/oce/weather/pubs/Other/MWCACP/Graphs/USA/Corn2006to2010.pdf)

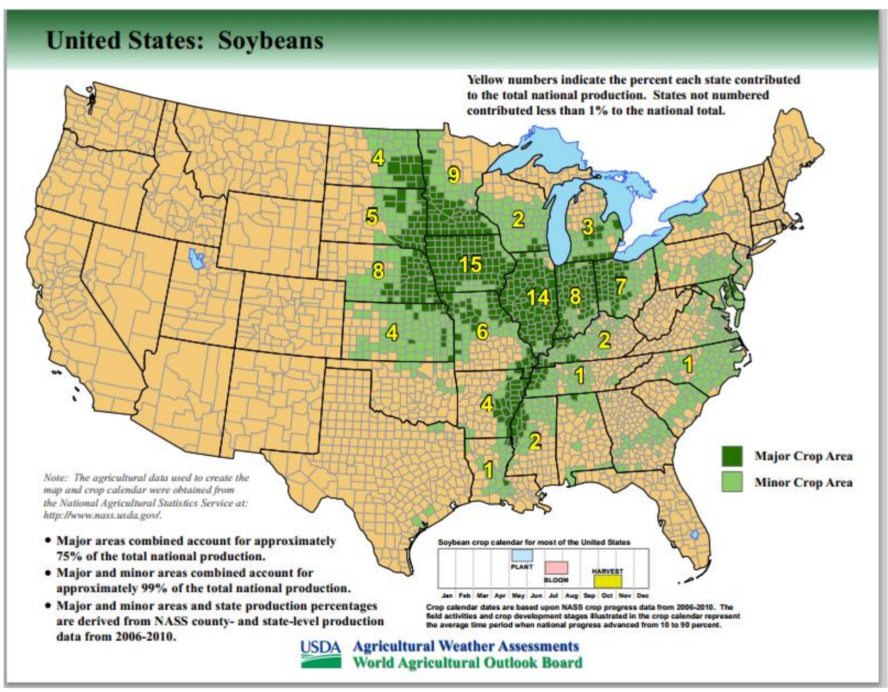

Figure 3 Major and minor soybeans fields in the U.S. (source: http://www.usda.gov/oce/weather/pubs/Other/MWCACP/Graphs/USA/Corn2006to2010.pdf)

In order to assess agricultural drought, we can make use of the crop classification data provided by the United States Department of Agriculture (USDA) National Agricultural Statistics Service (NASS), namely the CropScape -- Cropland Data Layer (CDL). CDL is hosting the cultivated crop mask data at a 30m or 51m spatial resolution over the continental U. S. (CONUS). Prior to 2006, CDL products relied primarily on Landsat 4, 5 and 7. Beginning from 2006, the CDL program switched to using the sensor(s) on the IRS-P6 Resourcesat-1. And in year 2011, CDL added two more sensors, the Deimos-1 and the UK-DMC2 to its data retrieval. Since it is over costly to use higher resolution satellites for crop acreage estimation over large areas, the products used in CDL are from medium resolution satellites.

The crop classifications provided by CDL are not one hundred percent faultless. For the dominant agricultural types, the accuracies can range from mid-80% to mid-90%. The detailed accuracy estimation for each crop type, state and year differs, and can be found out in the metadata file. For example, the accuracy for corn in Iowa of year 2012 is 96.61%, while that for soybeans the same state and year is 95.56%. For more info, check the metadata page at http://www.nass.usda.gov/research/Cropland/metadata/meta.htm.

CDL provides visualization for crop change between years, and displays in Figures 4 and 5 that the state of Iowa was subject to crop rotation during 2010 to 2012. The period of 2010 to 2011 tend to have less acreage of changed crop types compared to the period of 2011 to 2012. The tables (Tables 1 & 2) created by CDL's change analysis tool also support such changes. More than 24% of corn areas remain unchanged from

2010 to 2011, while for 2011 to 2012, less than 23% of corn areas stay the same for the state of Iowa.

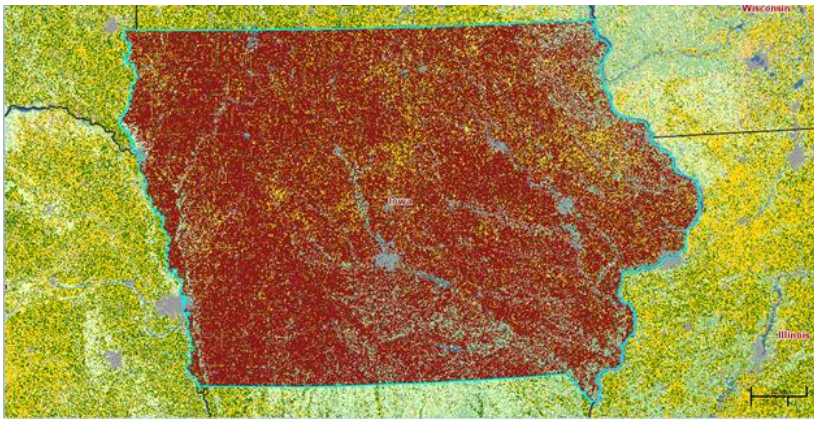

Figure 4 Changes in crop type from 2010 to 2011 in the state of Iowa (the color of red signifies change).

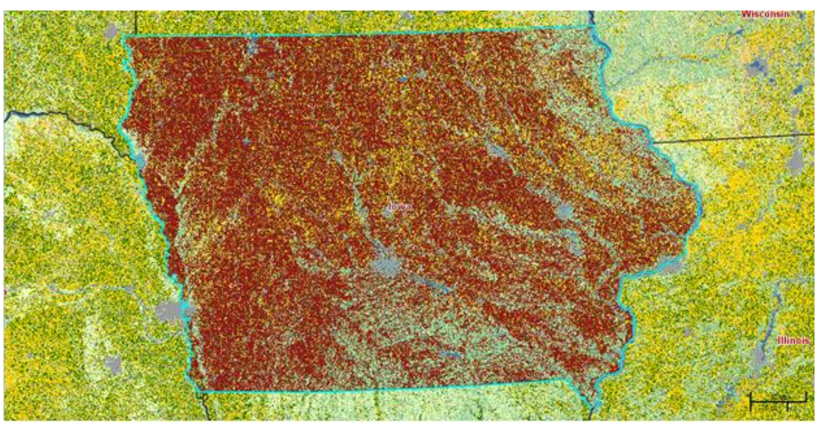

Figure 5 Changes in crop type from 2011 to 2012 in the state of Iowa (the color of red signifies change).

Table 1 Changes in crop type from 2010 to 2011 in the state of Iowa (top 5 in count of pixels)

From	To	Percent of Count
Corn	Corn	0.241
Corn	Sorghum	0.224
Corn	Soybeans	0.117
Corn	Sweet Corn	0.071
Corn	Pop or Orn Corn	0.046

Table 2 Changes in crop type from 2011 to 2012 in the state of Iowa (top 5 in count of pixels)

From	To	Percent of count
Corn	Corn	0.226
Corn	Sorghum	0.225
Corn	Soybeans	0.136
Corn	Sunflower	0.097
Corn	Sweet Corn	0.077

Section 1.7 Principal results

The principal results of this dissertation include a new approach to monitor vegetation drought stresses with the triple assurance from vegetation moisture, thermal, and health stresses, a new drought index that combines VIS/NIR/SWIR/TIR spectrums and ground observations for accurate monitoring of vegetation conditions and agricultural drought with remote sensing techniques, and two sets of Web Services that will enable online users to extract drought information from remote sensing based data, and customize and validate their own drought indicator.

CHAPTER 2 LITERATURE REVIEW: METHODS FOR MONITORING VEGETATION STRESSES, SOIL MOISTURE AND AGRICULTURAL DROUGHT

Section 2.1 Monitoring vegetation stresses in cropland

An agricultural drought refers to a drought event that has negative influence upon crops and pastures. According to the drought severity classification scheme used by USDM, the drought levels from D0 to D4 indicate possible impact to crops and pastures at different degrees: D0 is to slow down planting, growth of crops or pastures; D1 is to cause some damages to crops and pastures; D2 is leading to crop or pasture losses; D3 indicates major crop/pasture losses; and D4 refers to exceptional and widespread crop/pasture losses. This is to say, drought severity of an area can be determined from drought impact upon local vegetation conditions. For the past two decades, researchers have used remote sensing techniques along with ground measurements for monitoring, assessing and analyzing vegetation conditions (either stress or vigor). Numerous vegetation indices (VIs) have been adopted for these purposes. Subsections 2.1.1 and 2.1.2 will talk about the usage of VIs in detecting vegetation stresses.

Subsection 2.1.1 Vegetation Stresses

Monitoring drought stress of vegetation is a critical component of proactive drought planning designed to mitigate the impact of this natural hazard. Approaches that characterize the spatial extent, intensity, and duration of drought-related vegetation stress provide essential information for a wide range of management and planning decisions.

Much of the focus has been laid upon obtaining the value of satellite -based VI observations to assess vegetation conditions and, the considerable emphasis that has been placed on developing new VIs in support of drought monitoring. However, two major challenges exist among all these satellite-based VIs in terms of applying them for drought monitoring.

The first challenge is establishing the appropriate threshold(s) that discriminates between drought and non-drought conditions, as well as varying levels of drought stress (e.g., moderate, severe, and extreme). Typically, a relative VI value or a departure of a VI value from a baseline (e.g., low percentage of the average historical VI value) is used as an indicator of drought stress instead of classifying specific levels of drought severity. Selection of thresholds to classify drought conditions using VI information is difficult because they can vary by land cover types, geographic locations, and seasons. Also, the selection of thresholds shall be geo-location specific.

Operational drought definitions were developed by fitting an appropriate distribution function to a drought index. Five drought thresholds (ranging from abnormally dry to exceptional drought) were defined based on the percentiles used by the United States Drought Monitor. Using an objective approach for determining drought definitions ensures that droughts are accurately and correctly identified at the local level. It is inappropriate to use a single set of drought definitions for an entire state (especially a state the size of Texas). Also, because no single remote-sensing-based index can represent all aspects of drought including meteorological, hydrological and agricultural perspectives, integrating multiple indices into a “combined” drought indicator will provide a more comprehensive and accurate result for operational drought monitoring compared with what a single-index-approach will generate, and the new drought indicator, Combined Condition Index (CCI) to be proposed in this dissertation manages to combine the water, heat, and vegetation conditions into a single representation, and will serve as a more sensitive drought indicator.

The second challenge is the ability to discriminate drought-impacted areas from other locations experiencing vegetation stress due to other causes solely from remotely sensed VI information. A number of environmental factors (e.g., fire, flooding, hail, pests, plant disease, and human-induced land cover/use changes) can produce negative VI anomalies (Peters et al., 2003) that mimic a drought stress signal. Ancillary information such as climate data or ground observations (e.g., field reports of crop conditions) is needed to better define these negative VI anomalies within a drought context.

Generally, lack/excessive of heat, moisture, nutrient and other factors can all add up to the vegetation stress. The goal in managing and mitigating the stress of crop species is not simply to keep plants alive when the water is deficit, but to produce a profitable yield at harvest. In order to do so, the stresses crops most often experience (a.k.a. moisture, heat and nutrient stresses) shall be carefully monitored and mitigated.

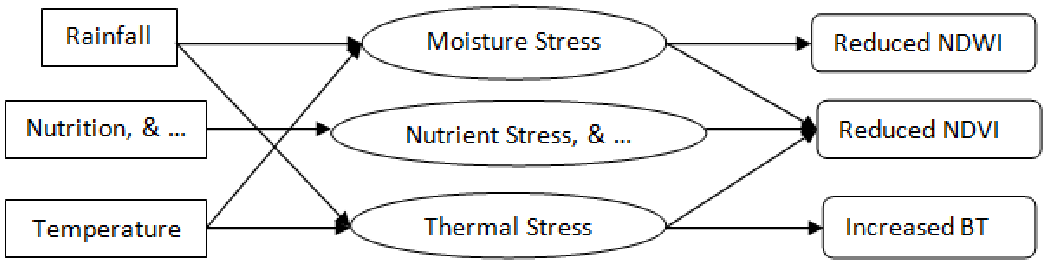

Figure 6 Vegetation stresses can be classified as moisture, nutrient, thermal stresses, etc.

2.1.1.1 Vegetation Water Stress

Studies have shown that crop water stress is directly affecting crop growth, development, and yield, and ultimately, farmers' profits. To achieve a delicate balance between water use and crop yield, farm managers need an operational means to quantify plant water deficit and evaluate the effects of stress on a given crop species at any stage of development.

Over the past 30 years, remotely sensed data have been used successfully for deriving information useful for irrigation scheduling and management. The basic approaches have focused on parameters related directly to crop water status (e.g., crop water loss (evaporation), metabolism, conductance, and photosynthesis) and plant manifestations of chronic crop water stress (e.g., phenologic stage and leaf expansion and loss).

For determination of crop water stress, several studies have proposed ratios of two complementary narrow-wavelength bands where the reflectance in one wavelength was sensitive to water or chlorophyll concentrations, and the reflectance of the other (a "reference") was relatively insensitive to such concentrations. Penuelas et al. (1997)

developed a water index (WI), defined as the ratio between reflectance at 0.97 and 0.90 μm for measurement of the percent plant water content for drought assessment. Gao (1996) introduced the Normalized Difference Water Index (NDWI), defined as the difference between reflectance at 0.86 and 1.24 μm divided by their sum. In a qualitative demonstration, the NDWI appeared to be sensitive to the liquid water content of vegetation canopies. Carter and Miller (1994) showed that the ratio of reflectance at 0.694 and 0.760 μm could be used to detect stress simultaneously with the crop physiological manifestation. Such indexes, based on narrow spectral bands, may have limited success with aircraft- and satellite-based sensors because they may be affected by atmospheric water absorption as well as plant water absorption.

All three of the above-mentioned spectral indices were found to be sensitive to measurements of plant stress as well as variations in ground coverage by leaves. To minimize the effects of ground cover variations and to maximize the assessment of plant stress condition, both Gao (1996) and Penuelas et al. (1997) suggest that the WI and NDWI be further normalized using a ratio or multiple regression with a vegetation index (e.g., NDVI) to correct for changing vegetation cover. This multispectral approach could circumvent the complexity associated with hyperspectral sensors by allowing a sensor to be designed with only a few spectral bands at strategic narrow and broad wavelength bands (assuming that wavelength and radiance calibrations are reliable). On the other hand, these indexes have been tested only for selected crops and they may be crop specific.

There is evidence that crop water stress can either hasten (Turner, 1977) or delay (Idso et al., 1980) crop development, depending on the crop phenologic stage at the time of water stress. Also, the time and duration of stress are of critical importance to ultimate yield (e.g., if a period of water stress occurs during heading or during the grain-filling period, the reduction of the grain yield is much greater than if this same stress condition occurs at some other time). For these reasons, knowledge of phenologic stage relative to planting date could provide important information on crop stress.

Multiple observations of the temporal-spectral characteristics of crops offer promise for use in estimating the crop development stages at the time of interest. Several approaches have been proposed to provide a spectral crop calendar. Tucker et al. (1979) showed that crop phenologic stage could be determined using a combination of spectral data and accumulated temperature units (growing degree-day). Badhwar and Henderson (1981) suggested that a given crop has a unique spectral profile in time and that the fractional area under the greenness profile curve was closely related to development stages in corn and soybeans. Malila et al. (1980) used the temporal changes in red and NIR reflectance of a wheat canopy related to crop development to develop a correlation between crop phenologic stage and canopy reflectance. That is, during the initial growth stage, NIR reflectance increased and red reflectance decreased due to corresponding differences in soil and green leaf reflectance. At heading, heads apparently cast shadows, causing both the NIR and red reflectance to decrease; and during ripening, the combined reflectance of the heads, the senescing leaves, and the exposed soil caused the red reflectance to increase while the NIR reflectance continued to decline.

There have also been attempts to determine stress effects by monitoring the temporal duration of specific phenologic stages. For example, Idso et al. (1980) reported that for wheat plots stressed for water, senescence appeared to be drawn out over a longer period of time than for well-watered plots. This was apparently due to an evolutionary strategy for annual plants to prolong their life span to increase grain production under stressful conditions. Idso et al. (1980) related the slope of the vegetation index (VI) over time to the rate of senescence and correlated this slope with final grain yield for wheat and barley under stressed and non-stressed conditions. In a similar study, Fernandez et al. (1994) found that the hydrologic stress of wheat could be determined by the slope of the NDVI along the maturity stage.

Besides lack of water, excessive water supplies may also lead to water stress for vegetation. A sudden localized heavy rainfall or lack of average rainfall can easily tip the balance toward flooding or drought. Monitoring whether the vegetation crop water is within the healthy range is a way to assure that the crop is not suffering from either drought or flood.

2.1.1.2 Vegetation Thermal Stress

LST can provide information about surface physical properties and climate, which plays a role in environmental processes (Javed et al., 2008). Weng et al. (2003) shows that LST varies with surface soil water content and vegetation cover -- the higher latent heat exchange is found with vegetated areas while the sensible heat exchange found in sparsely vegetation and urban areas. Because the LST is sensitive to vegetation and soil moisture, it can be used to detect land use and land cover changes (Javed et al., 2008).

However, validation of LST is difficult because (i) The surface emitted radiance is altered by atmosphere before reaching the sensors; (ii) Radiance measured by sensors are made in one direction which is not necessarily representing the entire upper hemisphere; and (iii) Separation of temperature from surface radiance cannot be done.

Traditionally, high temperature is believed to intensify the water stress for vegetation, and thus worsen the drought situations. The VHI raised by Kogan (1995) utilized the positive correlation between temperature index and vegetation index (i.e. when temperature increases, the vegetation performance worsens) to depict the vegetation vigor by 50% of temperature perspectives and other 50% of vegetation conditions. However, the pre-requisite might be wrong in many cases. High temperature is not making harm to vegetation performance all the time. For example, at the beginning of oats' growing season in Poland, abnormally high temperatures can provide an optimal soil environment for the newly planted crop to emerge. Thus to say, whether the temperature condition is good for the crop growth depends on the specific crop type, crop growing stage and location. Vegetation with a high resistance to evapotranspiration can have high VI and LST at the same time.

And also, during a specific growing stage of a crop when the optimal situation is to have lower temperature but the actual surface temperature appears higher than normal, the vegetation condition is not destined to reduce since the moisture level of the vegetation can be more than sufficient and the abnormal high temperature will not affect the water supply to the crop. For instance, though an area might be suffering from abnormal high temperature, an accidental rainfall can save the situation and provide enough water that the crop might need at its specific growing stage.

In summary, the relationship between surface temperature and vegetation condition is not linearly correlated. Many factors influence the way the change in temperature might interact with the change in vegetation conditions. Crop type, crop growing stage, soil type, soil moisture levels, wind speed, the evapotranspiration can all contribute to this issue. Among all, the soil moisture, or the vegetation water content is most important. When the vegetation is suffering from water stress, the thermal stress adding up to it might worsen the drought situations. However, when the vegetation is sufficient with water supply, abnormal high temperature might not cause such a disaster as when the water supply is deficient. There is no direct indication from high LST to severe drought.

The TCI, a remote sensing based thermal stress indicator is proposed to determine temperature-related drought phenomenon (Kogan, 1995). TCI is based on the thermal band of MODIS converted to brightness temperature (BT) and used to determine temperature-related vegetation stress and also stress caused by excessive wetness. The TCI algorithm is similar to the VCI algorithm, and is given as

Equation 1 Temperature Condition Index (TCI).

$$TCI = SCALE * \frac{BTmax\ -\ BT}{BTmax\ -\ BTmin}$$

Here, BT, BTmax and BTmin are the smoothed biweekly (or weekly) brightness temperature, maximum and minimum of the BT values for the same bi-week (or week) through multiple years, respectively, for each grid cell. The conditions are estimated relative to the maximum and minimum temperature envelopes. The above formula reflects different response of vegetation, to temperature. In most situations, high temperatures in the middle of the growing season indicate unfavorable conditions for drought, whilst low temperatures indicate mostly favorable conditions. Low TCI values correspond to vegetation stress due to high temperature and dryness. The TCI provides opportunity to identify subtle changes in vegetation health due to thermal effect as drought proliferates when moisture shortage is accompanied by high temperature (Kogan, 2002).

Subsection 2.1.2 Vegetation index (VI) for various crops

2.1.2.1 Performance of time-series NDVI

The NDVI, developed by Rouse et al. (1973), has been extensively used to monitor vegetation dynamics on a regional or continental scale (Tucker et al. 1985). However, the NDVI has its limitations when being applied for various locations different in latitude, elevation, climate zone, and other geospatial factors. If one compare the yearly NDVI time-series of any location (e.g. from 2000 to 2012), he/she can see that there is a fixed pattern of these NDVI peaks and valleys, no matter the studied year is suffering from drought or not. For example, the NDVI value of Corn Belt during drought period can still be higher than the NDVI value of Texas during normal times, and the NDVI value of wet winter is highly possible to be higher than that of dry summer as well.

NDVI can be considered as a variable consisting of two components – the short-term weather component and the long-term ecological component, and the weather component is weaker compared to the ecological component. Kogan (1990) thus introduced VCI to separate the weather-related fluctuations apart from the ecosystem changes. While NDVI's ability to indicate drought/non-drought is limited to geospatial and temporal difference, VCI as a ratio of current NDVI versus multi-year NDVI, reflects relative change in moisture conditions. In Figure 7, Blue lines represent the NDVI curve of corn, and the brown lines represent the NDVI curve of soybeans. Considering the peaks of the three states (IL, IA, and WI), the peak NDVI for corn lands is always lower than the peak values of soybeans. Also, there is a 16-32 days lag for the soybeans comparing to corn at their peaks (Johnson, 2010).

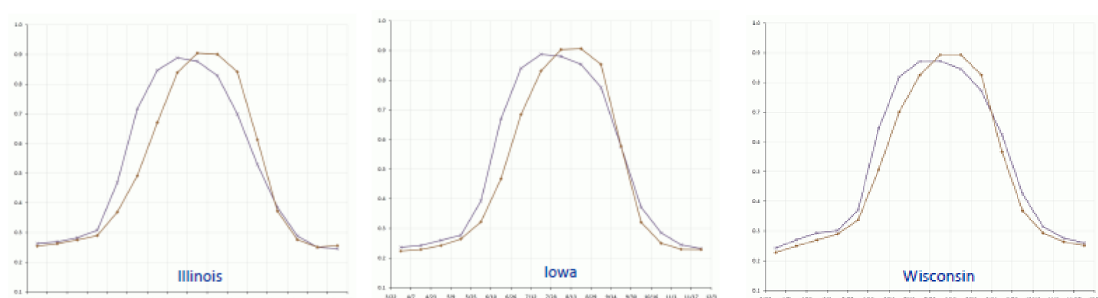

Figure 7 The NDVI curves of corn and soybeans for IL, IA, and WI (Johnson, 2010).

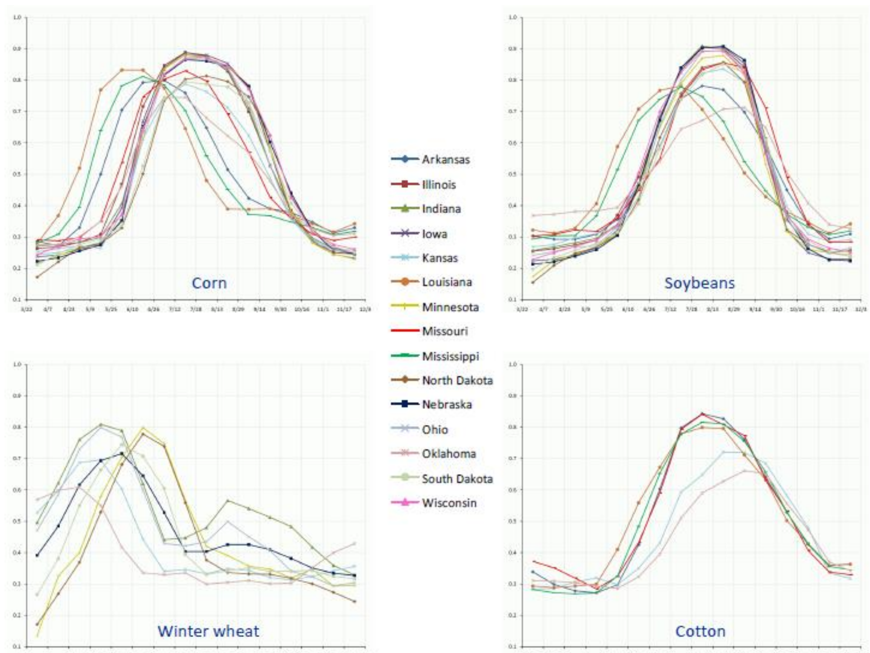

Figure 8 Even for the same crop in different states, the amplitude of NDVI differs. Also the timing could vary up to two months for some crops (Johnson, 2010).

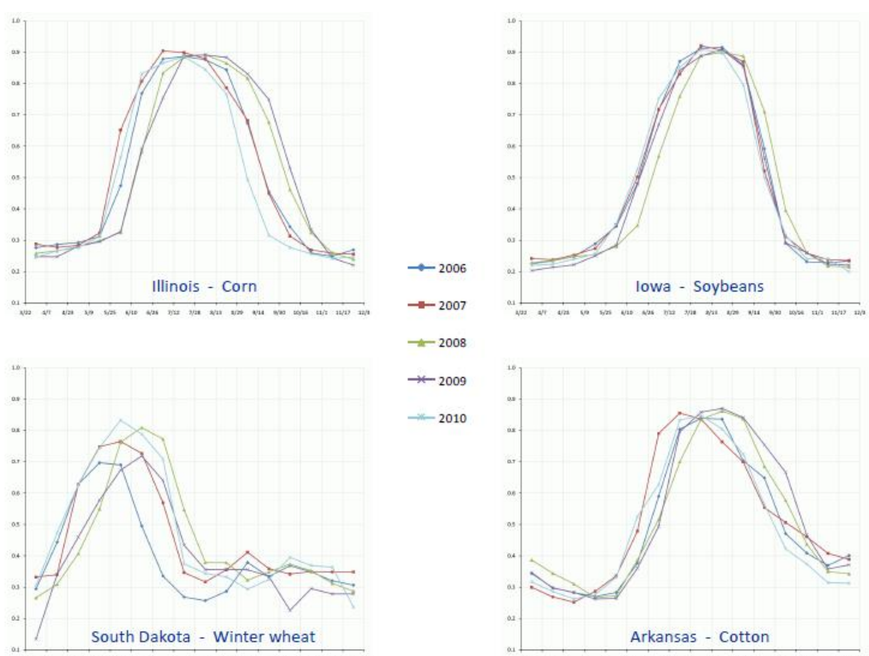

Figure 9 Even for the same crop in the same state, the NDVI performance could vary across years (Johnson, 2010).

Three rules can be concluded from the results above: (1) the amplitude and timing of NDVI varies by crop type, (2) the NDVI behaves differently based on the geophysical conditions, and (3) for each year, the timing and amplitude of NDVI differs.

2.1.2.2 Relationship between NDVI and NDWI

The calculation of NDVI is shown in Equation 2. The NDVI data provided by MOD13 product is derived from two bands – RED (620~670 nm) and NIR (841~876 nm), as listed in Table 3. Multiple studies have shown lagging NDVI responses to rainfall deficit and that, the red band used in NDVI calculation is highly absorbed by crop canopy and thus fails to return with strong signals (Chakraborty & Sehgal, 2010; Gao, 1996; Jackson et al., 2004). The NDVI value of a vegetated pixel getting saturated after the leaf area index (LAI) grows above three is another problem with NDVI, and therefore is not fully responsive during the full range of vegetation growing cycle. On the other hand, the Normalized Difference Water Index (NDWI), which is introduced by Gao (1996) and modified by Jackson et al. (2004), uses one band within NIR and the other within SWIR spectrum (as shown in Equation 3). And the two MODIS bands to represent NIR and SWIR spectrum are bands 2 and 6 (in Table 3), with spectral range of 841~876 nm and 1628~1652 nm, respectively.

Equation 2 NDVI

$$NDVI = \frac{R_{NIR} - R_{RED}}{R_{NIR} + R_{RED}}$$

Equation 3 NDWI

$$NDWI = \frac{R_{NIR} - R_{SWIR}}{R_{NIR} + R_{SWIR}}$$

Table 3 The corresponding wavelength ranges for the seven bands of MODIS surface reflectance products.

Band No.	Wavelength (nm)	Division
1	620-670	RED
2	841-876	NIR
3	459-479	BLUE
4	545-565	GREEN
5	1230-1250	NIR
6	1628-1652	SWIR
7	2105-2155	SWIR

NDWI manages to pick up vegetation water information in stronger signals, because the short infrared has high penetration through canopy cover. Unlike NDVI and its derivatives (e.g. VCI), NDWI remains sensitive to vegetation water content (and thus rainfall) until the LAI value reaches eight, and thus the effective duration for NDWI to reflect changes made in vegetation water is much longer than that for NDVI. Jackson et al. (2004) has illustrated the strengths of NDWI over NDVI using their time-series line plots, and the scatter plots of them versus VWC. In Figure 10, the line plot of NDVI-Corn series gradually ceases increasing and becomes constant after DOY 185, which means that NDVI for corn lands has reached saturation, while NDWI continues to change until several days after. The left plot of Figure 11 has shown that when corn VWC has risen above 4 kg/m^2, any additional increase of VWC is not reflected in NDVI changes. On the other hand, increase of VWC is still reflected via the increase of NDWI until VWC is larger than 4.6 kg/m^2, as shown in the right plot of Figure 11. The NDVI of soybeans also reaches saturation faster than NDWI, but the time lag is not as obvious as that of corn lands (Figures 10 & 11).

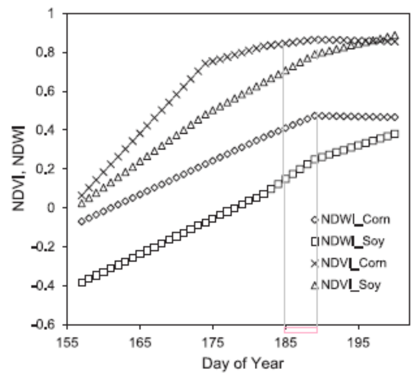

Figure 10 Jackson et al. (2004) pointed out that, for corn alone, NDVI reaches saturation during the middle of research period while the NDWI continues to change.

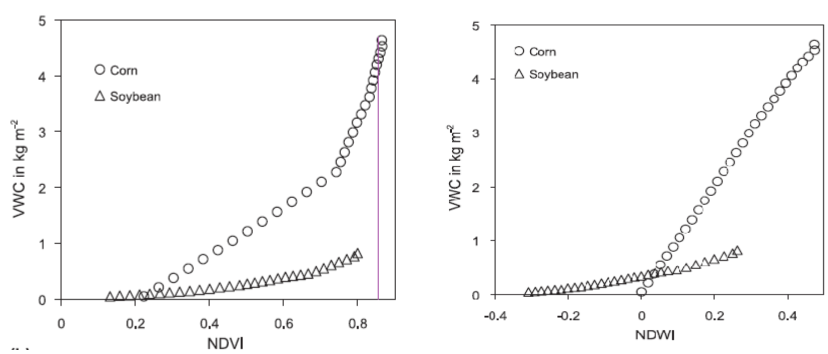

Figure 11 Jackson et al. (2004) pointed out that, for corn alone, NDVI reaches saturation during the middle of research period while the NDWI continues to change.

Because NDWI is more sensitive to vegetation moisture conditions in a longer span of time, adoption of NDWI and its derivatives will lead to better early detection and monitoring of agricultural drought in comparison to NDVI. This dissertation is to consider crop NDWI aside NDVI for drought monitoring.

2.1.2.2 Relationship between LST and NDVI

A large number of water- and climate-related applications, such as drought monitoring, are based on space-borne derived relationships between LST and the NDVI. The majority of these applications rely on the existence of a negative slope between the two variables, as identified in site- and time specific studies. Karnieli et al. (2008) investigated the generality of the LST–NDVI relationship over a wide range of moisture and climatic/radiation regimes encountered over the North American continent (up to 60 degrees North) during the summer growing season (April–September). Information on LST and NDVI was obtained from long-term (21 years) datasets acquired with the AVHRR. Research has found that when water is the limiting factor for vegetation growth (the typical situation for low latitudes of the study area and during the midseason), the LST–NDVI correlation is negative. However, when solar radiation is the limiting factor for vegetation growth (in higher latitudes and elevations, especially at the beginning of the growing season), a positive correlation exists between LST and NDVI.

Multiple regression analysis revealed that during the beginning and the end of the growing season, solar radiation is the predominant factor driving the correlation between LST and NDVI, whereas other biophysical variables play a lesser role. Air temperature is the primary factor in midsummer. It is concluded that there is a need to use empirical LST–NDVI relationships with caution and to restrict their application to drought monitoring to areas and periods where negative correlations are observed, namely, to conditions when water, instead of heat, is the primary factor limiting vegetation growth. The validity of the VHI as a drought detection tool relies on the assumption that NDVI and LST at a given pixel will vary inversely over time, with variations in VCI and TCI driven by local moisture conditions. However, when examined over spatially expanded areas and long periods, the relationship between LST and NDVI is found to be not only not a fixed one but also not always a negative correlation. The combination of 0.5*VCI + 0.5*TCI to represent vegetation health conditions might not work as efficiently in all regions. Kawashima (1994) distinguished between urban and suburban sites and observed positive relationships on a clear winter night as a result of higher vegetation density in the suburban area than in the urban area. Lambin and Ehrlich (1996) worked on a continental scale in Africa and found positive correlations over an evergreen forest and negative correlations over drier biomes. A positive slope was also shown for the native evergreen forests in southern Australia (Smith and Choudhury 1991). Karnieli et al. (2006) demonstrated that the slope of LST versus NDVI over Mongolia changes with respect to geo-botanical regions and latitude. A negative slope was observed in the arid regions of southern Mongolia, whereas the slope was positive in the northern part of the country. Olthof and Latifovic (2007) showed that the NDVI of trees and shrubs in Canada correlates positively with LST, whereas Sun and Kafatos (2007) found that these correlations over the North American continent are season and time-of-day dependent. A positive correlation was found in winter, whereas strong negative correlations were found during the warm seasons. The global distribution of the LST and NDVI relations shows negative correlations over drylands and mid-latitudes and positive correlations over the tropics and high latitudes (Schultz and Halpert 1995; Churkina and Running 1998; Nemani et al. 2003; Julien and Sobrino 2009).

In summary, positive relationships between LST and NDVI tend to develop in areas where vegetation growth is energy or temperature limited. Several studies confirmed via warming experiments in high-latitude regions that warming generally induces an increase in plant biomass, abundance, height, cover, and net primary productivity (NPP) (Chapin et al. 1995; Graglia et al. 1997; Dormann and Woodin 2002; Van Wijk et al. 2003; Stow et al. 2004; Walker et al. 2006). In such areas, higher LST reflects conditions that are more conducive to plant development through various biochemical processes (Badeck et al. 2004). Increased LST also drives processes within the soil, such as microbial activity, nitrogen availability, and nutrient uptake (Nadelhoffer et al. 1991; Chapin et al. 1995). Therefore, in high latitudes, increasing LST should not be interpreted as a signal of vegetation stress.

In general, prior studies suggest that the sign of the LST–NDVI slope may be governed by whether vegetation growth is water limited (negative slope) or temperature limited (positive slope). The latter condition is prevalent at high latitudes or in the evergreen tropical forests, whereas the former may occur at lower latitudes, especially in drylands (Nemani and Running 1989; Nemani et al. 1993; Lambin and Ehrlich 1996).

Karnieli et al. (2008) studied the LST-NDVI relationship over continental United States (CONUS), from 25°N to 60°N, and found that, at the beginning of the growing season, the majority of the area was characterized by positive correlation; in the middle negative correlation; and at the end a weaker, yet statistically significant, correlation. The correlation relationship between LST and NDVI being classified into three groups $r<-0.2$, $-0.2<r<0.2$, and $r>0.2$, the spatial distribution of these three groups over the growing period can be seen in Figure 12, in which red pixels are within group 1, white pixels within group 2, and blue pixels within group 3. From April to May, negative correlation between LST and NDVI is true for 67% of the studied area, the majority of which resides north of the 40°N (Figure 12(a)). From June to July, the LST-NDVI correlation is valid for 48% of the entire region, mostly south of the 45°N (Figure 12(b)). Figure 12(c) shows that, from August to September, the entire study area is made up of 34% of group 1 (negative correlation), 41% of group 2 (weak positive/negative correlation) and 25% (positive correlation), and overall indicates a relatively weaker correlation. Researchers need to pay attention to this changing correlation relationship.

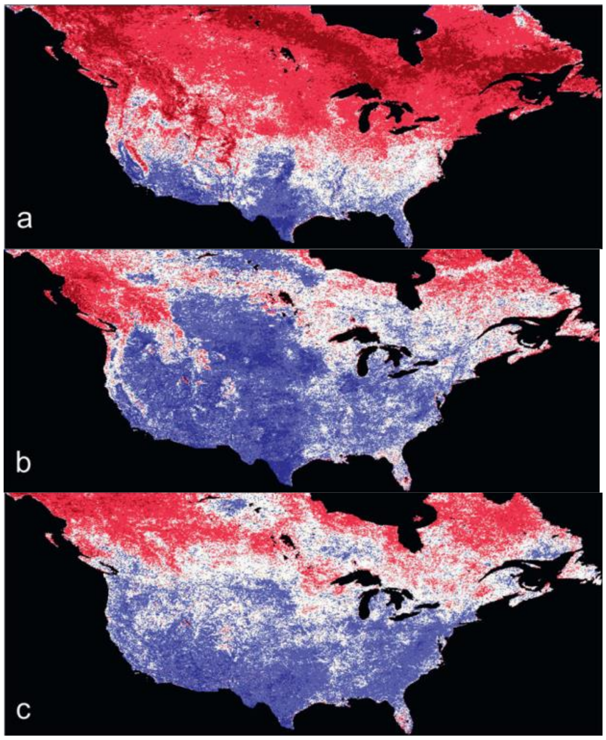

Figure 12 Spatial distribution patterns of pixels with positive, negative, or insignificant correlations for the (a)–(c) three sub-periods (April-May, June-July, and August-Sept.) of the growing seasons (Karnieli et al., 2008).

Section 2.2 Soil moisture estimation

Water held in the spaces between soil particles is called soil moisture. Surface soil moisture refers to the water being held in the upper 10 cm of soil, whereas root zone soil moisture is the water available to plants (generally considered to be) in the upper 200 cm of soil. Soil moisture is a limiting factor to vegetation growth in arid and semi-arid areas (Sandholt et al., 2002) where vegetation growth is heavily dependent on the water availability, and the vegetation index derived from satellite products may respond to the change of soil moisture and reflect the soil moisture to some degrees. Di (1991) has stated the complicated properties of soil moisture in that knowledge of soil moisture spans from surface to lower limit of root zone but most remote sensing methods can only cover the uppermost few micrometers of the soil. Sensitive to short-term changes in weather, the soil moisture in the top soil cannot be a strong carrier of long-term climate information, e.g. to indicate drought or non-drought. For instance, only a few days of dry weather can take away moisture from the topsoil, while the soil moisture down beneath in the root zone is still ample. On the other hand, there will be large deficiencies of soil moisture in the root-zone during a prolonged drought, yet a fast rain will immediately bring back the moisture level at the surface when the drought condition is not changed at all.

Among all methods to determine soil moisture, gravimetric sampling is the only direct and exact one; however, it is time and labor consuming to undertake, and therefore impractical to use for regional estimation (Wilson et al., 2003). Other ground-based methods can serve as alternative to save time and labor, e.g. Soil Climatic Analysis Network (SCAN) sites and COsmic-ray Soil Moisture Observing System (COSMOS) (Chrisman & Zreda, 2013) which take advantage of dielectric properties and neutron probes.

The advancements in remote sensing technologies have provided thriving perspective for timely measurement of soil moisture content across a large area. Thermal emissions from soils in the microwave region (i.e. passive microwave) are sensitive to the fluctuation of surface soil moisture – as the amount of water in soil increases, the energy emitted into space decreases (Jackson et al., 1995, 1996; Wang & Marsettb, 2004). Launched in 2002, the Advanced Microwave Scanning Radiometer (AMSR-E) of the Earth Observing System (EOS) instrument measures radiation at six frequencies in the range 6.9–89 GHz, all dual polarized. With its antenna scanning conically at a fixed incidence angle of 55 across a 1445-km swath, AMSR-E provides near-global coverage in two days or less. And its spatial resolution at the surface varies from approximately 60 km at 6.9 GHz to 5 km at 89 GHz. Moreover, the Aqua orbit is sun-synchronous with equator crossings at 1:30 P.M. and 1:30 A.M. local solar time. As a representation of a new data source for global observations of soil moisture, AMSR-E extends the variability of soil moisture information from regional to global scale (Njoku et al., 2003).

At moderate resolution, the soil moisture levels can be estimated from MODIS land parameters and ground measured soil moisture. With lower spatial resolution, AMSR-E microwave measurements provide a global picture of the soil moisture at the top soil layer. These measurements are typically less affected by clouds, and can be used as complementary to MODIS over regions of clouds.

From 2002 to 2005 a series of Soil Moisture Experiments (SMEX) were conducted to validate the space borne soil moisture measurements (e.g. from the AMSR-E instrument). Not only evaluation of the accuracy of AMSR-E soil moisture data is accomplished, but these objectives have also been realized with SMEX: to assess and refine soil moisture algorithm performance; to verify soil moisture estimation accuracy; to investigate the effects of vegetation, surface temperature, topography, and soil texture on soil moisture accuracy; and to determine the regions that are particularly useful for AMSR-E soil moisture measurements (SMEX Website, 2014).

Soil moisture, as a direct indicator for drought, can be used as a validation source to evaluate any agricultural drought indicator, either using the ground-based observations for points, or remotely sensed data for large areas.

Section 2.3 Methods for monitoring agricultural drought

Conventionally there are four types of defined droughts –meteorological, agricultural, hydrologic and socio-economic droughts. Targeting at each different type of drought, methods used for monitoring and assessment shall be distinguished. The United States has long been bothered by droughts, one of the most recent happened in 2012, which caused millions of dollars of crop/pasture losses. With recent advancements in remote sensing and other technologies, scientists are better equipped to have droughts monitored and forecasted at higher temporal and spatial frequencies, and hence in a more timely and accurate fashion. These will be enunciated in subsections 2.3.1, 2.3.2, 2.3.3 and 2.3.4.

Subsection 2.3.1 Definition of drought

Merriam-Webster Dictionary defines drought to be "a prolonged period of abnormally low precipitation; a shortage of water resulting from this". The National Drought Mitigation Center (NDMC) has its own definition of drought – an insidious hazard of nature, creeping, with its impact varying region by region (NDMC website). And it further classifies the definitions into two types: conceptual and operational definitions. Conceptually drought is defined as "a protracted period of deficient precipitation resulting in extensive damage to crops, resulting in loss of yield", which we can see how it emphasizes on the drought's impact to agricultural productions.

Operationally drought definitions take into consideration: "drought frequency, severity, and duration for a given historical period" (NDMC website). As Tannehill (1947) wrote in Drought and Its Causes and Effects, "We have no good definition of drought. We may say truthfully that we scarcely know a drought when we see one. We welcome the first clear day after a rainy spell. Rainless days continue for a time and we are pleased to have a long spell of such fine weather. It keeps on and we are a little worried. A few days more and we are really in trouble. The first rainless day in a spell of fine weather contributes as much to the drought as the last, but no one knows how serious it will be until the last dry day is gone and the rains have come again … we are not sure about it until the crops have withered and died."

Everyone has a different definition for drought. However, more commonly, drought can be viewed as the result of when demands for water exceed the natural availability of water. Lack of any clear definition of drought has compounded the difficulty since drought can be defined by all sorts of elements such as rainfall, temperature, vegetation conditions, agricultural productivity, or soil moisture, levels in reservoirs and stream flows, or economic impact.

In general, there are four main types of drought: meteorological, hydrologic, agricultural, and socio-economic droughts. By definition, a meteorological drought happens to a region when its level of precipitation is abnormally low, and duration of dryness is abnormally long. A hydrological drought is defined on a watershed or river basin scale and it measures the effects of periods of deficient water precipitation on surface and subsurface water supply, such as stream flow and groundwater. The National

Oceanic and Atmospheric Administration (NOAA) defines agricultural droughts as a combination of temperature and precipitation over a period of several months leading to substantial reduction (less than 90%) in yield. An agricultural drought is considered to have set in, when the soil moisture availability to plants has dropped to such a level that it adversely affects the crop yield and hence agricultural production. It emphasizes the response of the region's soils, plants, and animals to water stress. However, the actual impact of drought on agricultural crops depends on the biological characteristics of crops, stage of growth, and the physical/biological properties of soil. And the socio-economic drought occurs when water supply falls short to meet human and environmental needs, and when a meteorological, hydrological or agricultural drought adversely affects the supply-demand chain of economic goods in the society (Nagarajan, 2009). Other than this classification, drought can be sorted into long-term drought and short-term drought as well.

The meteorological, agricultural and hydrologic droughts are inter-connected. As shown in Figure 13, precipitation deficiencies and abnormally high temperatures are two major reasons for meteorological droughts, and as the drought situation intensifies, with the emergence of plant water stress and biomass reduction caused by soil water deficiency, a meteorological drought can become an agricultural drought. Moreover, as the situation gets worse, with reduction in streamflow, inflow, wetlands and wildlife habitat, a hydrologic drought will come into being.

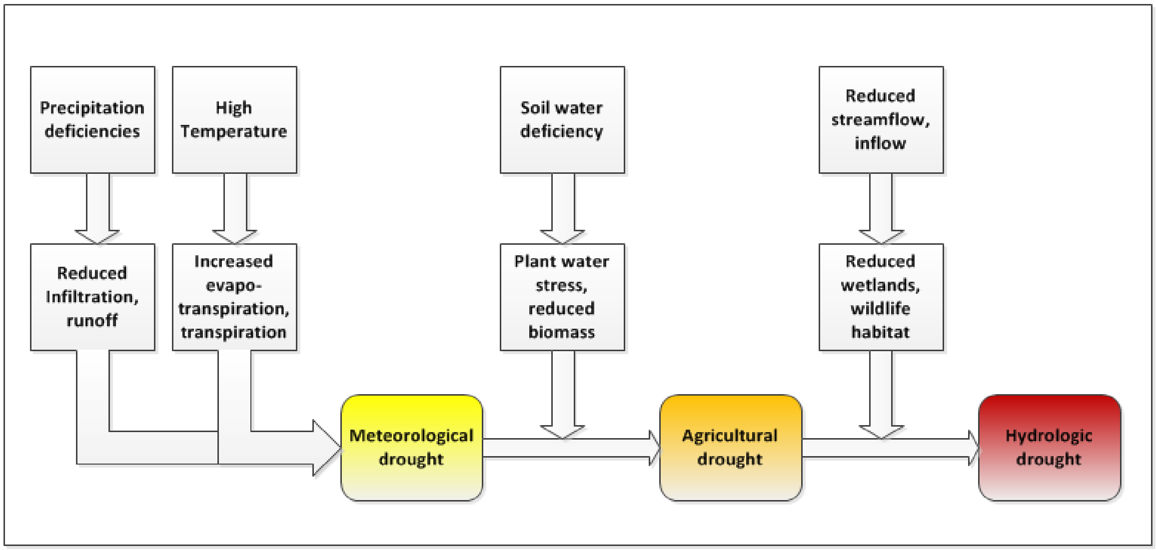

Figure 13 Transitions between meteorological, agricultural and hydrologic droughts.

Researchers have a tendency towards a specific type of drought when they are representing the interest of a special group of people. For example, when farmers or ranchers' interests are concerned, the research will focus on agricultural drought, because people in the grocery and meat business or farm communities depend on agricultural income for their livelihoods. Thus the spot light of assessing, monitoring, and predicting agricultural drought is around the drought impact to be seen on crops or livestock, and how these results into changes in food production and market price. On the other hand, urban planners are mostly concerned with hydrological drought because water supplies and reserves are key components in managing urban growth. In addition, mostly researchers care about meteorological drought, because that is the drought condition most familiar to the general public and the one most easily identified. Also, this is the set of information that decision makers will look into in the first place.

Subsection 2.3.2 Drought in the United States

Compared to floods, tornadoes, and hurricanes, droughts can be less spectacular, yet they are often more costly than other types of natural disasters, and not a single region in North America has been immune to periodic drought.

Drought has afflicted portions of North America for thousands of years. According to the NOAA, the year of 2012 is the hottest year, and July in 2012 is the hottest month ever recorded in the United States since 1895. The federal assessment in August 2013 has shown that the 2012 drought has affected 87% of the land dedicated to growing corn, 63% of land for hay and 72% of land used for cattle. The breadth of this 2012 drought is particularly striking. From the weekly (dated 2012/10/02) report of U.S. Drought Monitor, about 65.45% of the CONUS (and about 54.77% of the U.S. including Alaska, Hawaii, and Puerto Rico) was experiencing a drought classified as moderate to exceptional (D1-D4) at the end of September. Also, the Palmer Drought Index for the end of August has revealed that severe to extreme drought affected about 39% of the CONUS, and about 55% fell into the moderate to extreme drought categories. According to government historic monitoring records, such area of impact is the largest since 1956.

The worst drought in nearly half a century has set food prices up. After favorable spring weather in 2012, corn productions for the United States had been projected to hit record high (approaching nearly 15 billion bushels), as farmers had planted the most acreage since the late 1930s to profit from what were already the highest corn prices ever. Then the drought set in, projections of a bumper crop evaporated, and prices began to climb. As of mid-July, more than half of the corn in seven states was in poor condition or very poor condition, according to the U. S. Department of Agriculture (USDA). For corn planting areas in Kentucky, Missouri, and Indiana, more than 70% of them were in poor or very poor conditions. Fewer crops were in good to excellent conditions in 2012 – for instance, 66% of the nation's corn was in good to excellent condition in 2011 while in 2012 only 31% was in good to excellent condition. Some farmers have been cutting their corn early to use for feed, which is to profit much less than the other venture. More just sit watching their cash crops "burn to the point of no return". On June 25, 2012, corn prices on the Chicago Board of Trade rose 40 cents to $5.94 a bushel, as reported by Agriculture.com.

Withering of corn has put stress on cattle farmers by increasing feed prices and depleting available feeding land. By record of the U. S. Dept. of Agriculture (USDA), 54% of pasture and rangeland where cattle feed or hay is harvested for feeding, was in poor/very poor condition. Many farmers have not been able to keep their animals and have to sell them.

Figure 14 shows the deviation from trend for non-irrigated corn yield since 1960. The 2012 drought had been devastating to the non-irrigated corn yields in the U.S. and the deviation below trend was 34.1 bushels, which can only be rivaled in the last half-century by 1988 when yield dropped 33.8 bushels below trend. On the other hand, if deviation computation is based on percentage instead of bushels, then 2012 is the third worst of the last half-century with -29.3% below trend while 1988 is the worst with a -44.5% shortfall. If this deviation of corn yields is split into separate states, some states are with higher loss in corn yields. For instance in 2012, as shown in Figure 15, Illinois and Indiana suffered a steep drop in their corn productions, while Mississippi encountered an exceptionally good corn harvest. Illinois, the 2nd corn producing state by record, had to "import" corn from N. Dakota and Minnesota to make up for its shortfall.

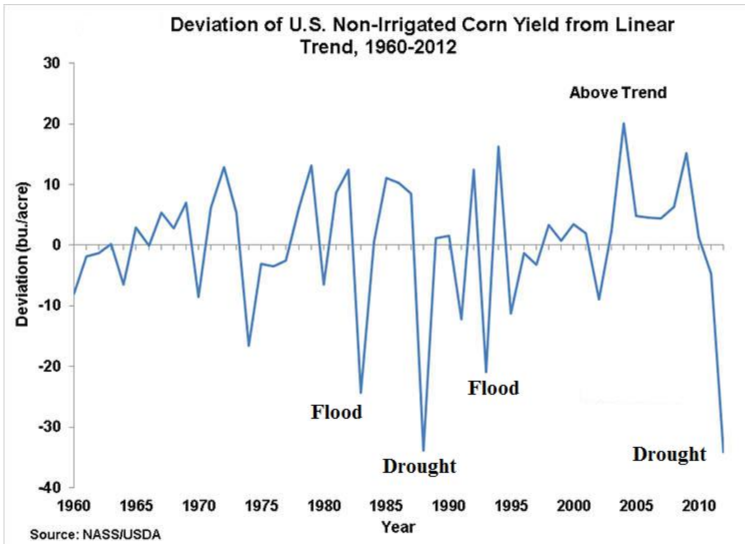

Figure 14 The deviation from trend for non-irrigated corn yield since 1960 (USDA NASS Crop Report, 2013).

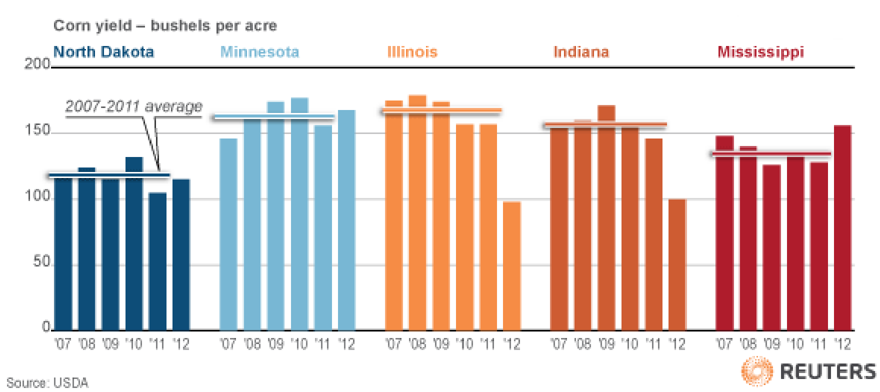

Figure 15 The corn yield for five states from 2007 to 2012. (Source: http://www.desdemonadespair.net/2012/10/in-aftermath-of-drought-us-corn.html)

Besides this 2012 drought that devastated U. S. agriculture, during the past century, the nation had several experiences with "big" droughts in 1930s, 1950s and

1980s respectively. During the 1930s, the Dust Bowl drought which severely affected much of the United States came in three waves, 1934, 1936, and 1939-1940. For some regions of the High Plains, the drought conditions lasted for as many as eight years. The cause of the "dust bowl" effect was the sustained drought conditions compounded by years of land management practices which left the topsoil susceptible to the forces of wind. After being depleted of moisture, wind lifted the soil into great clouds of dust and sand and thus was called "black blizzards". Because of this drought, farmers of the Great Plains adopted new cultivation methods to help control soil erosion in dry land ecosystems.

A five-year drought caused many residents of the Great Plains and southwestern United States to suffer during the 1950s and within three years the drought conditions expanded from coast to coast. The first signal of drought was felt in the south western United States in 1950 and by 1953 it had spread to Oklahoma, Kansas and Nebraska. Until 1954, the drought had swept a massive area consisting of 10 states, from mid-west to the Great Plains, and southward to New Mexico. Reaching a peak in 1956, the drought remained strong in the Great Plains area. It was not until the spring rains of 1957 had the drought conditions in most areas subsided. Characterized by both low rainfall amounts and excessively high temperature, the drought devastated the region's agriculture – crop yields in some areas dropped as much as 50% (Smith et al., 2004).

The drought from1987 to 1989, beginning along the west coast and extending into the northwestern U. S., had its greatest impact in the northern Great Plains. At its peak, the drought covered 36% of the states. Compared to the Dust Bowl drought which covered about 70% of the states, this drought might not seem as significant. Yet it had not only been the most costly drought in the U. S. history, but also the most expensive natural disaster of any kind that impacted the U. S. during the 20th century. The total cost to energy, water, ecosystem, and agriculture was estimated to be at $39 billion. The vulnerability of the farm land was due in part to farming on marginally arable lands and pumping of ground water to the point of depletion.

Scientists still cannot completely understand how and why these three drought episodes occurred. From a societal perspective, maybe the more important question we should ask is how unusual are these events? Because most instrumental records (thermometer and rain gauges) are only about 100 years old, we are short of historic data to answer this question. Also, the characteristics and the conditions that lead to the persistence of drought remain unsolved. Although droughts related to El Niño and the Southern Oscillation (ENSO) are now more predictable on a seasonal scale, longer, multi-year droughts cannot be predicted still.

Table 4 Drought timeline of the U. S. (source: http://www.circleofblue.org/waternews/2012/world/infographic-u-s-drought-impacts-2012-corn-crops/)

Year	Event
1930s	The Dust Bowl -- Considered worst U. S. drought, covering 70% of nation at its peak.
1932	Record Planting -- 113 million acres (46 million ha). The next largest planting were in 1937 and 2012 at 97 million acres (39 million ha).
1951-1956	Great Plains & SW Drought -- Crop Yields drop 50% in some areas of the country, and the PDSI reached a record low in Kansas during Sep. 1956.
1987-1989	Costliest drought -- Covering 36% of the country, the costliest drought in U. S. history totaled $39 billion losses.
2009	3.1% of corn planted was Monsanto's genetically modified insect-resistant or herbicide-tolerant corn.
2009	Record Corn Numbers -- Record Production: 13.1 billion bushels (332.2

	million metric tons); Record yield per area planted: 164.7 bushels per acre (10.33 metric tons per ha).
2012	25.8% of corn planted was Monsanto's genetically modified insect-resistant or herbicide-tolerant corn.
2012	Record planting since 1937 -- Expected record yield per acre, before the drought.
2012	Most Expansive Drought since 1956 -- Record corn price: $8.16 per bushel ($321.50 per metric ton).

Subsection 2.3.3 Major methods of drought monitoring over large areas

Traditionally weather station data (e.g. precipitation, temperature) and climate-based indices (e.g. PDSI) are used for drought monitoring. However, this approach has a limited spatial precision at which drought patterns can be mapped since the meteorological measurements are collected in points. Also, weather stations are scarce in remote areas and not distributed in a uniform manner. Thus, the traditional approach can only provide broad-scale point-based data using statistical spatial interpolation techniques, and the spatial detail in those patterns is highly dependent on the density and distribution of weather stations. Remotely sensed data can be used to monitor drought over large areas with relatively higher spatial resolution than the weather station data. The satellite observations can provide timely, spatially continuous information for monitoring drought (and specifically vegetation dynamics and conditions) over large geographical area (Tadesse et al., 2008).

Scientists tend to monitor drought using the changes in the conditions of vegetation dynamics, LST and soil moisture. And there are plenty of satellite products providing the information. For instance, MODIS products provide gridded data of surface reflectance, LST, thermal anomalies, and land cover type, leaf area index (LAI), Fraction of Photosynthetically Active Radiation (fPAR) and others at different temporal and spatial scales. Alternative to MODIS, AVHRR, Système Pour l'Observation de la Terre – Vegetation (SPOT-Vegetation), Landsat Thematic Mapper (TM), and Landsat Enhanced Thematic Mapper Plus (ETM+) can also provide data for calculation of vegetation indices (e.g. NDVI, VCI, NDWI, TCI and EVI). As to calculate soil moisture, daily gridded AMSR-E Level 3 soil moisture data provided by the National Snow and Ice Data Center (NSIDC) and, Daily gridded Level 2 Tropical Rainfall Measuring Mission (TRMM) Microwave Imager (TMI) soil moisture data from Princeton's Land Surface Hydrology Research Group made from using vegetation indices (e.g. NDVI) or temperature (e.g. TCI) can be applied.

The obtained datasets can either be directly used for visualization or analysis, or be used for an estimate model of another information (e.g. vegetation water content can be estimated using NDVI or NDWI), or be integrated with the meteorological data to achieve better accuracy. Inside Box 1 is a sample procedure of how to achieve a drought condition estimate from Vegetation indices.

Box 1.

Step 1 -- *Retrieving or/and calculating Vegetation Index (e.g. VCI being calculated from NDVI, TCI being calculated from LST, and VHI calculated from VCI and TCI) derived from MODIS.*

Step 2 -- *Merge the resulting tiled images of step 1 into a continental or global picture*

Step 3 -- *Analyze the relationship between the VI values and the drought severities, and set up threshold values for each drought class*

Step 4 -- *Visualize the global or continental map with the new color scheme for each drought class, and mark the areas impact by drought.*

Using Remote Sensing techniques for large-area drought monitoring is advantageous at its large, uniformly distributed, and temporally continuous coverage. The traditional way of using in-situ observations for drought monitoring is not realistic to be extended to a global scale, since the spatial and temporal observations at weather stations have proven to be sparse and not uniformly distributed. However, using Remote Sensing data has its disadvantages: (1) The drought information obtained from merely remote sensing data or indices can sometimes be erroneous due to noise effects or other factors (e.g. for NDVI, the asymptotic or saturated signals over high biomass conditions, and its sensibility to canopy brightness, according to Emutrain Website), requiring validation from weather data. (2) The VI or soil moisture index can cause inherent linearity since they are often ratio based indices. (3) It is not considering the structural properties of land surface features.

Subsection 2.3.4 Key research issues in agricultural drought monitoring for the global communities

In the realm of monitoring global agricultural drought, there are three most heated topics. First, some scientists have focused onto obtaining a most appropriate drought indicator (and providing proof for the new indicator being better correlated with drought conditions than the currently used ones). This new drought indicator is sometimes a combination of two or more existing (hydrological or meteorological or agricultural or socio-economical) indices. For example, Kogan (1995, 1996) managed to combine VCI and TCI, and created a new index – VHI, which is a better drought indicator than merely using the VCI because VHI represents both thermal stress and moisture stress. Another way to create better drought indicators is to revise the existing one by changing the composite wavelength. For instance, Gao (1996) introduced NDWI for depicting the vegetation soil moisture conditions using two NIR bands, while Jackson et al. (2004) used one NIR and one SWIR bands for the same concept, and proved that the new NDWI is superior to the old one. The advantages of adopting a good drought indicator are (1) to detect and monitor drought conditions efficiently, (2) to determine the starting/ending time, duration and level of drought severities or impact, (3) to characterize a single drought event, and compare multiple droughts either at the same time or at the same location, and (4) to tie together levels of drought severity with drought responses thereby forming an operationally workable drought management plan (Nagarajan, 2009).

The second trend is to analyze the relationship (i.e. whether there is a significant correlation) between the estimated drought variables (e.g. hydrology, crop yield, or vegetation conditions) created from remote sensing indices and meteorological parameters, and the statistical ground truth. Once the correlation is established, scientists integrate the indices or parameters into some empirical models such as regression functions, and use the model for a broad region. The Vegetation Drought Response Index (VegDRI) is a good example, in which the 1-km NDVI images providing detailed spatial patterns of vegetation conditions are analyzed in combination with dryness information represented in the climate-based drought index data to identify and characterize the intensity and spatial extent of drought conditions. Biophysical parameters such as the land cover type, soil available water holding capacity, irrigation status, and ecological setting of an area are also taken into consideration because these environmental characteristics can influence specific climate-vegetation interactions (Wardlow et al., 2008). Hence in order to discover the relationship between each factor, and decide the influential weights this factor exerts upon drought, scientists are encouraged to integrate satellite-based observations (e.g. NDVI), climate-based drought index data (e.g. precipitation), and several biophysical characteristics of the environment (e.g. crop phenology) to produce an indicator that serves as a sensitive expression for the level of drought stress affecting vegetation.

Third, the interoperability issue is also of great concern. The global drought research community calls for the development of a drought observatory or monitoring system, which provides consistent and timely information of drought conditions and patterns at various scales – from local, regional to continental scales – and a detailed risk assessment mechanism that is capable of information collecting/archiving/publishing, and also analysis/learning/forecasting. The first half of the mechanism requires the following components to be continuously monitored over long time periods: soil moisture, stream flow, lake and reservoir levels, groundwater, and direct impact on vegetation cover, since drought is a slowly developing phenomenon affecting the entire water cycle. And the second half requires the system to perform analysis for drought hazards (i.e. the likelihood of the occurrence of a drought of a certain extent, severity and duration) and the societal vulnerability to drought. The Open Geospatial Consortium (OGC) standardized Web Map Service (WMS), Web Coverage Service (WCS), and Catalogue Service with Web (CSW) are most widely used among agencies/organizations supporting drought data, information, and knowledge, yet the collaboration between providers has been limited, and sharing and reusing of data, processes, methods and results are still insufficient. There is still a long way to go in extending the interoperability with national and regional drought information systems, and testing medium-range probabilistic drought forecasting products.

Moreover, for each new drought indicator being created, each new relation between drought and indices/parameters/ground measurements to be found, and each new method or system to be established, the validation process is always the key.

In future such a system will be built to provide a wide range of data, information, knowledge, and decision-making capability that the public and decision makers in policy and water resource management as well as for the research community can find useful. Furthermore, the short to medium term forecasting of the occurrence and likely evolution of droughts, as well as the prediction and analysis of likely impact of climate change on drought hazard in different regions, are important to support the development of efficient drought management plans, and should be developed as an extension to the drought monitoring (JRC Website, 2013; Peng, 2013).

CHAPTER 3 DETERMINATION OF VEGETATION PHENOLOGICAL PHASES FROM GROWING DEGREE DAYS (GDD)

A "crop growing season" is the period during a year when seasonal weather is favorable for crop growth. The "growing season" of the Corn Belt is often defined as the freeze-free period beginning with the last freezing temperature (in spring) and ending with the first freezing temperature (in the autumn). This definition is based on the fact that water (in soil or plant) as the most important factor to living plants is highly dependent on temperature. In this sense, the "growing season" is determined by temperature. The crop season for each crop type is different. For corn, its growing cycle consists of vegetative, reproductive, and maturation phases, and these phases can be further classified into more detailed stages of development (Figure 16). For example, corn will germinate and grow slowly at about 50°F (10°C), and poor germination will result from below-normal temperatures (when corn is planted in early spring). The most commonly seen stress imposed at the beginning of the crop season is that of cold soil temperatures. High temperature stress is detrimental to yield during the stages of ear formation, reproduction, and grainfill. Specifically during tasseling, silking and grainfill (TSG), corn under rain-fed conditions begins to suffer heat stress when air temperature exceeds 90°F (32°C). A study performed upon Nebraska has showed that the yield of dry-land corn may be reduced by 1.5 bushel/acre for each day when the temperature reaches 95°F (35°C) or higher, during the TSG period.

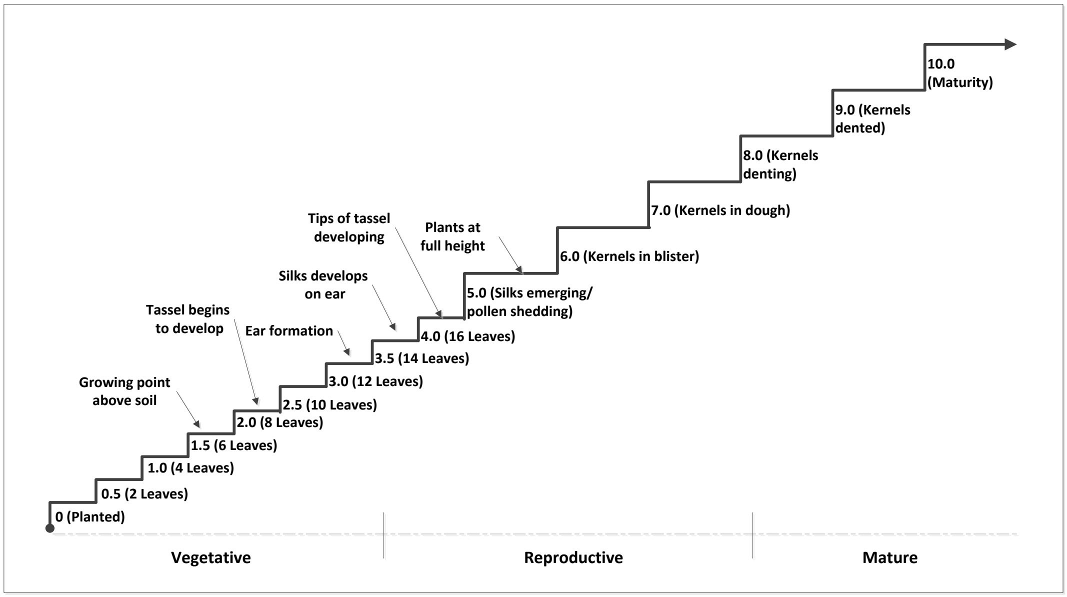

Figure 16 The vegetative, reproductive, and mature stages of corn can be divided into 11 sub-phases.

Multiple ways exist for decision makers to determine the integration period for agricultural areas, including (1) to find out the planting and harvesting dates for crops at each state every year by the National Agricultural Statistics Service (NASS) handbook published by United States Department of Agriculture (USDA) which is written based on historic crop calendar, (2) to determine the SOS (start of season) and EOS (end of season) by the NDVI time series, and (3) to calculate the accumulated GDD values for the area, and map to the corresponding growing stage of the specified crop. Detailed approaches are discussed in sections 3.1 and 3.2.

Section 3.1 Determination of SOS and EOS by crop calendar

The agricultural handbook published by NASS provides state-level usual planting and harvesting dates for major field crops, and has been used as reference of crop calendar for the broad range of public users including scientists and farmers. The SOS and EOS in this section are determined by crop calendar written in this handbook.

The planting and harvesting dates for each crop differ. For example in Table 5, for the state of Iowa in 1996, corn planting dates range from April 22nd to June 3rd while corn harvesting started from September 17th and ended on November 17th. Yet for soybeans, the planting did not start until May 4th, and the last date for harvesting was October 27th which together represents a much shorter growing period for soybeans. The growing period of soybeans is more or less 1 month shorter than that of corn.

Also, the planting and harvesting dates for the same type of crop and the same state can be different across years. Table 6 shows that corn planting of 2009 began from April 19th and ended on May 26th, representing a later and shorter planting period compared to year 1996.

The differences in planting and harvesting dates of the same type of crop in each state can be seen in Table 7. For instance, corn in the state of Arizona was planted since March 15th, and was harvested until December 1st in year 1996. Compared to corn growing in Iowa, the growing period of the former was much longer.

Table 5 The usual planting and harvesting dates by crop in the state of Iowa based on observations of year 1996 (Source: http://www.nass.usda.gov/Publications/Usual_Planting_and_Harvesting_Dates/uph97.pdf).

Iowa: Usual Planting and Harvesting Dates, by Crop

Crop	1996 Harvested Acres (000)	Usual Planting Dates			Usual Harvesting Dates		
		Begin	Most Active	End	Begin	Most Active	End
Corn, for Grain	12,450	Apr 22	May 2 - May 16	Jun 3	Sep 17	Oct 7 - Oct 31	Nov 17
Corn, for Silage	220	Apr 22	May 2 - May 16	Jun 23	Sep 1	Sep 10 - Sep 20	Sep 25
Hay, Alfalfa	1,200				May 26		Sep 27
Oats, Spring	190	Mar 24	Apr 4 - Apr 23	May 17	Jul 3	Jul 15 - Jul 29	Aug 9
Soybeans	9,450	May 4	May 14 - Jun 2	Jun 17	Sep 21	Oct 1 - Oct 15	Oct 27
Wheat, Winter	45	Sep 6	Sep 26 - Oct 15	Oct 30	Jun 24	Jul 6 - Jul 22	Aug 7

Table 6 The usual planting and harvesting dates by crop in the state of Iowa based on observations of year 2009 (Source: http://usda01.library.cornell.edu/usda/current/planting/planting-10-29-2010.pdf).

Usual Planting and Harvesting Dates by Crop – Iowa

State	2009 Harvested acres	Usual planting dates			Usual harvesting dates		
		Begin	Most active	End	Begin	Most active	End
	(1,000 acres)						
Corn for grain	13,400	Apr 19	Apr 25 - May 18	May 26	Sep 21	Oct 5 - Nov 9	Nov 21
Corn for silage	220	Apr 19	Apr 25 - May 18	Jun 23	Aug 15	Aug 25 - Sep 20	Sep 25
Hay, alfalfa	920	(NA)	(NA)	(NA)	May 24	May 30 - Sep 15	Sep 29
Hay, other	300	(NA)	(NA)	(NA)	Jun 5	Jun 14 - Aug 17	Sep 3
Oats, spring	95	Mar 25	Apr 2 - May 2	May 13	Jul 9	Jul 17 - Aug 5	Aug 11
Soybeans	9,530	May 2	May 8 - Jun 2	Jun 16	Sep 21	Sep 28 - Oct 20	Oct 31
Wheat, winter	22	Sep 6	Sep 26 - Oct 15	Oct 30	Jun 24	Jul 6 - Jul 22	Aug 7

(NA) Not available.

Table 7 The usual planting and harvesting dates of corn (for grain) by state based on observations of year 1996 (Source: http://www.nass.usda.gov/Publications/Usual_Planting_and_Harvesting_Dates/uph97.pdf).

Corn for Grain: Usual Planting and Harvesting Dates, by State

State	1996 Harvested Acres (000)	Usual Planting Dates			Usual Harvesting Dates		
		Begin	Most Active	End	Begin	Most Active	End
AL	280	Mar 5	Mar 25 - Apr 25	May 18	Jul 21	Aug 11 - Sep 20	Nov 2
AZ	40	Mar 15	Apr 1 - May 15	Jun 1	Sep 1	Oct 1 - Nov 1	Dec 1
AR	230	Apr 3	Apr 10 - May 18	May 25	Aug 16	Aug 27 - Sep 18	Oct 11
CA	220	Mar 15	Apr 1 - Jul 1	Jul 15	Sep 1	Oct 1 - Nov 15	Dec 1
CO	940	Apr 15	May 1 - May 15	Jun 1	Oct 1	Oct 15 - Nov 10	Dec 1
DE	150	Apr 19	Apr 30 - May 16	May 28	Sep 10	Sep 20 - Oct 15	Nov 5
FL	112	Mar 1	Mar 15 - Apr 15	Apr 25	Jul 15	Aug 1 - Sept 10	Oct 1
GA	525	Mar 1	Mar 20 - Apr 15	May 5	Jul 25	Aug 15 - Sep 5	Oct 10
ID	40	Apr 21	May 5 - May 26	Jun 9	Sep 29	Oct 20 - Nov 10	Nov 24
IL	10,800	Apr 22	Apr 30 - May 18	May 28	Sep 24	Oct 9 - Nov 3	Nov 19
IN	5,450	Apr 25	May 5 - May 20	Jun 10	Sep 20	Oct 10 - Nov 25	Dec 10
IA	12,450	Apr 22	May 2 - May 16	Jun 3	Sep 17	Oct 7 - Oct 31	Nov 17

The year-by-year planting and harvesting dates for a single state do not change much – there is only one week's time lag between that of 1996 and of 2009 (Tables 5 & 6). However, in order to achieve monitoring and assessment at finer spatial and temporal scales, it is critical to align the VI or drought information organized in calendar dates to be comparable by crop growing stages. The information provided by the agricultural handbook on SOS and EOS is not sufficient to form a complete crop growing calendar for the alignment. A better approach to create such a crop growing calendar is to use growing degree days (GDD), which is introduced in section 3.2.

Section 3.2 Identification of crop phenologic stage with GDD

Subsection 3.2.1 Calculation of GDD

Crops have different water demands along their growth stages. Crop water stress directly reflects agricultural drought intensity and affects crop growth, development, and yield, and ultimately, farmers' profits. Studies have shown that crop water stress can either hasten or delay crop development, depending on the crop phenologic stage at the time of water stress. Also, the time and duration of stress are critical to ultimate yield (e.g., if a period of water stress occurs during heading or during the grain-filling period, the reduction of the grain yield is much greater than if this same stress condition occurs at some other time). Take field corn for example (as shown in Figure 21), the three growing stages when it is most sensitive to water deficits are tasseling, pollination, and yield formation, in which under watering by 10% might cause a 20-25% reduction in yield (Hane et al., 1984). For these reasons, knowledge of phenologic stage relative to planting date could provide important information on crop water stress and agricultural drought conditions.

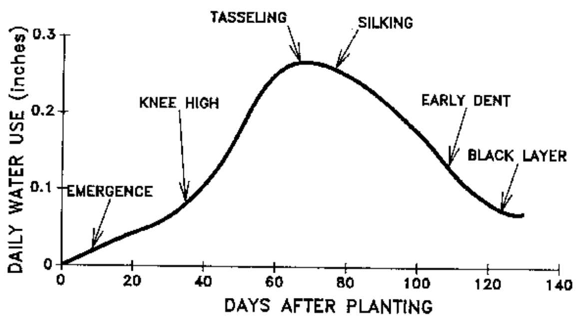

Figure 17 Daily water use by corn as influenced by stage of development. Irrigation scheduling decisions should be adjusted to reflect changes in water consumption by the crop during the growing season (Image Source: http://www.bae.ncsu.edu/programs/extension/evans/ag452-4.html).

Since the growth rates of many biological organisms are controlled primarily by temperature, the accumulated Growing Degree Days (AGDD), sum of daily GDD values from beginning of the growing period till the studied day, are useful in tracking the development of several important crops and insect pests. Each corn hybrid has a certain requirement for the AGDD value to reach maturity. For instance, for those grown in the central Corn Belt, the AGDD required is anywhere from 2100°F to 3200°F depending on the hybrid (Gibson, 2003), which is equivalent to the AGDD(°C) required from 1149 to 1760°C if using Celsius instead of Fahrenheit. The equations used to calculate daily GDD and accumulated GDD are shown in Equations 4 and 4b.

Equation 4 Growing Degree Days (GDD)

$$GDD = (Tmax + Tmin)/2 - Tbase$$

Here, T_{max} is maximum daily temperature and is set equal to 86°F (or 30°C) when temperatures exceed 86°F, T_{min} is the minimum daily temperature and is set equal to 50°F (or 10°C) when temperatures fall below 50°F, T_{base} is the base temperature for the crop. Only temperatures within a specific range can sustain growth rate, and temperatures falling out of 50~86°F (10~30°C) are always set to boundary values.

The GDD concept is under the assumption that: First, there is a value or base temperature below which plants do not grow or grow very slowly; Second, the rate of growth increases as temperature increases above a base temperature; Third, plant growth and development are more closely related to daily temperature mean accumulations above a base value in the absence of other limiting conditions (NCH, 2014).

Equation 4b Accumulated Growing Degree Days (AGDD)

$$AGDD(DOY) = \sum_{day=SOS}^{DOY} \mathrm{GDD(DOY)}$$

In Equation 5, the accumulated GDD value of any DOY that is within the growing period is computed by summing up the GDD values of each day from the start of season to the current day DOY. Depending on the units of temperature, AGDD can be in Celsius or Fahrenheit. Figure 18 shows the GDD accumulation slopes for years 2005 to 2011 for an observation station (SCAN site #2031). In year 2007, the GDD accumulates fastest than other years, which means crops reach maturity stage ahead of those in other years; while in year 2009, the GDD accumulation slope is flatter than other years, so the crops in 2009 would have a longer growing cycle. Also, the growing seasons of years 2005, 2009 and 2011 started earlier than those of other years, and the crop growing cycle of years 2005, 2007, 2010 ended sooner than other years.

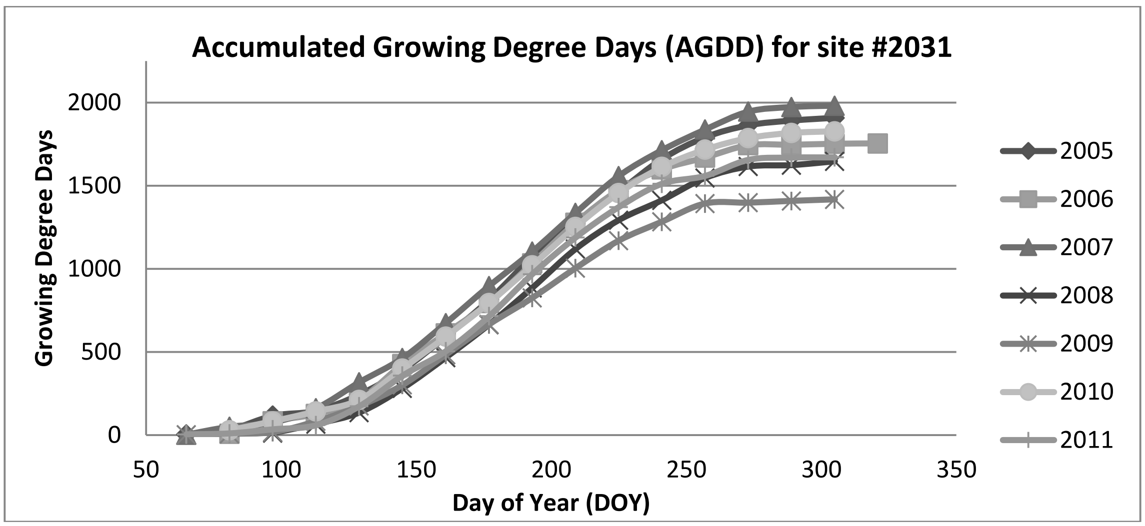

Figure 18 GDD time-series made with the temperature data collected from SCAN site #2031.

Subsection 3.2.2 Mapping GDD to corn phenologic stages

Crops have different water demands along their growth stages, with AGDD serving as an indicator for phenologic stages, water demands can be seen as a variable depending on the change of AGDD. Existing studies have utilized AGDD to indicate phenologic stages of crops. Take healthy maize shoot as an example, as shown in Figure 19, germination starts when AGDD is zero, then as AGDD increases to 120~180, tiler/shoot appears, and when AGDD reaches 780~810, kernel development starts. Unlike healthy maize, corn shoots suffering from drought stress do not have the same amount of AGDD at each growing stage. Also in Figure 19, the AGDD value at the stage of VT/R1 (tasseling/silking) is 885 for healthy maize shoots and 860 for those impacted by drought, while the AGDD at maturity is 1635 for healthy ones and 1510 for drought impacted ones. Thus, given day of year, we can accumulate GDD values from SOS to the specific DOY, and use the mapping relationship between AGDD and growing stages to decide which growing stage it is for current DOY. The resulting mapping relationship between DOY and growing stages for every year is illustrated in Figure 20.

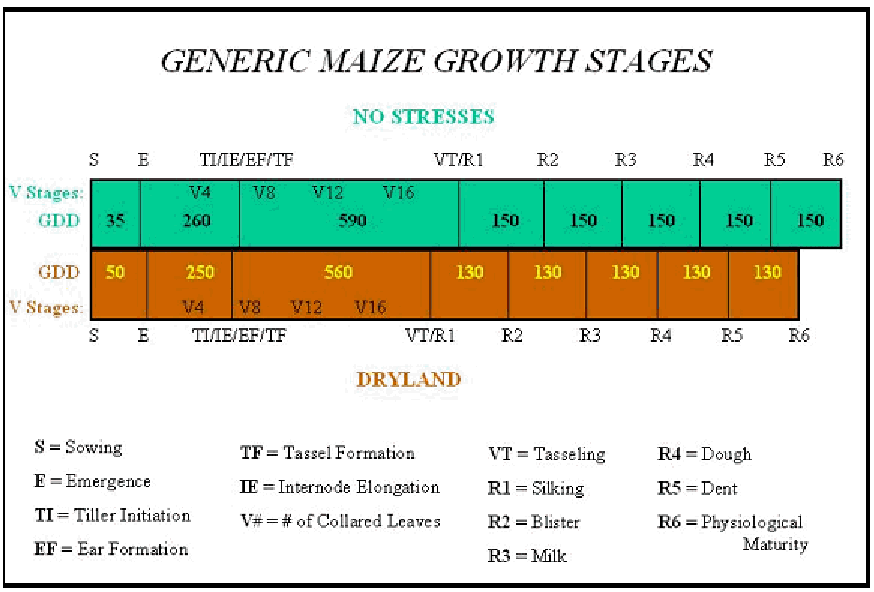

Figure 19 Generic maize growth stages for (1) those with no stresses and (2) those grown on dryland. As shown in the specific case of generic maize, the AGDD at maturity is 1510 for the dryland, and 1635 when there is no drought and other stresses (source: http://www.cropscience.org.au/icsc2004/poster/2/8/607_mcmaster.htm).

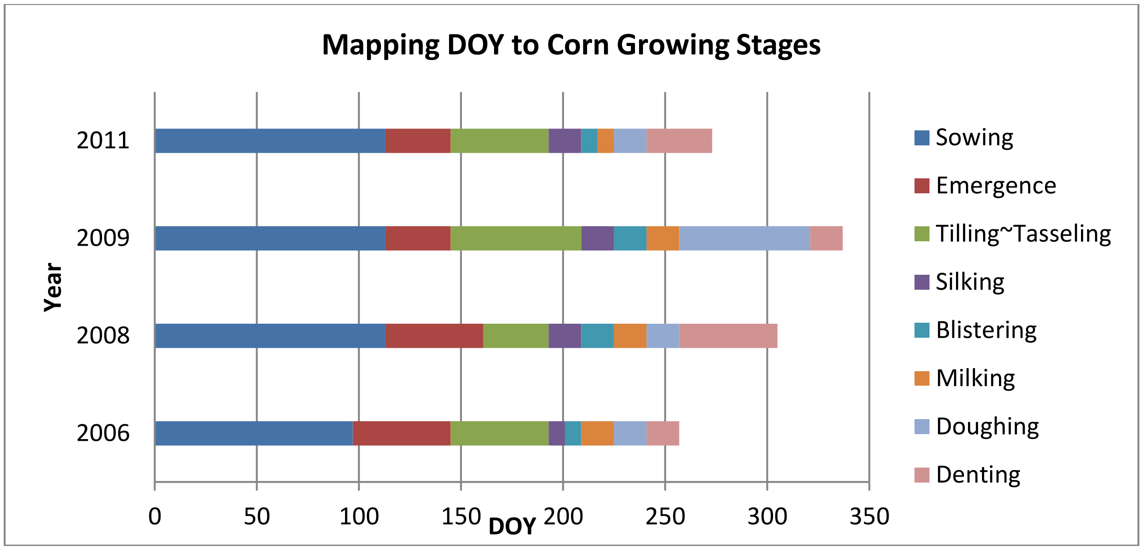

Figure 20 This bar chart is mapping DOY to corn growing stages of SCAN site #2031 in years 2006, 2008, 2009 and 2011.

Section 3.3 The relationship between crop phenologic stages and crop yields

One may conclude from Figures 19 and 20 that drought causes crop yield losses when the crop growing cycle starts late but ends early. However, this point of view that early planting dates are likely to provide more yields than the later dates, does not always quadrates with the facts. For instance, corn yield of Iowa in year 2008 is rated the third best in the state's history – 172 bushels per acre, but the corn progress in field for year 2008 started out late. Usually the recommended date to plan corn in Iowa is by May 10th. However, in year 2008, due to rain and cold weather, only half of the acres were planted in the western third of the state by then. It took until May 15th for the rest of the state to reach 50% planted. Iowa's corn was not completely planted until the end of June 2008 (Figure 21).

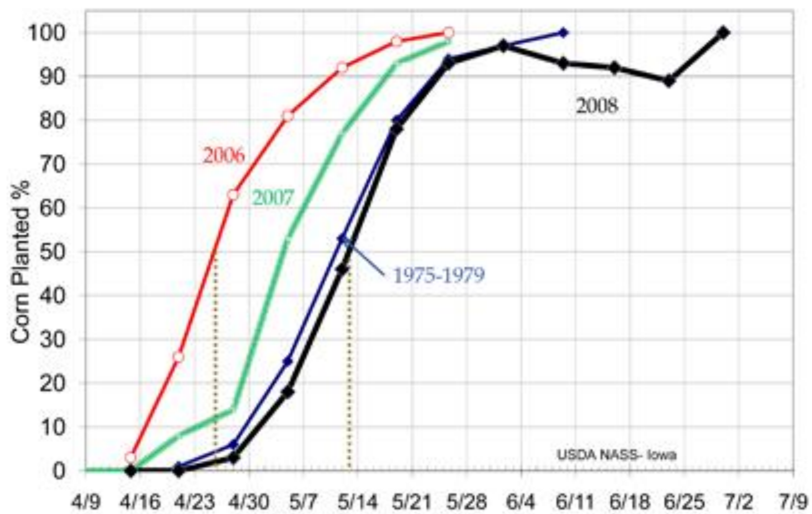

Figure 21 Iowa corn planting progress (source: http://www.extension.iastate.edu/CropNews/2008/1208elmoreabendroth.htm)

Also, the common belief that a late silking date correlates to lower yields cannot be accepted as the rule-of-thumb. Silking dates in 2008 are clearly lagging behind those of last few years. 50% of corn silking occurred 15 days later in 2008 than in 2007 and 2006. In fact, 2008 was the slowest year on record. Silking is the most critical growth stage for corn with late silking dates typically causing greater yield reductions. However, because the crop yield is dependent on weather conditions after silking, if the weather conditions are extremely suitable for crop growing after silking, the crop yield can still be satisfying despite of delayed silking. Note that corn in 2004 was also behind in silking yet resulted in the highest Iowa corn yields ever (Figure 22).

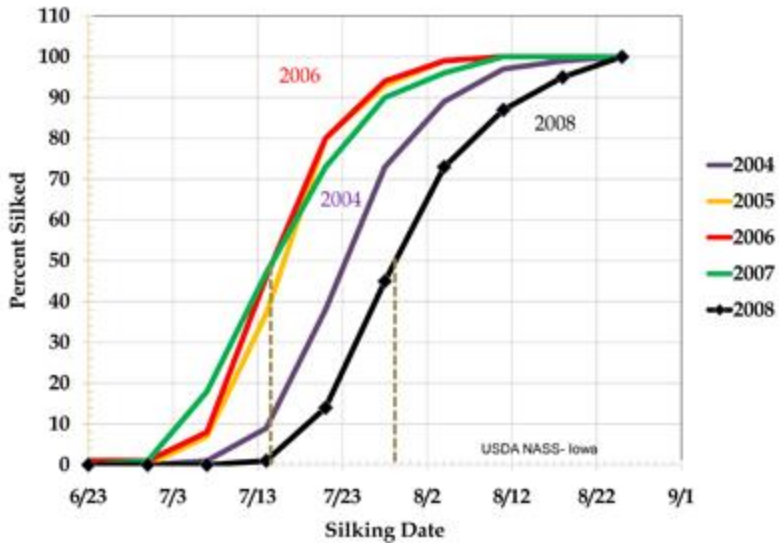

Figure 22 Iowa corn silking dates (source: http://www.extension.iastate.edu/CropNews/2008/1208elmoreabendroth.htm)

A delayed harvest is an obvious outcome of delayed planting and silking, and 2008 is much slower than an average year and is two weeks behind 2007. Average corn yield in Iowa continues to increase 2.25 bushels per acre per year. The 2008 yield, 172 bushels, is four bushels above the trend line. Though the state of Iowa as a whole is reported to have surprisingly high corn yields, various cropping districts within the state behaved differently -- the northwest cropping district posted exceptional yields for year 2008 due to normal heat unit accumulation, ordinary planting dates and less saturated soils in the spring, while the yields in southwest cropping district were reduced from drought and storm damage.

Scientists are curious about the reasons for lagging crop progress in Iowa to result in an exceptionally high crop yields in 2008, and research has shown that weather conditions of 2008 provided an excellent opportunity to maximize corn yield. Sunlight and rainfall after silking, 32572 Langley of solar radiation and 8.1 inches of rain, were similar to those of the best year (34344 Langley, and 9.7 inches). The maximum temperature after silking, 75.9°F, was close to that of median year (75°F), while the minimum temperature, 55°F, was close to that of best year (54°F). This, coupled with slow heat unit accumulation, resulted in slow crop development and subsequently longer grain-fill period. Moreover, a late frost also added to the advantages. Thus, it is the late-season weather that contributed to the high corn yields in 2008.

From the analysis above, the weather conditions after silking are determining factors to crop yields. Less-than-satisfying weather conditions including abnormally high temperatures, or low precipitation before silking dates do not exert as much influence to the crop yields. Thus when deciding if an area has been exposed to agricultural drought, it is more reasonable to consider its vegetation conditions after silking, since an agricultural drought is defined as a drought event related to crop/pasture yield losses.

Section 3.4 Summary

Crops have distinguishing requirements for water and thermal conditions at each growing stage. In order to decide whether (1) the meteorological parameters are over, within, or under the required conditions, (2) the vegetation conditions are better than, similar to, or worse than the "normal" crop progress, (3) the crop growing period is longer, equal to, or shorter than an ordinary growing cycle, researchers who are cross-comparing the vegetation conditions of two different years also need crop calendar to decide the starting and ending DOYs of every growing stage for these years.

CHAPTER 4 APPLICATION OF SATELLITE-BASED VEGETATION VIGOR

NDVI, a good indicator of various vegetation biophysical parameters, such as biomass, green leaf area index, percent green cover, and net primary production, as well as fraction of absorbed photosynthetically active radiation, has been widely used in applications related to vegetation vigor. NDVI also demonstrates strong linear relationships with environmental variables, such as temperature and precipitation, under various environmental circumstances. Study of the temporal response and spatial pattern of vegetation to climate fluctuations can be conducted using NDVI data. Moreover, the NDVI data have been used to explore trends of vegetation under climatic variation. In addition, previous studies showed that NDVI could be quantified to measure the deviation of vegetation condition from the normal conditions. In summary, NDVI can be used to study vegetation response to climatic variation at a range of time and spatial scales.

Section 4.1 Variation of vegetation vigor for the entire globe

Many studies already investigated the impact of climate change and climate variability on vegetation at global and continental scale. In this section, we will explore the usage of MODIS-based NDVI as an indicator for vegetation greenness under various climatic conditions worldwide.

Subsection 4.1.1 Data and Methods

As shown in Figure 23, the MODIS sinusoidal grids are made up of 36 by 18 tiles, each with a resolution of approximately 10° by 10°. However, due to the distortion of projection system, 177 out of 648 tiles do not exist. For the rest of tiles that do exist, about 290 tiles are classified as "land" or "land & water", and the other 290 or so tiles are considered "water". In Figure 23, dark blue squares represent the "water" tiles and light blue squares represent the "water & land" tiles, while the green squares are representing "land" tiles. The MOD13 algorithm does not produce products over oceans and deep inland water, and thus only around 290 tiles should be fed into this global calculation.

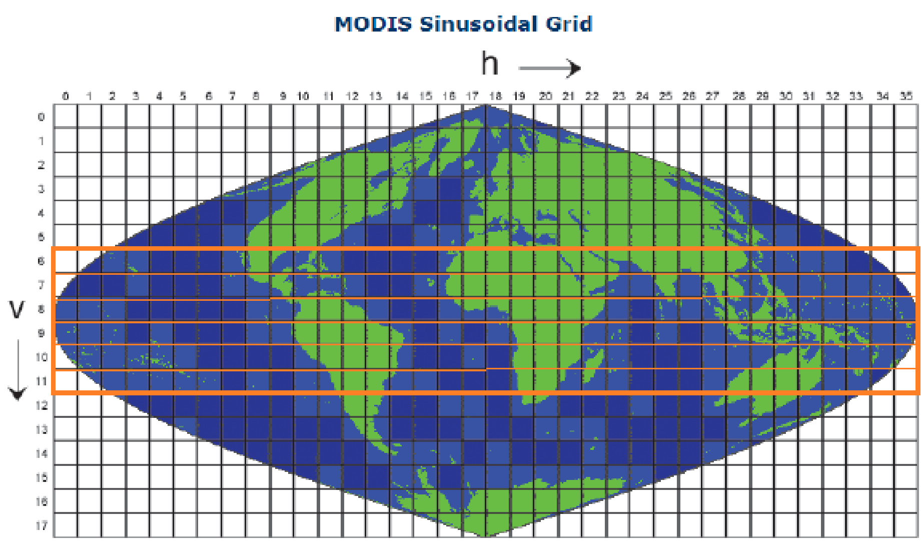

Figure 23 Circled strips are from V6 to V11, each compositing 36 MODIS tiles from H00 to H35 (source: http://nsidc.org/data/modis/data_summaries/landgrid.html).

Also, due to weather conditions, limitations of sensors, and other reasons that may cause errors for measurements, some of the collected surface reflectance data are considered unreliable, and they should be excluded from consideration as well. In fact, among the 12 Science Data Sets (SDSs) provided in the MOD13Q1.005 products, there are two SDSs carrying quality assurance information – namely "250m 16 days VI Quality detailed QA", and "250m 16 days pixel reliability summary QA", and these two bands can be combined to make a pixel quality mask in which 1 represents good quality and 0 represents bad quality. Three steps need to be done in order to generate quality mask for each pixel. First, the QA summary layer shall be checked. This layer provides five rank keys to describe the quality level of each pixel: -1 meaning Fill/No data, 0 meaning Good Data, 1 meaning Marginal data, 2 meaning Snow/Ice, and 3 meaning cloudy. When the pixel value in the QA summary layer is 0, the according pixel of the desired quality mask should be 1 and the according pixel of the reflectance band can be used with confidence. When the pixel value in QA summary is 1, the second step shall be taken, in which the pixel value in the same row and column within the detailed QA dataset is used. Each pixel of this layer is stored in a 16-bit unsigned integer, and these 16 bits are grouped into 9 fields – "MODLAND_QA", "VI usefulness", "Aerosol quantity", "Adjacent Cloud detected", "Atmosphere BRDF correction performed", "Mixed Clouds", "Land/water flag", "Possible snow/ice", and "Possible Shadow". The "MODLAND_QA" field is made up of the last two bits of each 16-bit pixel value. When it reads "00" from right to left, the according pixel in the resulting quality mask shall be 1. When it reads "01", the third step shall be taken, which is to look at the "VI usefulness" field (the 2nd to 5th bit reading right to left). The VI quality is acceptable when this field reads "0000", "0001", "0010", "0100", "1000", "1001","1010", or "1100". The quality mask will be set to 0 when this field reads in “1101”, “1110” or “1111”. The C code used to implement steps one to three can be found in Box 2. With these three steps, the VI quality mask is now complete.

Box 2.

```
for(int i = 0; i < PixelNum; i++){
	/*
	Layer "250m 16 days pixel reliability summary QA"

	Rank Key		Summary QA	Description
	-1	Fill/No Data	Not Processed
	0	Good Data	Use with confidence
	1	Marginal data	Useful, but look at other QA information
	2	Snow/Ice	Target covered with snow/ice
	3	Cloudy	Target not visible, covered with cloud
	*/

	if (QA_summary[i] == 0) QA_mask[i] = 1;
	else if(QA_summary[i] == 1) {
		/*
		MODLAND_QA		read from right to left (bits 0 - 1)
		00	VI produced, good quality
		01	VI produced, but check other QA
		10	Pixel produced, but most probably cloudy
		11	Pixel not produced due to other reasons than clouds
		*/
		if (QA_detailed[i]%4 == 0) QA_mask[i] = 1;
		else if(QA_detailed[i]%4 == 2) {
			/*
			bits 2–5 VI usefulness
			(0)0000 Highest quality
			(8)0001 Lower quality
			(4)0010 Decreasing quality
			(2)0100 Decreasing quality
			(1)1000 Decreasing quality
			(9)1001 Decreasing quality
			(5)1010 Decreasing quality
```

```
                        (3)1100 Lowest quality
                        (11)1101        Quality so low that it is not useful
                        (7)1110 L1B data faulty
                        (15)1111        Not useful for any other reason/not processed

                        */
                        int tmp = ( QA_detailed[i] - QA_detailed[i]%4)%16;

        if((tmp==0)||(tmp==8)||(tmp==4)||(tmp==2)||(tmp==1)||(tmp==9)||(tmp==5)|| (tmp==3))
QA_mask[i] = 1;
                        else ((tmp==11)|| (tmp==7)||(tmp==15)) QA_mask[i]=0;
                }else QA_mask[i]=1;
                //end of MODLAND_QA
        }else QA_mask = 0;
}
```

Downloading tiles and creating VI quality mask are just part of the workflow. A complete list of necessary procedures to calculate 16-day average NDVI time-series for the globe is shown in Box 3.

Box 3.

Step 1 – Download all "land" tiles of MOD13Q1.005 for any Year from 2000 to 2011, any DOY from 001 to 321.

Step 2 – Derive from each tile three subdatasets "250m 16 days NDVI", "250m 16 days VI Quality summary QA", and "250m 16 days VI Quality detailed QA", create quality mask and perform quality masking upon the NDVI dataset.

Step 3 – Merge the resulting good-quality tiled images of step 2 into a global image, and assign the other areas which are not covered by tiles Fill Values.

Step 4 – Traverse each pixel of the global image, get the sum and count of all valid pixels, and calculate the average (average = sum/count). Convert the 16-bit scaled NDVI average value to within its original range [-0.2, 1].

Step 5 – Repeat steps 1 through 4 for all available days during 2000-2011.

Subsection 4.1.2 Results

The global vegetation cover changed with an undulating trend from 2000 to 2011 (shown in Figure 24). Wave crests of the average yearly NDVI values occurred in 2000, 2006 and 2009, while troughs are found in 2003 and 2007. In 2003, the annual average NDVI dropped to 0.495, while the average NDVI in 2009 reached 0.505 – the highest value from yearly average since 2001. The global NDVI average calculated every 16 days throughout the years explains why year 2003 is of the lowest yearly average and year 2009 is of the highest from how the seasonal NDVI changes (in Figure 25). During the entire growing period, the NDVI curve of 2009 resides above the 11-year average except the time period from DOY 145 to 160, and that of 2003 resides beneath the 11-year average except the same period.

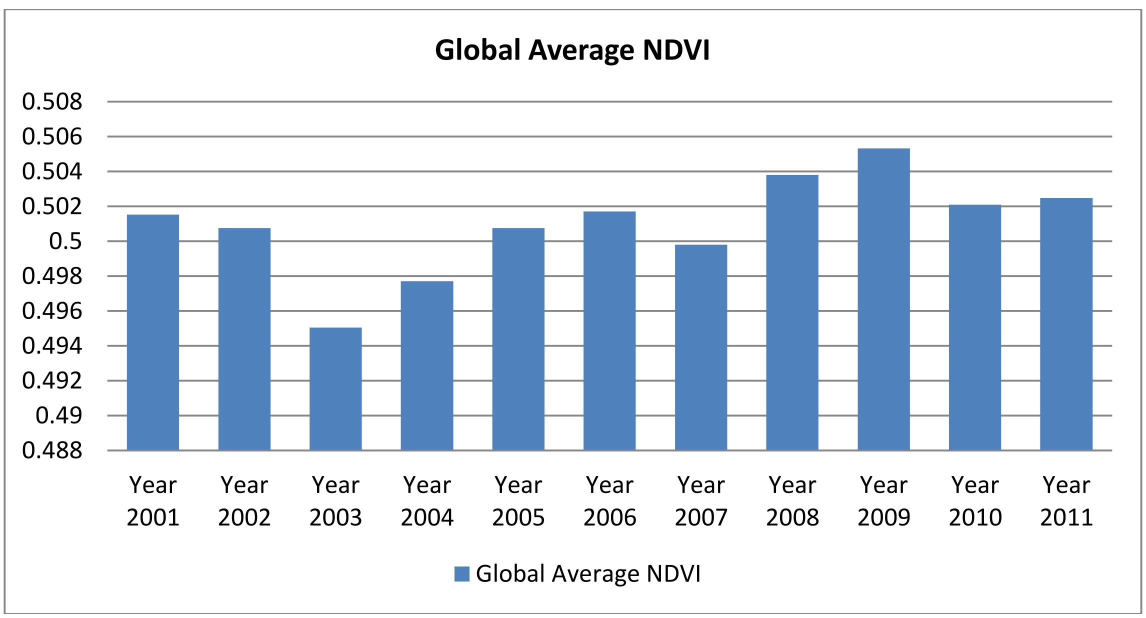

Figure 24 The yearly average NDVI for the entire globe from 2001 to 2011.

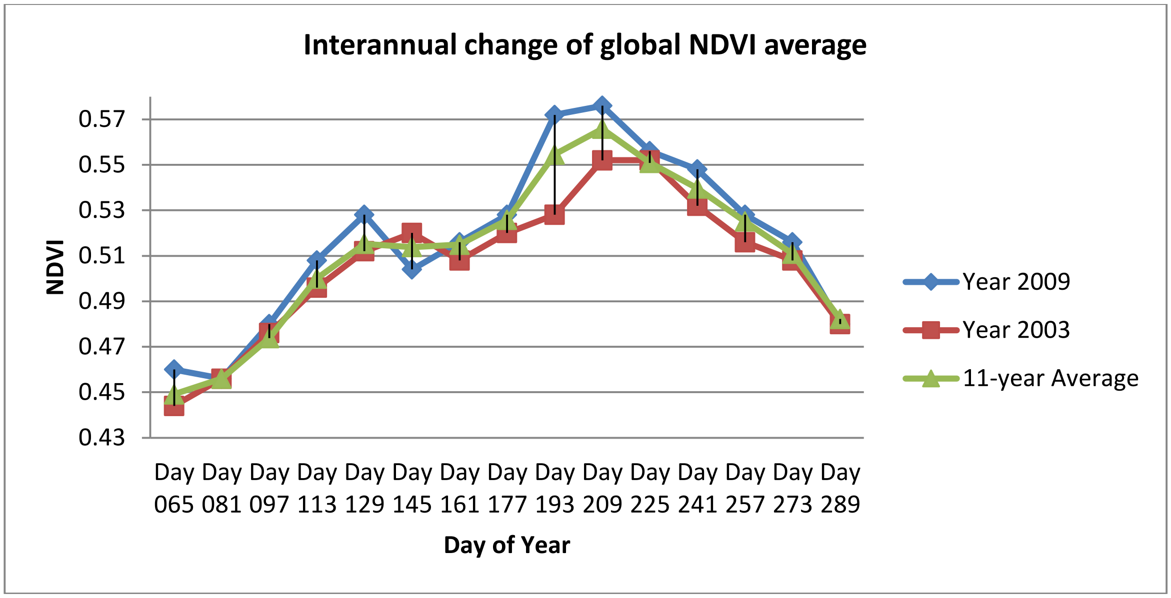

Figure 25 The inter-annual change of global NDVI average of years 2003, 2009 and the 11 year average from 2001 to 2011.

Section 4.2 Variation of vegetation vigor in latitudes

In this section, tiles of the same vertical order (e.g. V06) are grouped together into a horizontal belt. Because all the pixels located within oceans, rivers, and other water bodies are marked with Fill Values in MODIS datasets, the research only concerns about the land pixels. As a result, only the NDVI values of reliable land pixels are fed into the computation process for area average, and here average NDVI of the same belt are listed for V06 to V11. As mentioned before, theoretically speaking, NDVI takes values between -1 and 1, with values larger than 0.1 indicating vegetation, values larger than 0 and less than 0.1 indicating bare soils or cloud (that cloud is always very close to 0, e.g. 0.002), and values less than 0 indicating water, snow and ice. Thus, the NDVI average obtained here shall be positive, and larger than 0.1.

We can see from Figure 26 that the yearly NDVI average values for each belt are confined into specific ranges – for V08, V09 and V10, 0.55 to 0.61, for V07 and V11, 0.45 to 0.55, and 0.40 to 0.45 for V06. The differences between belts are more significant than the yearly differences of any single belt, which indicates that latitude has larger influence upon vegetation vigor than climate change and other temporally evolving factors. Since V08 and V09 are two closest belts to the equator, their yearly average NDVI values are the highest among all six belts. The maximum and minimum values for V08 from 2000 to 2011 are 0.602 and 0.584, and those for V09 are 0.592 and 0.577. As the most distant belt from the equator, V06 has the lowest NDVI values – the yearly NDVI average for V06 ranges from 0.418 to 0.435. Generally speaking, vegetation vigor increases as the study area gets closer to the equator.

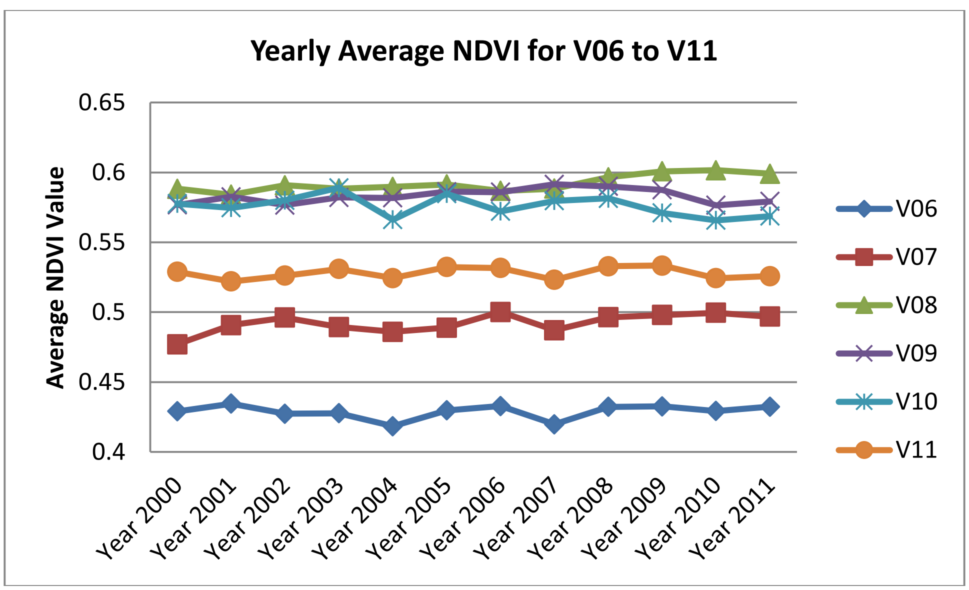

Figure 26 The yearly average NDVI value for parallel belts from V06 to V11.

Latitude and other geo-spatial characteristics define the basis of vegetation performances, and these properties are temporally stable. In order to tell whether the study area is suffering from drought or other vegetation stresses, one has to look at the temporal changes of its vegetation vigor. As shown in Figure 27, the belt-wise NDVI average curves of V06 in 2004 and 2007 lie beneath the 12-year average during the typical growing period (from DOY 97 to 257), thus belt V06 as an entity experienced vegetation suppression (compared to other years from 2000 to 2011) during both years. On the other hand, belt V07 encountered vegetation stresses in 2000 as shown in Figure 28. Although the belt-wise NDVI average of V07 is higher than its 12-year average during DOY 177 to 192, for most of its growing season, the NDVI values are below average.

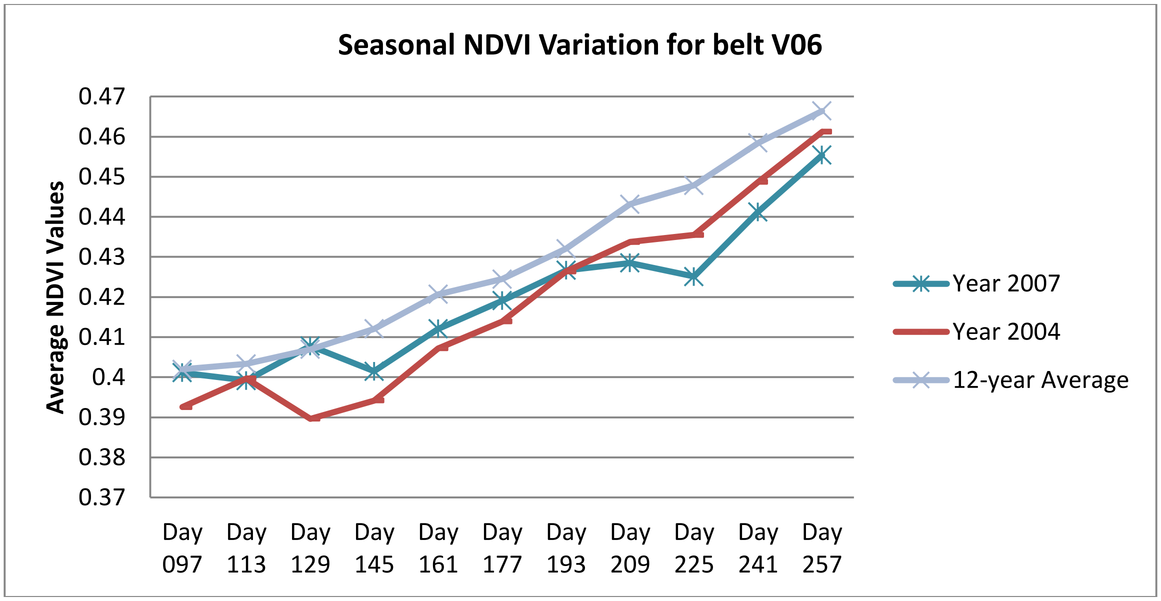

Figure 27 The seasonal NDVI curves of belt V06 for years 2004, 2007 and the 12-year average NDVI.

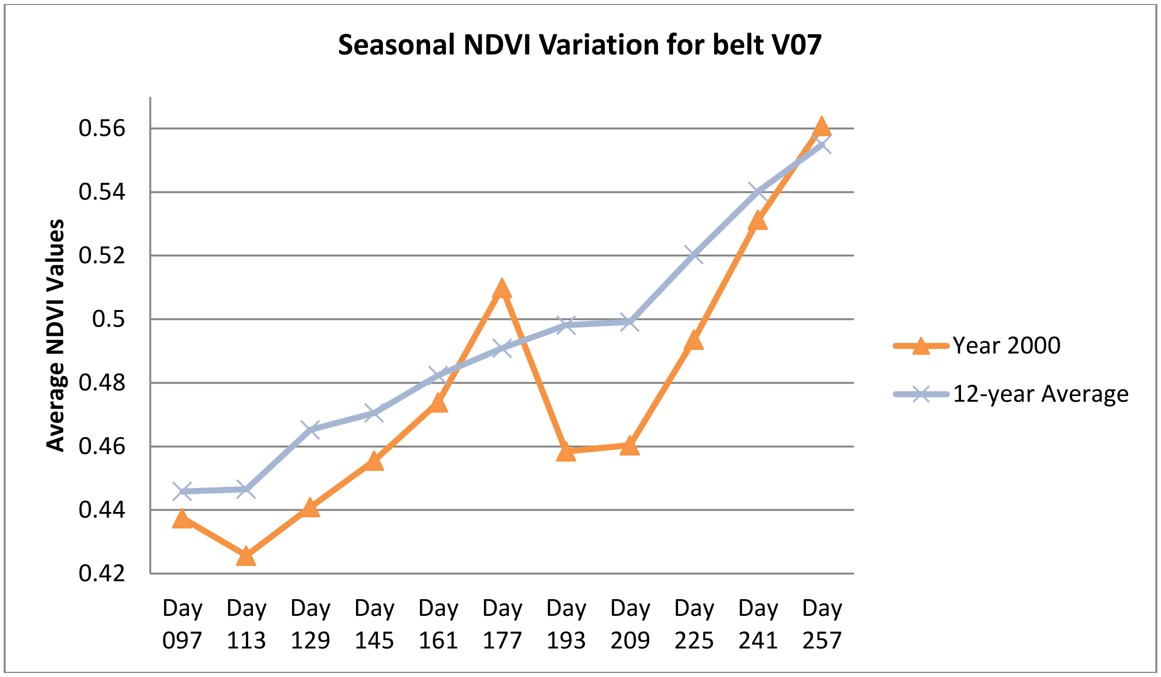

Figure 28 The seasonal NDVI curves of belt V07 for years 2004, 2007 and the 12-year average NDVI.

Section 4.3 Variation of vegetation vigor in climate zones

Drought is a serious climatic condition that affects nearly all climatic zones worldwide, with semi-arid regions being especially susceptible to drought conditions because of their low annual precipitation and sensitivity to climate changes. The effect of drought on vegetation varies noticeably between areas, and its pattern is determined mainly by the location of land-cover types. In subsections 4.3.1, 4.3.2, 4.3.3, and 4.3.4, four regions with different climate types are to be discussed, and they are Nile Delta (desert/subtropical Mediterranean), Great Lakes (Warm Summer Continental), Texas (humid subtropical, semi-arid, etc.), and southwest China (humid subtropical, alpine, etc.), respectively.

The agriculture in Great Lakes states or provinces has been diverse and productive; nearly 25% of total Canadian and 7% of U. S. production come from this area. With plenty of precipitation and snow/ice, the area's agriculture is not as dependent on moisture levels as semi-arid regions. Opposite to Great Lakes, other three regions constantly suffer from agricultural drought, and are highly dependent on precipitation for crop growth. Vegetation Indices, such as NDVI, reflect vegetation responses to climatic and weather conditions. Studying the multi-year inter-annual NDVI performances of each region helps us understand the relationship between precipitation, temperature, drought and vegetation responses. NDVI performances vary by location, and the influences of precipitation and temperature upon NDVI are especially significant in semi-arid regions such as Nile Delta, and some climate divisions of Texas.

Subsection 4.3.1 Case study of Nile Delta

Figure 29 displays how the NDVI 16-day-average changes throughout each year, starting from the first 16-day-period DOY 001 to 015, and ending at the last period of DOY 321 to 336. Years 2002 and 2005 stand out from other years for presenting abnormally high and low values than average, especially before DOY 177. The NDVI curves of each year drop sharply from DOY 177 (end of June) to 193(mid-July), indicating a sudden depression to vegetation vigor of the area, caused by its unique climate pattern. The monthly average rainfall of Nile Delta drops to 0 mm for June, and stays 0 till the end of September, while its monthly average temperature climbs above 90°F in June and keeps heating up until the end of August. Low precipitation and high temperature are two major causes for such vegetation suppression.

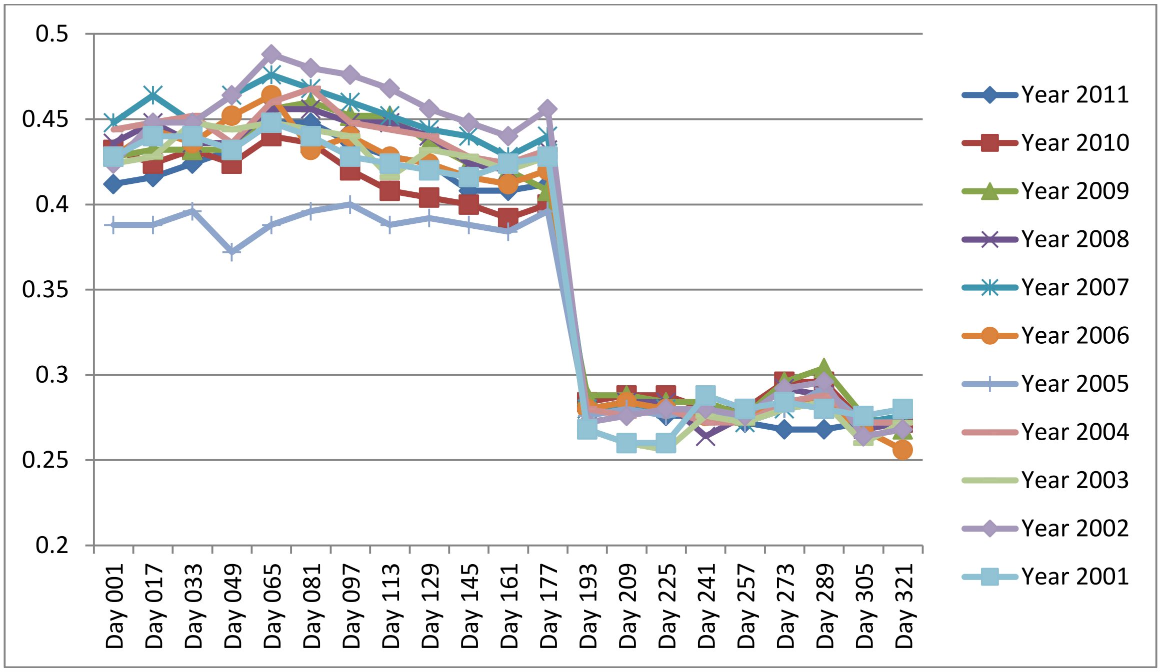

Figure 29 The inter-annual NDVI average for Nile Delta from years 2001 to 2011.

Subsection 4.3.2 Case study of the Great Lakes

Figure 30 displays how the NDVI average changes for the Great Lakes throughout each year, starting from duration of DOY 049 to 064, and ending at the duration of DOY 321 to 336. Overall speaking for an ordinary year, the NDVI climbs up fast till DOY 161 (the 16 day period ranges from early- to mid-June), then increases slowly until it peaks at DOY 209 (ranges from late July to early August); the NDVI value starts to decrease slowly until DOY 241 (ranges from late August to early September) and then climbs down sharply starting from DOY 257 (ranges from mid- to late September). NDVI curves of 2003 and 2010 start lower than other years at the beginning of the growing season, and instead of reaching a peak value at DOY 209, the NDVI curve of 2008 submerged to a locally minimum value, and also comparatively lower than that of all other years.

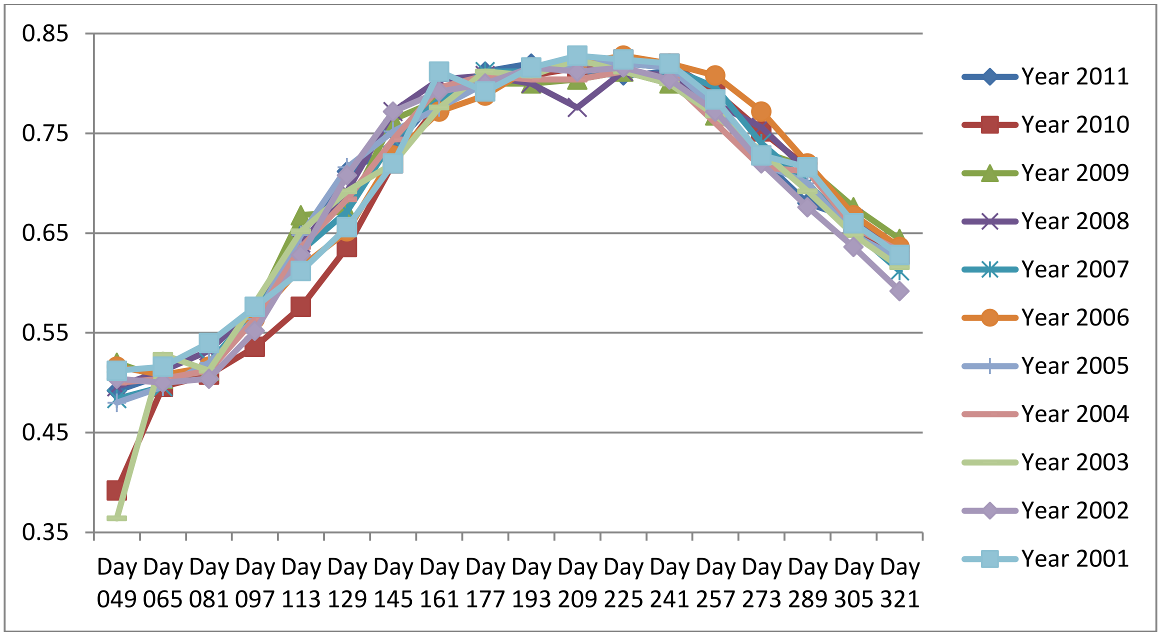

Figure 30 inter-annual NDVI average for the Great Lakes from years 2001 to 2011.

Subsection 4.3.3 Case study of Texas

Figure 31 displays how the NDVI average changes for Texas throughout the growing period each year (which is from DOY 049 to 321). Unlike the similar year-to-year NDVI trends shown in Figures 29 and 30, the yearly NDVI curves of Texas do not look alike, and this is largely due to the fact that Texas is large in size, and has heterogeneous climate divisions.

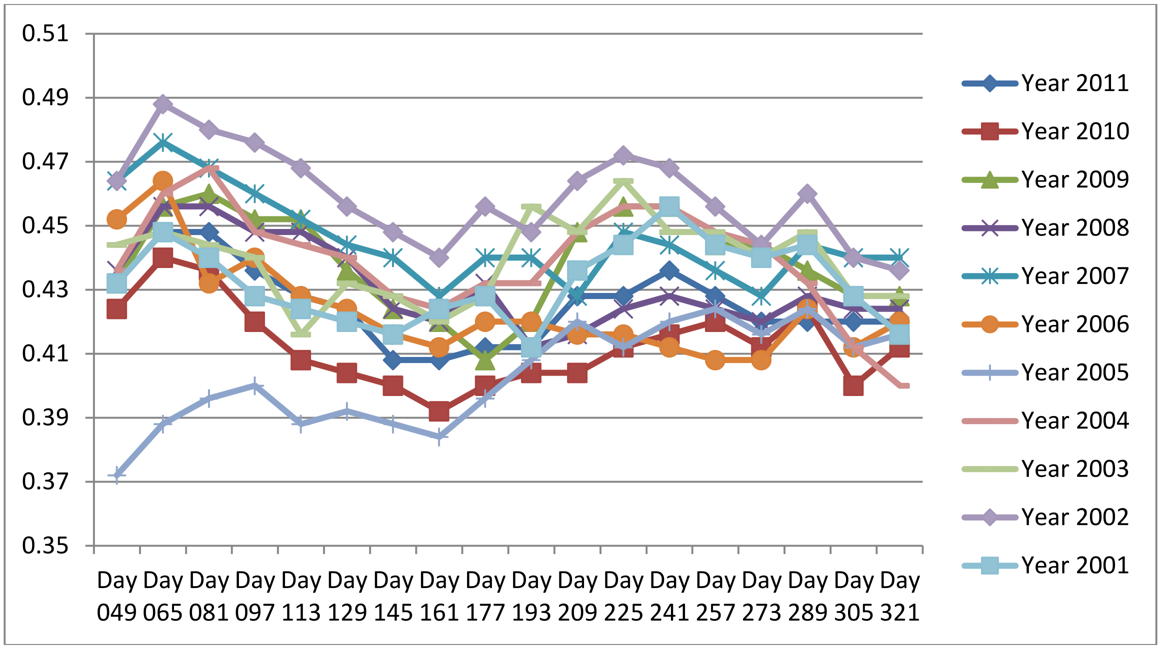

Figure 31 The inter-annual NDVI average for Texas from years 2001 to 2011.

Due to its large size, Texas's climate varies widely, from arid in the west to humid in the east. The National Climatic Data Center (NCDC) divides the state into 10 climate divisions (CDs): Northern Plains (CD#1), Low Rolling Plains, Cross Timbers, Piney Woods, Trans-Pecos Region (CD#5), Edwards Plateau, Post Oak Savanna, Gulf Coastal Plains, South Texas Plains, and Lower Rio Grande Valley. A climate division is a region within which similar characteristics such as vegetation, temperature, humidity, rainfall, and seasonal weather changes are shared. CD#1 and CD#5 in Texas are selected as our study areas here because they are 1) both vulnerable to drought and extreme water deficiency, 2) having clear sky for the majority of the days in growing season, and 3) having obvious wetter and drying months each year. The green area in Figure 32 represents CD#1 while the brown area signifies CD#5. Compared to CD#1 which is mostly continental steppe or semi-arid savanna, most areas of CD#5 are subtropical arid desert has higher temperature and lower precipitation all year long.

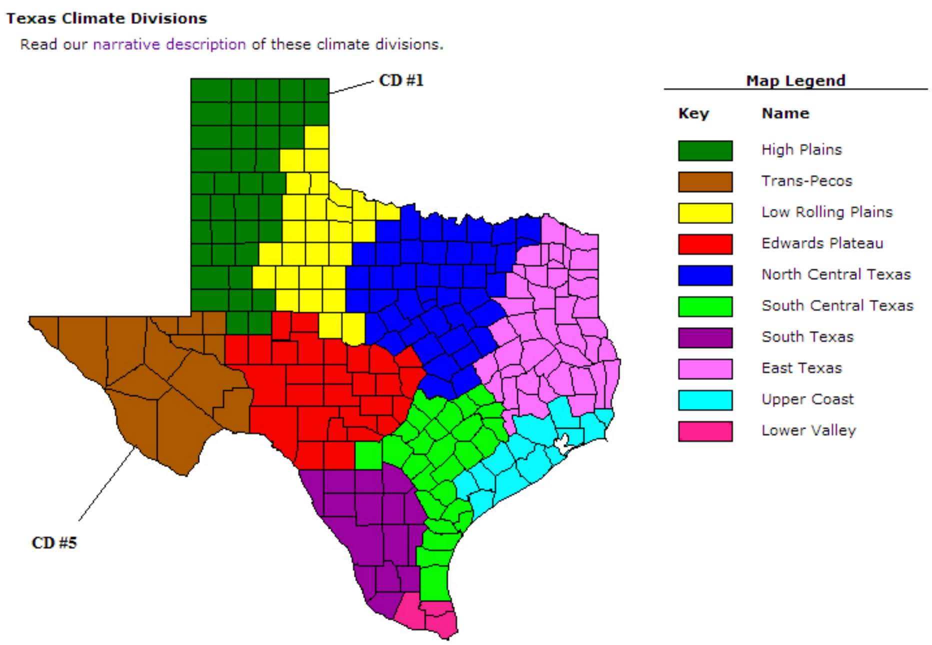

Figure 32 Climate divisions (CD) inside the state of Texas (http://www.nass.usda.gov/Statistics_by_State/Texas/Charts_&_Maps/cwmap.htm).

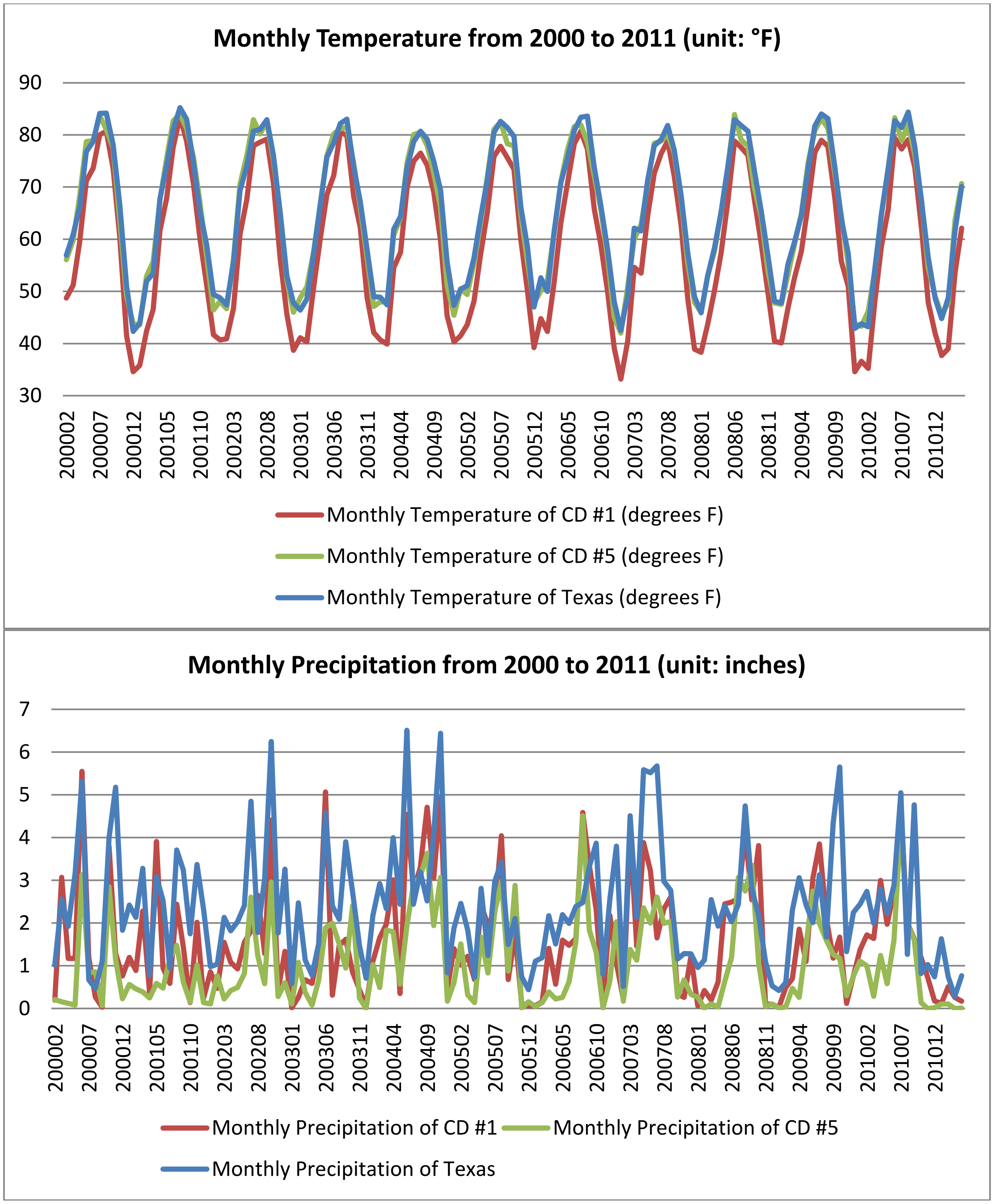

Figure 33 Monthly Temperature (upper panel) and Precipitation (bottom panel) for CD1, CD5 and Texas from 2000 to 2011 (source: NOAA NCDC).

Lack of precipitation and excess of temperature are two most significant causes of drought, and we can roughly pick out drought years based on the precipitation and temperature reports of the area. For example, during the year 2011, precipitation of the Texas state ranked #1 lowest among 13 years (2000-2012), while its temperature ranked #12 and second highest within years. Thus, the difference of the two rankings would be -11, lowest among all ranking differences, which indicates Texas is highly likely to be suffering from drought during year 2011.

Table 8 Yearly Precipitation and Temperature for Texas (source: NOAA NCDC).

Texas	Precipitation			Temperature			Precip - Temp
YearMonth-YearMonth	Value	Rank	Anomaly	Value	Rank	Anomaly	Rank Difference
200001 - 200012	28.28"	7	0.36"	66.4°F	0	1.4°F	-3
200101 - 200112	29.56"	10	1.64"	65.7°F	8	0.7°F	2
200201 - 200212	31.36"	11	3.44"	65.1°F	3	0.1°F	8
200301 - 200312	24.35"	3	-3.57"	65.5°F	6	0.5°F	-3
200401 - 200412	39.90"	13	11.98"	65.2°F	4	0.2°F	9
200501 - 200512	22.16"	2	-5.76"	65.8°F	9	0.8°F	-7
200601 - 200612	25.59"	6	-2.33"	67.0°F	1	2.0°F	-5
200701 - 200712	37.23"	12	9.31"	64.8°F	1	-0.2°F	11
200801 - 200812	24.80"	5	-3.12"	65.4°F	5	0.4°F	0
200901 - 200912	29.19"	9	1.27"	65.6°F	7	0.6°F	2
201001 - 201012	28.76"	8	0.84"	64.8°F	1	-0.2°F	7
201101 - 201112	15.18"	1	-12.74"	67.2°F	12	2.2°F	-11
201201 - 201212	24.56"	4	-3.36"	67.5°F	13	2.5°F	-9

Table 9 Yearly Precipitation and Temperature for CD#1 (source: NOAA NCDC).

CD#1	Precipitation			Temperature			Precip - Temp
YearMonth -	Value	Rank	Anomaly	Value	Rank	Anomaly	Rank

YearMonth							Difference
200001 - 200012	18.66"	8	-0.18"	59.7°F	9	1.4°F	-1
200101 - 200112	16.48"	4	-2.36"	59.8°F	10	1.5°F	-6
200201 - 200212	18.37"	7	-0.47"	58.7°F	3	0.4°F	4
200301 - 200312	12.77"	2	-6.07"	59.6°F	8	1.3°F	-6
200401 - 200412	31.87"	13	13.03"	58.6°F	2	0.3°F	11
200501 - 200512	17.62"	6	-1.22"	59.0°F	7	0.7°F	-1
200601 - 200612	19.57"	10	0.73"	60.2°F	11	1.9°F	-1
200701 - 200712	22.40"	11	3.56"	58.0°F	1	-0.3°F	10
200801 - 200812	19.50"	9	0.66"	58.8°F	4	0.5°F	5
200901 - 200912	16.94"	5	-1.90"	58.9°F	6	0.6°F	-1
201001 - 201012	22.78"	12	3.94"	58.8°F	4	0.5°F	8
201101 - 201112	8.14"	1	-10.70"	60.5°F	12	2.2°F	-11
201201 - 201212	13.65"	3	-5.19"	61.3°F	13	3.0°F	-10

Table 10 Yearly Precipitation and Temperature for CD#5 (source: NOAA NCDC).

CD#5	Precipitation			Temperature			Precip - Temp
YearMonth - YearMonth	Value	Rank	Anomaly	Value	Rank	Anomaly	Rank Difference
200001 - 200012	9.78"	3	-2.61"	65.9°F	10	2.2°F	-7
200101 - 200112	7.31"	2	-5.08"	65.8°F	9	2.1°F	-7
200201 - 200212	11.10"	4	-1.29"	65.1°F	7	1.4°F	-3
200301 - 200312	11.32"	5	-1.07"	65.6°F	8	1.9°F	-3
200401 - 200412	22.46"	13	10.07"	64.1°F	1	0.4°F	12
200501 - 200512	14.26"	11	1.87"	64.9°F	5	1.2°F	6
200601 - 200612	11.58"	7	-0.81"	66.1°F	11	2.4°F	-4
200701 - 200712	16.98"	12	4.59"	64.3°F	2	0.6°F	10
200801 - 200812	12.63"	9	0.24"	64.4°F	3	0.7°F	6
200901 - 200912	12.11"	8	-0.28"	65.0°F	6	1.3°F	2
201001 - 201012	13.96"	10	1.57"	64.4°F	3	0.7°F	7
201101 - 201112	3.94"	1	-8.45"	66.7°F	13	3.0°F	-12
201201 - 201212	11.58"	6	-0.81"	66.6°F	12	2.9°F	-6

Vegetation Condition Index (VCI) developed by Kogan (1995) is used in the following analysis as to reflect the extreme changes of the climate, and to roughly eliminate the spatial diversification of NDVI, and hence make the vegetation conditions between different regions comparable. Its definition is as below,

Equation 5 Vegetation Condition Index (VCI)

$$VCI = SCALE * \frac{NDVI - NDVImin}{NDVImax - NDVImin}$$

And here, in order to obtain *VCI* of a specific pixel for any year *YYYY*, and any day *DOY*, the parameters required for computation include *NDVI* (NDVI value of the same day YYYY/DOY), $NDVI_{max}$ (the maximum of all NDVI values in day *DOY* through all years), and $NDVI_{min}$ (the minimum of all NDVI values in day *DOY* through years) of the pixel. VCI is an indicator of “relative greenness”, a percentage value that expresses how green each pixel is in relation to the average greenness over the historical record for a pixel location at a given time (Peters & Walter-Shea, 2002).

The VCI time-series displayed in Figure 34 match accordingly the previous diagnoses from the ranking difference between precipitation and temperature. The VCI curve of Texas goes below 0.2 since 2011/113 and stay below for a long period of time (until 2011/321), indicating the vegetation vigor of such period is suppressed likely to be caused by drought.

The vegetation performance for CD#1, CD#5, together with the entire state of Texas will be studied in this section, and the results will be verified using Palmer Drought Severity Index (PDSI), as shown in Figure 35. For instance, for CD#1, VCI stays above 0.6 for a long period of time (from 2004/177 to 2005/273, i.e., June 25th, 2004 to September 29th, 2005), while its PDSI values are higher than 2.5 from August, 2004 to August, 2005. As for CD #5, VCI values are higher than 0.6 from 2004/225 to 2005/177 (i.e. August 12th, 2004 to June 25th, 2005) and the PDSI stays above 2.5 from August, 2004 to October, 2005. The drought patterns are detected in both VCI and PDSI curves, yet their duration does not match exactly.

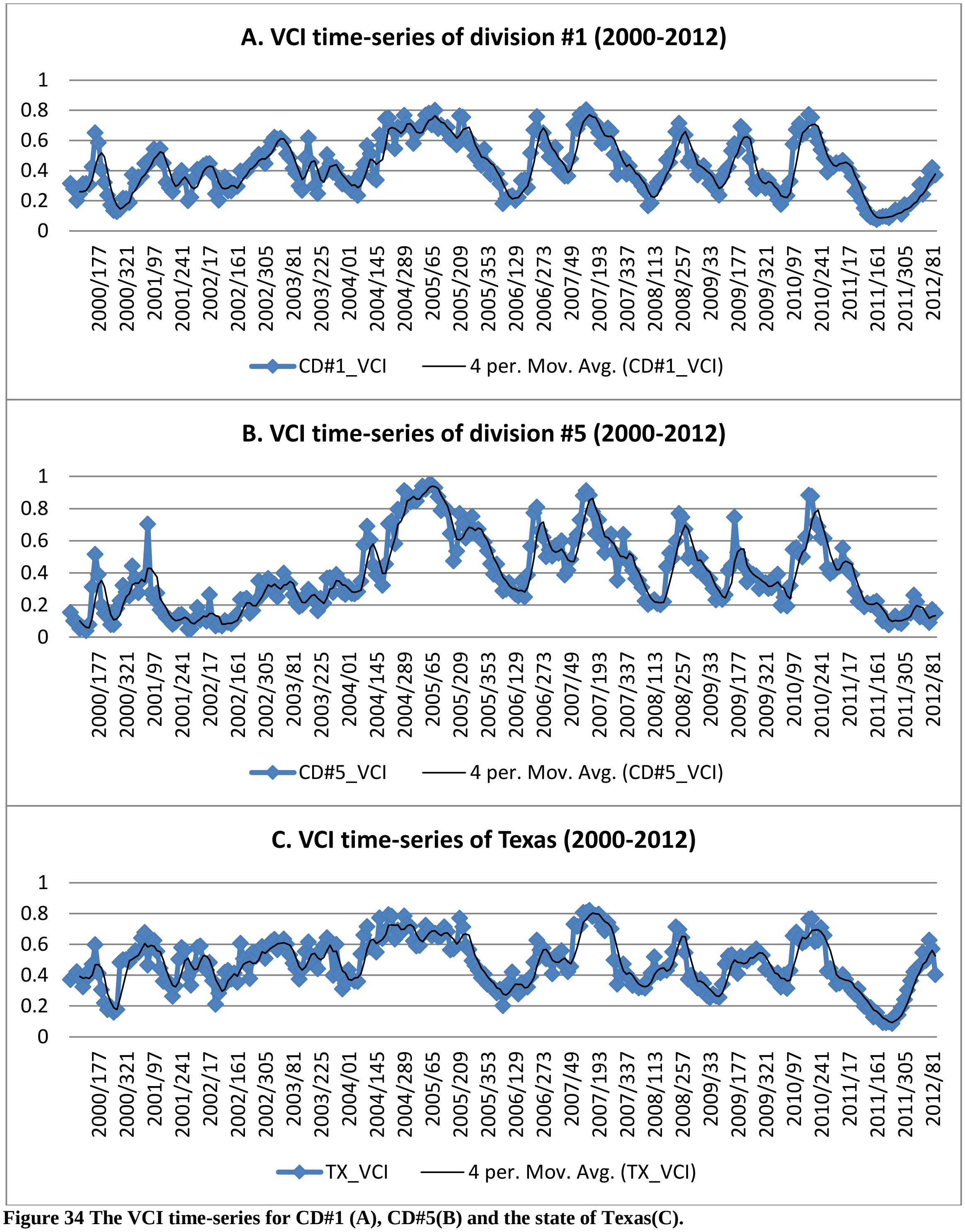

Figure 34 The VCI time-series for CD#1 (A), CD#5(B) and the state of Texas(C).

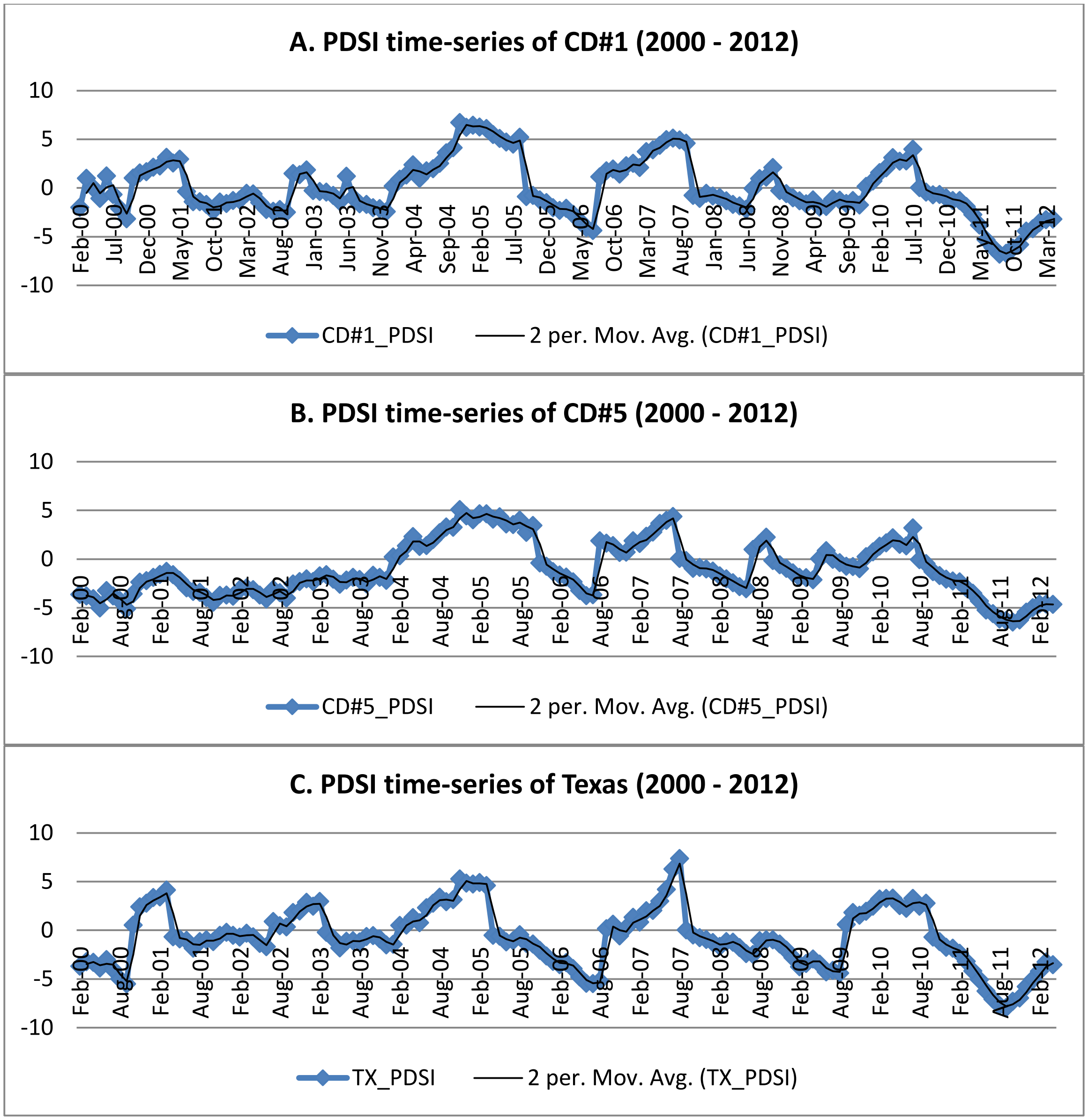

Figure 35 PDSI time-series of CD#1(A), CD#5(B), and the entire state of Texas(C).

Figure 36(A) displays the correlation between yearly VCI average and the 12-month PDSI for CD#1 from year 2000 to 2011. The PDSI values of year 2006 and 2011 are lower than -2, signaling moderate droughts or more severe. The VCI values of year 2000 and 2011 are lower than 0.32, which based on fixed threshold classification, indicates moderate drought or more severe for years 2000 and 2011. Using a linear regression model, the coefficient of correlation between PDSI and VCI for CD#1 is 0.839.

The correlation relationship, between yearly VCI average and the 12-month PDSI for CD#5 from year 2000 to 2011, is very obvious from Figure 36(B). The PDSI values are lower than -2 in years 2000 to 2003 and 2011, while the VCI values are lower than 0.32 in the exact same years. It is not surprising to find that the correlation coefficient for CD#5 is 0.978, indicating a very high positive correlation.

For the entire state of Texas, PDSI values are below -2 in years 2000, 2006, 2009 and 2011 while the VCI curve is lower than 0.32 only in year 2011, and the correlation coefficient for the area is 0.849. Thus, the correlation coefficients between VCI and PDSI are 0.978 (CD#5), 0.849 (TX), and 0.839 (CD#1). One of the reasons for CD#5 to have such a high correlation is its relatively vegetation composition – according to CropScape, there are 20 major crop types in CD#5, and shrubland is the most important of them all taking up 87% of all vegetated lands.

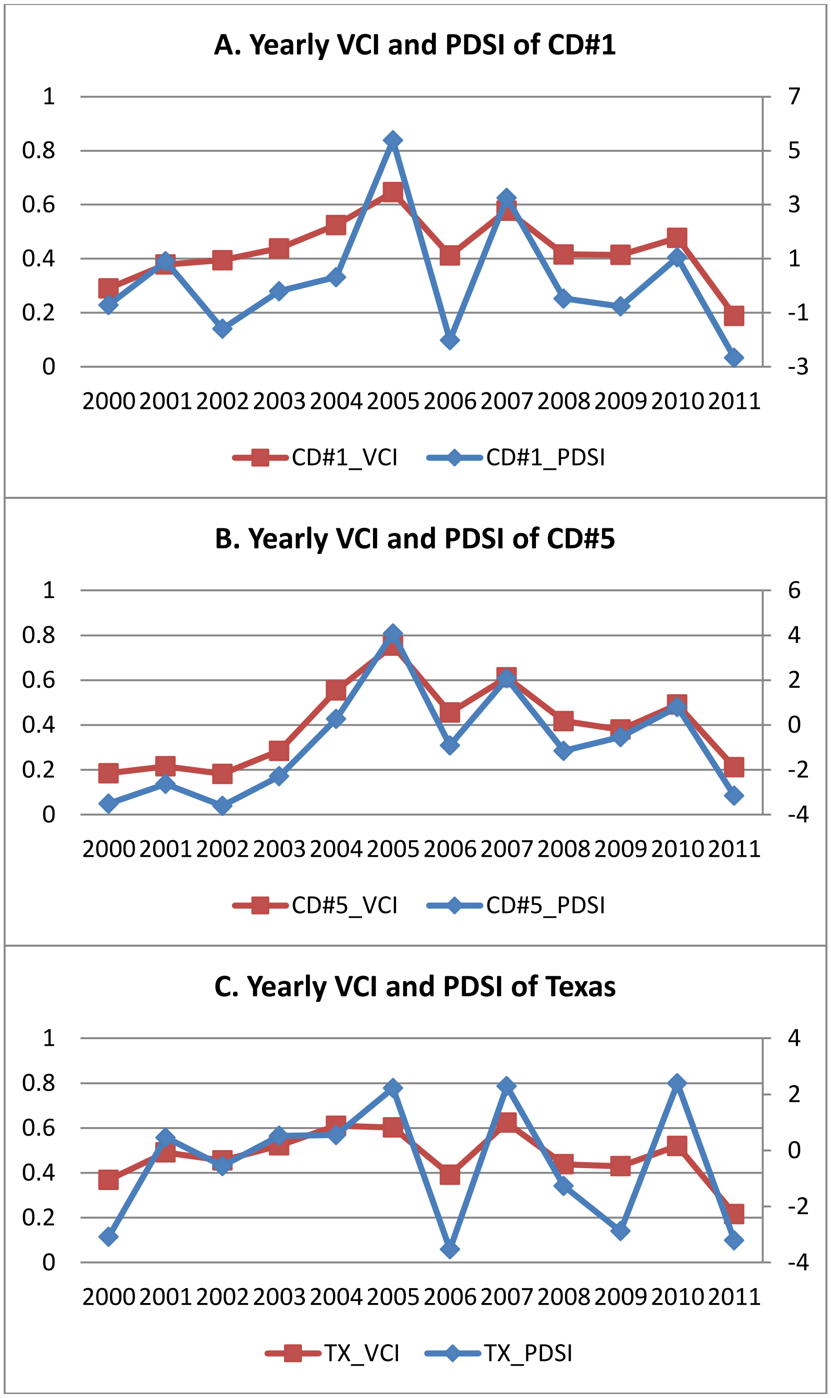

Figure 36 The yearly VCI and PDSI values for CD#1(A), CD#5(B) and Texas(C).

Because VCI of year *YYYY* is in fact a relative measure of NDVI of year *YYYY* compared to the maximum and minimum NDVIs of a valid range of time, if the NDVI datasets consist of only a small number of years, then the resulting VCI can be biased. If the maximum and minimum NDVI values of the area within the short list of years reside solely on part of the real historic NDVI range, then the VCI calculated using the former can be of no meaning in indicating drought or non-drought. Since the NDVI calculated from MODIS datasets can only be traced back to year 2000, with such a short list of years the VCI values tend to be biased. For instance, row (1) of Figure 37 represents a non-biased VCI calculated with minimum and maximum NDVI values of 30 years of historic data, and rows (2) and (3) represent biased VCI calculated from a short list of NDVI data. When the NDVI values of the studied years are higher than the 30-year average (as shown in row 2), a low VCI value being calculated does not necessarily mean vegetation depression. Vice versa, when the maximum NDVI is lower than 30-year maximum, a high VCI value calculated this way may not indicate high vegetation vigor in real applications.

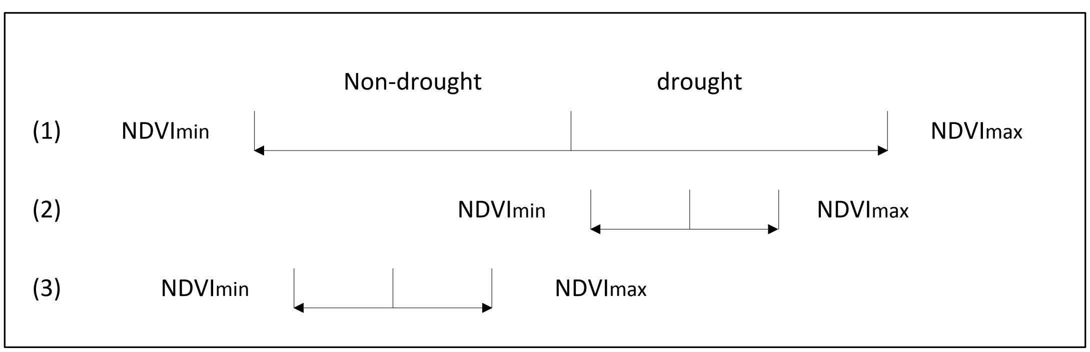

Figure 37 Non-biased VCI (row 1) and the biased VCI (rows 2 &3).

VCI performance has a high correlation to the crop yield – usually high VCI values for the year indicate promising crop yield. From Figure 36(C), we can find the year with the highest yearly average – 2007, within the 2001 to 2010 time periods, which is also the year with the highest cotton yield from both harvested and planted areas as shown in Figure 38.

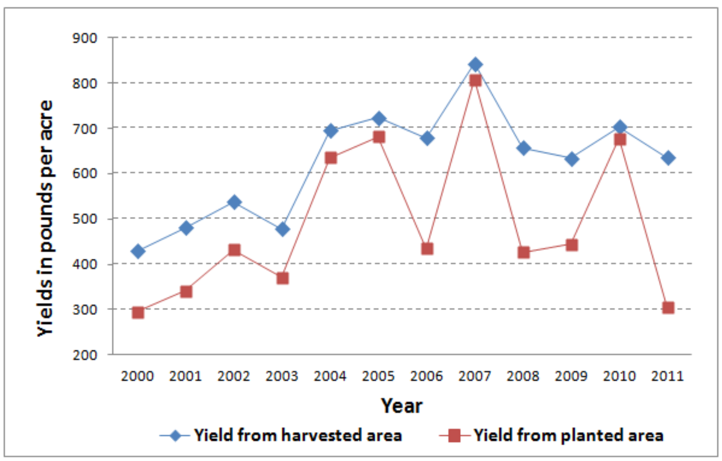

Figure 38 Yearly cotton yields for the state of Texas from 2000 to 2011.

Subsection 4.3.4 Case study of SW China

The severe drought of 2010 for southwestern China affected more than 600 million people and ruined billions of dollars worth of crops. Due to crop failure on 3.1 million hectares of arable land, 9 million people face a grain and water shortage. Centering on southeastern Yunnan, this drought affected 125 of 129 counties of the province. For some regions, it is the worst drought in a century. The loss from agricultural production cost 20 billion RMB, and rice price increased from $0.225/lb to $0.375/lb. From September 2009, the drought had made its debut in some areas of

Yunnan, Guizhou, and Guangxi provinces. Since Oct. 2009, large areas of the south west provinces – Yunnan, Sichuan, Guizhou and Guangxi had been experiencing droughts of levels D2 to D4 for almost 6 months. During this period, the number of days Yunnan endured droughts of levels of D3 to D4 is at an average of 84 days, and that of Guizhou is at an average of 50 days – both are at the record high of history (BBC News, 2010).

The 2010 drought is different from other droughts not only in the long duration of its developing and ending, but also in its widespread range of affected areas, huge impact to people's life and agricultural yields and other socio-economic factors. In Jan. 2010, up to 85% of all the counties in Yunnan Province had been experiencing droughts of levels D3 to D4. Until Mar. 2010, 81% of counties in Guizhou were under D3-D4 leveled drought. There was a great lack of drinkable water for citizens, and water to feed stock animals or irrigate crops. The yields from agricultural products (e.g. sugar cane) had decreased sharply. Also this spring drought had a lasting effect to cause the winter wheat to drop its production.

The Lancang River in China flows southward to become the Mekong River in the downstream countries – Thailand, Vietnam, Myanmar, Laos and Cambodia. During the same period when southwestern China was suffering from severe drought, farmers and fishermen in the downstream countries were battling with water to keep their crops and fisheries alive. Half of the 76 provinces in Thailand faced severe drought, especially the north and northeast partitions. Over 4 million people were affected by the drought and nearly 20 thousand hectares of lands were due to reduce production. Rice produced from the Mekong River basin had taken up nearly 40% of the total market share in the world.

The 2010 drought had a severe impact on the growth of rice in these regions, and the rice production dropped sharply which in turn resulted in a great economic loss for these countries.

There has been scientific evidence that low rainfall was responsible for the plunging levels of the river and hence the devastating agricultural drought in the southwest China. Developing countries, with agriculture being their backbone properties, are very much dependent on the seasonal rainfall and climatic conditions and hence more vulnerable to droughts. According to the statistics provided by USDA, up to year 2004, more than 500 million people live in the drought-prone areas of the world and 30% of the continental surfaces are affected by droughts or desertification processes (Murthy & Sasha, 2008). The substantial reduction of forest cover in many areas might be another reason of this drought. Other likely causes to drought include El Nino effect, intensive water consumption by industry and household usage, pollution and waste in natural lakes and reservoirs, and energy production from coal, etc. (Asian Sustainability Ratings, 2010)

An agricultural drought can be caused by a meteorological drought event. A meteorological drought can develop quickly and end abruptly since after all it is a due to the absence or reduction of precipitation – a result of atmospheric conditions which could literally change overnight. In an agricultural drought, the surface layers (or the root zone) are suffering from short-term dryness (i.e. for a few weeks) during the growing season, even though the deeper soil levels may be saturated. Thus, the onset of an agricultural drought may lag that of a meteorological drought, depending on the prior moisture status of the surface soil layers (Heim, 2002). The immediate impact of drought is on crop area, crop production, and farm employment. Speculation of poor farm harvest drives food prices upwards. Shortage of drinking water and starvation of food are later to emerge.

4.3.4.1Study area

Three adjacent provinces Yunnan, Guizhou, and Sichuan and the city of Chongqin have been selected to form the study area (shown in Figure 39). These areas had experienced devastating drought situations in year 2010, and this study demonstrates how vegetation indices can be used to reflect drought severities and evolutions in the area.

Figure 39 The study area compositing of Yunnan, Guizhou, Sichuan, and the city of Chongqin.

4.3.4.2 Analysis of 2010 SW China Drought

The left and right plots of Figure 40 show the severity degrees of agricultural drought affecting China, on 04/17/2010 and 05/12/2010, respectively. The red areas are those suffering from severe drought, orange areas are suffering from medium-leveled drought, yellow areas are prone to light droughts, and green areas are without any drought conditions. We can see that the northeast of Yunnan and adjacent areas located in Sichuan and Guizhou were suffering from severe drought during April 17, 2010 to May 12, 2010, and the impact area had been shrinking during this time period. (CRAN, 2010)

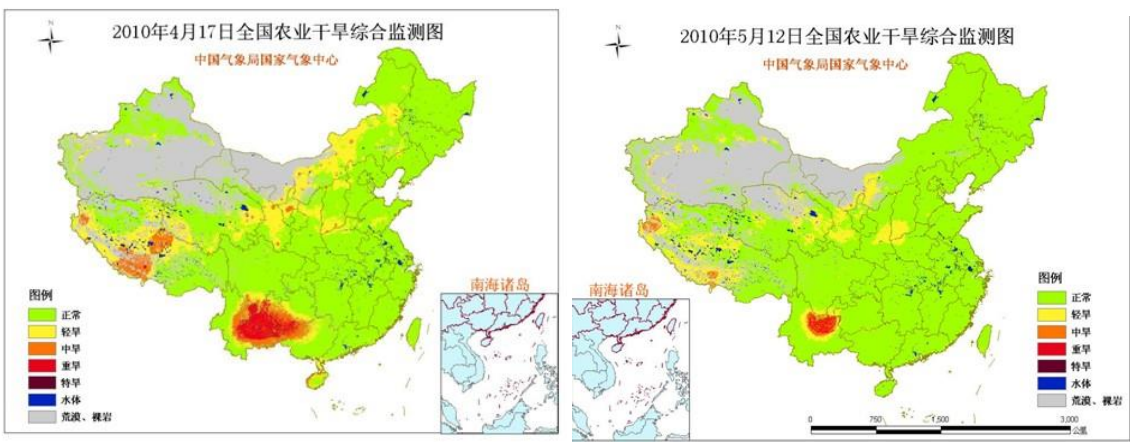

Figure 40 The Severity Degrees of Agricultural Drought for China, 04/17/2010 (left) and 05/12/2010 (right) (Source: CMA).

The left and right plots of Figure 41 display the NDVI layer on top of the satellite basemap in Google Earth, of two 8-day periods 05/01/2009 – 05/08/2009, and 05/01/2010 – 05/08/2010, respectively, while plots in Figure 41 are VCI layers for the same 8-day periods. Comparing the VCI maps for the same period during May, 2009 and 2010, we can see for most part of the Yunnan-Guizhou-Sichuan area, the VCI values are higher in the former, indicating a less idealistic picture for the vegetation growth in 2010 – since the color of blue represents a fairly well or normal vegetation growth condition, while red means that the vegetation in the area are suffering from the stress of wilting. On the right of Figure 42, vegetation growth in most part of Yunnan and Sichuan provinces is worse than previous year, and as shown the situation is especially not optimistic for the bordering areas between Yunnan and Sichuan, and between Yunnan and Guizhou.

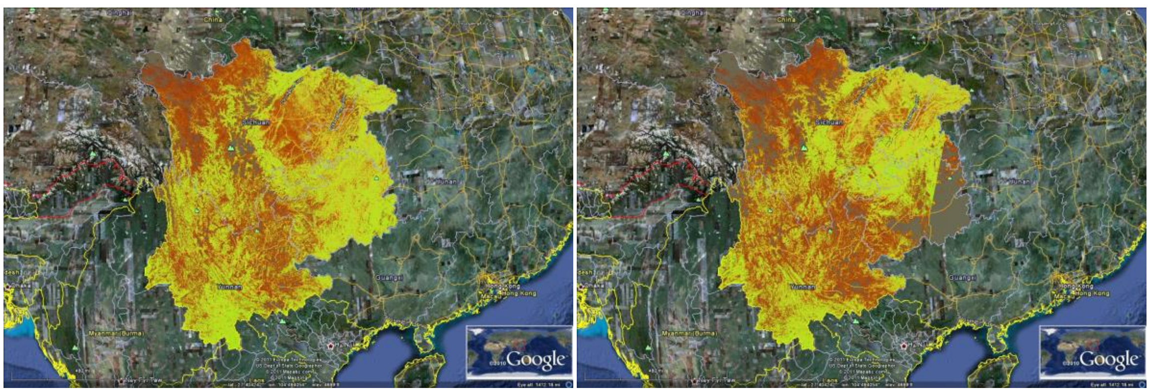

Figure 41 NDVI maps of the three provinces (Yunnan, Guizhou, and Sichuan) for the eight days periods (left) 05/01/2009 – 05/08/2009, and (right) 05/01/2010 – 05/08/2010.

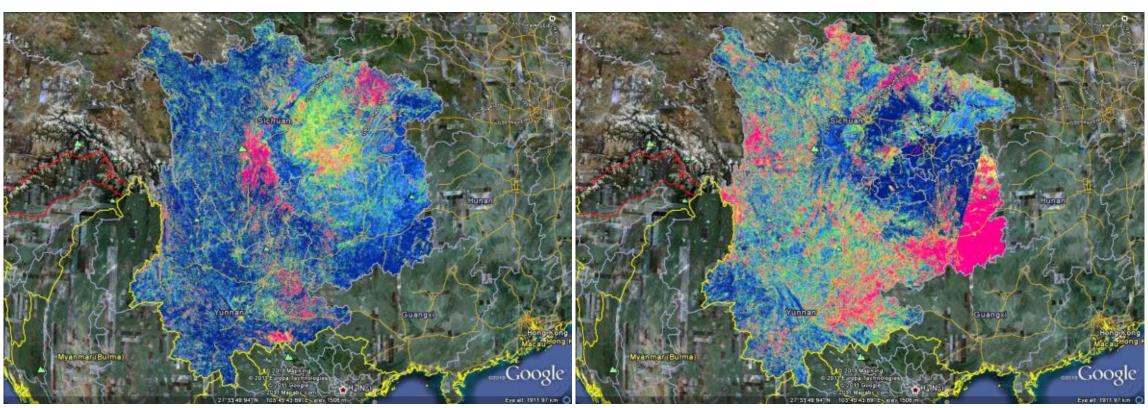

Figure 42 VCI maps of the three provinces (Yunnan, Guizhou, and Sichuan) for the eight days period (left) (left) 05/01/2009 – 05/08/2009, and (right) 05/01/2010 – 05/08/2010.

As shown in Figures 43 and 44, the day- and night-time TCI maps of the area have shown the majority of the eastside are under thermal stress for May 2009, and only a small strip of the area is influenced by high temperature. This is irreconcilable to the ground truth, possibly due to the fact that the NDVI and VCI represent the accumulating drought impact upon vegetation while the TCI is solely a modest display of current temperature. Though the Yunnan-Guizhou-Sichuan area was suffering from severe drought in May 2010, with temperature dropping back to normal, the drought impact to the area would not be found in TCI maps. Also, even though the soil moisture level for the region was much lower than historic average, an immediate rainfall to the drought prone area will move the TCI value back to the normal level overnight, and thus TCI alone cannot serve as a drought indicator.

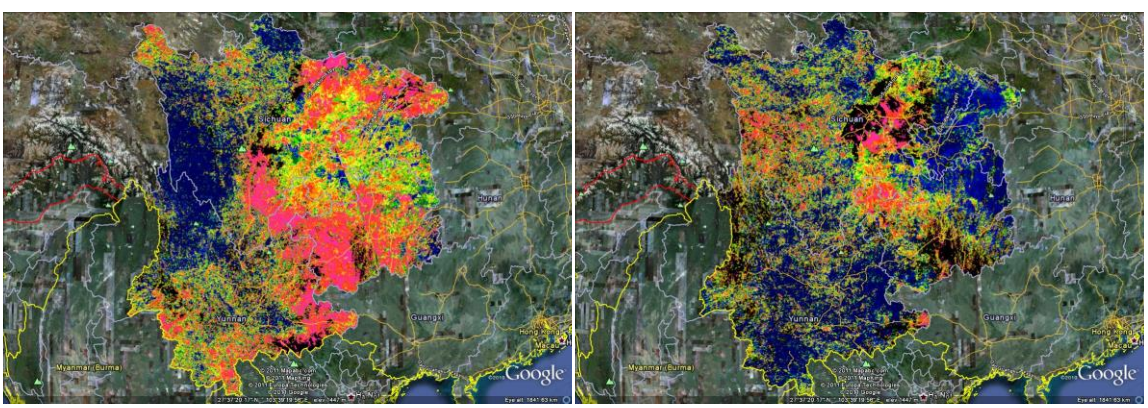

Figure 43 Day-time TCI maps of the three provinces (Yunnan, Guizhou, and Sichuan) for the eight days period 05/01/2009 – 05/08/2009, and (right) 05/01/2010 – 05/08/2010.

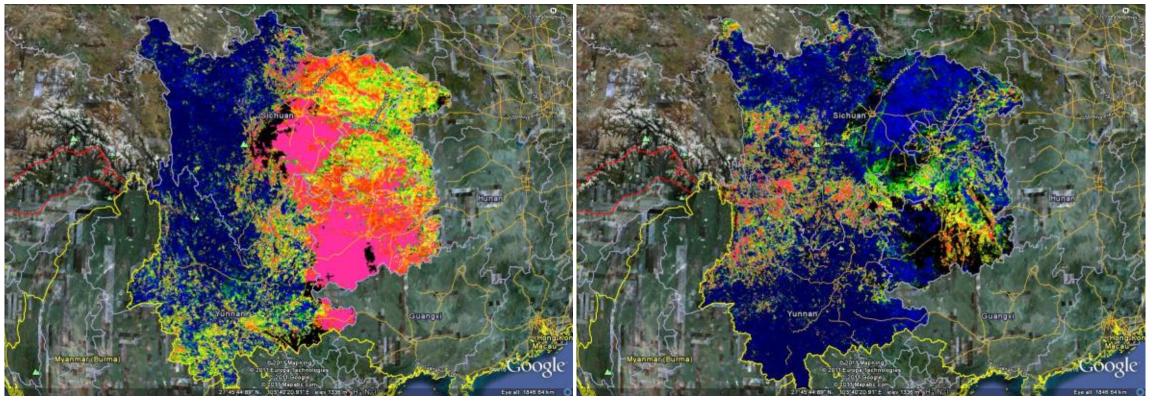

Figure 44 Night-time TCI maps of the three provinces (Yunnan, Guizhou, and Sichuan) for the eight days period 05/01/2009 – 05/08/2009, and (right) 05/01/2010 – 05/08/2010.

In summary, the NDVI and VCI are direct indicators of vegetation conditions, displaying the accumulating influences of climates upon vegetations. In the case of SW China drought, the correlations between NDVI, VCI and agricultural drought, respectively, are significant. However, TCI is less relevant to drought, since TCI can be greatly changed within one day due to some extreme weathers while drought is more about accumulating effects.

Section 4.4 Summary

This chapter aims to prove that the temporal response and spatial pattern of vegetation to climate fluctuations can be reflected in NDVI/VCI changes. For the entire globe, comparisons of yearly NDVI average values tell us in which year the global vegetation as a whole is under stress and thus crop/pasture yields decrease and food price increases. For different latitudes, the “normal” NDVI value differs; as latitude decreases (approaching the equator), the year-long NDVI average increases, which is to say, vegetation greenness increases from high latitudes to low latitudes. Also, the inter-annual change of NDVI/VCI is a reflection of the climate pattern of an area. The VI time-series of a climate zone is correlated to the precipitation and temperature parameters. The anomalies from “normal” VI time-series can possibly be due to a drought or flood event. However, it is often difficult to deduct what is the main cause for the VI anomalies. Chapter 6 provides a better interpretation to the outliners.

CHAPTER 5 RELATIONSHIP BETWEEN REMOTE SENSING BASED AGRICULTURAL DROUGHT INDICATORS AND ROOT ZONE SOIL MOISTURE

Section 5.1 Introduction

For more than 30 years, VI derived from RS-based measurements has been widely applied to monitor land surface vegetation, and indirectly infer root zone soil moisture and agricultural drought conditions. Compared with meteorological or hydrological measurements collected from scattered observation stations, these RS-based VIs provide spatially and temporally continuous monitoring to vegetation greenness, soil moisture levels and the occurrence/severities of drought for the entire globe. For example, NDVI, VCI and VHI are often used for these purposes.

Despite the popularity of using NDVI in monitoring global vegetation phenology, primary productivity, and drought condition, NDVI has many limitations. For instance, it is insufficient to characterize vegetation and drought conditions due to an apparent time lag between precipitation and NDVI responses, effects from the soil background, atmospheric attenuation, and asymptotic saturation over areas with moderate-to-high density of vegetation (Di et al., 1994; Huete et al., 1985; Kaufman & Tanré, 1992; Gitelson, 2004). Thus a number of new indices have also been developed for monitoring vegetation condition and/or drought. For example, NDWI (Gao, 1996) is calculated as the differences between the NIR and SWIR reflectance. The SWIR reflectance shows changes in both the vegetation water content and the spongy mesophyll structure in vegetation canopies, while the NIR reflectance is affected by leaf internal structure and leaf dry matter content but not by water content. The combination of the NIR with the SWIR removes variations induced by leaf internal structure and leaf dry matter content, improving the accuracy in retrieving the vegetation water content. NDWI is thus a good indicator for vegetation liquid water. Moreover, it is less sensitive to atmospheric scattering effects than NDVI. Comparing NDWI of the current state with that of previous reference year, or plotting the time series of NDWI through the years, is able to show the evidence of water availability, water stress, or drought condition. Another example, Enhanced Vegetation Index (EVI) (Huete at al., 2002) makes use of measurements in the blue, red and NIR bands -- EVI is a more sensitive indicator to vegetation responses since the visible blue band is also included to allow for an extra correction of aerosol scattering. Besides, EVI does not saturate as easily as NDVI, and thus performs better over high biomass areas. NDDI, as a result of division between the difference of NDVI and NDWI and the sum of them, can be used to describe drought intensity of an area (Gu et al., 2007). NDDI is believed to have a stronger response to drought situations than VCI (which is based on NDVI only) or NDWI used alone. Whether or not the NDDI has a stronger response to root zone soil moisture at depths under various canopies will be discussed in this chapter as well. However, NDWI, EVI and NDDI have their limitations. Though bearing less sensitivity to atmospheric effects than NDVI, these indices cannot remove completely the background soil reflectance effects. The RS-based VIs may raise false alarms to agricultural drought due to the limitations and problems associated with them, e.g., a reducing NDVI value can also be due to flood, bad weather, fire, pesticides, and/or other factors in addition to drought. Thus, investigations about how those RS-based indicators work under different conditions (e.g., weather, biophysical environments and land-cover types) and validation of the RS-based agricultural drought indicators with ground-station observations are very important. However, so far no (or little) such study has been performed.

This chapter aims to fill some gaps of the current researches by studying the relationships between those RS-based agricultural drought indicators (including NDVI, NDWI, EVI and NDDI) and root zone soil moistures at different cropland layers. As a key factor that influences the interactions among soil, vegetation, and atmosphere, soil moisture plays an important role in surface energy balances, vegetation productivity, and the occurrences/severities of drought/flooding (Shukla & Mintz, 1982; Goward et al., 2002). Soil moisture, particularly at the root zone, can substantially influence vegetation health and surface energy balance through the process of transpiration. Soil moisture measurements are conventionally collected from in situ sensors at discreet stations, and the results do not account for local scale variation in soil properties, terrain, and vegetation cover. In order to characterize the spatial heterogeneity of soil moisture over extended geographic areas, spatial extrapolation of these isolated measurements is performed, and usually causes large uncertainties. Constructing a dense network of observation points is overly expensive, and thus will not be a good solution. Remote-sensing techniques have successfully supplemented data from ground-based sensors to retrieve spatially integrated information on soil moisture over large area with varying soil and land-cover conditions. The research hypotheses to be tested in this chapter include,

(1) Null hypothesis: The trends in time-series of soil moisture and in that of vegetation greenness do not relate to each other; (2) Null hypothesis: There is no significant correlation between VIs and soil moisture; (3) Null hypothesis: There is no significant correlation between VIs and soil moisture with lag periods; (4) Null hypothesis: Correlation between VIs and soil moisture is not influenced by cover type and soil texture across an area.

In addition, there is an increasing demand on managing and mitigating the drought condition of different crop species with a persistent and timely monitoring method for every major crop grown on various regions throughout the crop's growing cycle. This work will provide an experimental study on the effect of drought on crop fields in the U. S. Corn Belt. Remotely sensed data of vegetation dynamics and soil moisture content, in particular NDVI, NDWI, EVI, and NDDI time series from 2005 to 2011, derived from MODIS datasets are used for the study. The potential of proximally sensed VIs simulated to the band passes of contemporary space-borne sensors (e.g. MODIS) in characterizing soil moisture at variable depths within the root zones of corn and soybean will be evaluated. This work will help to answer many concerned questions, such as, which VI can serve as a better agricultural drought indicator for a specific cropland type under specified environmental conditions, what the confidence level is to use an agricultural drought indicator in a local area or globally, and how to reduce the uncertainties and improve the reliability in drought monitoring, analysis and prediction.

Section 5.2 Methodology

Agricultural drought is described as reduced root-zone soil moisture and crop yields (Gu et al., 2007). The proposed approach here is to find out the optimized drought indicator among NDVI, NDWI, EVI and NDDI which best correlates with soil moisture observations consists of four major steps of work: (a) use GDD to determine crop growing stage, (b) calculate agricultural drought indicators, align them neatly along the GDD axis, and scale them separately based on maximum and minimum values, (c) adopt a bivariate regression model upon time-series VI and the station-based soil moisture data at various depths, and (d) obtain the correlation coefficient of VIs versus the time lagged soil moisture data at various depths. Some details of these procedures will be given in the following.

Subsection 5.2.1 Bivariate Linear Regression Model for Evaluation

Agricultural drought indicators should reflect the reduced level of root-zone soil moisture. It is straightforward to assess the performance of RS-based drought indices (by drought impact category) with observed soil moisture levels, particularly at the root-zone. Experiments done so far indicate that all VIs exhibited a linear monotonic association with soil moisture observations. In this chapter, the evaluation of Vegetation Indices (VIs) as agricultural drought indicators uses bivariate least square regression model through Equation 6.

Equation 6 The bivariate least square regression model used to simulate soil moisture using VI.

$$Y = X\beta + \varepsilon$$

, where Y is an N by 1 vector of observed soil moisture from a particular soil depth, X is an N by 2 matrix composed of 1 and VI, β is a regression function vector calculated from X and Y, and ε is the random error component. The correlation coefficient R^2 is used to validate the model – a large R^2 can guarantee a better performance of estimation.

Relationships between root zone soil moisture at five depths and corn/soybean VIs are evaluated using the correlation coefficient. VI observations are correlated with the concurrent soil moisture values. In order to evaluate the effect of antecedent soil moisture on the canopy reflectance signals, soil moistures lags up to 64 days are also correlated with VIs.

Subsection 5.2.2 Remotely Sensed Drought Indices

In addition to NDVI, NDWI, and NDDI which have been mentioned in previous sections, another RS-based indicator, EVI is also used in this study. Believed to be a better indicator for vegetation conditions than NDVI, EVI is calculated as

Equation 7 Calculation of EVI (Huete et al., 2002)

$$EVI = SCALE * \frac{R_{NIR} - R_{RED}}{R_{NIR} + C1 * R_{RED} - C2 * R_{BLUE} + L}$$

In the equation, R_{NIR}, R_{RED}, and R_{BLUE}, are atmospherically-corrected (partially or fully) surface reflectance, and $C1$, $C2$, and L are coefficients to correct for atmospheric condition (i.e., aerosol resistance). For the standard EVI data derived from MODIS product, SCALE=2.5, L=1, C1=6, and C2=7.5.

Section 5.3 Study Area and Data

Iowa has been selected as the study area since its yearly productions in corn and soybeans top other states (contributing 18% of corn productions for the U. S.). Almost all corn fields in Iowa are rain-fed rather than irrigated (Duvick & Cassman, 1999). The study site is located at 42.1°N, 93.85°W, approximately 16 miles northwest of Ames, Iowa, with a typical crop-rotation pattern of corn and soybean alternatively.

Different crops have different growing patterns even they are planted in the same soil and climate system. In order to investigate how crops respond to agricultural drought stress, a crop mask needs to be applied first to the selected study data and separate the images into several crop layers (depending on how many crops the research is concerned). The CropScape CDL is hosting the cultivated crop mask data at a 30m or 51m spatial resolution with the coverage over the continental United States. Applying the crop mask generated from the CDL downloads, the crop type for the site varies by each year. This study is undertaken using data acquired during 2006, 2008, 2009, and 2011 growing seasons when the field was under corn cover, and during 2005, 2007 and 2010 growing seasons when the field was planted with soybeans (Table 11).

Table 11 The crop rotation patterns for the study site (SCAN site #2031) from year 2005 to year 2011.

Year	2005	2006	2007	2008	2009	2010	2011
Crop	Soybeans	Corn	Soybeans	Corn	Corn	Soybeans	Corn

This area experiences a humid continental climate (Dfa), with warm to hot summers, and cold to severely cold winters. The soil type varies significantly even for a small area surrounding the observation station (Table 12, Figure 45). The observation station is located in the center of the Figure 45, classified as soil type 507 (Canisteo Silty Clay Loam (with 0 to 2% slope)). Only a few meters away from the station, soil types of 138B and 55 are spotted as well, namely, Clarion and Nicollet Loam respectively.

Table 12 Top three soil types for the neighborhood of the study site.

Map Unit Symbol	Map Unit Name	Percentage
507	Canisteo Silty Clay (0~2% slope)	34.6
138B	Clarion Loam, 2~5% slope	24.0
55	Nicollet Loam, 1~3% slope	19.8

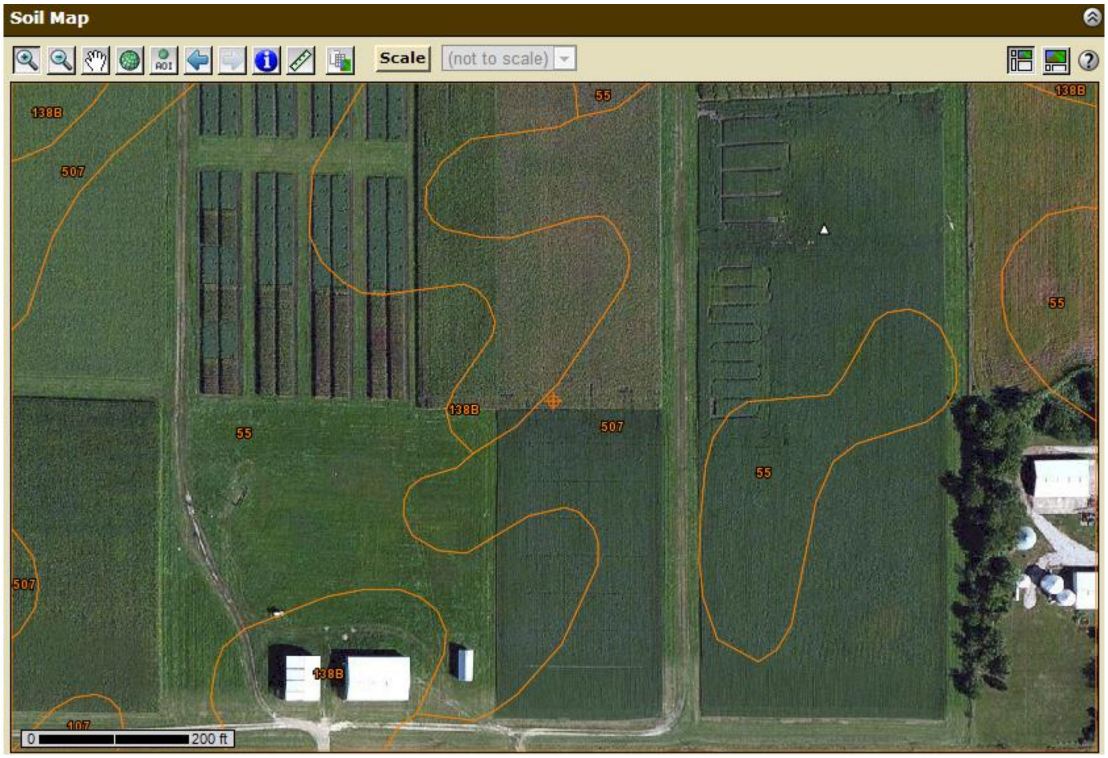

Figure 45 Soil Type Classification map for the neighborhood near SCAN site #2031, in which soil types 507, 138B and 55 are shown in contours. (Source: http://websoilsurvey.nrcs.usda.gov/app/WebSoilSurvey.aspx)

The soil moisture (a.k.a. volumetric water content) levels were measured hourly at five depths (2, 4, 8, 20 and 40 inches, i.e. 5, 10, 20, 50, and 100cm), and averaged to generate daily values for each of the depths. The soil moisture and precipitation data were collected by the Soil Climate Analysis Network (SCAN) supported by National Water and Climate Center (NWCC). The temperature parameters collected by SCAN are used to calculate the GDD for the crops growing at the fields. The soil moisture parameters recorded are used for validation and analysis of correlations with vegetation indices. Parameters collected by SCAN that are used in this study are shown in Table 13, and Box 4 describes the essential information of SCAN site #2031 located within Ames, IA.

Table 13 Soil moisture and temperature parameters collected by SCAN (source: SCAN Website).

Label	Element	Unit	Instrument*	Ecode	Function Interval	Ordinal	Sensor Height
SMS.I-1:-2	Soil Moisture Percent	Pct	Hydraprobe Analog (2.5 Volt) - 1 Of 4	SMS	Instantaneous	1	-2"
SMS.I-1:-4	Soil Moisture Percent	Pct	Hydraprobe Analog (2.5 Volt) - 1 Of 4	SMS	Instantaneous	1	-4"
SMS.I-1:-8	Soil Moisture Percent	Pct	Hydraprobe Analog (2.5 Volt) - 1 Of 4	SMS	Instantaneous	1	-8"
SMS.I-1:-20	Soil Moisture Percent	Pct	Hydraprobe Analog (2.5 Volt) - 1 Of 4	SMS	Instantaneous	1	-20"
SMS.I-1:-40	Soil Moisture Percent	Pct	Hydraprobe Analog (2.5 Volt) - 1 Of 4	SMS	Instantaneous	1	-40"
STO.I-1:-2	Soil Temperature Observed	Degc	Hydraprobe Analog (2.5 Volt) - 1 Of 4	STO	Instantaneous	1	-2"
STO.I-1:-4	Soil Temperature Observed	Degc	Hydraprobe Analog (2.5 Volt) - 1 Of 4	STO	Instantaneous	1	-4"
STO.I-1:-8	Soil Temperature Observed	Degc	Hydraprobe Analog (2.5 Volt) - 1 Of 4	STO	Instantaneous	1	-8"
STO.I-1:-20	Soil Temperature Observed	Degc	Hydraprobe Analog (2.5 Volt) - 1 Of 4	STO	Instantaneous	1	-20"
STO.I-1:-40	Soil Temperature Observed	Degc	Hydraprobe Analog (2.5 Volt) - 1 Of 4	STO	Instantaneous	1	-40"

Box 4.

SCAN Site: Ames
State: Iowa
Site Number: 2031
Latitude: 42 deg; 1 min N
Longitude: 93 deg; 44 min W
Elevation: 1073 feet
Reporting since: 2001-09-19

Two types of MODIS products, MOD13Q1 and MOD09A1, are used to study the agricultural drought occurred in the selected study area during the growing period each year. The MOD13Q1 is a level-3 product. Among 11 scientific datasets (SDS) of this product, 16-day composite NDVI, EVI, VI quality assurance bit fields, and view zenith angle bands are utilized for the study. The NDVI or EVI is encoded in 16-bit signed integer, ranging from -2000 to 10000. As a result, these NDVI and EVI values stored in the MOD13Q1 products should be divided by 10000 to obtain its original range from -0.2 to 1. Different from NDVI or EVI, NDWI is not a standard MODIS product, and cannot be simply derived from existing HDF datasets. Instead, the NDWI is calculated using the reflectance data (bands 2, and 6) from MOD09A1, which is an 8-day gridded level-3 product estimating surface spectral reflectance at a 500-m resolution in the sinusoidal projection (as shown in Equation 3).

The data used are within the growing periods of 2005 to 2011 as to provide uniform temporal resolution. Reflectance data is rescaled to the 16-day temporal resolution and to a 500-m spatial resolution. Atmospheric correction, cloud removal, and bi-directional reflectance distribution function (BDRF) correction have been applied to MOD13Q1 and MOD09A1 products before the release of the products, and thus no more correction needs to be taken for the experiments to be conducted. The NDDI can be then calculated with values of NDVI and NDWI in Equation 9.

The reasons for using 16-day MODIS products rather than other products with different temporal resolutions have been explained in details in subsection 1.6.1. In simple language, it is because 16-day MODIS datasets are closest one can get in MODIS series that is with less cloud and error. The sole purpose being to discover the relationship between MODIS VIs and ground-based soil moisture data, and decide root zone soil moisture at which depth is best suited for validation with MODIS VIs, the experiments conducted here are based on 16-day temporal resolution for both VIs and soil moisture data (satellite- or ground-based).

Section 5.4 Results and discussions

Subsection 5.4.1 Temperature and Precipitation

The averaged daily precipitations and temperatures for the SCAN site 2031 for years 2011, 2010, 2007 and 2006 are illustrated in Table 14. It is easy to see from the figure that the precipitation of the observed area increased from March to early September, and dropped sharply in mid-September. During the periods of 2007/113-2007/128 (as in the format of YEAR/DOY) and 2010/049-2010/064, the precipitation levels are 5-10 inches lower than multi-year average, which could cause drought in the crop fields. From October to next spring, the precipitation climbed up slowly, and the temperature of the area ranged from lower than -10°C in January to more than 25°C in July.

Table 14 Averaged daily precipitation and temperature for the SCAN site 2031 for years 2011, 2010, 2007 and 2006.

Year	Precipitation (inches)	Temperature (°C)
2011	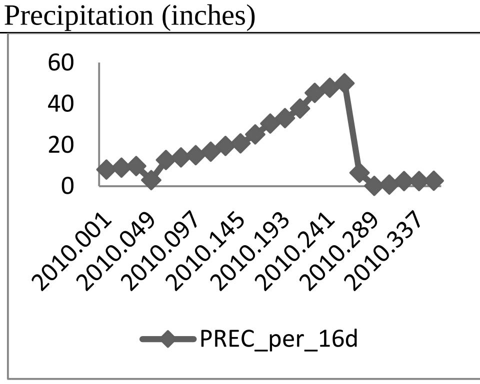	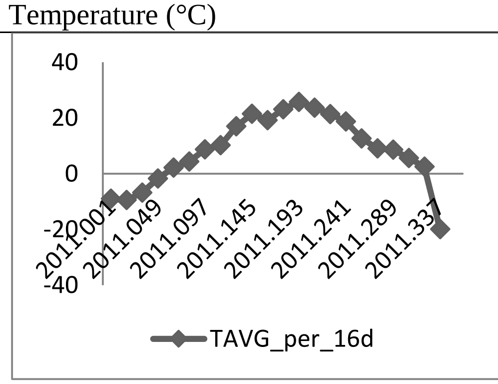

2010

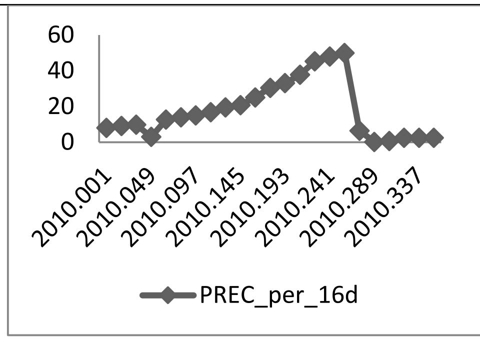

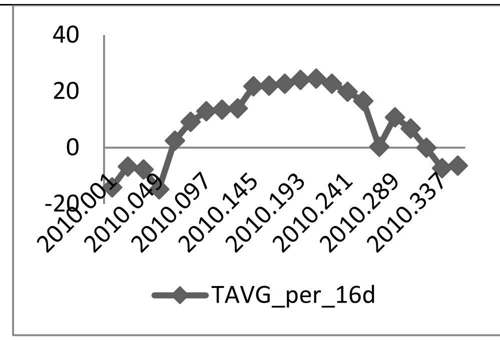

2007

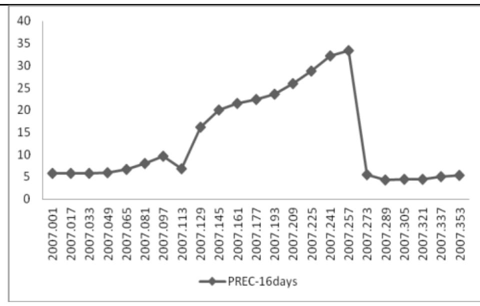

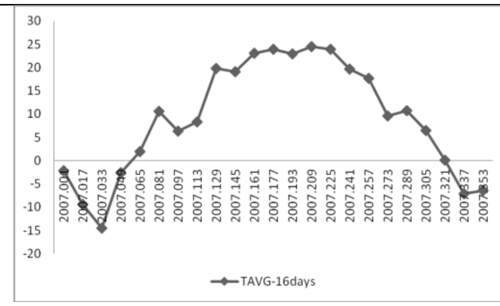

2006

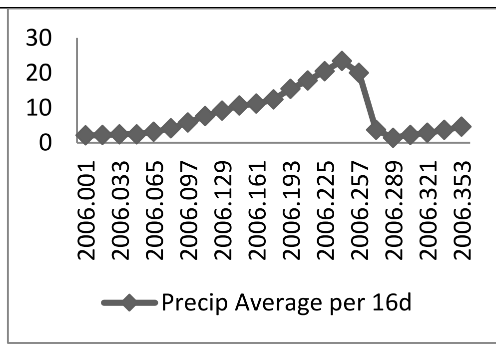

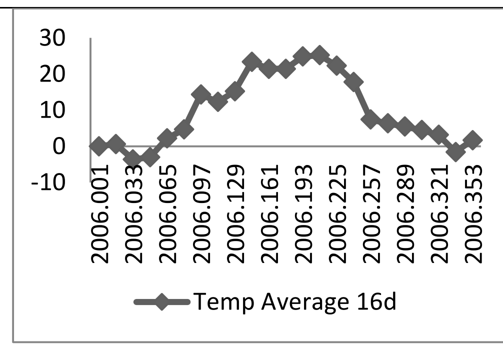

Subsection 5.4.2 Growing Season Time-series Soil Moisture and VI Profiles

Time-series soil moisture profiles at five depths for the year 2011 are presented in Figures 46, 47, 48 and 49 to illustrate the temporal trends of soil moisture at the study site #2031. Soil moisture of -2, -4 and -8 inches exhibited high frequency variations compared to those at -20 and -40 inches. In the beginning of the growing season (approx. from day 65 to 129), soil moisture content at the shallower depths show variations because of snowmelt and other hydrologic activities. Since day 161, the soil moisture content progressively declined because the vegetation roots started to suck water from shallower depths.

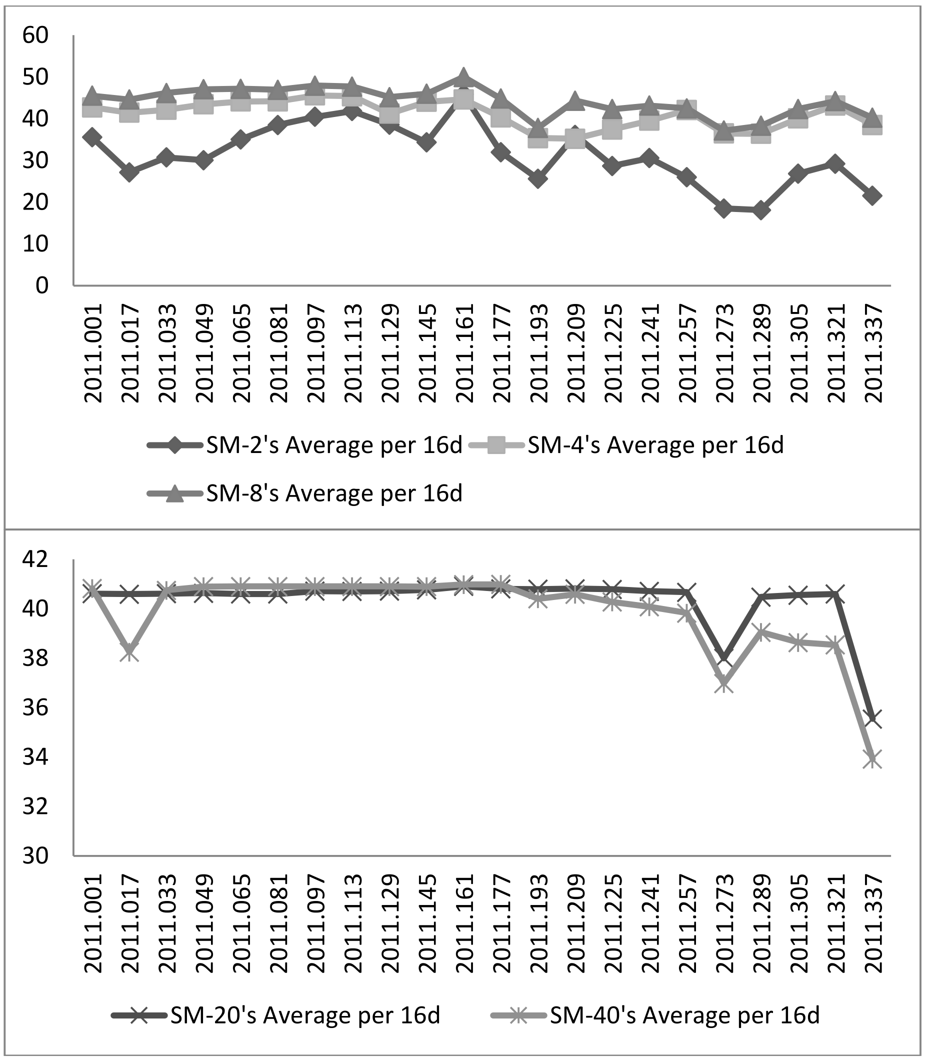

Figure 46 Corn field's soil moisture content at 5 depths (2, 4 and 8 inches (upper panel), 20 and 40 inches (bottom panel)) from SCAN (year 2011, site #2031).

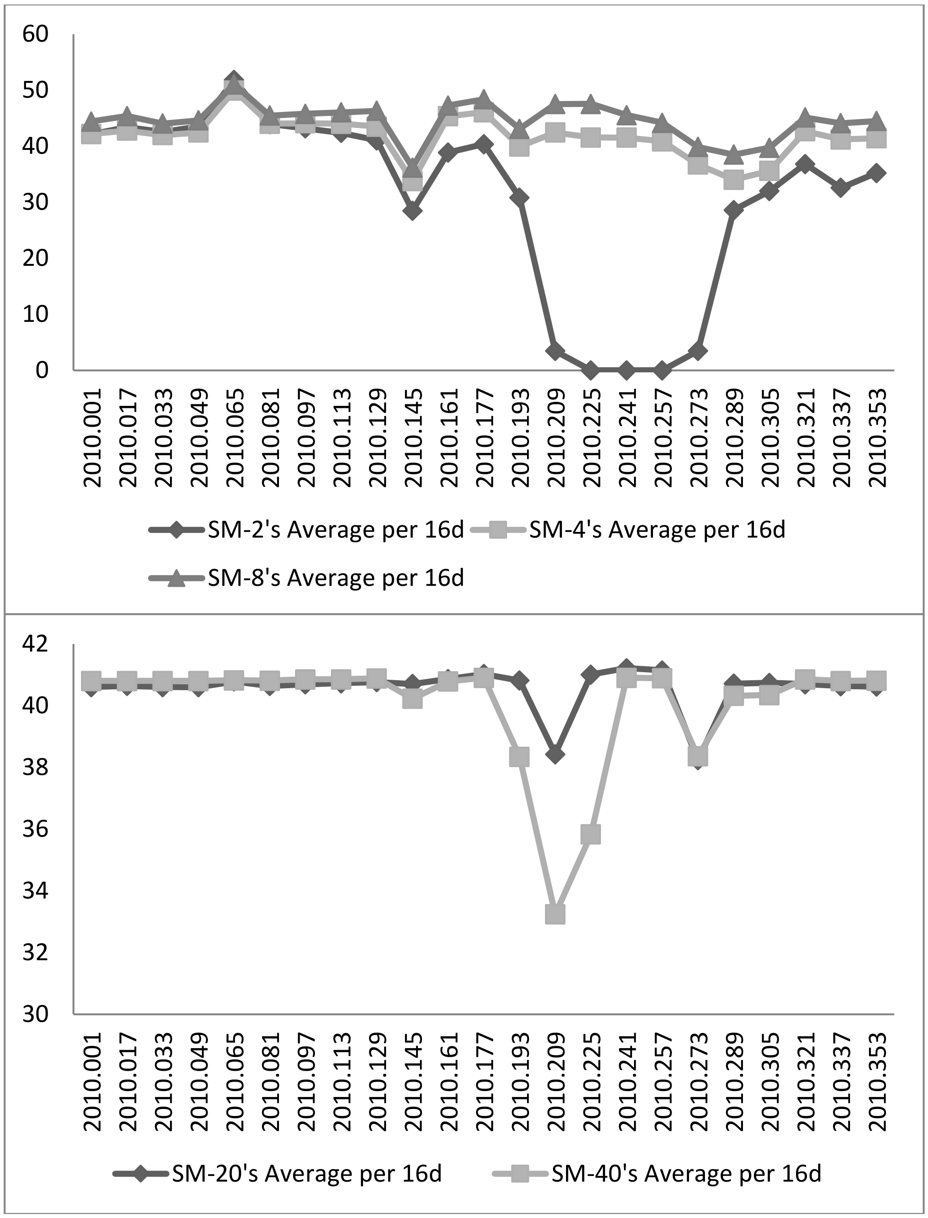

Figure 47 Soybeans field's soil moisture content at 5 depths (2, 4 and 8 inches (upper panel), 20 and 40 inches (bottom panel)) from SCAN (year 2010, site #2031).

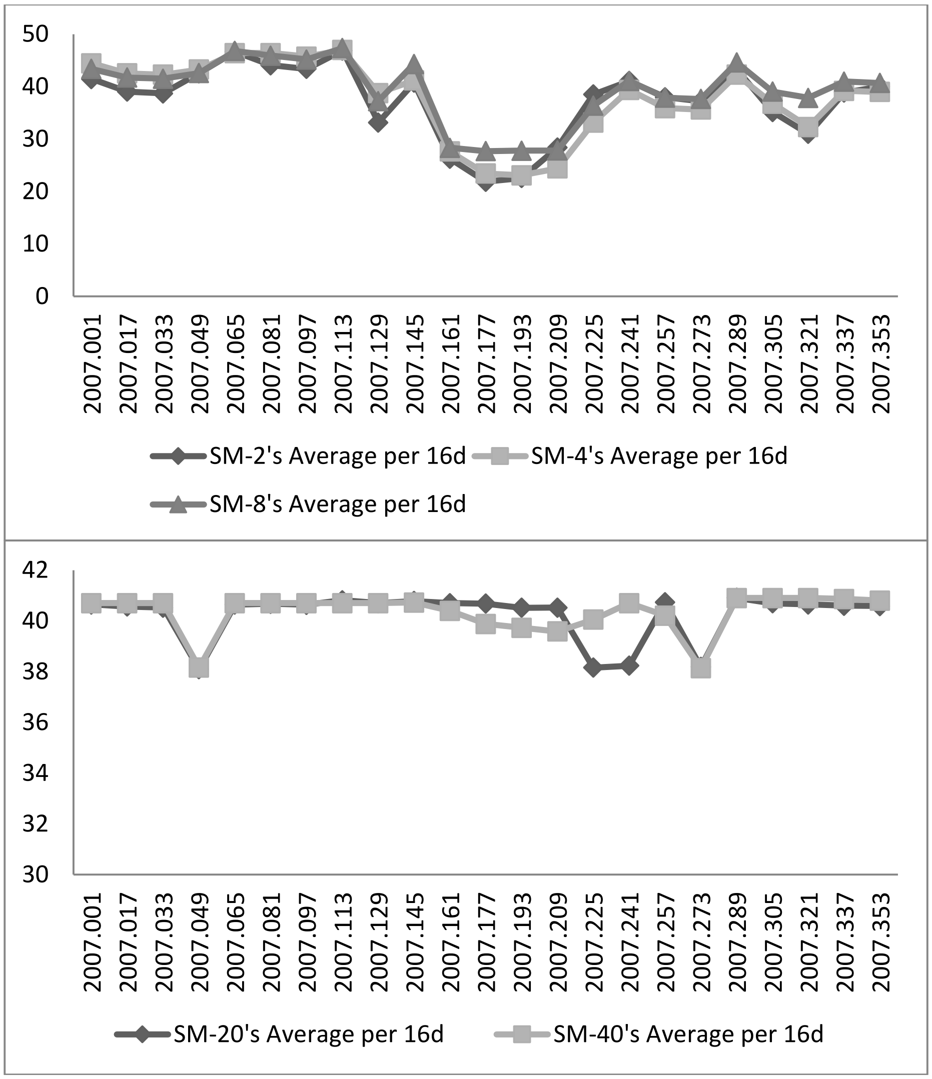

Figure 48 Soybeans field's soil moisture content at 5 depths (2, 4 and 8 inches (upper panel), 20 and 40 inches (bottom panel)) from SCAN (year 2007, site #2031).

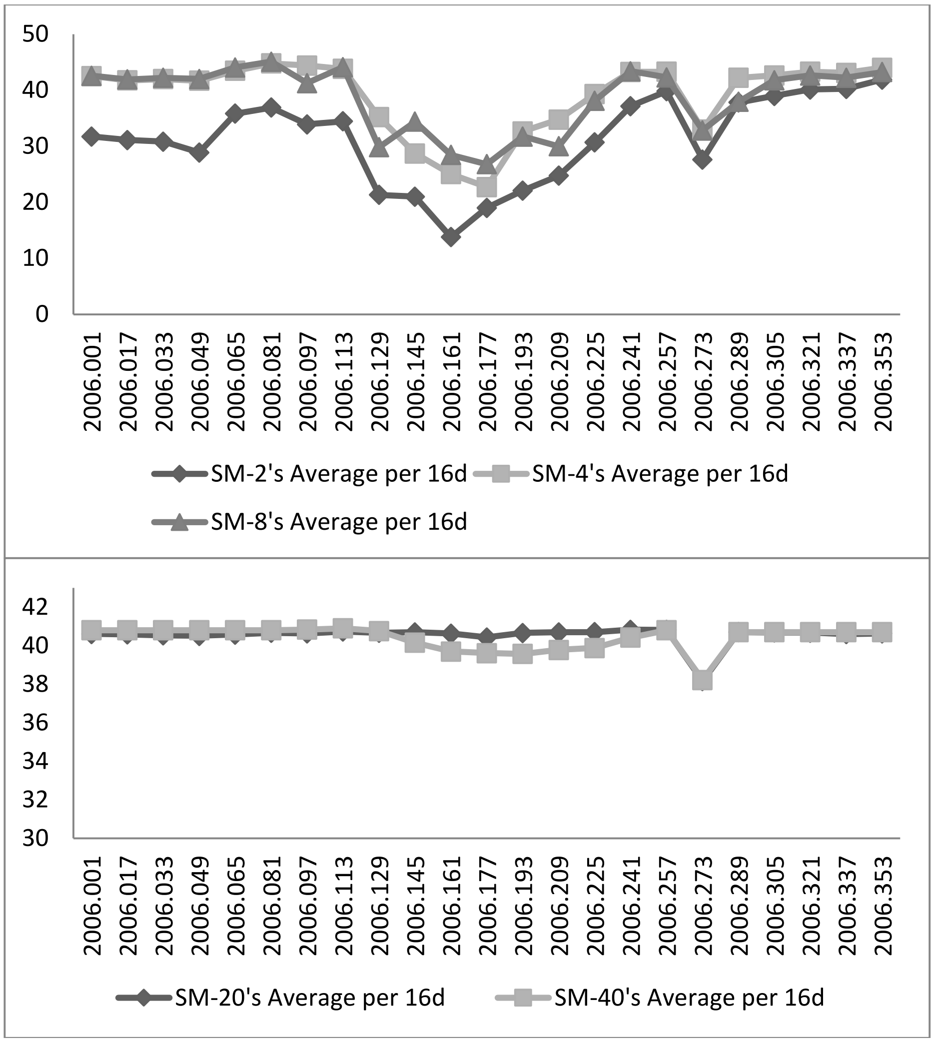

Figure 49 Corn field's soil moisture content at 5 depths (left: 2, 4 and 8 inches, right: 20 and 40 inches) from SCAN (year 2006, site #2031).

The growing season variations in the corn (2011, 2006) and soybeans (2010, 2007) VIs are shown in Figures 50 and 51. The onset of greenness increases with increasing NDVI and NDWI values or decreasing NDDI values which starts in May. The four VIs behave differently across a given growing season. For example, corn NDVI values during the 2011 growing season ranged between 0.23 and 0.87, while corn NDDI values during the same growing season ranged between 0.07 and 0.62. In order to visually compare the changes in the VIs across the growing season, and to contrast its inter-seasonal differences, the index values need to be scaled between 0 and 1 according to Equation 8.

Equation 8 VI being rescaled to the range of 0~1.

$$Rescaled\ VI\ =\ (VI - VImin)\ /\ (VImax - VImin)$$

Here, VI_{min} and VI_{max} are the minimum and maximum VI values throughout the observed period. The reason for new VIs after normalization being named ‘rescaled VIs’ instead of ‘normalized VIs’ is that the latter has been already used to define the VI ratio between maximum and minimum VI values for the same DOY across all the years. During corn’s vegetative stage, the rescaled NDVI has showed increasing trends and reached maximal values on DOY 209. The rate of increase in rescaled NDVI is maximal compared to the rate of increase of other VIs, between DOYs 145 and 161. In the reproductive and senescence stages of corn, NDWI has showed sharper decline than NDVI or EVI (between DOYs 257 and 273).

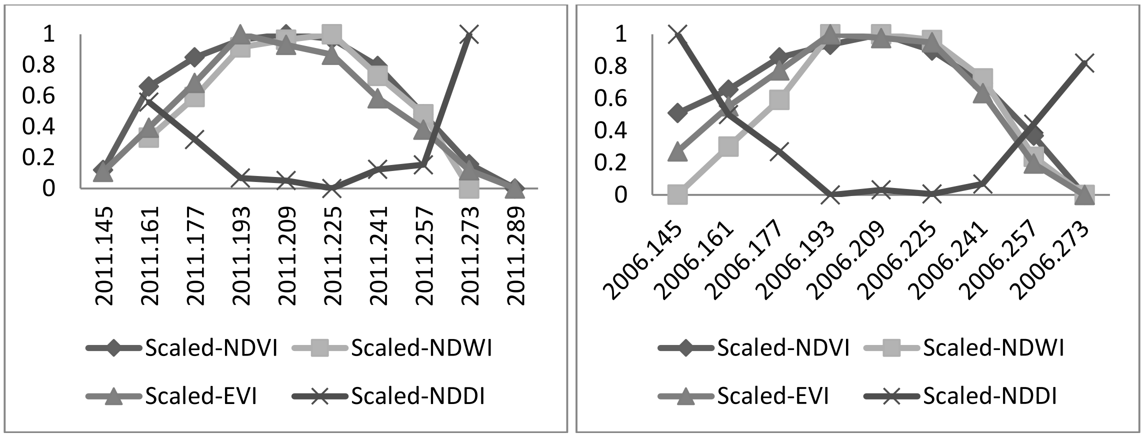

Figure 50 Temporal variations of rescaled VIs for corn during the growing season of 2011 (left) and 2006 (right).

The NDVI, NDWI, and EVI curves have showed increasing trends and reached maximal values on DOY 209, while the NDDI curve displayed decreasing trend and reached minimal values on the same day. Soybean EVI values decreased rapidly during the reproductive and senescence stages compared with NDVI and NDWI values. Among the four VIs for soybean fields, EVI has showed the largest variations during the growing season, especially between DOYs 225 and 257. In contrary to NDVI, NDWI, or EVI, which are indicators for vegetation greenness, NDDI values are correlated with the dryness of an area. As the NDDI increases, the drought intensities of an area climb high. Also, NDDI has showed a higher sensitivity than other VIs in responding to changes of greenness.

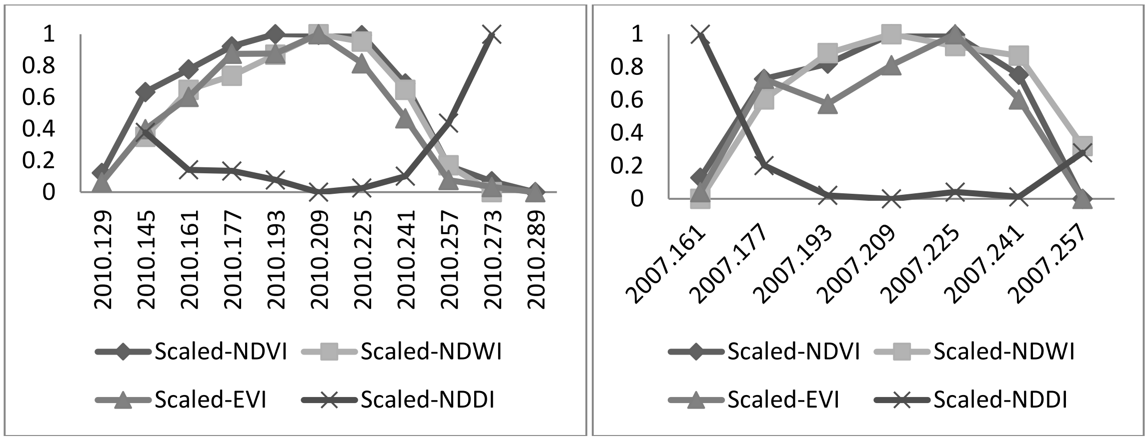

Figure 51 Temporal variations of rescaled VIs for soybean during the growing season of 2010 (left) and 2007 (right).

Subsection 5.4.3 Correlation between soil moisture and VIs

The relationships between corn VIs and soil moisture at all five depths are illustrated in Table 15. Results show that the relationships of NDVI, NDWI and EVI with soil moisture with lag periods from 16 to 48 days at 2, 4, and 8 inches are statistically significant. The peak correlation lies between soil moisture at the depth of 8 inches and these three VIs with a 32 days' lag period. The correlations of corn NDDI with soil moisture of 48 days' lag period at 20 and 40 inches depth are highly significant (R = -0.975). Correlations of soybean VIs with the soil moisture have revealed that NDVI, NDWI, and EVI exhibit significant relationships with soil moisture at 2, 4 or 8 inches, while the relationships of these three VIs with soil moisture at deeper depths with a lag period of 16 days are also statistically significant. The correlations of soybean NDDI with soil moisture of 32 days' lagging period at 20 and 40 inches depth are significant (R = -0.597).

Soil moisture, as a determining factor for whether an agricultural drought is taking place, is not always positively correlated with vegetation conditions. Excessive soil moisture levels can also harm vegetation performance. For regions or vegetation types that are not water-limited (e.g. high latitudes), soil moisture levels can be negatively correlated to vegetation greenness, indicating that the abnormally high water supplies from the soil has limited vegetation growing conditions in the area. For example, in (a1) of Table 15, the correlation coefficients between SM at shallower depths (2, 4, and 8 inches) and NDVI appear to be negative.

Table 15 Correlation Coefficient (r) between soil moisture (SM) at 2, 4, 8, 20 and 40 inches depths and corn VIs with time lags up to 64 days during the growing season of 2006 and 2007. For each row, (a1, a2): NDVI vs. SM, (b1, b2): NDWI vs. SM, (c1, c2): EVI vs. SM, and (d1, d2): NDDI vs. SM.

<table>
<tr>
<td>
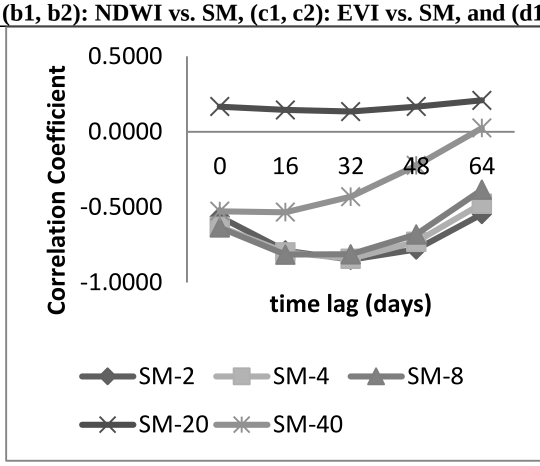

</td>
<td>
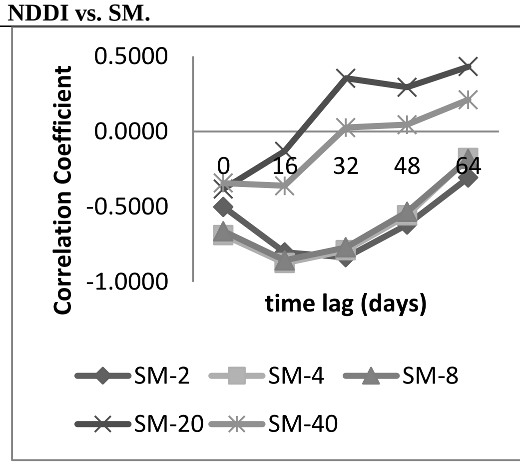

</td>
</tr>
<tr>
<td>(a1) Corn NDVI 2006</td>
<td>(a2) Soybean NDVI 2007</td>
</tr>
</table>

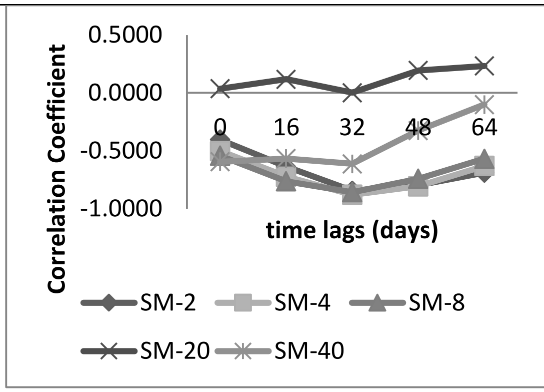	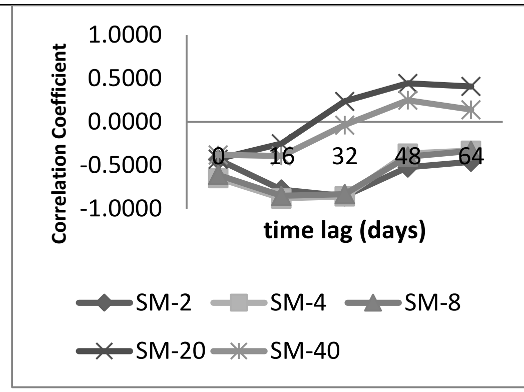
(b1) Corn NDWI 2006	(b2) Soybean NDWI 2007
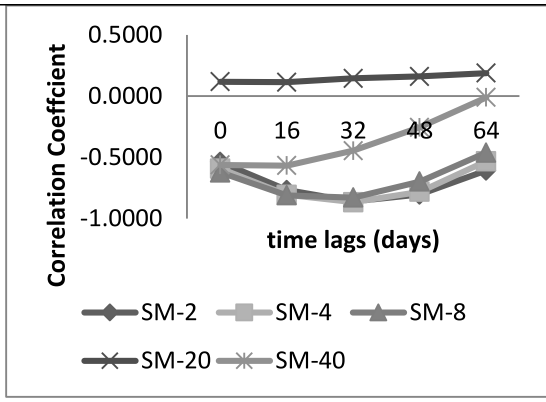	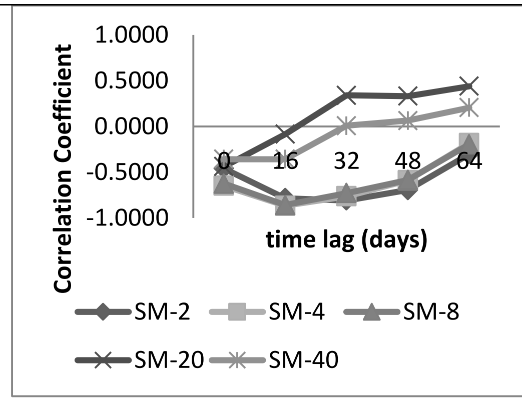
(c1) Corn EVI 2006	(c2) Soybean EVI 2007
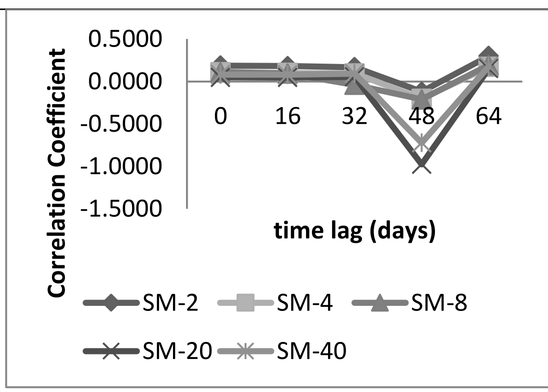	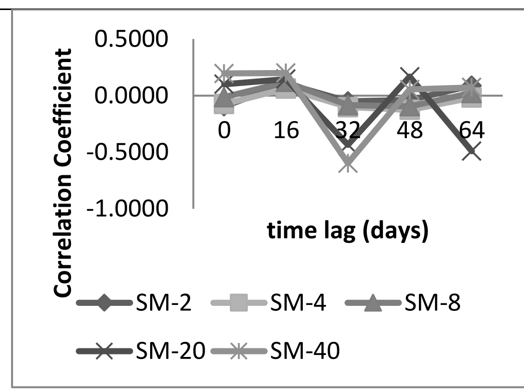
(d1) Corn NDDI 2006	(d2) Soybean NDDI 2007

The hypothesis is that relationships between VIs and soil moisture would be stronger if any inherent time delays (lag periods) that plants need to respond to soil moisture changes were considered. We tested the hypothesis by correlating the VIs with the averaged soil moisture using lag periods up to 64 days. On average, the correlation of corn VIs peaked at the lag period from 32 to 48 days for the 4 to 8 inches depth. On the other hand, the correlation of soybean VIs peaked at the lag period from 0 to 16 days for the 2 to 4 inches depth, and then followed a decreasing trend with increasing time lags. These results have shown soybean VIs respond to changes in the soil moisture more rapidly and maintain a fairly short soil moisture memory compared to corn.

Results have shown that the water extraction patterns of corn and soybean plants within the root zone areas are distinct. Corn VIs exhibit strong relationships with soil moisture at deeper depths, while the soybean VIs are highly sensitive to changes in soil moisture at much shallower depths. The difference between corn and soybeans is a reflection of their different rooting depths and structures. In the U.S. Corn Belt area, the roots of corn can extend to 42~46 inches or more (Weaver, 1926), while soybean is a comparatively shallower rooted plant. Depth and distribution of roots are also determined by climate, soil properties, and management practices such as irrigation and tillage treatments. For instance, when grown in clayey-textured soil with no-till system, the root length density of soybeans can be twice higher than that of corn in the shallower depths (Filho et al., 2004). Also, Tufekcioglu (1999) pointed out that, the density of corn roots is higher in 20 ~ 40 inches depth in the soil profile at a riparian buffer site in central Iowa, compared to that of corn grown in other areas. What we have found in this research, e.g., the corn VIs respond to soil moisture in deeper depths while the soybean canopy VIs respond to the soil moisture in the 4 ~ 10 inches depth, is consistent with such evidence.

In summary, the relationships between four RS-based agricultural drought indicators (NDVI, NDWI, EVI and NDDI) and the root zone soil moisture under corn and soybean canopies collected in the Corn Belt area have been uncovered through this experimental study. Time-series VI data for six growing seasons are correlated with concurrent as well as antecedent soil moisture (up to 64 days) at five different depths (2, 4, 8, 20 and 40 inches) in the soil profile. The indicators applied to Corn have been found significantly related to soil moisture lagging 32 days at the 20 inches depth. Among the four indicators analyzed, NDDI has showed the strongest correlation at this depth but with soil moisture lagging 48 days. Correlations of corn VIs with soil moisture improve when the time required by the plant to respond to the changes in the soil moisture are taken into consideration. Correlations of soybean VIs with soil moisture show that NDVI, NDWI, and EVI are significantly related to concurrent soil moisture at the 4, and 8 inches. Correlations of soybean NDVI, NDWI, and EVI are highest with 16 day lagged soil moisture at 4 and 8 inches depths, and the NDDI shows the strongest correlation when there is a 32 days of lagging period. These findings suggest that, unlike corn, RS-based indicators for soybean are highly sensitive to soil moisture at shallow depths with short lagging periods. Thus, the potential and limitation of using NDVI, NDWI, EVI and NDDI for characterizing root zone soil moisture and identifying agricultural drought severities under corn and soybean canopies have been tested and clarified.

Section 5.5 Summary

This work has accurately characterized the detailed relationships between different RS-based agricultural drought indicators and root zone soil moisture at various depths, by way of (1) applying crop mask to filter out irrelevant crop type, (2) calculating GDD to determine growing stages of crops, and hence lining up the datasets of the same growing phase every year onto the same comparison platform, (3) deriving the correlation coefficients between concurrent VIs and soil moisture at various depths, and (4) analyzing the relationships between time-lagged VIs and soil moisture observed at various depths . The method integrates VIS, NIR and SWIR bands from remotely sensed MODIS data, and also considers weather and environmental factors including precipitation, temperature, and soil moisture. The relationships between soil moisture and the VIs found in this study will form the basis of modeling simulation for root zone soil moisture estimation and largely improve the accuracy of agricultural drought monitoring and analysis in corn and soybean croplands in the Corn Belt area of the United States. The major contribution of this work is to have discovered the relationships between per-16-day MODIS-based crop specific VIs and the SCAN root zone soil moisture data under different canopies, and to indicate the root zone soil moisture at which depth is good for validation specifically for different crop types. This finding is to be utilized in Chapters 6 and 7 in order to facilitate the optimized source for validation.

Section 5.6 Future Work

One of the limitations of this study is that the regression models used have not considered the situation when root zone soil moisture at various depths with different lag periods all contribute to the current vegetation greenness, because of the “memory” properties of soil. That is to say, RZSM (64 days' lag), RZSM (48 days' lag), RZSM (32 days' lag), RZSM (16 days' lag), and RZSM (current) can all become a variable in the regression model for VI, such as, VI (current) = function (RZSM (64 days' lag), RZSM (48 days' lag), RZSM (32 days' lag), RZSM (16 days' lag), RZSM (current)). More efforts need to be taken in order to find out the relationship between these variables.

In the future, the following work will also be conducted to improve the accuracy of agricultural drought monitoring: First, soil mask shall be applied to the satellite images, since the soil type (loam, clay, and sand) largely affects how much water can be stored for a specific area. Secondly, the correlation analysis will be based on the VI time series not only from the recent decade, but also reaching backwards to the latest 30 years as provided by the AVHRR data. Thirdly, since NDVI, NDWI and combined NDVI and NDWI curves have different performances throughout crop growing season for dry years and wet years, the rules of how these indices reflects whether each crop is undergoing drought or non-drought situations for each county, the per crop, per location, per growing stage analysis of whether or not the crop is suffering from agricultural drought will be studied. Establishing a library containing the performance curves for all these VIs throughout the years can serve as a footing stone for better understanding the impact of agricultural drought upon crop performances.

CHAPTER 6 ASSESSING IMPACT OF AGRICULTURAL DROUGHT ON THE VARIATION OF VEGETATION VIGOR

Section 6.1 Introduction

As stated in 2.1.2.2, the correlation relationship between NDVI and LST is negative for regions where crop growth are limited by water (e.g. semi-arid areas) and is positive for where crops growth are energy-limited (e.g. in high latitudes). Because the LST/NDVI relationship is not simply linear, in order to accurately interpret the LST/NDVI space, some scientists suggested the triangle method (Price, 1990; Carlson et al., 1994; Gillies & Carlson, 1995; Gillies et al., 1997), which uses the calculation of a point falling into the triangle between the slope of the LST and the NDVI, while some others developed the Vegetation Index Temperature Trapezoid (VITT) (Moran et al., 1994) that is based on a trapezoid model. The Vegetation Temperature Condition Index (VTCI) developed by Wang et al. (2001), and the Vegetation Water Temperature Index (VWTI) by Katou and Yamaguchi (2005) both fall into the second category. With the purpose of integrating vegetation conditions and thermal properties to monitor drought, the VTCI is defined as the ratio of the LST differences among pixels with a specific NDVI value in a sufficiently large study area (Wang et al. 2001). Considering that vegetation conditions and thermal stresses are sufficient for drought detection and water stresses serve as direct indicators for agricultural drought, Katou and Yamaguchi (2005) used NDWI, NDVI and LST for the calculation of VWTI1 and VWTI2, which are measurements of the strength of stress and the influence of stress upon vegetation, respectively.

Whether an area is experiencing thermal or moisture stresses can be answered by the trapezoid interpretation of LST/NDVI space. However, since NDVI fails to represent the vegetation moisture levels through the years, esp. after the vegetation has reached the saturation point, using NDVI for detection of moisture levels will not be appropriate by then. In fact, the NDVI and NDWI curves tend to have similar trends until the saturation point when NDWI still climbs up and NDVI stays constant ever since. Thus, NDWI can better depict water levels within vegetation throughout the growing cycle, including the period when NDVI has been saturated.

The LST/NDVI/NDWI approach, on the other hand, is not entirely efficient because the process to extract the warm and cold edges for NDVI-NDWI, and LST-NDVI spaces respectively, and nest the former into the latter is time-consuming and CPU-exhausting. Using the NDDI or RNDDI to depict the relationship between NDWI and NDVI not only saves time in calculation, but also makes the difference between these two indices more contrasting. In brief, the proposed approach aims to construct an LST/RNDDI space, and extract the patterns of temperature and wetness performances into a single Index, called the Combined Condition Index (CCI). The definition and usage of RNDDI can be seen in section 6.2.1, and later in section 6.2.2, CCI is introduced and discussed in details.

Section 6.2 Methodology

Subsection 6.2.1 Reversed Normalized Difference Drought Index (RNDDI)

As the ratio between the difference and sum of NDVI and NDWI, NDDI combines both vegetation and water conditions, and thus serve as an appropriate indicator for dryness of a particular area. Also derived from the radiances of VIS, NIR, and SWIR data, NDDI has a stronger response to summer drought situations than a simple difference between NDVI and NDWI, or NDVI/NDWI being used alone. Experiments by Liu and Wu (2008) have showed that the goal of drought monitoring could be reached with satisfied accuracy and quickness. The definition for NDDI is shown in Equation 9.

Equation 9 Normalized Drought Difference Index (NDDI).

$$NDDI = SCALE * \frac{NDVI\ -\ NDWI}{NDVI +\ NDWI}$$

NDDI values are strongly correlated with the dryness of an area. As the NDDI increases, the drought intensities of an area climb high. Liu and Wu (2008) applied the NDDI method to Jiangsu province in China, and validated the results of NDWI and NDDI with the 10cm soil moisture data. Judging from the correlation coefficients, where R^2 is 0.0714 for that between NDWI and soil moisture, and is 0.2783 between NDDI and soil moisture, NDDI is more sensitive to the changes in 10cm soil moisture than NDWI. In most situations, for any vegetated pixel, the NDVI curve is above the NDWI curve, and when the gap between two curves grows thick, the NDDI value becomes larger which indicates higher drought intensity. Before rescaling, the NDDI ranges from -1 to 1;

as NDDI approaches 1, the drought severity of the area gets upgraded, which is opposite to how NDVI, NDWI and other vegetation indices relate to drought severities, since higher VI values always represent lesser drought severities. One way to reverse the correlation direction between NDDI and drought severities is simply to subtract NDDI from 1, divide the difference by 2, and obtain the reverse NDDI (RNDDI) value ranging from 0 to 1 (as shown in Equation 10). For example, if the NDDI of an area is 0.95, its drought situation would be extremely severe, and accordingly the RNDDI value is 0.05 signaling its wetness level being rather low. Negatively correlated to drought intensities, RNDDI along with LST are used in subsection 6.2.2 for calculation of CCI.

Equation 10 Reversed Normalized Drought Difference Index (RNDDI).

$$RNDDI = \left(1 - \frac{NDVI\ -\ NDWI}{NDVI +\ NDWI}\right)/2 = \frac{NDWI}{NDVI +\ NDWI}$$

In real life implementation, RNDDI is often scaled to 0~255 to save storing space and computation efforts, since an 8-bit integer is easier to store, manipulate and display than a 32-bit float. The rescaling equation is shown in Equation 11. Opposite to NDDI, which is positively correlated to drought severity, the RNDDI is correlated to drought severity degrees in a negative way. As the RNDDI increases (up to 1.0), the NDDI decreases accordingly (down to -1.0), and thus representing the dryness severity of the area is reducing.

Equation 11 Scaled RNDDI.

$$RNDDI' = SCALE' * \frac{NDWI}{NDVI + NDWI}$$

Subsection 6.2.2 Combined Condition Index (CCI)

A trapezoid shape can be identified in the pixel distribution of an area, of which these requirements are met: (1) there are a large number of valid pixels, (2) a wide range of soil wetness, and (3) a broad range of fractional vegetation cover. The base of the trapezoid shape (i.e. edge BD) and the upper slope of the trapezoid (i.e. edge AC) represent the wettest and the driest condition of respectively (Figure 52). The way to construct the RNDDI-LST space for an area of N pixels is to draw a point with RNDDI value as x-coordinate, and LST value as y-coordinate to represent each of these N pixels. Here, the LST is in Kelvin, while the RNDDI is a ratio. The location of a pixel in this RNDDI-LST space is influenced by many factors, one of which is evapotranspiration (ET). ET can largely control the surface temperature through the energy balance occurring at the surface. The more the ET, the more intensive heat removal from the surfaces and thus bring the surface temperature down. More specifically, the process of water vapor being released from the plant stomata, namely transpiration, is partially controlled by soil moisture availability; when the soil moisture is in deficiency, the transpiration process is slowed down, or even shut down. The relationship between evaporation and LST, and that between transpiration and LST are shown in Figure 52 as well.

Points A and B represent dry bare soils (low RNDDI and high LST) and moist bare soils (low RNDDI and low LST) respectively. As the fractional vegetation increases, surface temperature drops for vegetated land. Points C and D both represent continuous vegetation canopies, among which C (with high RNDDI and high LST) corresponds to those with a high resistance to evapotranspiration probably resulting from a low water availability, while D (with high RNDDI and low LST) corresponds to those with low resistance to evapotranspiration probably occurring on well-watered surfaces (Liang, 2005). Within the trapezoid space, for vegetated pixels, LST value decreases as the RNDDI value increases; this is especially significant on the dry edge. However, there can be no significant variability of LST along the wet edge. Densely vegetated pixels are located where the dry and wet edges start to merge, and a slight LST variation is exhibited compared to other pixels.

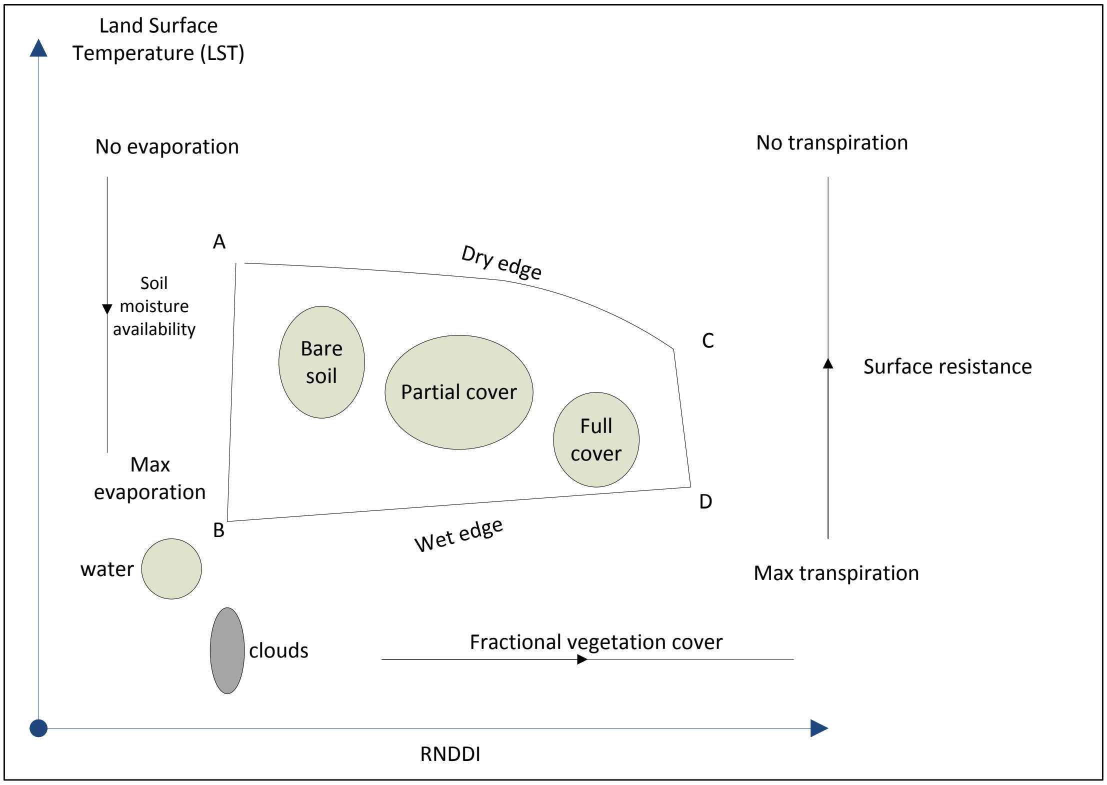

Figure 52 The schematic plot of land surface temperature and RNDDI space, and the conceptual relationships with evaporation, transpiration, and fractional vegetation cover (RNDDI, units: 1; LST, units: Kelvin).

To determine dry and wet edges is critical to understanding the distribution of vegetation wetness across the area and hence obtaining the CCI results. These two edges can be found in the scatter plot for a large area of pixels, where the RNDDI and LST values for each pixel serve as x and y co-ordinates. Here, the RNDDI values are computed with NDVI, MIR, and NIR bands from the 16-day MOD13Q1 product. Also, two temporally adjacent 8-day MOD11A1 products will be set for input, so the two brightness temperature datasets can be merged into a 16-day LST layer. With the RNDDI and LST values of each pixel ready, a scatter plot for the pixel distribution of the study area can be drawn, and the dry edge is higher than all valid pixels, which means the LST value of any point residing on the edge is the maximum among all points sharing the same RNDDI value. Likewise, the wet edge is lower than all valid pixels, that the LST value of any point residing on it is the minimum among all points sharing the same RNDDI value. A polynomial curve fitting needs to be run against the maximum and minimum LST values, respectively, to find the wet and dry edges represented in polynomial functions (Equation 12 Warm and Cold Edges of RNDDI/LST space (polynomial fit) below). Detailed steps in calculating the coefficients of dry and wet edges, namely p0, p1, …, pn, and q0, q1, …, qn, are shown in Box 5.

Equation 12 Warm and Cold Edges of RNDDI/LST space (polynomial fit)

$$LST_{RNDDIi.max} = p0 * RNDDI_i^{\mathrm{n}} + p1 * RNDDI_i^{\mathrm{n}-1} + \dots + pn$$

$$LST_{RNDDIi.min} = q0 * RNDDI_i^{\mathrm{n}} + q1 * RNDDI_i^{\mathrm{n}-1} + \dots + qn$$

Box 5.

Step 1: Download MOD13Q1 dataset for the desired date and location, derive NDVI, MIR, and NIR bands from the former, calculate NDWI from the last two bands, and compute RNDDI using NDVI and NDWI.

Step 2: Download MOD11A1 dataset for the desired date and location, derive BT band, merge two adjacent 8-day LST into a single 16-day LST product.

Step 3: Draw scatter plots with the RNDDI-LST values, obtain the maximum LST array, and minimum LST array corresponding to each RNDDI entry, and simulate these RNDDI-max LST, and RNDDI-min LST data into polynomial fit (called f1, and f2).

Step 4: Get the maximum absolute value of the difference between real max LST (called Error1) and simulated max LST, and also that between real min LST and simulated min LST (called Error2).

Step 5: Draw the two edges on the scatter plot – one is f1+Error1, and the other f2-Error2.

Considering any point plot in the RNDDI-LST space, the closer it is to the dry edge, the more likely it is enduring water stress; Vice versa, the closer a point approaches the wet edge, the less likely it is suffering from water stress. Computed as a ratio of temperature differences among pixels with the same RNDDI, CCI combines vegetation water stress and thermal stress into a single index. The following equation (Equation 13) to calculate CCI measures the data position within the trapezoid (as shown in Figure 52), and determines its proximity to dry edge.

Equation 13 Combined Condition Index (CCI).

$$CCI = SCALE * \left(\frac{LST_{RNDDIi.max} - LST_{RNDDIi}}{LST_{RNDDIi.max} - LST_{RNDDIi.min}} \right)$$

Here, LST_{RNDDIi}, is the LST value of any specified pixel. $LST_{RNDDIi.max}$, and $LST_{RNDDIi.min}$ are two points residing on the dry and wet edges representing the maximum and minimum LST values of any specified $RNDDI_i$ value. The two edges are decided previously (in Equation 12), that are in fact two polynomial functions of $RNDDI_i$. As an indicator for the point's proximity to the dry edge, the CCI range from 0 to 1 before scaling, and the lower the value of CCI, the higher the degree of drought happens to the point.

Subsection 6.2.3 Correlation and Regression Analysis

In order to assess CCI's performance as an indicator for vegetation drought stress, the root-zone soil moisture (RZSM) data will be used to compare against the CCI calculated. If a pixel is having low RZSM and CCI value at the same time, which signifies high drought severities, the CCI performance is considered as "hit". On the other hand, if low CCI values happen along with high RZSM, then the CCI performance for the specified pixel is considered as "miss". Correlation and least square regression analysis will be used to assess the strength of association between RZSM and CCI. Because the soil moisture available for vegetation is largely influenced by the depth of rooting systems, RZSM used for validation needs to be picked according to crop type. Then, the statistical relationships between RZSM anomalies, time lag periods of RZSM and CCI are investigated using Pearson correlation analysis for selected SCAN sites.

Five models have been tested in search of the fittest match for the regression model between CCI and soil moisture, and they are namely, linear, quadratic, and cubic regression, and logarithmetic, and power equations. Table 16 lists these regression models used to create trend lines in the scatter plot of CCI vs. Soil Moisture.

Table 16 Regression models used to create trend lines for CCI vs. Soil Moisture.

CCI vs. soil moisture	Equation
Linear regression model	$y = a + bx$
Quadratic regression model	$y = a + bx + cx^2$
Cubic regression model	$y = a + bx + cx^2 + dx^3$
Logarithmetic function	$y = a + b * \ln(x)$
Power function	$y = a * b^x$ or $\ln(y) = \ln(a) + x * \ln(b)$

Section 6.3 Study area and data

Subsection 6.3.1 Study area

For validation purposes, the meteorological data for seven observation stations were collected by the Soil Climate Analysis Network (SCAN), and each station was picked from a different state. The parameters, including site number, location, and elevation, for these seven stations are listed in Table 17.

Table 17 Parameters for the seven SCAN sites chosen for the study.

SCAN SITE	Site No.	State	County	Longitude	Latitude	Elevation (FT)
Sidney	2120	Montana	Richland	104 deg; 15 min W	47 deg; 46 min N	2274
Eros Data Center	2072	S. Dakota	Minnehaha	96 deg; 37 min W	43 deg; 44 min N	1602
Mandan #1	2020	N. Dakota	Morton	100 deg; 55 min W	46 deg; 46 min N	1930
Ames	2031	Iowa	Boone	93 deg; 44 min W	42 deg; 1 min N	1073
Crescent Lake #1	2002	Minnesota	Sherburne	93 deg; 57 min W	45 deg; 25 min N	980
Mason #1	2004	Illinois	Mason	89 deg; 54 min W	40 deg; 19 min N	570
UW Platteville	2196	Wisconsin	Lafayette	90 deg; 23 min W	42 deg; 42 min N	1075

Crop rotation is a practice of growing a series of dissimilar types of crops (usually alternating between deep-rooted and shallow-rooted plants) in the same area in sequential growing seasons, aiming to give various benefits to the soil, and also mitigate the build-up of pathogens and pests. Based on the crop classification data derived from NASS CDL datasets, the crop types grown on some of these SCAN sites have displayed a crop rotation pattern (as shown in Table 18 the crop types for each site during years 2009 and

2010). The crop types rotated for three SCAN sites from 2009 to 2010 while for the rest of observation stations, the crop type remained the same. Table 19 lists the crop maps surrounding the observation sites. The SCAN site #2072 (inside South Dakota) and site #2031 (inside Iowa) are shown to be growing corn in 2009 and then soybeans in 2010. The similar situations happen to #2196 as well, grass growing in 2009 and corn in 2010. Because different crops behave separately to drought stress, the experiment though based on the same geo-location along the timeline, needs to be conducted separately according to crop types. For instance, for site #2031, the crop rotation pattern from 2005 to 2011 is, S\C\S\C\C\S\C, where S means soybeans and C means corn, then the time-series of experiment dataset needs to be separated into 2 groups: {2005, 2007, 2010}, and {2006, 2008, 2009, 2011}.

Table 18 The Crop type distribution for these seven SCAN sites.

SCAN SITE No.	XY Location (meters)	Crop Type 2009	Crop Type 2010
2120	-7791586.34, 5311454.05	Spring Wheat	Spring Wheat
2072	-7767800.05, 4862893.21	Corn	Soybeans
2020	-7686335.66, 5200259.00	Woody Wetlands	Woody Wetlands
2031	-7743465.7, 4672082.5	Corn	Soybeans
2002	-7333027.72, 5050145.68	Deciduous Forest	Deciduous Forest
2004	-7622045.8, 4483050.91	Open Water	Open Water
2196	-7385996.32, 4748028.72	Grass	Corn

Table 19 Crop Mask surrounding study sites in year 2010.

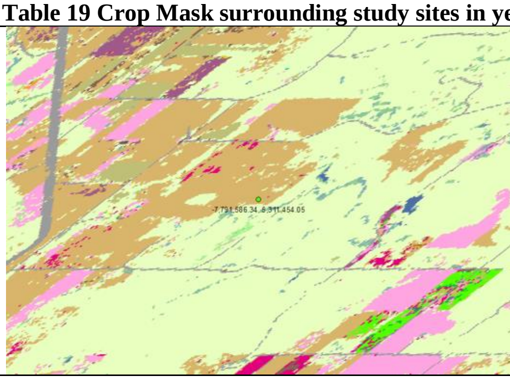	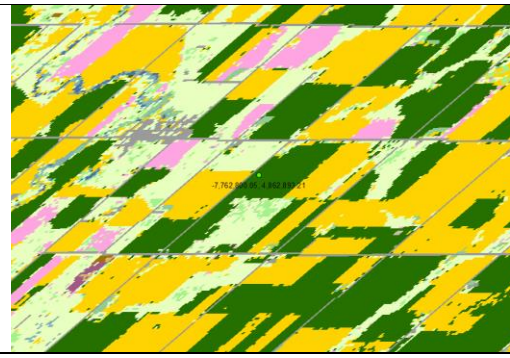
#2120 (MT)	#2072 (SD)
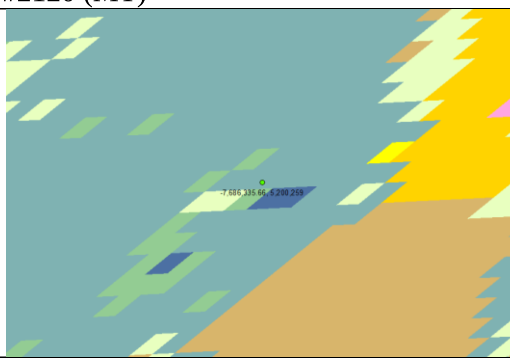	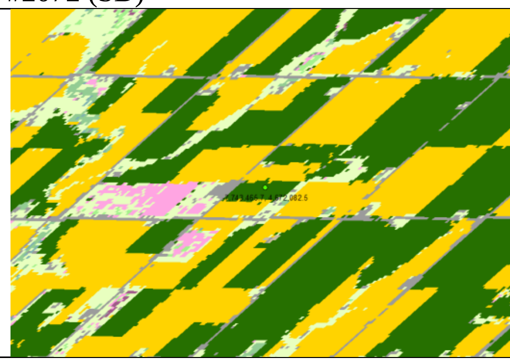
#2020 (ND)	#2031 (IA)
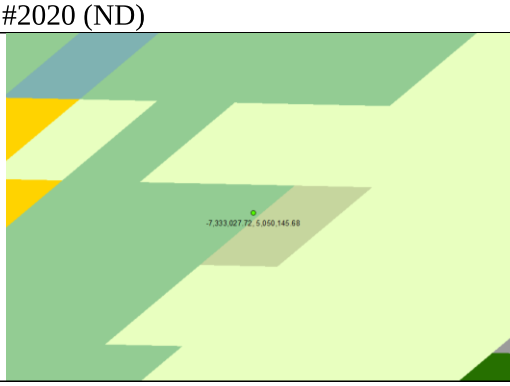	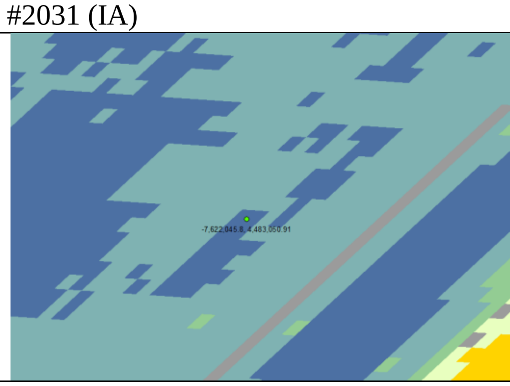
#2002 (MN)	#2004 (IL)
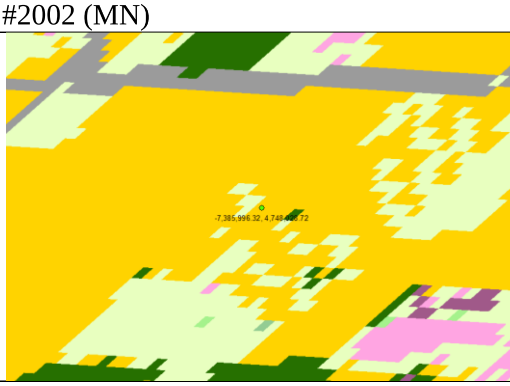	
#2196 (WI)	

Subsection 6.3.2 Remotely Sensed Indices as input

With MIR and NIR bands derived from MOD13Q1 products, the NDWI can be calculated as NDWI = (NIR-MIR) / (NIR+MIR), and would range from -1 to 1. For easier display, these NDWI values can be scaled into Scaled NDWI as SNDWI = 125*(NDWI+1), ranging from 0 to 250. Then these values can be stored as 8-bit integers, and mapped to wetness legend, which is using black/red/orange/yellow/white color scheme to represent the values of Scaled RNDDI from 0 to 250. Here, 0 means very dry, and 250 means very wet. The NDWI maps drawn for four 16-day periods (a) 2009/193 – 2009/208, (b) 2010/193 – 2010/208, (c) 2011/193 – 2011/208, and (d) 2012/193 – 2012/208, using such an approach are displayed in Figure 53.

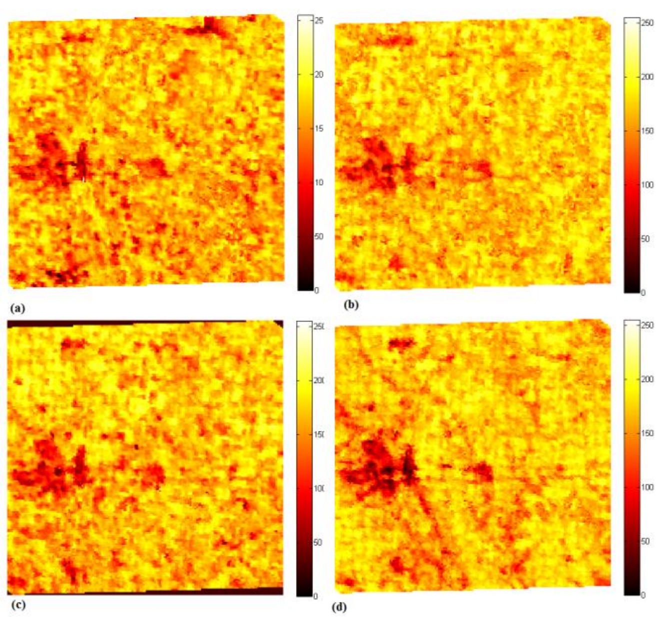

Figure 53 The NDWI images of Ames, Story on (a) 2009/193, (b) 2010/193, (c) 2011/193, and (d) 2012/193.

Directly derived from NDVI dataset in MOD13Q1 products, the NDVI data needs to undo the scaling, from a range of -3000, 10000, to its original range of -0.3, 1. The negative NDVI values are then abandoned since valid vegetated pixels are always with an NDVI value larger than zero. For display purposes, NDVI can be rescaled into Rescaled NDWI, which equals 250*NDVI, ranging from 0 to 250. The NDVI data obtained for four 16-day periods (a) 2009/193 – 2009/208, (b) 2010/193 – 2010/208, (c) 2011/193 – 2011/208, and (d) 2012/193 – 2012/208 are displayed in Figure 54.

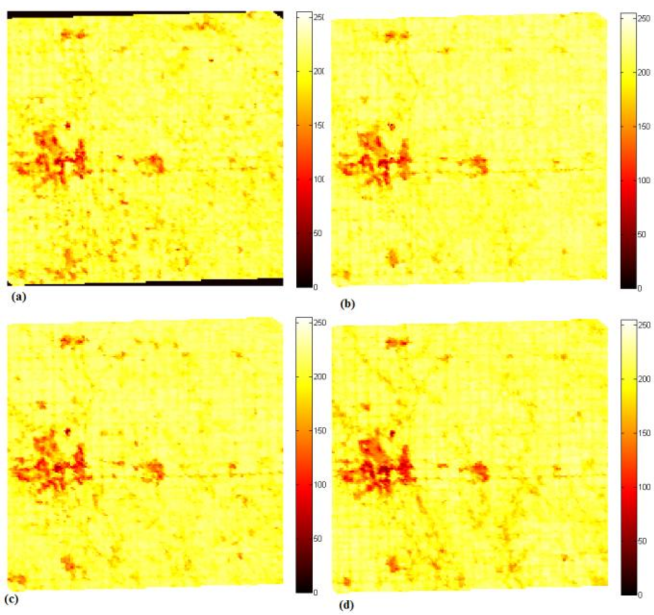

Figure 54 The NDVI images of Ames, Story on (a) 2009/193, (b) 2010/193, (c) 2011/193, and (d) 2012/193.

Subsection 6.3.3 Crop Mask Data

The crop mask data downloaded from NASS CropScape portal is projected to world sinusoidal coordinate system, and clipped to the same areal extent of tile h11v04 (shown in Figure 55). The pixel value ranging from 1 to 255 indicates different types of canopies (vegetation, urban, etc.), and value of 0 indicates no data. Extracting the pixels with desired vegetation type from the composite image, assigning them to be of value 1, and assigning the rest to be of value 0, we can derive crop mask for each specific crop type. The four major crop types of this area are deciduous forest, grass, corn, and soybeans, and the crop mask for each of these crop types are displayed in four subplots of Figure 56. These crop masks will be applied in the process of generating crop-specific CCI and other VIs.

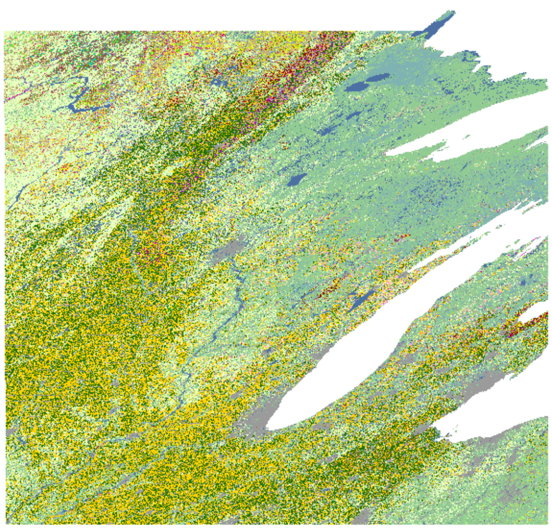

Figure 55 Crop Mask of tile h11v04 for year 2009.

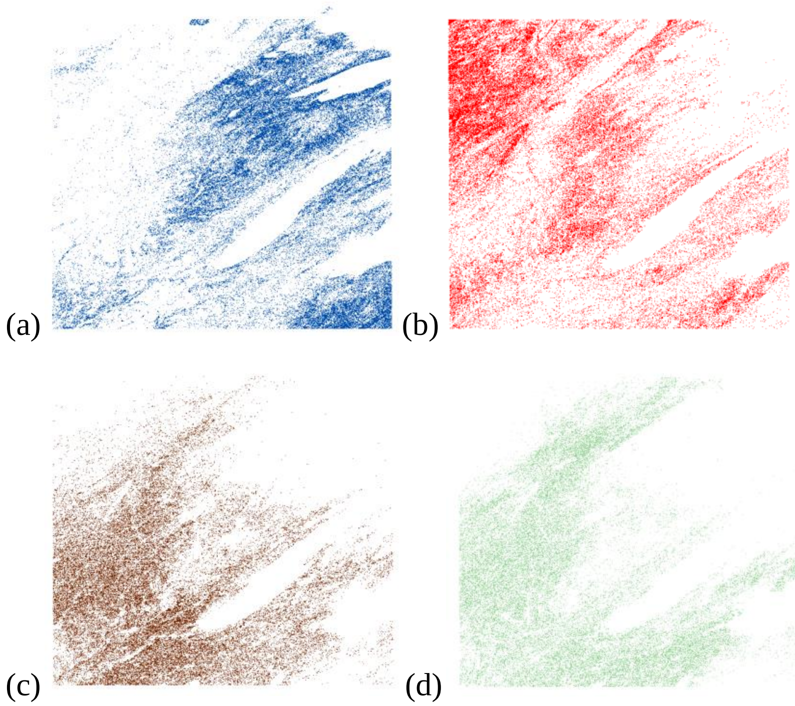

Figure 56 Crop Mask for tile h11v04 of various crop types in 2009: (a) Deciduous forest, (b) Grass, (c) Corn, and (d) Soybeans.

Section 6.4 Results and discussion

Subsection 6.4.1 Intermediate and Final Products

With the maximum and minimum LST values of each RNDDI value, polynomial fit regression model can be used upon these RNDDI-LST sets respectively, to find the dry and wet edges for the study area. Detailed steps are shown in Box 5. For three different 16-day periods, namely, 2009/193-2009/208, 2010/193-2010/208, and 2011/193-2011/208, and the same area (tile h11v04), the warm and cold edges derived are shown in Figure 57. Though the polynomial fit regression model allows the degree of polynomial equation to be any positive integer N, the regression equations obtained from these experiments turned out to be in quadratic or linear form (shown in Table 20), either

$y=a_0*x^2 + a_1*x + a_2$ or $y = b_0*x + b_1$. The slope of dry edge, which is always negative, indicates the $LST_{RNDDImax}$ decreases as RNDDI increases for each incremental step. The positive slope of wet edge indicates the $LST_{RNDDImin}$ increases as RNDDI increases.

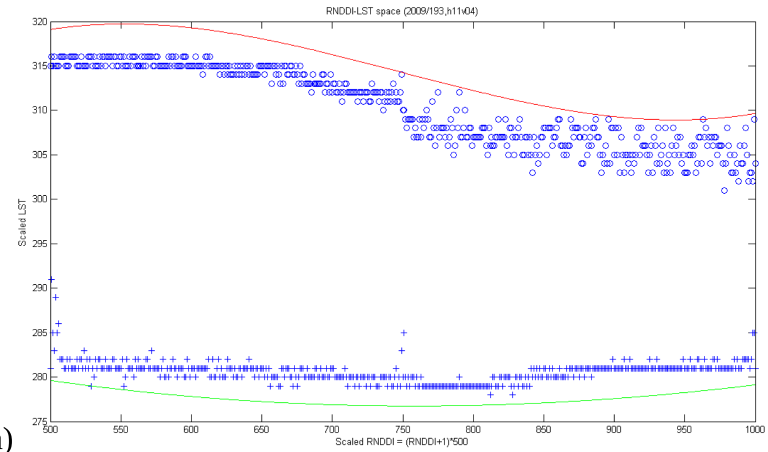

(a)

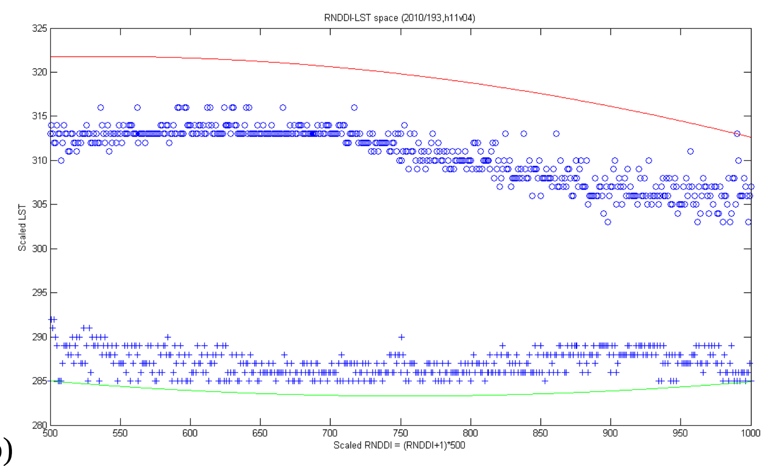

(b)

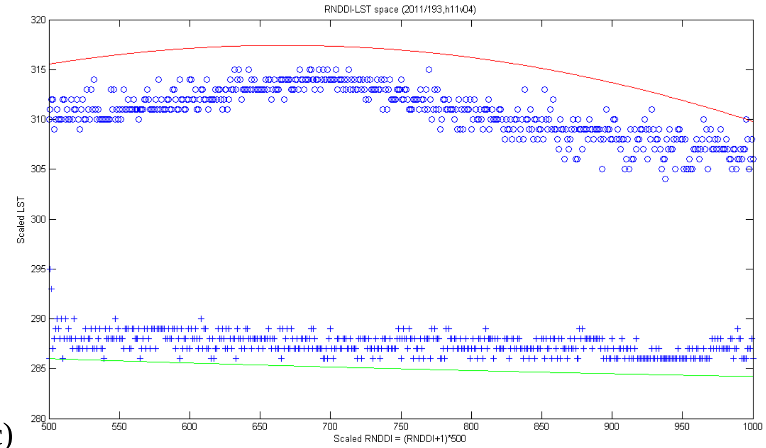

(c)

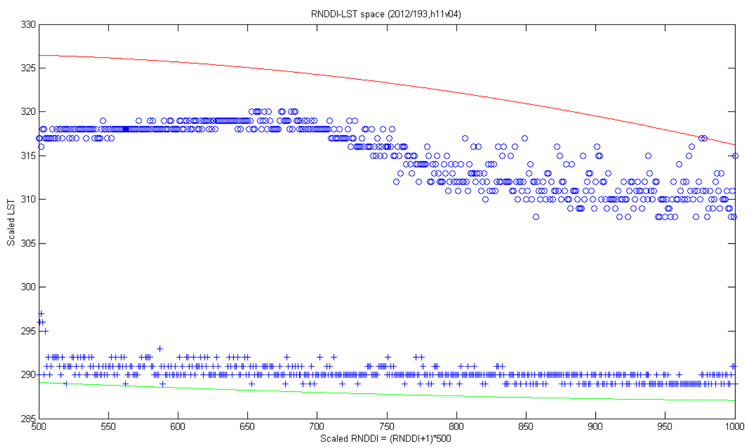

(d)

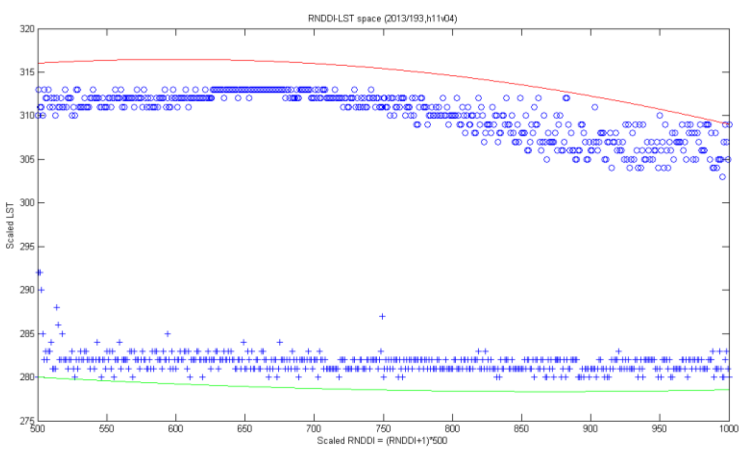

(e)

Figure 57 Scatter plot of pixels with the maximum, and minimum LST values, and the warm and cold edges derived via polynomial fit for the RNDDI/LST space of tile h11v04 for (a) 2009/193 – 2009/208, (b) 2010/193 – 2010/208, (c) 2011/193 – 2011/208, (d) 2012/193 – 2012/208, and (e) 2013/193 – 2013/208.

Table 20 Regression Equations for dry and wet edges.

DOY	Year	Dry Edge
193	2009	$LST_{RNDDIi,max} = -0.0008* RNDDI_i{}^2+0.563*RNDDI_i+190.6055$
	2010	$LST_{RNDDIi,max} = -0.0007* RNDDI_i{}^2+0.5169*RNDDI_i+188.8826$
	2011	$LST_{RNDDIi,max} = -0.0001* RNDDI_i{}^2+0.0916*RNDDI_i+282.0772$
	2012	$LST_{RNDDIi,max} = -0.001* RNDDI_i{}^2+0.7465*RNDDI_i+141.5928$
	2013	$LST_{RNDDIi,max} = -0.0006* RNDDI_i{}^2+0.4346*RNDDI_i+205.1171$
DOY	Year	Wet Edge
193	2009	$LST_{RNDDIi,min} =0.0001* RNDDI_i{}^2+0.0719*RNDDI_i+305.8931$
	2010	$LST_{RNDDIi,min} =0.0005* RNDDI_i{}^2-3.78*RNDDI_i+382.1718$
	2011	$LST_{RNDDIi,min} =-0.0065*RNDDI_i+291.1853$
	2012	$LST_{RNDDIi,min} =-0.0001* RNDDI_i{}^2+0.0607*RNDDI_i+307.7737$
	2013	$LST_{RNDDIi,min} =-0.0001* RNDDI_i{}^2-0.1006*RNDDI_i+309.3591$

With the polynomial curves representing warm and cold edges found, the CCI can now be computed with the RNDDI and LST value sets for each pixel (Equation 9). CCI is a ratio signifying the pixel's proximity to dry edge, ranging from 0 to 1. For display purposes, CCI is multiplied by 250, to yield an 8-bit integer ranging from 0 to 250 (with 253~255 as Fill Values). The Scaled CCI maps for five 16-day periods, namely, 2009/193-2009/208, 2010/193-2010/208, and 2011/193-2011/208, and the same area (tile h11v04), are put as Figure 58. The symbology used for the raster images generated here is "Unique Values" instead of "Stretched", since each of the pixel value is already a ratio. Each value from 0 to 250 is assigned a color continuously from red to green. Red color represents a low CCI value, meaning this pixel is experiencing drought; while the color shifts from reddish to greenish, the drought situation is mitigated; green color represents a high CCI value, meaning the pixel is of healthy vegetation. Cloud-polluted, or water/snow/ice covered pixels are here colored in white.

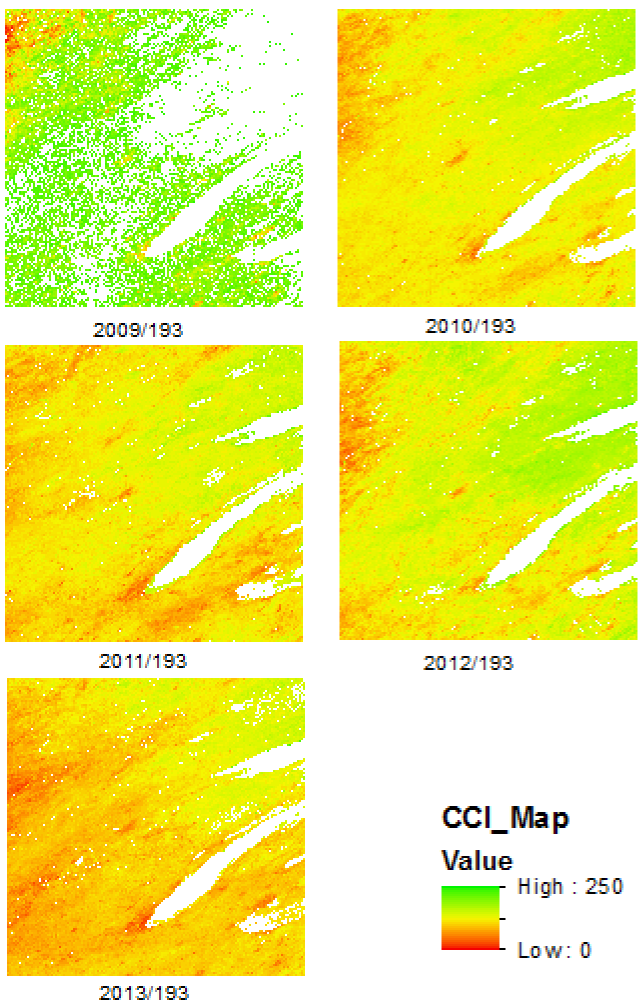

Figure 58 The CCI maps of tile h11v04 for 2009/193, 2010/193, 2011/193, 2012/193 and 2013/193.

Subsection 6.4.2 Temporal Pattern of CCI

CCI, as a measure to assess whether an area is suffering from vegetation drought stress, can be used to observe the temporal patterns of the areal vegetation growth conditions through crop growing seasons. In Figure 59, the CCI maps for the growing season of year 2009 are shown in a series. Comparing the vegetation growth conditions before and after 2009/193 (YEAR/DOY), the former is more likely to be experiencing drought stress. The CCI map of 2009/193, displaying large areas of green pixels, appears to be the healthiest during the period, or the peak of growing conditions. Because CCI is considering the dry/wet conditions of an area from a regional perspective (i.e. the wet and dry edges are drawn according to the minimum and maximum LST values of the region), compared to VCI which is calculated on a pixel basis, difference between CCI values of two neighboring pixels is not as large as that of VCI pixels. Unlike VCI maps on which pixel values change abruptly between neighbors (as in Figure 60), CCI maps by nature display smoothing patterns and thus resembles a real-life situation. For two adjacent fields, it is hardly possible for one to be suffering from severe drought while the other to be entirely stress-free.

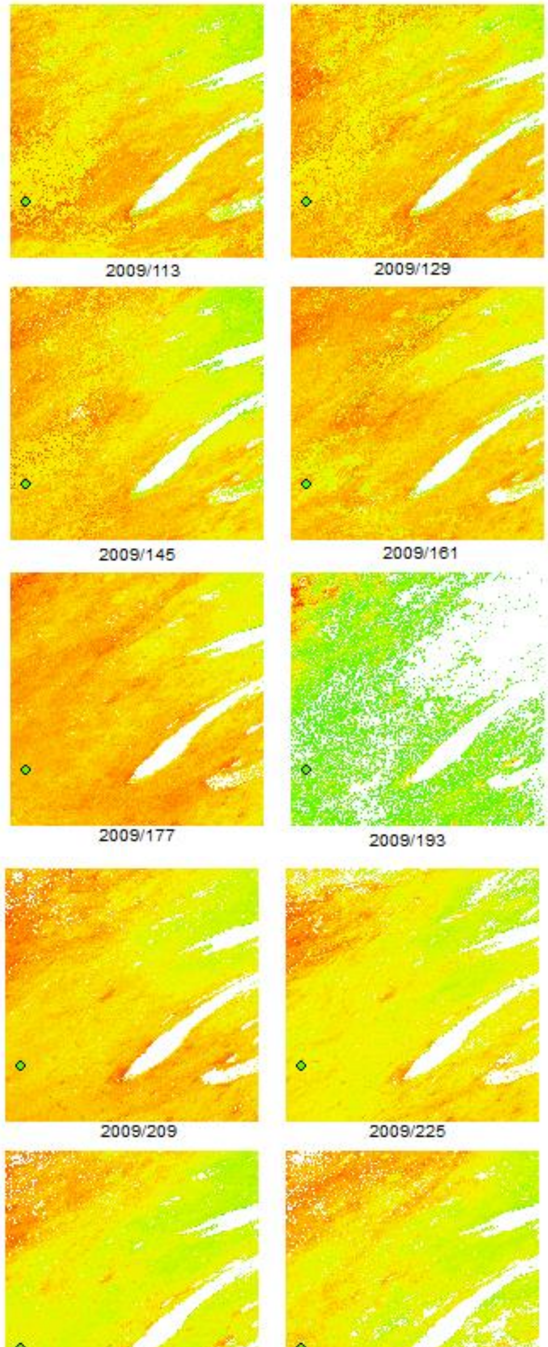

Figure 59 The CCI maps of tile h11v04 for the growing season of 2009 (which is from DOY 113 to 257).

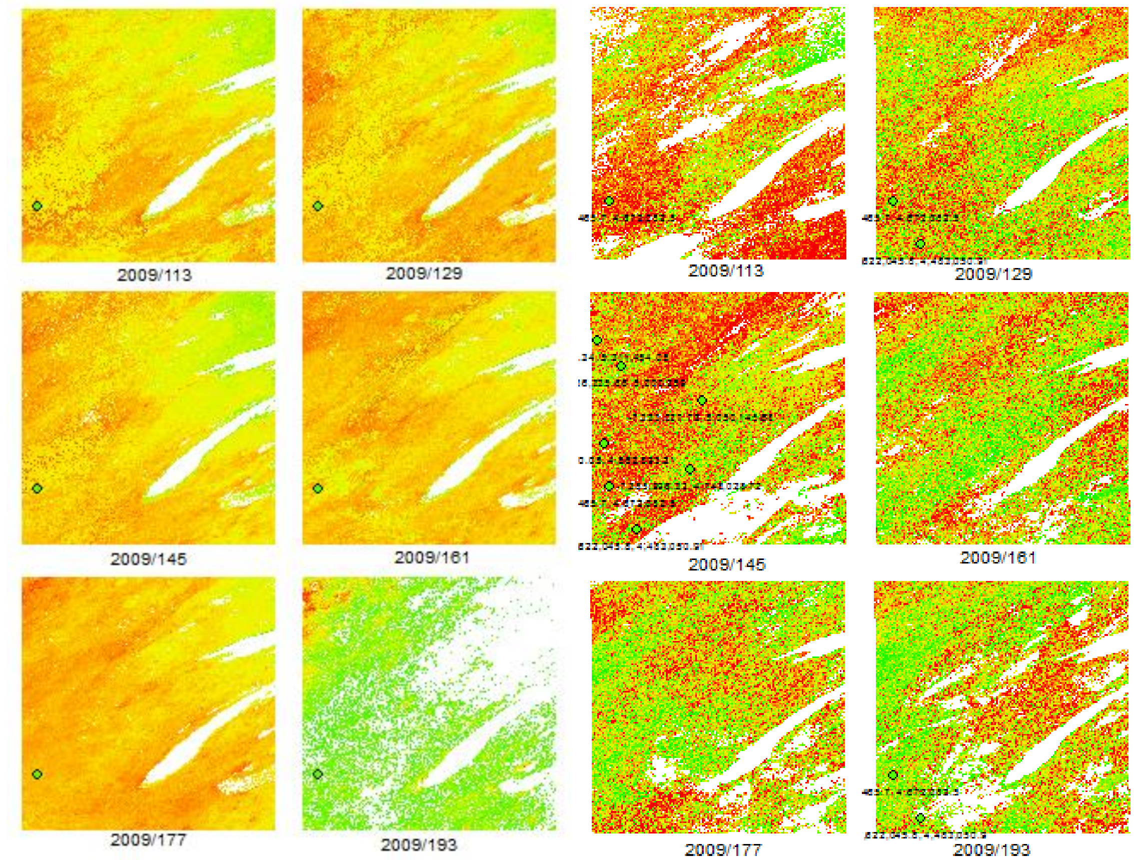

Figure 60 The CCI maps (left) VS. VCI maps (right) of tile h11v04 for the first half growing season of 2009 (which is from DOY 113 to 193).

Subsection 6.4.3 Spatial Pattern of CCI

Areas with accumulated low CCI values are those drought-affected areas most vulnerable to drought stresses. Shown in Figure 61 is the accumulated CCI for the area during the peak growing seasons through years 2009-2012. Reddish pixels represent areas most frequently suffering from drought stress during growing seasons, while greenish pixels are those areas least likely to be experiencing vegetation drought stress. At least three patterns can be observed from Figure 61: (1) green areas with high CCI values on the northeast, (2) red areas with low CCI values on the northwest, and (3) yellow areas with mid CCI values for the rest of the area. This spatial distribution of high to low CCI values through multiple years correspond to the crop distribution patterns for the area: (1) deciduous forest at the northeast, (2) grass at the northwest, and (3) corn or soybeans for rest of the area. The fact that CCI shares a similar distribution pattern with crop types has led us to two conclusions: First, vegetation dryness/wetness represented by CCI is relative to crop type, for instance, the CCI value of deciduous forest is often higher than that of grass. Second, in order to illustrate a site or an area is wetter or dryer than previous year, it is crucial to make sure the comparison is established on the same site or area that is of the same vegetation type; or else, the comparison is meaningless.

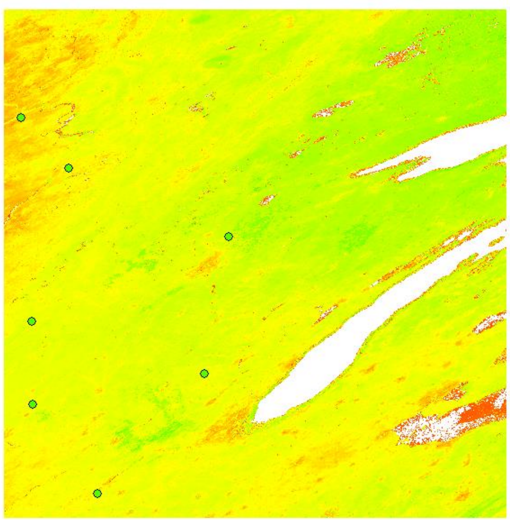

Figure 61 Areas with accumulated CCI values during peak growing seasons through multiple years, and seven points representing SCAN sites from multiple states.

Subsection 6.4.4 CCI and Root-zone soil moisture Observations

In order to validate CCI as an effective measure to monitor drought stresses, root-zone soil moisture observations under different canopies at various depths are chosen, since soil moisture is a direct indicator for drought or non-drought. Daily observations at each of the SCAN sites (starting from spring of 2000) were composited into 16-day precipitation or soil moisture data, masked with a dominant crop type, and input as dependent variables for regression models established with CCI or VCI.

Tables 21 and 22 display the Pearson Correlation Coefficient between CCI/VCI and precipitation/soil moisture at various depths with lag periods of 0, 16, 32 and 48 days. Because crop growing conditions are influenced by soil moisture at various depths with different lag periods, depending on crop type and geo-location, using soil moisture as a validation source for CCI needs to be performed with the correct depth and lag period. Take site #2031 as an example, the best correlation result for linear regression between CCI and root zone soil moisture takes place at depth of 4 inches and when lag period is 32 days (r = -0.901), and the best result for that between VCI and root zone soil moisture (r=0.456) happens at the same depth (-4 inches) and lag period (32 days). Site #2031 is planted with corn during the selected years, and from conclusions of Chapter 5, corn-specific VIs have higher correlation to root zone soil moisture levels at deeper earth (>=4 inches) and with longer lag period (>=32 days), which corresponds to the result as shown in Tables 21 and 22. As a result of the comparison, CCI is correlated to RZSM at higher degrees than VCI is for site #2031.

Site #2020, planted with soybeans, is another example. The best correlation result for linear regression between CCI and root zone soil moisture takes place at depth of 2 inches and when lag period is 16 days (r = -0.644), and the best result for that between VCI and root zone soil moisture (r=0.609) happens at the same depth (-2 inches) and lag period (16 days). Site #2020 is planted with soybeans during the selected years, and from Chapter 5, soybeans-specific VIs have higher correlation to root zone soil moisture levels at shallower earth (<=2 inches) and with shorter lag period (<=16 days), which corresponds to the result as shown in Tables 21 and 22. As a result of the comparison, CCI is correlated to RZSM at higher degrees than VCI is for site #2020 as well.

Table 21 Pearson Correlation Coefficient between CCI and precipitation or soil moisture at various depths.

SCAN Site	Lag Period	Precip	SM-2	SM-4	SM-8	SM-20	SM-40
#2020 (ND)	Concurrent	0.426	-0.224	-0.204	-0.292	-0.359	-0.297
	16days	-0.131	-0.644	-0.604	-0.595	-0.343	-0.406
	32days	0.416	-0.424	-0.189	-0.242	-0.222	-0.386
	48days	0.235	-0.369	0.303	-0.262	-0.276	-0.438
#2120 (MT)	Concurrent	0.179	0.360	0.376	-0.339	-0.153	-0.147
	16days	0.330	-0.538	-0.568	-0.636	0.356	0.595
	32days	-0.746	-0.714	-0.720	-0.153	0.438	-0.222
	48days	0.724	-0.086	0.025	0.013	0.274	-0.111
#2072 (SD)	Concurrent	-0.703	0.366	0.010	-0.079	NaN	0.447
	16days	0.094	0.386	0.232	-0.300	NaN	0.737
	32days	0.185	0.371	0.179	-0.197	NaN	0.219
	48days	0.156	0.026	-0.120	0.174	NaN	0.710
#2031 (IA)	Concurrent	-0.552	-0.662	0.513	0.323	-0.450	-0.535
	16days	0.095	-0.492	-0.480	-0.741	-0.468	-0.530
	32days	-0.744	-0.389	-0.901	-0.807	-0.352	-0.488
	48days	0.096	0.249	-0.236	-0.346	0.457	-0.175
#2002 (MN)	Concurrent	-0.182	-0.236	0.092	-0.020	0.419	0.692
	16days	0.170	0.139	0.093	0.164	0.185	0.060
	32days	0.371	-0.235	0.256	0.063	0.296	0.581
	48days	0.088	0.789	0.989	0.776	0.888	-0.697

Table 22 Pearson Correlation Coefficient between VCI and precipitation or soil moisture at various depths.

SCAN Site	Lag Period	Precip	SM-2	SM-4	SM-8	SM-20	SM-40
#2020 (ND)	Concurrent	-0.452	-0.557	-0.555	-0.498	-0.482	-0.428
	16days	-0.031	-0.609	-0.602	-0.550	-0.544	-0.502
	32days	0.236	-0.537	-0.586	-0.554	-0.529	-0.483
	48days	0.548	-0.498	-0.072	-0.262	-0.166	0.093
#2120 (MT)	Concurrent	-0.245	-0.127	-0.086	-0.306	-0.120	-0.396
	16days	0.439	-0.369	-0.374	-0.671	0.014	0.158
	32days	-0.387	-0.665	-0.680	-0.602	0.283	-0.280
	48days	0.428	-0.721	-0.650	-0.446	0.502	0.278
#2072 (SD)	Concurrent	0.164	0.590	0.606	0.135	NaN	0.173
	16days	0.284	0.304	0.167	0.104	NaN	0.511
	32days	0.463	0.056	-0.285	-0.103	NaN	0.170
	48days	0.045	-0.671	-0.783	-0.612	NaN	-0.080
#2031 (IA)	Concurrent	-0.182	-0.236	0.092	-0.020	0.419	0.692
	16days	0.170	0.139	0.093	0.164	0.185	0.060
	32days	0.371	-0.235	0.456	0.063	0.296	0.381
	48days	0.088	0.189	0.189	0.176	0.188	-0.197
#2002 (MN)	Concurrent	-0.032	0.066	0.480	0.465	0.716	0.852
	16days	0.867	0.620	0.780	0.624	0.609	0.467
	32days	0.353	-0.925	-0.696	-0.833	-0.647	-0.426
	48days	-0.905	0.132	-0.368	0.154	-0.845	-0.268

The “residuals versus fitted” plots for both sites are shown in Figures 62, and 63 respectively. The y-axis of Figure 62 is displaying the RZSM values observed at sites #2031 (at the depth of 4 inches, and with a lag period of 32 days) and that of Figure 63 is showing the RZSM values collected at #2020 (at the depth of 2 inches, and with a lag period of 16 days). Fitted values, drawn as x-axis on both figures, are the differences between observed and estimated RZSM levels at the sites. The estimated RZSM is either derived from the linear regression model using CCI as an independent variable as in Y = a*CCI + b (e.g. the first plot in Figure 62), or from that using VCI as an independent variable as in Y' = a'*VCI + b' (e.g. the second plot in Figure 62). The residuals bounce randomly around the 0 line, suggesting that the assumption that the relationship between vegetation index and root zone soil moisture is linear is reasonable.

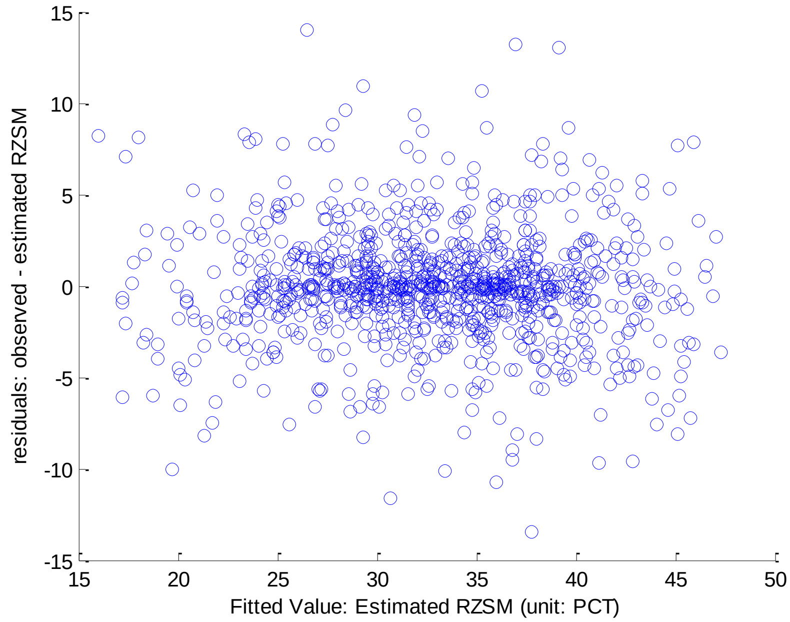

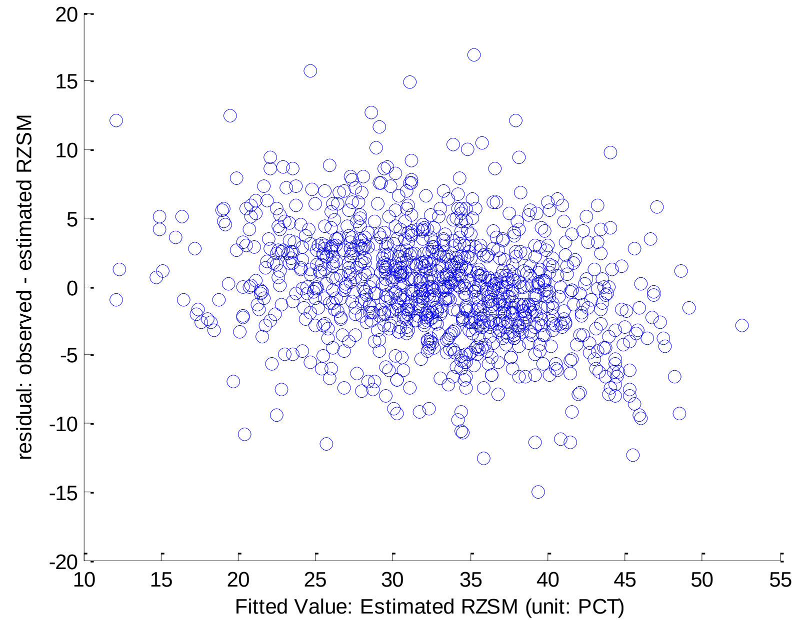

Figure 62 The residuals vs fits plots for site #2031; estimated RZSM is displayed on the x-axis, while the residual of subtracting estimated from observed RZSM is shown on y-axis. (Top) Estimation of RZSM is made with linear regression model of CCI; (Bottom) Estimation of RZSM is made with linear regression model of VCI.

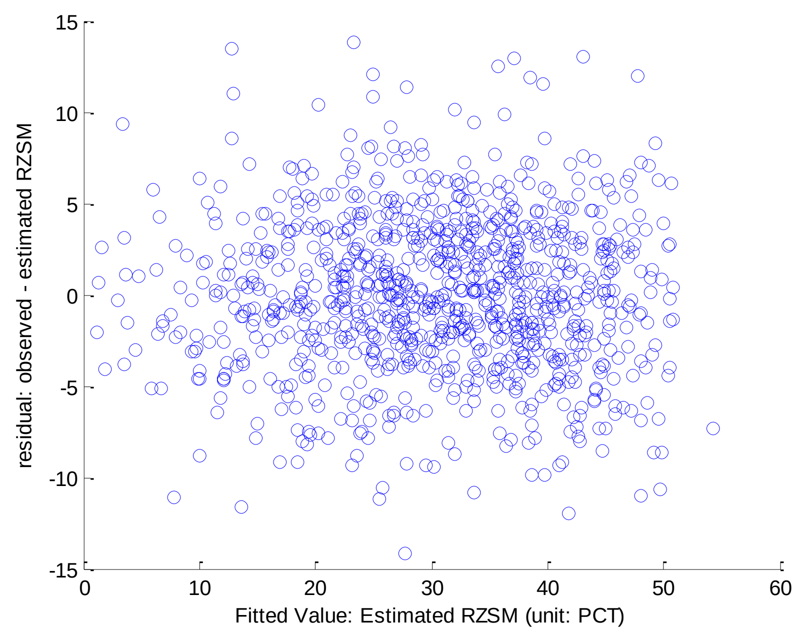

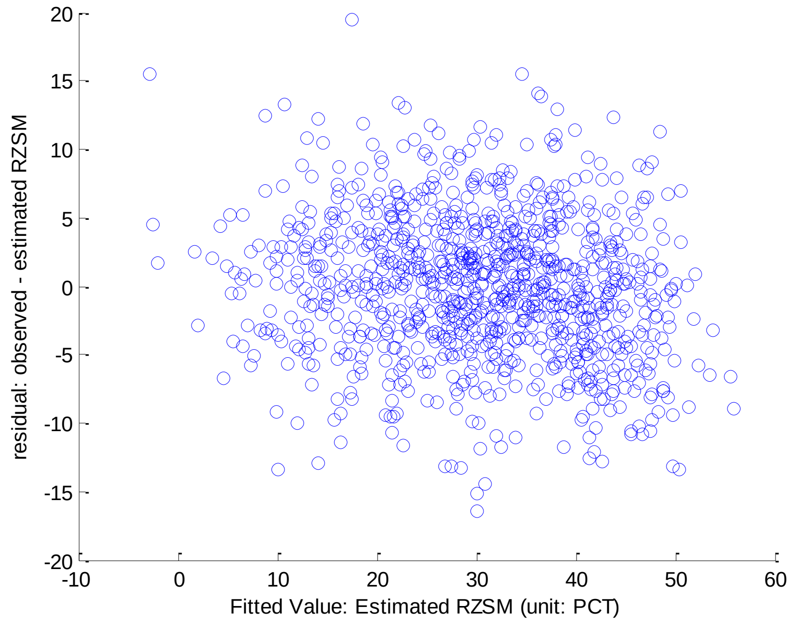

Figure 63 The residuals vs fits plots for site #2020; estimated RZSM is displayed on the x-axis, while the residual of subtracting estimated from observed RZSM is shown on y-axis. (Top) Estimation of RZSM is made with linear regression model of CCI; (Bottom) Estimation of RZSM is made with linear regression model of VCI.

Other regression models have been applied onto RZSM vs. CCI and RZSM vs. VCI as well. For instance, cubic regression models have yielded good correlation results as well. For corn-vegetated site (#2031), the best correlation result for cubic regression between CCI and root zone soil moisture takes place at depth of 4 inches and when lag period is 32 days (r = 0.912), and the best result for that between VCI and root zone soil moisture (r=0.651) happens at the same depth (-4 inches) and lag period (32 days). As for soybean-vegetated site (#2020), the best correlation result for cubic regression between CCI and root zone soil moisture takes place at depth of 2 inches and when lag period is 16 days (r = 0.673), and the best result for that between VCI and root zone soil moisture (r=0.419) happens at the same depth (-2 inches) and lag period (16 days). From the results shown above, CCI has higher correlation to RZSM than VCI for soybeans fields under the assumption that cubic regression model is valid for RZSM and VI as in RZSM $= a*VI^3 + b*VI^2 + c*VI + d$.

Section 6.5 Results and Conclusions

Results of the experiments have shown that, fitting CCI or VCI as independent variable, and RZSM as dependent variable into a linear or cubic regression model, correlation coefficient between CCI and RZSM is higher than that between VCI and RZSM. Soil moisture observations at various depths and with different lag periods have been investigated in this experiment and results indicate that for corn field of #2031, RZSM at depth of 4 inches and 32 days lagging behind is more sensitive than others as an indicator for drought or non-drought, while for soybeans field of #2020, RZSM at depth of 2 inches and 16 days of lag period performs better as in indicating drought or non drought for vegetation.

CCI, as a drought indicator, will provide a new foundation of physics based indices for monitoring vegetation health, moisture and thermal conditions from space. Combining information from multiple channels makes CCI response to vegetation drought conditions in opposite directions and therefore, a promising indicator for vegetation drought monitoring. Its highest overall performance and discrimination power compared to other vegetation indices (either single VI, or indices that have not considered moisture, thermal and vegetation health all at a time) demonstrated its ability for active drought detection. This index can be applied to the next generation of satellite instruments to extract information about vegetation drought condition.

Section 6.6 Future Directions

Though CCI has been shown to be an exact indicator for vegetation drought condition, it is limited in these aspects: (i) it ignores the errors in NDWI and NDVI values when being collected from different soil wetness conditions; (ii) experiments have been performed under the assumption that users have a clear idea of which RZSM source should be used for regression models, and this knowledge is hard to obtain in the sense that users may need to study root depth, water intake habit, and growing patterns of each crop; (iii) the research has focused onto corn and soybeans fields within the Corn Belt area; more studies need to be done for multiple crop types over various climate regions in order to achieve a general knowledge of whether CCI can be applied as a global drought indicator.

Recommendations for future research fall into three categories, namely: (i) develop a general CCI approach that would consider group behaviors of crops having the similar rooting depths; (ii) extensive applications of CCI for drought monitoring and vegetation drought stress detecting for various crop types across the globe; (iii) apply different regression models to make sure if there will be any other fitting models between VI and RZSM, e.g. Taylor series approximation, and Natural Spline Smoothing; (iv) improvements of drought information web service; and (v) development of an operational system for global drought monitoring.

CHAPTER 7 AGRICULTURAL DROUGHT INFORMATION WEB SERVICES

Section 7.1 Background

The unprecedented data-collecting capability of earth observing satellites has brought considerable challenges to geospatial research and applications, one of which is the difficulties in deriving high-level information and knowledge from the massive amount of data in an effective and timely manner. This is an era of data richness and analysis poverty, and thus the world is calling for semi- or fully-automated geospatial knowledge discovery and dissemination to take care of geospatial data and applications.

Service-Oriented Architecture (SOA) has shown prospects for providing valuable geospatial data and processing functions for worldwide open use. With SOA, previously used software applications and supporting infrastructure are re-organized into an inter-connected set of services, and each of these services are accessible through standard interfaces and messaging protocols (Papazoglo, 2003). In real practices, the Web Services technologies have been explored by multiple agencies or organizations, such as the Global Earth Observation System of Systems (GEOSS) (GEOSS, 2012) and the U. S. NASA GES-DISC (Goddard Earth Sciences Data and Information Services Center) Interactive Online Visualization ANd aNalysis Infrastructure (Giovanni) (Berrick et al., 2009).

Web Service technologies, aiming to implement SOA, allow such an infrastructure to be set up for collaborative sharing of distributed resources as geospatial data, processing modules, and process models. A Web Service is designed to support interoperable machine-to-machine interaction over a network, via a standard interface that enables the interoperation between various software systems or web portals, so a set of Web Services developed by various organizations can be connected and applied in a chain to fulfill users' requests (Booth et al., 2004; Yue). Open Geospatial Consortium (OGC) standard-compliant services, including Web Feature Service (WFS), Web Map Service, Web Coverage Service (WCS), Catalogue Services for the Web (CSW) and Web Processing Services (WPS), are the most notable services being interoperable in publishing, discovery, chaining, and execution through the Web (Vretanos, 2010; de la Beaujardière, 2006; Baumann, 2010; Bröring et al., 2012; Nebert et al., 2007; Schut, 2007).

However, in order to support problem-solving and scientific discovery in the geospatial Cyberinfrastructure, development of high-level intelligent services (acting as middleware) and domain-specific services is in urgent need. The heavy analysis and synthesis demands of such services have been challenging to researchers (Hey & Trefethen, 2005; Brodaric et al., 2009). As addressed by Di (2004), the upcoming task is to extend capabilities on dynamically and collaboratively developing interoperable, Web-executable geospatial service modules and models, which can be applied online to any part of the peta-byte archives to obtain customized information products rather than only raw data.

Section 7.2 Web Services for Aggregational Agricultural Drought Information

Subsection 7.2.1 Introduction

This section explores the advantages of providing on-demand web-based agricultural drought analysis on top of an existing platform that is ready for data downloading and visualization. With the widespread adoption of GIS technologies and the availability of continuous or fine-scale meteorological and hydrological information in recent years, drought information can be collected and processed as a continuous geo-referenced data set with as fine a spatial resolution as observing technologies allow. The information can be aggregated to appropriate physical and jurisdictional domains as the user group desires. On a statewide basis, standard aggregational units should include counties as well as river drainages relevant to surface water storage. In addition, the geo-referenced information should be available for individual planners and users for user-specific extraction and aggregation.

Russell Ackoff (1989) pointed out that the human perception and recognition process includes four steps – data, information, knowledge and wisdom. In this sense the process for researchers to understand agricultural drought can also be divided into four phases: (1) access/download remotely sensed images or meteorological ground measurements from various data providers, (2) process and calculate the agricultural drought indicators representing several perspectives: vegetation conditions, crop phenology, soil moisture levels, climate types, etc., (3) integrate major indicators according to user-customized analysis model to generate drought severity maps for the chosen area and create drought reports based on statistical results, and (4) form an applied knowledge of the geospatial patterns and temporal frequencies of agricultural drought, and what are the environmental factors that exert the most important influences to drought severities of an area. In this article, the transition from data to information and knowledge is accomplished using web-based GIS services.

In addition to (i) aggregation of vegetation indices (VI) based on different spatial units, (ii) classification of aggregated VI into according drought severity groups, (iii) providing percentage analysis of each drought severity group, and (iv) generating time-series VI and drought severity information for selected area, the Web Services covered in this article also take care of presentation of (a) attribute information, and (b) display information (Nagarajan, 2009).

In this chapter, the transition from data to information and knowledge is accomplished by automated delivery of agricultural drought information and knowledge using web-based GIS services (Bonham-Carter, 1994; Huang et al., 2001; Satti & Jacobs 2004). In specifics, four Web services will be presented in details for illustration purposes: GetROI to visualize the drought patterns of a selected area and time, GetVCIStats to capture the mean VCI value for the chosen region of interest, GetDroughtPercentageByStates to depict the distribution of various drought severity groups for multiple chosen states, and GetDroughtTimeSeries to describe the time-series drought information of the county, Agricultural Sciences Division (ASD) or state specified in a request.

This research work aims to fill a major gap of existing studies in sharing and disseminating agricultural drought information. With the availability of continuous and finer-scale remote sensing data (Kumar & Panu, 1997; McKee et al., 1993; Shiau & Shen, 2001; Steinemann et al., 2005; Peng et al., 2012; Yagci et al., 2013) in recent years, drought information have been collected and processed as a continuous geo-referenced data set with finer spatial resolution. The information can be and should be aggregated into as appropriate physical or jurisdictional domains as a user group desires (Issaks & Srivastava, 1990; Raper, 2000; Tucker & Sellers, 1986). For example, standard aggregation units on a statewide basis should include counties as well as river drainages relevant to surface water storage. In addition, the geo-referenced information should be online available for individual users to extract and aggregate user-specific knowledge. USDM labels droughts by intensity, with D1 being the least intense and D4 being the most intense (and D0 is either drying out, or recovering from drought). Besides the weekly maps displaying broad-scale drought conditions, USDM also supports a tabular data archive that shows percent area in the array of drought categories for each state, region (High Plains, Midwest, Northeast, South, Southeast, and West), Contiguous U. S., or the entire U. S. (USDM Website, 2014). However, users will find this information insufficient and hard to manipulate. First, a randomly selected area cannot be used as the geospatial unit for drought analysis. Second, historic drought information (esp. through years) will be hard to gather since USDM returns weekly result per single request. Last, comparison across different areas and visualization to facilitate comparing are difficult using USDM because users may need to collect values for different areas into spreadsheet, and create bar charts or other illustrative graphs using software (e. g. Excel). Due to the fact that existing research cannot fully explore the potentials of Web Service technologies or realize the desired capabilities by users, there is an urgent need to extend the capabilities of drought portals in an online and on-demand manner, namely, providing Web Services which can efficiently support the agricultural drought management and decision-making.

Subsection 7.2.2 Presentation of Agricultural Drought Information

There are two major parts in presenting agricultural drought information – attribute and display information. Attribute information used to characterize a drought event includes where (location and spatial extent of drought), when (start time and duration of drought), and how (severity or intensity of drought, and the distribution of drought severity groups). On the other hand, display information shall contain how the information is to be shown – either by scatter plots, bar charts, pie charts, lines or by maps – and the thresholds and color representation of each drought group if shown in maps. Without dual consideration into presenting attribute and display information simultaneously, the delivery of drought data, information, and knowledge will not succeed.

7.2.2.1 Choose the optimized thresholds to classify drought severities

In purpose to map the value of VI to a drought severity ranking, and hence give users a straight view of the spatial distribution patterns of various degrees of agricultural drought, the classification scheme need to be selected with care.

USDM has become one of the most respected tools for characterizing drought in the United States. One of the keys to its success is the establishment of drought intensity scale, which is likened to the Enhanced Fujita scale for tornadoes and Saffir-Simpson scale for hurricanes. USDM uses a percentile ranking approach allowing authors to compare different parameters which have different units and lengths of record regardless of location. The USDM approach also adds duration and both regional and seasonal influences into consideration, as well as whether a given location is improving or worsening in terms of drought conditions.

Table 23 Drought Intensity Scale used by USDM (source: http://www.drought.gov/drought/content/understanding-drought-printable-version#p2_4)

Drought Level and description
D0: At this level, an area experiences short-term dryness that is typical with onset of drought. This kind of dryness can slow crop growth and elevate fire risk to above average. Also, this level can refer to an area coming out of drought, with lingering water deficits and pastures or crops not fully recovered. Drought level 0 is noted when a convergence of indicators fall into the 30th percentile, which is to say, roughly a 1-in-3-year dryness.
D1: "Moderate Drought", the first drought class and falls into the 20th percentile, or a 1-in-5-year type event.
D2: "Severe Drought", within the 10th percentile, which roughly equates to a 1-in-10-year drought.
D3: "Extreme Drought" that falls into the 5th percentile, or a 1-in-20-year type of drought.
D4: "Exceptional Drought". Worst on the scale, D4 can be loosely defined as a "once-in-a-generation" type of drought noted by the 2nd percentile, or a 1-in-50-year drought.

As shown in Tables 23 and 24, D0 conditions have a 21-30% chance of occurring in any given year at a given location, while D1 events occur 11-20% of the time. A D2 drought would be expected 6-10% of the time, and the chances of D3 or D4 droughts happening are at 3-5% and 2% or less, respectively. Kogan (1995) has linked the value of Vegetation Health Index (VHI) to these five categories of drought severities, with a VHI ranging from 0 to 1, a VHI value equal to or lower than 0.05 represents a D4 drought, while that equal to or larger than 0.45 means the area is not suffering from drought at all.

Table 24 Alternate representation of the Drought severity classification used by USDM.

Category	Description	Drought Indicator (Percentiles)	Satellite Vegetation
D0	Abnormally dry	21-30	0.36-0.45
D1	Moderate drought	11-20	0.26-0.35
D2	Severe drought	6-10	0.16-0.25
D3	Extreme drought	3-5	0.06-0.15
D4	Exceptional drought	0-2	0.01-0.05

7.2.2.2 Choose the optimized spatial unit for drought assessment

In order to effectively determine the spatial areal extent of drought impact area, the first thing is to decide at which spatial level the drought assessment takes place.

Aside from the pixel-by-pixel drought assessment provided by current coarse or fine resolution drought monitoring information systems, it is also important to consider the drought situations from the point of view of potential or likely users of the drought information, in the sense that users might have a preference towards a certain level of administrative units, or hydrant basin, etc. Many applications use the county as a logical unit for drought assessment. The size of counties is more or less similar to each other, compared to that of states, and the county is a standard unit of local government, of which most disaster declarations are made on the basis. Meteorological information is generally available on a county scale, but no smaller, except for radar-estimated precipitation. The county is probably the most appropriate scale on which to make subjective assessments of drought severity.

However, there are other jurisdictional units for which moisture and drought information would be critical. For example, all individual water suppliers require information over the geographical area for which they supply water, to understand past, current, and future water demand. In addition, for surface water supplies and aquifer recharge, the water suppliers require information over the drainage that supplies their reservoir or the recharge area for their aquifer, to understand past, current, and future water supply. Finally, if other water suppliers make use of the same water supply and possess priority of water rights, the water supplier will require information about drought conditions in all other locations for which water from their source is used. For such users of drought information, any single geographical unit for drought information reporting will provide suboptimal or possibly useless information.

Calculation of drought indices from raw data and aggregation of pixel-level information to county-level or higher levels will require considerable care with the geospatial units. First, raw data or drought indices are not always based on the same spatial unit – for example some are designed for climate divisions while others made for counties – and adjustment (or say, re-sampling) is required before being applied to a finer scale. Second, a few common drought indices assess drought severity using historical records as reference, and challenge is raised when the drought indices are to be computed at a finer scale – there can be no historical record existing at such fine resolution. Third, aggregated information cannot be used for further aggregation, and drought indices must be recomputed separately for each aggregation level. For instance, if there are two counties of a studied area– one is characterized as a D1 drought (i.e. 11-20% of chances for drought to happen in 100 years) and the other as a D3 drought (i.e. 3-5% of chances for drought to happen in 100 years) – simply adding these two ranks together and making the conclusion that the studied area is experiencing a D2 drought (i.e. 6-10% of chances for drought to happen in 100 years) is not reasonable. Instead, the preferred approach is to compute the vegetation index for the area and map the value to a corresponding drought severity level whenever to up- or down- scale the aggregational unit.

7.2.2.3 Quantify the confidence of agricultural drought

Data quality issue is very important to the information coming out of aggregation of spatial units. With the pixel-level drought information being aggregated into county-, ASD-, state-, or even country-level, the data quality of this piece of drought information becomes a big concern.

The measures proposed to quantify drought are the percentage of different levels of drought severities, the median of drought severities within the area, and the degree of uncertainty of agricultural drought.

For example, if for a county, the percentage of pixels residing on six drought severity levels is distributed as: D4 (0.112916), D3 (0.021477), D2 (0.027017), D1

(0.762346), D0 (0.042318) and No-Drought (0.033926). Since the majority of pixels are ranked as D1, and for all the pixels, median of their drought severities reside on D1, the entire county can be categorized as D1.

To describe the effect of transition range, or say, to describe how uncertain drought characterization is, the dissertation proposes another measure called vagueness (defined in Equation 14). This measure takes values in the unit interval [0, 1], with values close to 1 showing high uncertainties, and values close to 0 showing low uncertainties. Hence in this example, vagueness of the county residing in D1 is 1 – 0.762346 = 0.237654.

Equation 14 Drought Vagueness of any area residing in drought severity of median.

$$DV = 1 - percentage(median)$$

Here, *median* is the drought severity ranking which has the highest percentage among D4, D3, D2, D1, D0 and non-drought. In the example mentioned above, the *median* value will be 1, and *DV* represents the percentage of pixels within the selected area that are not residing on drought severity of *median*, and thus is a reflection of how uncertain the statement (of the area is experiencing degree median drought) is compared to the real situations.

Subsection 7.2.3 The foundations of Web Service

Web Services are defined as self-contained and self-describing application components communicating on the Web using open protocols; they can be discovered using UDDI (short for “Universal Description, Discovery and Integration”), usable by other applications, and based on HTTP and XML (W3Schools Website). Web services have been around since 2000, and they were originally developed by IBM, Microsoft, Ariba, and many others, and then submitted to the World Wide Web Consortium (W3C) (IBM Website).

In order to make services discoverable over the web, an XML document which specifies the location of the service and the operations (or methods) the service exposes is necessary, and it is called Web Services Description Language (WSDL). Speaking of where to search for and publish a WSDL file, UDDI comes into the picture. A UDDI is a directory service where businesses can register and search for Web services. This platform-independent framework is in charge of describing services, discovering businesses, and integrating business services over the Internet (W3Schools Website).

The Service-oriented architecture (SOA) is where everything happens. It provides the core mechanism for publishing, finding, and binding Web services with three key elements: Web service provider, Web service directory, and Web service client (service requester). For example, the service provider firstly publishes a WSDL to the UDDI (which is a web service directory). Then the Web service requestor discovers services that are published in the UDDI, and uses the WSDL to generate a Web service client. The latter can interact in an interoperable way by sending and receiving XML-based Simple Object Access Protocol (SOAP) messages, which is a protocol based on XML for accessing web services. Hence the communication between service provider and service requestor has been established (Figure 64). The Web Services mentioned in the research have been developed in such a manner.

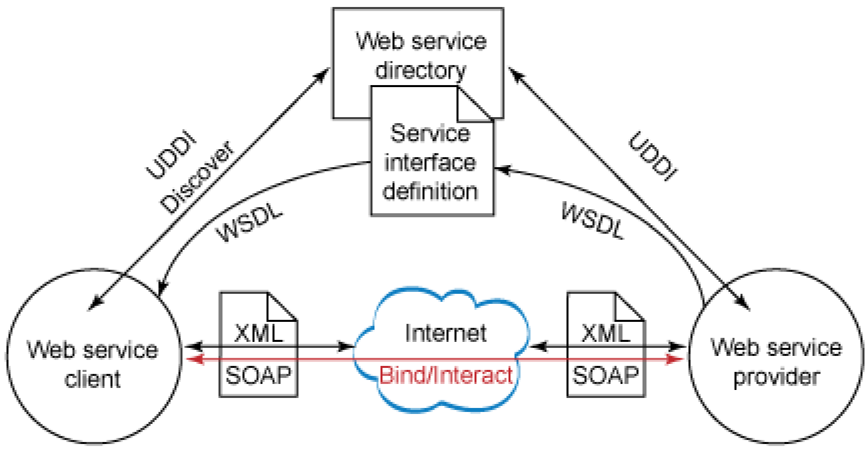

Figure 64 An SOA model (source: IBM website)

Subsection 7.2.4 Implementation of Drought Information Web Service

The Web Services developed for drought analysis and information management have four major characteristics (1) Service Oriented Architecture (SOA) and AJAX enabled web applications, (2) interoperable and ready to be incorporated into other web processing workflows, (3) providing powerful time series drought data analysis, and (4) compliant to Open Geospatial Consortium (OGC) standard-compliant services, including Web Feature Service (WFS), Web Map Service, Web Coverage Service (WCS), Catalogue Services for the Web (CSW) and Web Processing Services (WPS), and the functionalities to be implemented via these services include (i) aggregation of vegetation indices (VI) based on different spatial units, (ii) classification of aggregated VI into according drought severity groups, (iii) providing percentage analysis of each drought severity group, (iv) generating time-series VI and drought severity information for selected area, and (v) presentation of attribute information and display information.

The developed Web services are integrated in the Global Agricultural Drought Monitoring and Forecasting System (GADMFS) (Deng et al., 2012, 2013), which provides access, downloading, and visualization of daily, weekly, and per-16-day Normalized Difference Vegetation Index (NDVI) and Vegetation Condition Index (VCI) at global scales. With the deployment, the information output from the agricultural drought information system is in an organized manner to yield useful knowledge, often as maps and images, but also as statistical graphics, tables, and in-browser responses in various forms to interactive requests. Figure 65 depicts the required input to invoke drought analysis including data of remotely sensed and meteorological sources, vector data of administrative units, and socio-economic reports, and the expected output of drought analysis Web Services, such as drought maps, and drought statistics reports. A detailed picture of the transition steps from data to information can be seen in Figure 66. The functional capabilities for data capture, input, manipulation, transformation, visualization, combination, analysis, query, and output are all considered as manipulative/analytic operations.

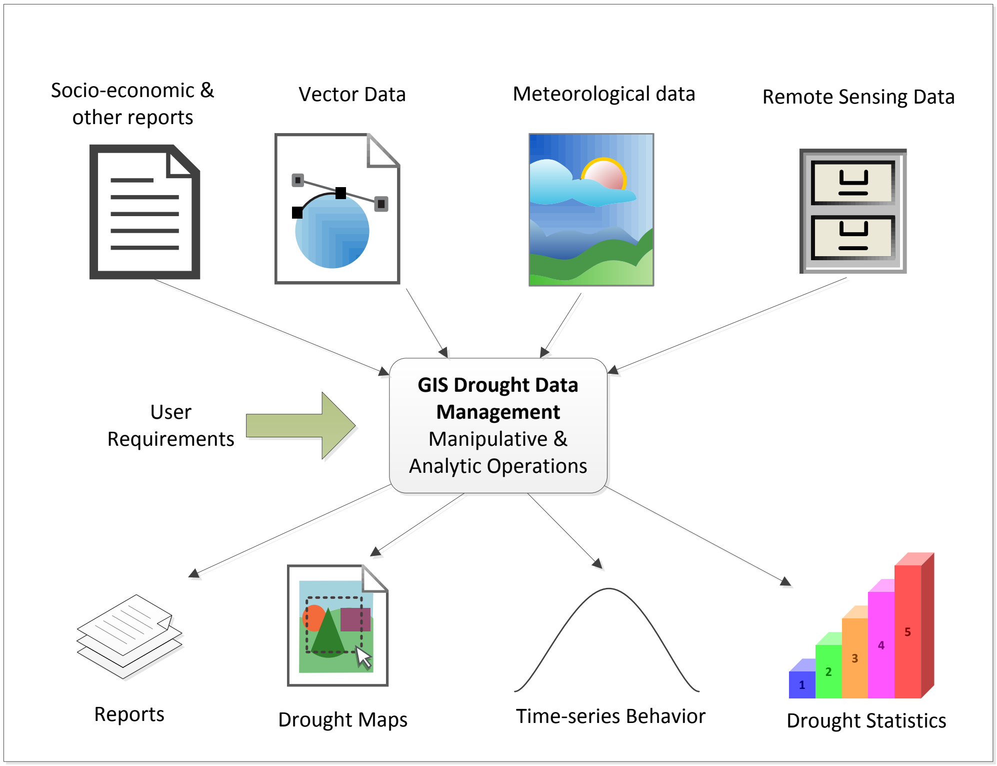

Figure 65 Schematic diagram showing generalized input and output of an agricultural drought information system.

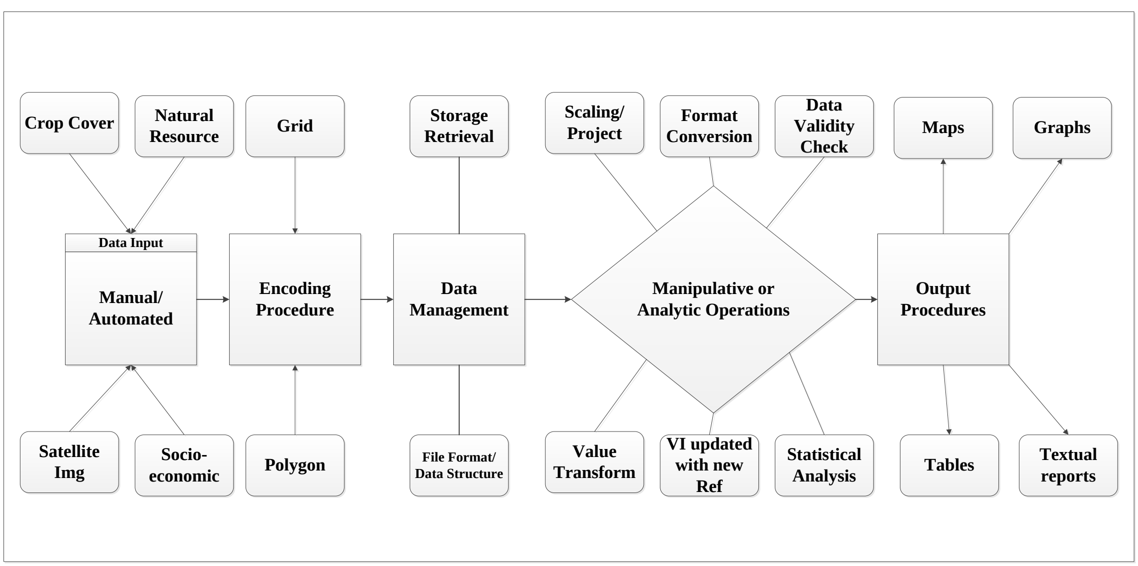

Figure 66 Functional modules of agricultural drought information system.

The business objects are modeled using XML schema and the client side will talk to the server side over Web Service using AXIS2. Also, the business logic of drought analysis has been packaged and deployed with AXIS2. Figure 67 shows the data exchange path between the business logic, AXIS2 server, AXIS2 Client, and the client side. The data exchanged between the client and server side will be drought analysis request containing location, and time, and function name, and the drought analysis response pointing to the URL address where users can view or download their requested resources/answers.

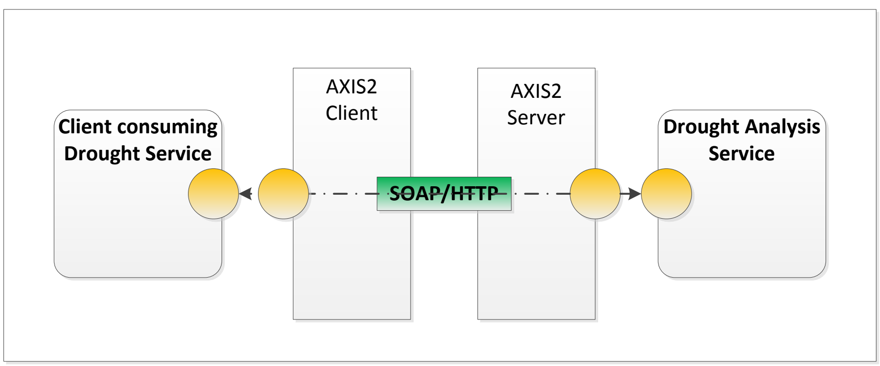

Figure 67 The data exchanged between the client requesting drought information and server side that is performing drought analysis.

Syntactical interoperability of Web services is archived mainly using two common standards: Web Services Description Language (WSDL) (Christensen et al., 2001) and Simple Object Access Protocol (SOAP) (W3C, 2007). The WSDL snippet as shown in Figure 68 lists the required key-value pairs needed to trigger the drawROI service. A valid HTTP request for this Web Service will need to include all required key-value pairs, including in_year, in_day, and four parameters of the bounding box (as shown in Box 6). WSDL not only describes the HTTP GET/POST bindings, but also the SOAP binding. Sample SOAP request and response can be found in Figures 69 and 70 respectively.

Box 6.

http://gis.csiss.gmu.edu:8080/axis2/services/DroughtPercentBBoxWorkflow/drawROI?in_year=2003&in_day=129&left=-95.7766&top=43.4373&right=-94.7566&bottom=42.4293


```xml
▼<xs:element name="drawROI">
  ▼<xs:complexType>
    ▼<xs:sequence>
       <xs:element minOccurs="0" name="in_year" nillable="true" type="xs:string"/>
       <xs:element minOccurs="0" name="in_day" nillable="true" type="xs:string"/>
       <xs:element minOccurs="0" name="left" type="xs:float"/>
       <xs:element minOccurs="0" name="top" type="xs:float"/>
       <xs:element minOccurs="0" name="right" type="xs:float"/>
       <xs:element minOccurs="0" name="bottom" type="xs:float"/>
     </xs:sequence>
   </xs:complexType>
 </xs:element>
▼<xs:element name="drawROIResponse">
  ▼<xs:complexType>
    ▼<xs:sequence>
       <xs:element minOccurs="0" name="return" nillable="true" type="xs:string"/>
     </xs:sequence>
   </xs:complexType>
 </xs:element>
```


Figure 68 Sample WSDL snippet describing drawROI request.

```xml
<soapenv:Envelope xmlns:soapenv="http://schemas.xmlsoap.org/soap/envelope/"
                  xmlns:edu="http://edu.gmu.gadmfs">
   <soapenv:Header/>
   <soapenv:Body>
      <edu:drawROI>
         <!--Optional:-->
         <edu:in_year>2003</edu:in_year>
         <!--Optional:-->
         <edu:in_day>129</edu:in_day>
         <!--Optional:-->
         <edu:left>-95.7766</edu:left>
         <!--Optional:-->
         <edu:top>43.4373</edu:top>
         <!--Optional:-->
         <edu:right>-94.7566</edu:right>
         <!--Optional:-->
         <edu:bottom>42.4293</edu:bottom>
      </edu:drawROI>
   </soapenv:Body>
</soapenv:Envelope>
```

Figure 69 Sample SOAP message requesting drawROI service.

```xml
<soapenv:Envelope xmlns:soapenv="http://schemas.xmlsoap.org/soap/envelope/">
   <soapenv:Body>
      <ns:drawROIResponse xmlns:ns="http://edu.gmu.gadmfs">
         <ns:return>
         http://gis.csiss.gmu.edu/drought_data_cache/data/subset_20130618155303_333558473.tif
         </ns:return>
      </ns:drawROIResponse>
   </soapenv:Body>
</soapenv:Envelope>
```

Figure 70 Sample SOAP response returned by drawROI request.

After the drawROI request is sent in HTTP or SOAP messages, server recognizes and handles the request in the following sequence: (1) receives the selected polygon, determines whether it is a valid polygon within the contiguous United States, and cut the shapefile of the U. S. into the selected shape; (2) receives the selected duration, and picks the available dates in the archive, and writes these dates into the execution sequence; (3) clip the Vegetation Index (VI) dataset with the new shapefile, and obtains the new VI dataset of the selected area; (4) generate drought mapfiles for datasets created in step 3;

(5) open access of the new dataset and mapfiles, so users can query drought maps using OGC WMS requests; (6) apply Cairo APIs to put map elements (e.g. title, legend) together with the map image, and concatenate maps of different dates to output. Figure 71 shows processes to handle drawROI request at the server side.

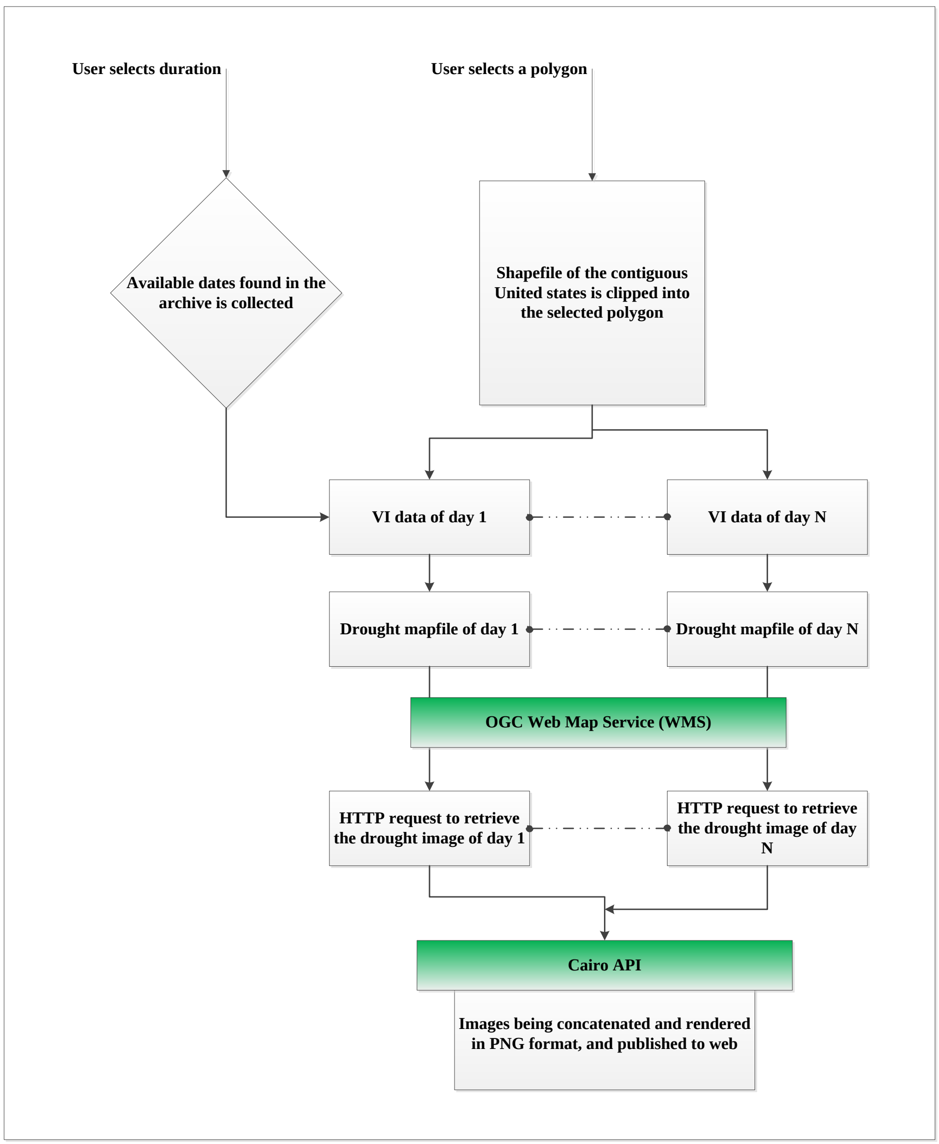

Figure 71 How server handles drawROI request at the back end.

Subsection 7.2.5 A case study of the U. S. Corn Belt

Droughts are often more costly than other types of natural disasters, and no region in North America is immune to periodic drought. According to the National Oceanic and Atmospheric Administration (NOAA), the year of 2012 is the hottest year ever recorded in the United States since 1895, and this year's drought had affected 87% of the land dedicated to growing corn, 85% of land for soybeans, 63% of land for hay and 72% of land used for cattle (statistics by Drought Monitor). The agricultural drought maps of the U. S. Corn Belt can be drawn via DrawROI Web Service, and the returned images are displayed in Figure 72.

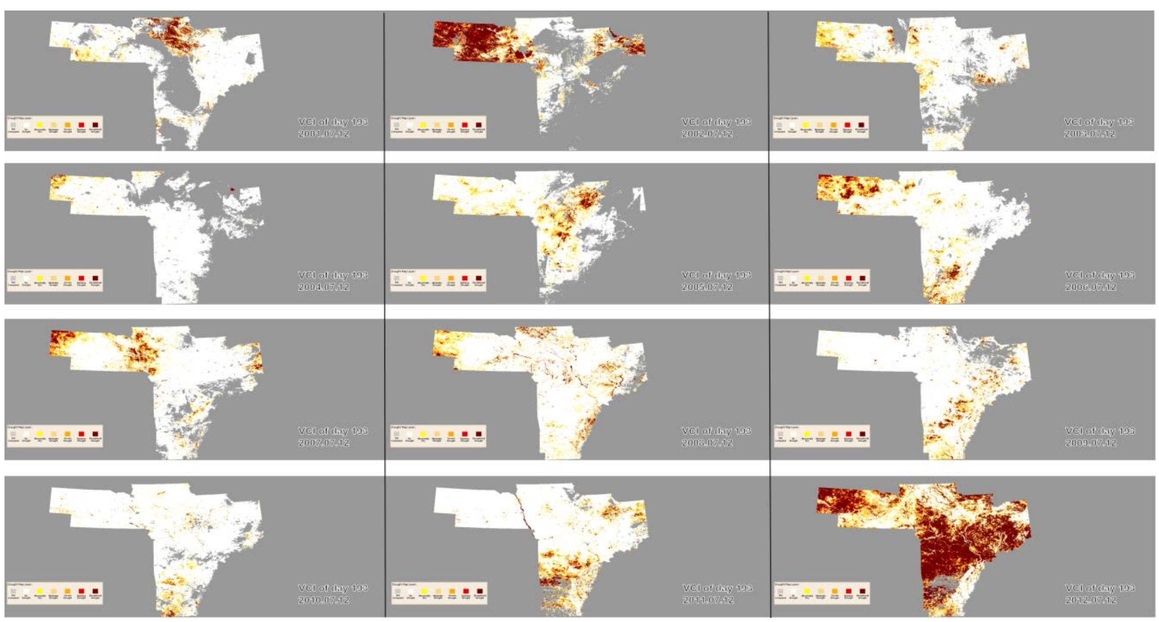

Figure 72 Drought maps returned from DrawROI Web Service (requested area: the U. S. Corn Belt, and requested day: 20XX/193).

In year 2012, almost 30% of the Corn Belt area was suffering from exceptional drought (D4), and less than 47% of the area was not prone to drought, compared to year

2011 when less than 7% of the area was in D4, and more than 80% was not in drought. From Figure 73, the mean VCI value of year 2011 is 159 while that of year 2012 is 91, which also indicates that latter is experiencing drought of a higher intensity.

Box 7.

http://gis.csiss.gmu.edu:8080/axis2/services/DroughtPercentBBoxWorkflow/getVCIstats?ROI=/tmp/subset_20130618155303_333558473.tif

Another Web Service GetDroughtPercentageByStates returns a set of bar charts displaying the drought percentage distribution of selected states, helping users to understand on a specific day which of the drought severity groups for each state is taking the major role. For instance, in Figure 74, the majority of Illinois is of D0, while for Idaho, both the D0 and D4 severity groups are of high percentage (respectively 28%, and 37%).

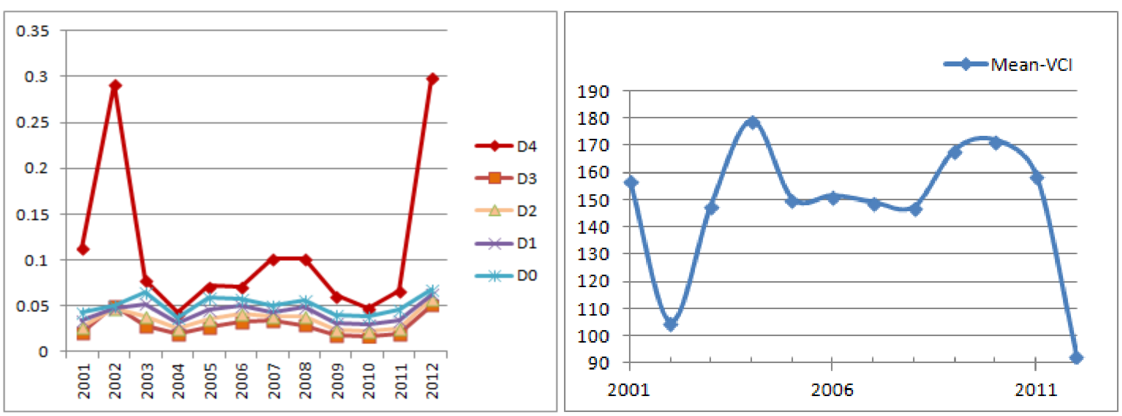

Figure 73 (Left) Percentage of crop area suffering from different degrees of drought (D4 to D0) in the period of 2001 to 2012. (Right) The mean VCI of the Corn Belt area from 2001 to 2012

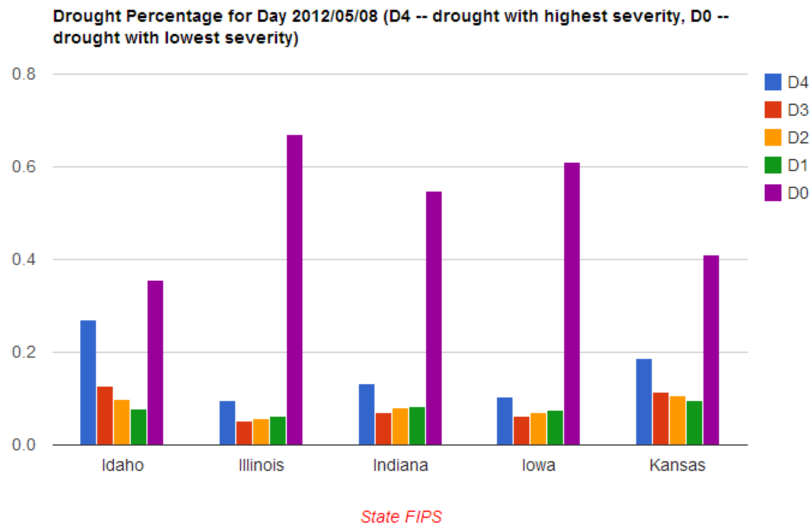

Figure 74 Response per GetDroughtPercentageByStates request – bar charts of distribution of drought severity groups per state for Idaho, Illinois, Indiana, Iowa and Kansas for the day of 2012/05/08.

In order to view the time-series performance of the vegetation index, users need to send a GetDroughtTimeSeries request and will receive in the response (Figure 75) the percentage of various drought groups throughout the year. Looking at the yearly time-series of VCI for the state of Iowa, the percentage of D4 pixels is lower than 20% from June to October in 2011, starts to climb up since October 2011, and climbs down from January 2012. The percentage of D4 drops under 10% in April 2012 and remains low till July, and from August 2012, D4 percentage mounts above 70% and stays high until November. These indicate a high possibility of agricultural drought in Iowa from October 2011 to March 2012, and from July to November 2012.

Figure 75 (Top Left) Percentage of crop area suffering from different degrees of drought (D4 to D0) in the period of 2011 and 2012 of day 129 in time series returned by GetDroughtTimeSeries request.

Subsection 7.2.6 Summary

A drought data and information system serving only raw data or drought indices can provide researchers or experts with the data needed for creation of drought maps and reporting of drought events, yet the general public may find themselves lack of experiences and guidance to complete the drought analysis process. With the on-demand geospatial Web Services in a system to provide dynamic drought analysis, the drought monitoring, forecasting and related applications are much more facilitated and the general public does not have to worry about lack of resources or capabilities.

The Web Services introduced in this article and deployed in GADMFS provide online and on-demand drought analysis and information management, which largely facilitate agricultural drought monitoring, forecasting and decision-making. The Web Service drawROI is meant for visualizing the drought patterns of a selected area and time. Other services, GetVCIStats is to capture the mean VCI value for the chosen region of interest, and GetDroughtPercentageByStates is used to depict the distribution of various drought severity groups for multiple chosen states, while GetDroughtTimeSeries is designed to describe the time-series drought information of the county, ASD or state specified in a request. With these Web Services, users can not only access and manipulate drought data, but they can also obtain an improved understanding of drought information, and hence form their drought knowledge base.

Subsection 7.2.7 Future Work

Although the Web Services in this paper facilitates users to better understand the characteristics of drought, the information returned is insufficient for timely decision-making or quick disaster response. There is an increasing demand to establish an Agricultural Drought Knowledge Base (ADKB) that stores the knowledge and expertise required for decision-making, including a number of facts and rules for different objectives (e.g. the ones for drought severity of D4 to happen), and their corresponding actions for different combinations of each objective's attributes. The ADKB can be divided into two systems -- the Rule Based System (RBS) and the Expert System (ES). The RBS is a computerized system that uses knowledge about some domain to arrive at a solution to a problem from that domain. The various stages of development are: (a) problem definition and expert selection, (b) knowledge engineering (climatological, hydrologic, and hydrogeologic attributes, agricultural attributes, and socio-economic attributes), (c) inference engine, and (d) verification and validation. Some researchers have used fuzzy rule-based modeling to assess and predict regional droughts by applying two forcing inputs, El Nino/South Oscillation (ENSO) and large scale atmospheric circulation patterns (CPs) in a typical Great Plains state, Nebraska (Pongracz et al., 1999; Pesti et al., 2010).

On the other hand, an ES reproduces the performance of one or more human experts, most commonly in a specific problem domain, and is a traditional application and/or subfield of artificial intelligence. The most common form of an ES is a computer program that analyzes information with a set of rules about a specific class of problems, and recommends one or more courses of user actions. The ES may also provide mathematical analysis of the problems, and utilizes what appears t be reasoning capabilities to reach conclusions (Nagarajan, 2009). The ES proposed by Palmer & Holmes (1988) incorporates operator experience and intuition using a rule base developed through interviews with management personnel from the Seattle Water Department, and also integrates the other programming techniques in a single system, thus being a great aid in drought decisions.

In the future research, our goal will be to establish such an ADKB, which is a rule-based expert system that helps users to detect, analyze, and handle agricultural drought events, monitor and predict agricultural impact (delay in sowing, sown area, crop vigor, change in cropping pattern, supply and demand of agriculture input), and react to the disaster.

Section 7.3 Agricultural Drought Information Cluster

Agricultural droughts, usually due to abnormally high temperature, low precipitation, and insufficient soil moisture, can cause devastating impact to a region's agriculture. Lack of proper drought warning and assessment systems may lead to enormous decrease in crop production and also in the amount of poultry and livestock, and thus endangering food security and economics. Thus an increasing number of scientists and researchers have their attention focused onto the causes and outcomes of agricultural drought, and are yearning for a clustering tool that would enable easy data accessing/downloading, calculation, analysis, visualization and decision-making, not just for experts with deep domain knowledge of drought and agriculture, but also for the general public who needs step-by-step guidance through the entire working process.

The DIKW (data, information, knowledge, and wisdom) processes (Ackoff, 1989) being interpreted in the sense of understanding agricultural drought can be as follows: (1) access/download remotely sensed images or meteorological ground measurements from various data providers, (2) process and calculate the agricultural drought indicators representing several perspectives: vegetation conditions, crop phenology, soil moisture levels, climate types, etc., (3) integrate major indicators according to user-customized analysis model to generate drought severity maps for the chosen area and create drought reports based on statistical results, and (4) form an applied knowledge of the geospatial patterns and temporal frequencies of agricultural drought, and what are the environmental factors that exert the most important influences to drought severities of an area. But several problems still exist in efficiently accessing, analyzing, visualizing, interpreting and understanding the agricultural drought information. The most critical of them all is the difficulty in sharing the raw data (collected), agricultural drought indicators (calculated), drought information (assembled) and drought theory (abstracted).

The reusability of data and technologies is the most difficult part of this challenge. First, huge amount of satellite data, station-based observations, and drought related statistical information are stored separately in different servers (ftp, http or others) by the data providing agencies or groups. Two researchers performing analysis on the same drought prone area are making duplicated efforts in downloading and storing data which are often isolated from each other, and not always reusable (usually being abandoned after being used for indicator calculation). Besides the big data challenge brought to drought researchers, the second challenge is the reusability of technologies or methods. Algorithms or methods that each individual or organization used for calculating drought indices and analyzing drought are unique in some parts and similar in others, and most of these have not been made completely understandable by the general public. There are hundreds of drought indicators in the field, yet not a platform exists for users to view how each of the existing indicators is being formed and should be used – a non-expert user has to look into publications or user manuals for the detailed information of the data source, processing methods, calculation formula, reliability and other meta-data. Such a platform that displays how each index is being made at each processing stage (from data collection to result analysis) needs to be urgently sought (Deng et al., 2012, 2013; Peng et al., 2012).

Subsection 7.3.1 Background

Not a single definition of drought can be used under all circumstances (Whilhite, 2000; Svoboda, 2002), and experts/users in various domains (e.g. hydrology, or agriculture) might adopt completely different sets of indicators to measure drought conditions. Take the short-term drought indicator as an example, the percentiles of the five input indicators are 35% of Palmer Z-index, 25% of 3-month precipitation, 20% of 1-month precipitation, 13% of CPC Soil Moisture Model, and 7% of Palmer Drought Index. On the other hand, six indicators are needed to blend into a long-term drought indicator, and the composition of each indicator is different from that of the short-term drought indicator. For the western states, the percentiles are 30% (PHDI), 30% (60-month Average Z-index), 10% (60-month precipitation), 10% (24-month precipitation), 10% (12-month precipitation) and 10% (CPC Soil Moisture Model). Yet for the rest of the states, the input indicators and percentiles are Palmer Hydrologic Index (25%), 12-month precipitation (20%), 24-month precipitation (20%), 6-month precipitation (15%), 60-month precipitation (10%), and CPC Soil Moisture Model (10%) (USDM Predictions Webpage, 2014).

Subsection 7.3.2 Methodology

The two regression models provided by Agricultural Drought Information Cluster are Least Squares and Multi-Variate Linear Regression models.

7.3.2.1 Multivariate Linear Regression Model

The multivariate linear regression model has the form

Equation 15 multivariate linear regression model for simulation.

$$Y = \beta 0 + \beta 1X1 + \beta 2X2 + \cdots + \beta rXr + \varepsilon,$$

where ε is a random error, and the $\beta i, i$ = 0, 1, …, r are unknown and fixed regression coefficients, and $\beta 0$ is the intercept under the assumption that $Xi, i = 0, 1, \ldots, r$ are a set of independent variables believed to be related to the response variable Y.

The following preconditions must be met for a linear regression model to be put in use. (a) For each value of the independent variable, the distribution of the dependent variable must be normal. (b) The variance of the distribution of the dependent variable should be constant for all values of the independent variable. (c) The relationship between the dependent variable and the independent variables should be linear, and all observations should be independent. To summarize these preconditions in simple words: independence; linearity; normality; homoscedasticity. In other words the residuals of a good model should be normally and randomly distributed, which is to say, the unknown does not depend on X ("homoscedasticity"). In order to check model assumptions, residual analysis can be applied. There are several kinds of residuals, most commonly used of which are the standardized residuals (ZRESID) and the studentized residuals (SRESID) (SPSS, 2010). If the model is correct, the residuals should have a normal distribution with mean zero and constant standard deviation. Here, we can plot residuals against X. If the variation alters with increasing X, then there is violation of homoscedasticity (Alexopoulos, 2010).

7.3.2.2 Least Squares Model (Polynomial Fit)

This model has its form as in Equation 16:

Equation 16 The least squares model (polynomial fit) for simulation.

$$Y = \alpha 0 + \alpha 1X + \alpha 2X^2 + \cdots + \alpha\gamma X^\gamma,$$

and in order to estimate the vector $\alpha = \{\alpha 0, \alpha 1, \alpha 2, \dots, \alpha\gamma\}$, we need to choose the value of α that minimizes the sum of squared residuals $(Y - X\alpha)'(Y - X\alpha)$. Here, the $\alpha i, i$ = 0, 1, …, γ are unknown coefficients, and $\alpha 0$ is the intercept under the assumption that $Xi, i =$ 0, 1, …, γ are a set of independent variables believed to be related to the response variable Y. When $\gamma = 1$, Equation 16 represents a straight line; when $\gamma = 2$, it becomes a quadratic equation and produces a parabola; when $\gamma = 3$, it is a cubic equation and produces an s-shaped curve.

Subsection 7.3.3 Implementation

The goal of this study is to provide a platform that can walk the general public from farmers to decision makers step-by-step through the process of collecting data, generating drought indices, analyzing time-series behaviors, compositing user-desired agricultural drought indicator, and creating easy-to-understand drought maps and reports. A one-stop self-service drought information cluster will serve as the solution, which allows users to view common templates used by agencies, and simulate selected remotely sensed indices to the in-situ data, and proceed to build up their own drought indicator by adjusting the weighting factors of each principal component. With its capability of sharing data, algorithms, and results, such a cluster will become an excellent model that carries out partnership and interoperability.

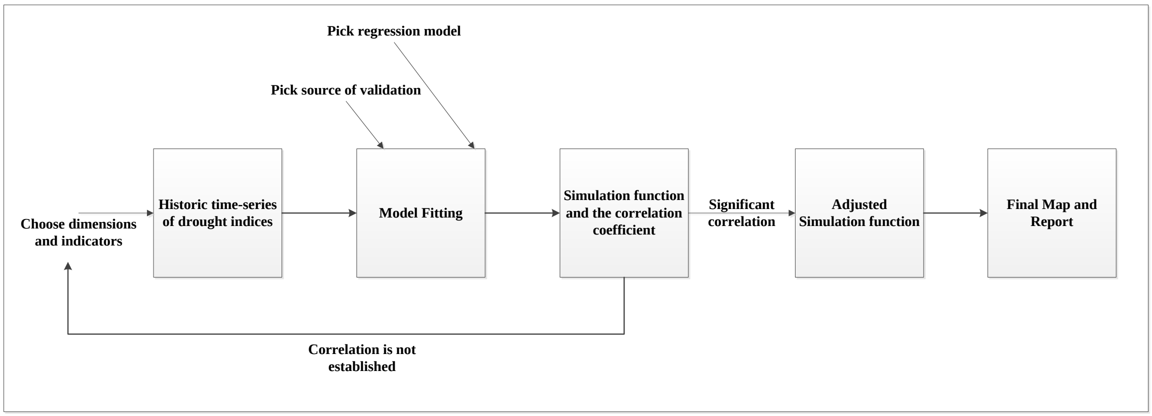

Figure 76 Scheme of the Agricultural Drought Information Cluster.

Such a system is to facilitate users to build up their own drought indicators in five steps (Figure 76):

(1) Choose dimension and indicators. Users get to choose one or more dimensions from Vegetation and Soil Moisture Conditions, Surface Temperature, and Crop Phenology, etc. If users would like to upload any data not present in the catalog, they can choose to import their own dimension. Also, users can decide the relationships of each dimension – e.g. D1+D2+D3+ … + D_n, or, (D1+D2) / (D3+ … + D_n). Next, choose indicators. Users need to specify one or more indicators for each selected dimension. For example, you can choose VCI and VHI for the first dimension. The user interface for step 1 is shown in Figure 77.

(2) Choose source of validation and regression model. There are four study sites (e.g. Ames station at Iowa) with their in-situ observing data such as soil moisture and precipitation to be validated against the remotely sensed indicators. Users need to choose one study site and a corresponding meteorological dataset. Also, it is user's right to choose one of the models – Least Squares and Multi-Variate Linear Regression for the validation, to which the time-series data for the set of independent variables and the unique dependent variable are fed.

(3) Obtain the simulation result and the correlation coefficient. As shown in the left of Figure 78, the example simulation web service returns Y= -0.0918706 + 0.760957*NDVI - 1.00754*NDWI + 1.02582*EVI in the case.

(4) Adjust the weighting factors. Now user is prompted to adjust the percentage (or, weight) of the indicator. For the sake of simplicity, user can make minor adjustments to the weighting factors of the independent variables. In this case, Y'= -0.1 + 0.76*NDVI – NDWI + EVI (shown in Figure 79).

(5) Generate the new drought map for the selected area, and compare the new map for the customized drought indicator against drought maps from official source (e.g. USDM). If the two are displaying similar drought/non-drought patterns, then the new customized indicator is considered to be an efficient agricultural drought index. With different validation source, the combination of drought indicators varies, and hence the simulated drought maps display different drought patterns, as shown in Figure 80.

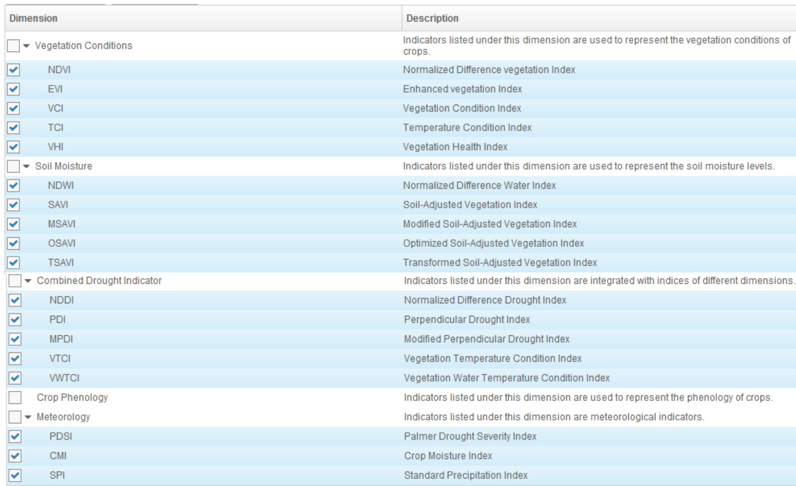

Dimension	Description
Vegetation Conditions	Indicators listed under this dimension are used to represent the vegetation conditions of crops.
NDVI	Normalized Difference vegetation Index
EVI	Enhanced vegetation Index
VCI	Vegetation Condition Index
TCI	Temperature Condition Index
VHI	Vegetation Health Index
Soil Moisture	Indicators listed under this dimension are used to represent the soil moisture levels.
NDWI	Normalized Difference Water Index
SAVI	Soil-Adjusted Vegetation Index
MSAVI	Modified Soil-Adjusted Vegetation Index
OSAVI	Optimized Soil-Adjusted Vegetation Index
TSAVI	Transformed Soil-Adjusted Vegetation Index
Combined Drought Indicator	Indicators listed under this dimension are integrated with indices of different dimensions.
NDDI	Normalized Difference Drought Index
PDI	Perpendicular Drought Index
MPDI	Modified Perpendicular Drought Index
VTCI	Vegetation Temperature Condition Index
VWTCI	Vegetation Water Temperature Condition Index
Crop Phenology	Indicators listed under this dimension are used to represent the phenology of crops.
Meteorology	Indicators listed under this dimension are meteorological indicators.
PDSI	Palmer Drought Severity Index
CMI	Crop Moisture Index
SPI	Standard Precipitation Index

Figure 77 Dimensions to be considered include Vegetation Conditions, Soil Moisture, Combined Drought Indicators, Crop Phenology, and Meteorology. For each dimension, user can choose none to all indicators for analysis.

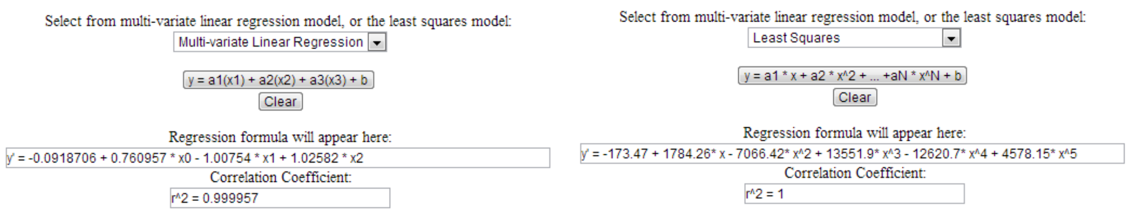

Figure 78 Select from multi-variate linear regression model, or least squares model to fit the chosen independent variables (indicators) to the verification source (e.g. soil moisture observations). A web service is to be invoked to calculate the correlation coefficient.

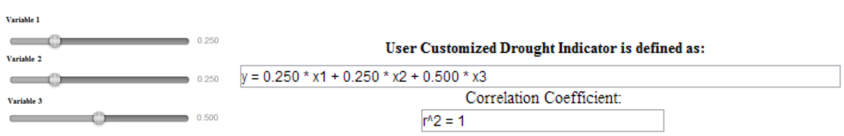

Figure 79 the slider bar to adjust the weights of each variable to be used to define the new drought indicator. User can look at the automatically generated CC to find the most appropriate weights for each variable.

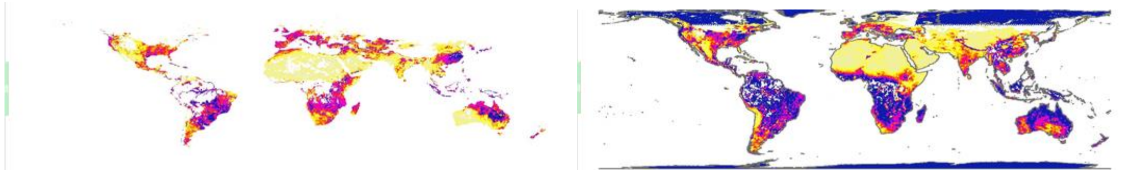

Figure 80 (Left) The global drought map based on the new combined drought indicator #1 which simulates the AMSR-E Vegetation Water Content. (Right) combined drought indicator #2 simulating the ECV Soil Moisture.

With such an agricultural drought information cluster, users define their own drought indicator which tailors their own needs targeted for various applications, and to enable data, technology, and drought information to be shared among different groups.

Subsection 7.3.4 Discussion & Summary

How to enable discovery across federated systems from multiple domains has become a heated topic these days. Yet technologies to share data traceability, reliability and extensibility are still limited. Further efforts need to be taken for users to understand how each organization makes their drought indicators and maps, and whether their results are trustworthy and compatible for extending research and applications.

Such an Agricultural Drought Information Cluster is to provide a comprehensive monitoring and forecasting system that incorporates all principal components necessary for the analysis of agricultural drought step-by-step from data, information, and knowledge to wisdom. Through the process, users can understand the behaviors of each indicator, what influences drought and proceed to create their own drought indicators.

CHAPTER 8 CONCLUSIONS AND DISCUSSION

Within this dissertation, the use of remote sensing technologies towards the monitoring of vegetation stresses, soil moisture, and agricultural drought has been explored. The study investigates the ability to estimate the spatial and temporal distribution of agricultural drought by utilizing remotely sensed and ground-based data for vegetation conditions and soil moisture assessment. Here, the root-zone soil moisture observations have been combined with remotely sensed VIs for evaluation of agricultural drought to achieve higher accuracy and spatial resolution. Remote sensing measurements from VIS, NIR, MIR, and TIR channels are used to monitor vegetation stresses and agricultural drought based on the spectral reflectance change responding to vegetation and climatic variations. The trapezoid model is the base for Combined condition Index (CCI), as it interprets the LST-NDVI-NDWI space efficiently and accurately by taking into account the distribution and temporal variation of crop conditions from three perspectives (water, vegetation growth, and thermal) which gained by MODIS reflectance measurements. Having these means integrated, information and knowledge of agricultural drought at high resolution can be gained.

Section 8.1 Conclusions

There are six categories for the main achievements of this dissertation, and they are namely: (i) estimation of vegetation drought stress by combining the strengths of multi-sensor and ground measurements to achieve higher accuracy and spatial resolution; (ii) investigation for the potentials of using a combination of multiple VIS-NIR-SWIR-TIR spectral signatures to estimate vegetation moisture, thermal, and health conditions from space and to find the algorithm that would differentiate vegetated pixels with or without drought stress; (iii) usage of root-zone soil moisture data for validation of the drought indicators being correlated to actual conditions of agricultural drought; (iv) investigation of the relationship between soil moisture and vegetation greenness, particularly when there is drought, thus ruling out the false VI signals when VI is low but soil moisture level is high; (v) development of an integrated drought condition index and a flexible drought severity classification standard as to form an accurate and comprehensive view for agricultural drought monitoring at the national or even global scale; (vi) development of Web Services to facilitate the community with not only drought data, but also drought information and knowledge. In the following sections, the applications of the research presented in this thesis and their impact on further studies are summarized.

Subsection 8.1.1 Vegetation Stresses Evaluation

Vegetation stresses can come from various sources, namely flood, extreme weather, lack of fertilizers, excessive use of fertilizers, pesticides, human/animal damage, etc., and drought is not the only reason. It is subjective to attribute the depression of vegetation conditions to drought, which is to say, the low VI value does not necessarily point to any drought occurrences. The study has summarized water, thermal, and crop growing conditions to be the three most important factors resulting into an agricultural drought, and NDWI, LST, and NDVI are the RS-based indicators for each condition. The trapezoid model is used here to interpret the 3D space composed of NDWI/LST/NDVI values of all vegetated pixels within a selected area. In implementing of the model, RNDDI is used to carry the information of NDWI and NDVI, and then combined with LST to form a 2D space. With the wet and dry edges drawn, the CCI value for each pixel is calculated, and later the CCI maps for the area shall be created. The validation process with meteorological data (e.g. PDSI, soil moisture, and precipitation) has proven that CCI is an efficient drought indicator at high accuracy.

Subsection 8.1.2 Root-zone soil moisture for validation

Soil moisture deficiency is a direct reflection of drought. Soil moisture at the root zone is of higher correlation to drought than that at the surface, because the latter is always fluctuating by weather changes in a short time. However, root-zone soil moisture refers to a depth of soil information, from 0 to 100 cm beneath the ground. Investigating the relationship between VIs and soil moisture at different depths is crucial, since soil moisture observations as a source for validation (i.e. the speaker for drought conditions) need to be accurate at the first place, or else linking VI performance to drought conditions can totally be of no foundation. The study has found that Corn VIs exhibit strong relationships with soil moisture at deeper depths (with longer lagging period), while the soybean VIs are highly sensitive to changes in soil moisture at much shallower depths (with shorter lagging time). Depending on the crop type, different soil moisture data shall be used as validation source. This finding will help correlation study related to soil moisture achieve higher accuracy.

Subsection 8.1.3 Web Services for Agricultural Drought Information

Although raw data or drought indices may suit the needs of researchers or experts who can download these data onto their desktop and perform analysis on their own, the general public may find themselves lack of experiences and guidance to complete the process to extract information or knowledge out of purely raw data. The on-demand geospatial Web Services introduced here can provide dynamic drought analysis, monitoring, and forecasting to online users, and can equip general user groups with sufficient domain knowledge such as spatial and temporal patterns of drought. For example, the Web Service drawROI is meant for visualizing the drought patterns of a selected area and time. Other services, GetVCIStats is to capture the mean VCI value for the chosen region of interest, and GetDroughtPercentageByStates is used to depict the distribution of various drought severity groups for multiple chosen states, while GetDroughtTimeSeries is designed to describe the time-series drought information of the county, ASD or state specified in a request. With these Web Services, users can not only access and manipulate drought data, but they can also obtain an improved understanding of drought information, and hence form their drought knowledge base.

Section 8.2 Applications of this research

The research conducted in this dissertation is expected to be useful for monitoring agricultural drought using maps, statistic reports, and Web Services.

The trapezoid model proposed here can provide decision makers detailed information on spatial distribution and temporal variation of vegetation conditions, which are valuable for many applications, such as drought or flood monitoring. Although the study was conducted in the U. S. Corn Belt, the trapezoid model of LST and RNDDI is expected to apply to other areas whose crop growth is mostly determined by thermal and water conditions. The CCI derived from this model serves as a better indicator for drought. Combining information from multiple channels makes CCI response to vegetation drought conditions in opposite directions and therefore, a promising indicator for agricultural drought monitoring. This index can be applied to larger areas (such as continents) to extract information of vegetation drought conditions.

The relationship found between VIs and soil moisture at various depths will provide a new foundation of correlation studies for choosing the optimized drought indicator. In order to achieve higher accuracy and efficiency in simulating drought conditions using RS-based indicators, using the appropriate soil moisture data (with correct depth and lagging period) for validation is the key. Researchers are now warned to select the soil moisture data based on depths of the rooting system, and the crop growing patterns.

Web Services (WS) developed in the study have enabled general users to access, analyze, extract and visualize drought information online, instead of the traditional expert-only desktop-based approach. These WS return to end-users the characteristics of droughts from spatial and temporal extent to severities and impact. Being standardized, interoperable, and concatenation-convenient, these services can be integrated with more functionality, either on the same server or across domains, to constitute an information cluster on which every GIS tool can be found and used for drought analysis.

The research presented in this thesis explores a new direction in the use of remote sensing science and technologies towards vegetation stresses and agricultural drought estimation. Not only will it provide a solid foundation for remote sensing-based approaches for assess and monitor vegetation conditions and drought at a finer spatial and temporal resolution, but it will also extend the web-based capabilities of accessing, analyzing, and visualizing agricultural drought on-demand.

Section 8.3 Limitations of this work

Due to data availability in time and space, the experiments conducted in this research are subject to some limitations. For example, the croplands are considered as non-irrigated and non-fertilized at the first place. Also, the self-examined laboratory in-field data collection is absent for the study site. Hence, some results are mainly based on model simulation and certain preconditions, and cannot represent the complex nature of agricultural drought.

The proposed new index, CCI, is currently experimentally used for croplands within Corn Belt which are covered with dense vegetation. More research needs to be done for areas with moderate or scarce vegetation coverage, which are common conditions found in reality. With fewer pixels carry valid values for thermal, moisture and vegetation conditions, the construction of a trapezoid can be difficult. Testing CCI on sparsely-vegetated lands is likely to yield inaccurate results.

Currently the validation functionality provided with Web Services only enables users to choose the regression model from multi-variate linear regression and the least squares model (polynomial fit), and has hence left some blank for other simulation patterns. In the future, logistic regression and genetic programming shall be added for studying the relationship (correlation or not) between VIs and ground measurements.

Section 8.4 Future works

Future research will fall into three categories, namely: (i) develop a general CCI approach that would consider group behaviors of crops having the similar rooting depths; (ii) extensive applications of CCI for drought monitoring and vegetation drought stress detecting for various crop types across the globe (on densely, moderately, and sparsely vegetated areas); (iii) apply different regression models to make sure if there will be any other fitting models between VI and RZSM, e.g. Taylor series approximation, and Natural Spline Smoothing; (iv) further development of standardized, interoperable, and concatenation-convenient Web Services to deliver agricultural drought information; and (v) development of agricultural drought knowledge base which clusters all the data, methods and services required for drought access, analysis, understanding, visualization and extraction into information and knowledge.

REFERENCES

Achard, F., and F. Blasco, 1990: Analysis of vegetation seasonal evolution and mapping of forest cover in West Africa with the use of NOAA AVHRR HRPT data. Photogramm. Eng. Remote Sens., 56, 1359–1365.

Ackoff, R., 1989: From Data to Wisdom. Journal of Applied Systems Analysis 16: 3–9.

Alexopoulos., E.C., 2010: Introduction to Multivariate Regression Analysis, Hippokratia, Dec. 2010; 14(Suppl 1): 23-28

Anderson, M. C., J. M. Norman, J. R. Mecikalski, J. A. Otkin, and W. P. Kustas, 2007: A climatological study of evapotranspiration and moisture stress across the continental United States based on thermal remote sensing: 1. Model formulation. J. Geophys. Res., 112, D10117, doi:10.1029/2006JD007506.

Asian Sustainability Ratings, 2010

Bäck, T., U. Hammel, and H. P. Schwefel, 1997: Evolutionary computation: Comments on the history and current state. IEEE Trans. Evol. Comput., 1, 3-17, doi: 10.1109/4235.585888.

Badeck, F. W., A. Bondeau, K. Bottcher, D. Doktor, W. Lucht, J. Schaber, and S. Sitch, 2004: Responses of spring phenology to climate change. New Phytol., 162, 295–309.

Baumann., P. 2010: OGC WCS 2.0 Interface Standard—Core, Version 2.0.0, OGC 09-110r3, Open Geospatial Consortium, Inc., p 53.

Bayarjargal, Y., Karnieli, A., Bayasgalan, M., Khudulmur, S., Gandush, C. and Tucker, C.J., 2006. A comparative study of NOAA–AVHRR derived drought indices using change vector analysis. Remote Sensing of Environment, 105, pp. 9–22.

BBC News, http://news.bbc.co.uk/2/hi/8587516.stm, last accessed on April 2010.

Bhuiyan, 2008: Desert Vegetation during Droughts: Response and Sensitivity, ISPRS Technical Commission VIII, WG VIII/9

Boegh, E., H. Soegaard, N. Hanan, P. Kabat, and L. Lesch, 1999: A remote sensing study of the NDVI-Ts relationship and the transpiration fromsparse vegetation in the Sahel based on highresolution satellite data – An overview. Remote Sens. Environ., 69, 224 – 240.

Boken, V. K., G. Hoogenboom, F. N. Kogan, J. E. Hook, D. L. Thomas, and K. A. Harrison, 2004: Potential of using NOAA-AVHRR data for estimating irrigated area to help solve an inter-state water dispute. Int. J. Remote Sens., 25, 2277–2286.

Bonham-Carter, G.F. 1994: Geographic information systems for geoscientists - modeling with GIS. Pergamon, 398 pp.

Bröring A, Stasch C, Echterhoff J. 2012: OpengGIS sensor observation service interface standard, Version 2.0, OGC 12-006, Open Geospatial Consortium, Inc., p 163.

Brown, J., C. Jenkerson, and Y. Gu, 2008: Using eMODIS Vegetation Indices for Operational Drought Monitoring, NIDIS Knowledge Assessment Workshop at Boulder, CO, Feb 6-7, 2008

Carlson, T.N., Gillies, R.R. and Perry, E.M., 1994, A method to make use of thermal infrared temperature and NDVI measurements to infer soil water content and fractional vegetation cover. Remote Sensing Reviews, 9, pp. 161–173.

Chakraborty & Sehgal, 2010: Assessment of Agricultural Drought Using MODIS Derived Normalized Difference Water Index, Journal of Agricultural Physics, Vol. 10, pp. 28-36

Chang, N. B., Z. Xuan, and B. Wimberly, 2012: Remote sensing spatiotemporal assessment of nitrogen concentrations in Tampa Bay, Florida due to a drought. Terr. Atmos. Ocean. Sci., 23, 467-479, doi: 10.3319/TAO.2012.04.10.01(WMH)

Chapin, F. S., G. R. Shaver, A. E. Giblin, K. J. Nadelhoffer, and J. A. Laundre, 1995: Responses of Arctic Tundra to Experimental and Observed Changes in Climate. Ecology, 76, 694–711.

Chen, D., Huang, J. and Jackson, T.J., 2005. Vegetation water content estimation for corn and soybeans using spectral indices derived from MODIS near – and short wave infrared bands. Remote Sensing of Environment, 98, pp. 225-236.

Cheng, Y-B., Ustin, S.L., Riaño, D., and Vanderbilt, V.C., 2008. Water content estimation from hyperspectral images and MODIS indexes in Southeastern Arizona. Remote Sensing of Environment, 112, pp. 363-374.

Choudhury, B. J., N. U. Ahmed, S. B. Idso, R. J. Reginato, and C. S. T. Daughtry, 1994: Relations between evaporation coefficients and vegetation indices studied by model simulations. Remote Sens. Environ., 50, 1–17.

Chrisman., B., & M. Zreda, 2013: Quantifying mesoscale soil moisture with the cosmic-ray rover, Hydrol. Earth Syst. Sci., 17, 5097–5108, 2013

Churkina, G., and S. W. Running, 1998: Contrasting climatic controls on the estimated productivity of global terrestrial biomes. Ecosystems, 1, 206–215.

Coll, C., V. Casselles, J. A. Sobrino, and E. Valor, 1994: On the atmospheric dependence of the split-window equation for land surface temperature. Int. J. Remote Sens., 15, 105–122.

CRAN, 2010: http://www.cnan.gov.cn/qxnq/hljc/t20100419_338202.phtml, last accessed in May 2010.

Dabrowska-Zielinska, K., F. Kogan, A. Ciolkosz, M. Gruszczynska & W. Kowalik, 2010: Modelling of crop growth conditions and crop yield in Poland using AVHRR-based indices, International Journal of Remote Sensing, 23:6, pp. 1109-1123

Dall'Olmo, G., and A. Karnieli, 2002: Monitoring phenological cycles of desert ecosystems using NDVI and LST data derived from NOAA-AVHRR imagery. Int. J. Remote Sens., 23, 4055–4071.

Defries, R. S., M. C. Hansen, and J. R. G. Townshend, 2000: Global continuous fields of vegetation characteristics: A linear mixture model applied to multi-year 8 km AVHRR data. Int. J. Remote Sens., 21, 1389–1414.

de la Beaujardière J, 2006: OpenGIS web map server implementation specification. Version 1.3.0, OGC 06-042, Open Geospatial Consortium, Inc., p 85.

Deng, M., L. Di, G. Yu, A.Yagci, C. Peng, B. Zhang, and D. Shen, 2012: Building an on-demand web service system for global agricultural drought monitoring and forecasting, Proceedings of 2012 IEEE International Geoscience and Remote Sensing, Munich, Germany, July 22–27. 4pp.

Deng, M., L. Di, A. Yagci, C. Peng, & G. Heo, 2013: Web-service-based Monitoring and Analysis of Global Agricultural Drought. In Photogrammetric Engineering & Remote Sensing, 79 (10).

Di, L., 1991. Regional-scale soil moisture monitoring using NOAA/AVHRR data, The University of Nebraska-Lincoln (doctorate dissertation)

Di, L., D. Rundquist, and L. Han. 1994. “Modelling Relationships between NDVI and Precipitation during Vegetative Growth Cycles.” International Journal of Remote Sensing 15: 2121–36.

Dormann, C. F., and S. J. Woodin, 2002: Climate change in the Arctic: Using plant functional types in a meta-analysis of field experiments. Funct. Ecol., 16, 4–17.

Dracup, A., K. Lee, and E. Pauson, 1980: On the definition of droughts. Water Resources Research, 16(2): 291-302

Duvick, D. N., and K. G. Cassman. 1999. “Post-green Revolution Trends in Yield Potential of Temperate Maize in the North-Central United States.” Crop Science 39: 1622–30.

Ehrlich, D., and E. F. Lambin, 1996: Broad scale land-cover classification and interannual climatic variability. Int. J. Remote Sens., 17, 845–862.

Ek, M. B., K. E. Mitchell, Y. Lin, E. Rogers, P. Grunmann, V. Koren, G. Gayno, and J. D. Tarpley, 2003: Implementation of Noah land surface model advances in the National Centers for Environmental Prediction operational mesoscale Eta model. J. Geophys. Res., 108, 8851, doi:10.1029/2002JD003296.

Eumetrain website, http://www.eumetrain.org/data/3/36/navmenu.php?page=4.1.0, accessed in 2012

Filho, V., B. J. Feigl, M. C. Piccolo, L. Fante Jr., M. S. Neto, and C. C. Cerri. 2004. “Root Systems and Soil Microbial Biomass under No-Tillage System.” Scientia Agricola 61: 529–37.

Fogel, L. J., A. J. Owens, and M. J. Walsh, 1966: Artificial Intelligence Through Simulated Evolution, John Wiley & Sons, New York, USA.

Francone, F. D. 1998: DiscipulusTM Software Owner’s Manual, version 3.0 DRAFT, Machine Learning Technologies, Inc., CO, USA.

Friedl, M. A., and F. W. Davis, 1994: Sources of variation in radiometric surface-temperature over a Tallgrass Prairie. Remote Sens. Environ., 48, 1–17.

Gagne, C. and M. Parizeau, 2004: Genericity in evolutionary computation software tools: Principles and case-study, Technical Report RT-LVSN-2004-01, Laboratoire de Vision et Systemes Numerique (LVSN), Universite Laval, Quebec, Canada.

Gao, B.C., 1996, NDWI – a normalized difference water index for remote sensing of vegetation liquid water from space. Remote Sensing of Environment, 58, pp. 257–266.

Gibson, 2003, Agronomy 212 – Grain and Forage Crops, [Online]. Available:http://agron-www.agron.iastate.edu/Courses/agron212/Calculations/GDD.htm

Gillies, R.R. and Carlson, T.N., 1995, Thermal remote sensing of surface soil water content with partial vegetation cover for incorporating into climate models. Journal of Applied Meteorology, 34, pp. 745–756.

Gillies, R.R., Carlson, T.N., Cui, J., Kustas, W.P. and Humes, K.S., 1997, A verification of the 'triangle' method for obtaining surface soil water content and energy fluxes from remote measurement of the Normalized Difference Vegetation Index (NDVI) and surface radiant temperature. International Journal of Remote Sensing, 18, pp. 3145–3166.

GOETZ, S.J., 1997, Multi-sensor analysis of NDVI, surface temperature and biophysical variables at a mixed grassland site. International Journal of Remote Sensing, 18, pp. 71–94.

Goward, S., Y. Xue, and K. Czajkowski. 2002. "Evaluating Land Surface Moisture Conditions from the Remotely Sensed Temperature/Vegetation Index Measurements: An Exploration with the Simplified Simple Biosphere Model." Remote Sensing of Environment 79: 225–242.

Gitelson, A. A., F. Kogan, E. Zakarin, L. Spivak, and L. Lebed, 1998: Using AVHRR data for quantitive estimation of vegetation conditions: Calibration and validation. Adv. Space Res., 22, 673–676.

Gitelson, A. A. 2004. "Wide Dynamic Range Vegetation Index for Remote Quantification of Crop Biophysical Characteristics." Journal of Plant Physiology 161: 165–73.

Graglia, E., S. Jonasson, A. Michelsen, and I. K. Schmidt, 1997: Effects of shading, nutrient application and warming on leaf growth and shoot densities of dwarf shrubs in two arctic-alpine plant communities. Ecoscience, 4, 191–198.

Gu, Y., Brown, J.F., Verdin, J.P. and Wardlow, B., 2007. A five-year analysis of MODIS NDVI and NDWI for grassland drought assessment over the central Great Plains of the United States. Geophysical Research Letters, 34, L 06407.

Ghulam, A., Qin, Q., Teyip, T. and Li, Z-L., 2007. Modified perpendicular drought index (MPDI): a realtime drought monitoring method. Journal of Photogrammetry & Remote Sensing, 62, pp. 150-164.

Gupta, R. K., T. S. Prasad, and D. Vijayan, 2002: Estimation of roughness length and sensible heat flux from WiFS and NOAA AVHRR data. Land Surface Characterization and Remote Sensing of Ocean Processes, R. K. Gupta, R. P. Singh, and Y. Menard, Eds., Pergamon Press, 33–38.

Gurney, R. J., J. P. Ormsby, and D. K. Hall, 1983: Observed relation between thermal emission and reflected spectral radiance of a complex vegetated landscape. Permafrost: Fourth Int. Conf., Fairbanks, AK, University of Alaska and National Academy of Sciences, 401–404.

Gutman, G. G., 1990: Towards monitoring droughts from space. J. Climate, 3, 282–295.

Hane, Dan C., and Floyd Vance Pumphrey, 1984: "Crop water use curves for irrigation scheduling", Corvallis, Or.: Agricultural Experiment Station, Oregon State University.

Hansen, M. C., R. S. Defries, J. R. G. Townshend, and R. Sohlberg, 2000: Global land cover classification at 1 km spatial resolution using a classification tree approach. Int. J. Remote Sens., 21, 1331–1364.

Heim, R. R., 2002: A review of twentieth-century drought indices used in the United States. Bull. Amer. Meteor. Soc., 83, 1149–1165.

Higuchi, A., 2005, Integrated use of vegetation indices and surface temperature space obtained from Earth observation satellites dataset. In Water and Carbon Cycles in Terrestrial Ecosystems. The Textbook for the Fifteenth IHP Training Course, pp. 111–134 (Nagoya: Hydrospheric Atmospheric Research Centre, Nagoya University and United Nations Educational Scientific and Cultural Organization (UNESCO)).

Holland, J. M., 1975: Adaptation in Natural and Artificial Systems, University of Michigan Press, Ann Arbor, MI, USA.

Hope, A. S., 1988: Estimation of wheat canopy resistance using combined remotely sensed spectral reflectance and thermal observations. Remote Sens. Environ., 24, 369–383.

Huang, B., B. Jiang, & H. Li. 2001. An integration of GIS, virtual reality and the Internet for visualization, analysis and exploration of spatial data. International Journal of Geographical Information Science 01/2001; 15:439-456.

Huete, A. R., R. D. Jackson, and D. F. Post, 1985: Spectral response of a plant canopy with different soil backgrounds. Remote Sens. Environ., 17, 37–53.

Huete, A.R., Lieu, H.Q., Batchily, K. and Vanleeuwen, W., 1997. A comparison of vegetation indices global set of TM images for EOS-MODIS. Remote Sensing of environment, 59, pp. 440-451.

Huete, A.R., Didan, K., Miura, T., Rodriguea, E.P., Gao, X. and Ferreira, L.G., 2002. Overview of the radiometric and biophysical performance of the MODIS vegetation indices. Remote Sensing of Environment, 83, pp. 195-213.

IBM Website, http://www.ibm.com/developerworks/rational/library/07/0515_woldemichael/, last access on 01/23/2014

Isaaks, E., & R. Srivastava. 1990: An Introduction to Applied Geostatistics. Oxford University Press, New York-Oxford, 592 pp.

Jackson, T.J., Vine, D.M.L., Swift, C.T., Schmugge, T.J. and Schiebe, F.R. 1995. Large area mapping of soil moisture using the ESTAR passive microwave radiometer in Washita'92. Remote Sensing of Environment, 53: 27-37

Jackson, T.J., Schmugge, J., Engman, E.T. 1996.Remote sensing applications to hydrology: soil moisture. Hydrological Sciences, 41(4), 517-530.

Jackson, T.J., D. Chen, M. Cosha, F. Li, M. Anderson, C. Walthalla, P. Doriaswamya, E.R. Hunt, 2004: Vegetation water content mapping using Landsat data derived normalized difference water index for corn and soybeans, Remote Sensing of Environment, Vol. 92, pp. 475-482.

Jang, J. D., A. A. Viau, and F. Anctil, 2006: Thermal-water stress index from satellite images. Int. J. Remote Sens., 27, 1619–1639.

Javed, M. Yogesh, K. and Bharath , B., 2008: Estimation of land surface temperature over Delhi using Landsat-7 ETM+. J.Ind. Geophys.Union Vol 12, No.3 pp131-140

Ji, L., and A. J. Peters, 2003: Assessing vegetation response to drought in the northern Great Plains using vegetation and drought indices. Remote Sens. Environ., 87, 85–98.

Johnson (2010) "A five-year analysis of crop phonologies from the united states heartland", 2010 American Geophysical Union Fall Meeting, B33C-0413

Julien, Y., and J. A. Sobrino, 2009: The Yearly Land Cover Dynamics (YLCD) method: An analysis of global vegetation from NDVI and LST parameters. Remote Sens. Environ., 113, 329–334.

JRC website, http://ies.jrc.ec.europa.eu/our-activities/scientific-achievements/drought-monitoring-assessment-and-forecasting.html, accessed in 2012

Karnieli, A., and G. Dall'Olmo, 2003: Remote-sensing monitoring of desertification, phenology, and droughts. Manage. Environ. Qual., 14, 22–38.

Kaufman, Y. J., and D. Tanré. 1992. "Atmospherically Resistant Vegetation Index ARVI for EOSMODIS." IEEE Transactions on Geoscience and Remote Sensing 30: 261–70.

Kawashima, S., 1994: Relation between vegetation, surface temperature, and surface composition in the Tokyo region during winter. Remote Sens. Environ., 50, 52–60.

Katou, A. and Yamaguchi, Y., 2005, Assessment of water and temperature stresses of vegetation in urban areas by the VWTI index. Proceedings of the Conference of the Remote Sensing Society of Japan, 39, pp. 201–202.

Kogan, F.N., 1990, Remote sensing of weather impacts on vegetation in non-homogeneous areas. International Journal of Remote Sensing, 11, pp. 1405–1419.

Kogan, F.N., 1995, Application of vegetation index and brightness temperature for drought detection. Advances in Space Research, 15, pp. 91–100.

Kogan, F. N., 1997: Global drought watch from space. Bull. Amer. Meteor. Soc., 78, 621–636.

Kogan, F. N., 2000: Satellite-observed sensitivity of world land ecosystems to El Nino/La Nina. Remote Sens. Environ., 74, 445–462.

Kogan, F. N., 2002: World droughts in the new millennium from AVHRRbased vegetation health indices. Eos, Trans. Amer. Geophys. Union, 83, 557–564.

Koza, and Poli, 2005: http://dces.essex.ac.uk/staff/poli/papers/KozaPoli2005.pdf

Kraak, M.J. & Ormlering, E.J. (1996). Cartography, visualization of spatial data. Harrow, London.

Lanscape toolbox wiki, http://wiki.landscapetoolbox.org/doku.php/remote_sensing_methods:enhanced_vegetation_index, last access on 01/23/2014

Lambin, E. F., 1996: Change detection at multiple temporal scales: Seasonal and annual variations in landscape variables. Photogramm. Eng. Remote Sens., 62, 931–938.

Lambian, E. F.,1997: Land-cover changes in sub-Saharan Africa (1982-1991): Application of a change index based on remotely sensed surface temperature and vegetation indices at a continental scale. Remote Sens. Environ., 61, 181–200.

Lambian, E. F., and A. H. Strahler, 1994a: Change-vector analysis in multitemporal space: A tool to detect and categorize land-cover change processes using high temporal-resolution satellite data. Remote Sens. Environ., 48, 231–244.

Lambian, E. F., and A. H. Strahler, E. F., 1994b: Indicators of land-cover change for change vector analysis in multitemporal space at coarse spatial scales. Int. J. Remote Sens., 15, 2099–2119.

Lambian, E. F., and D. Ehrlich, 1995: Combining vegetation indexes and surface temperature for land-cover mapping at broad spatial scales. Int. J. Remote Sens., 16, 573–579.

Lambian, E. F., and D. Ehrlich, E. F., 1996: The surface temperature-vegetation index space for land cover and land-cover change analysis. Int. J. Remote Sens., 17, 463–487.

Lambian, E. F., and D. Ehrlich, E. F., 1997: Land-cover changes in sub-Saharan Africa (1982-1991): Application of a change index based on remotely sensed surface temperature and vegetation indices at a continental scale. Remote Sens. Environ., 61, 181–200.

Lawrence, R..L. and Ripple, W.J., 1998. Comparisons among Vegetation Indices and Bandwise Regression in a Highly Disturbed, Heterogeneous Landscape. Remote Sensing of Environment, 64, pp. 91-102.

Liang S. L., 2005: Quantitative Remote Sensing of Land Surfaces, John Wiley & Sons, Mar 11, 2005, 560 pages.

Liu, C. L., and J. J. Wu, 2008: Crop Drought Monitoring using MODIS NDDI over Mid-Territory of China. IEEE International Geoscience & Remote Sensing Symposium, IGARSS 2008, July 8-11, 2008, Boston, Massachusetts, USA, Proceeding

Liu, H. Q., and R. T. Pinker, 2008: Radiative fluxes from satellites: Focus on aerosols. J. Geophys. Res., 113, D08208, doi:10.1029/2007JD008736.

Liu, H. Q., and R. T. Pinker, and B. N. Holben, 2005: A global view of aerosols from merged transport models, satellite, and ground observations. J. Geophys. Res., 110, D10S15, doi:10.1029/2004JD004695.

Liu, H. Q., and R. T. Pinker, M. Chin, B. Holben, and L. Remer, 2008: Synthesis of information on aerosol optical properties. J. Geophys.Res., 113, D07206, doi:10.1029/2007JD008735.

Liu, W. T., and F. N. Kogan, 1996: Monitoring regional drought using the Vegetation Condition Index. Int. J. Remote Sens., 17, 2761–2782.

MAKI, M., ISHIAHRA,M. and TAMURA, M., 2004, Estimation of leaf water status to monitor the risk of forest fires by using remotely sensed data. Remote Sensing of Environment, 90, pp. 441–450.

Makkeasorn, A., N. B. Chang, M. Beaman, C. Wyatt, and C. Slater, 2006: Soil moisture estimation in a semiarid watershed using RADARSAT-1 satellite imagery and genetic programming. Water Resour. Res., 42, W09401, 1-15, doi: 10.1029/2005WR004033.

Matlab PCA web page, http://matlabdatamining.blogspot.com/2010/02/principal-components-analysis.html, accessed in 03/2013

Matlab LDA web page, http://matlabdatamining.blogspot.com/2010/12/linear-discriminant-analysis-lda.html, accessed in 03/2013

McVicar, T. R., and P. N. Bierwirth, 2001: Rapidly assessing the 1997 drought in Papua New Guinea using compositeAVHRR imagery. Int. J. Remote Sens., 22, 2109–2128.

Mesinger, F., and Coauthors, 2006: North American regional reanalysis. Bull. Amer. Meteor. Soc., 87, 343.

Mesinger, F.,A. F.Rahman, J. C.Washburne,D. C.Goodrich,M.A.Weltz, and W. P. Kustas, 1996: Combining the Penman-Monteith equation with measurements of surface temperature and reflectance to estimate evaporation rates of semiarid grassland. Agric. For. Meteor., 80, 87–109.

Mongkolsawat, and coauthors, 2009: Exploration of Spatio-Temporal Drought Patterns using Satellite-Derived Indices for Crop management in Northeastern Thailand. ACRS 2009 proceedings, pp. unknown.

MORAN, M.S., CLARKE, T.R., INOUE, U. and VIDAL, A., 1994, Estimating crop water deficit using the relation between surface-air temperature and spectral vegetation index. Remote Sensing of Environment, 49, pp. 2467–263.

Murthy C. S. , and Sesha Agricultural Drought Monitoring and Assessment, Remote Sensing Applications, 2008

Nadelhoffer, K. J., A. E. Giblin, G. R. Shaver, and J. A. Laundre, 1991: Effects of temperature and substrate quality on element mineralization in six Arctic soils. Ecology, 72, 242–253.

Nagarajan, 2009: Drought Assessment, published by Springer, Oct. 2009, 370 pp.

NCH, 2014: National Corn Handbook, http://www.extension.purdue.edu/extmedia/nch/nch-40.html, last accessed on Jan. 2014

Narasimhan, B., R. Srinivasan, and A. D. Whittaker, 2003: Estimation of potential evapotranspiration from NOAA-AVHRR satellite. Appl. Eng. Agric., 19, 309–318.

Nebert D, Whiteside A, Vretanos P (eds), 2007: OpenGIS@ catalog services specification. Version 2.0.2, OGC 07-006r1, Open GIS Consortium Inc., p 218.

NEMANI, R.R. and RUNNING, S.W., 1989, Estimation of regional surface resistance to evapotranspiration from NDVI and thermal-IR AVHRR data. Journal of Applied Meteorology, 28, pp. 276–284.

NDMC Website, http://drought.unl.edu/DroughtBasics/WhatisDrought.aspx, accessed in 2012

Njoku, E.G., T.J. Jackson, V. Lakshmi, T.K. Chan, and S.V. Nghiem, 2003: Soil Moisture Retrieval From AMSR-E,IEEE TRANSACTIONS ON GEOSCIENCE AND REMOTE SENSING, VOL. 41, NO. 2, FEBRUARY 2003

Olthof, I., and R. Latifovic, 2007: Short-term response of arctic vegetation NDVI to temperature anomalies. Int. J. Remote Sens., 28, 4823–4840.

Ottle, C., and D. Vidalmadjar, 1994: Assimilation of soil moisture inferred from infrared remote sensing in a hydrological model over the HAPEX-Mobilhy region. J. Hydrol., 158, 241–264.

Palmer., R., & K.J. Holmes, 1988, Operational Guidance During Droughts: Expert System Approach." J. Water Resour. Plann. Manage., 114(6), 647–666.

Peng, C., L. Di, M. Deng, A. Yagci. 2012. Using time-series modis data for agricultural drought analysis in Texas, 1-6. 2012 First International Conference on Agro-Geoinformatics.

Peng, C., M. Deng, L. Di, W. Han, A. Yagci. 2013: A Comprehensive Agricultural Drought Stress Monitoring Method Integrating MODIS and Weather Data (A case study of Iowa). 2013 Second International Conference on Agro-Geoinformatics.

Peng, C., L. Di, M. Deng, W. Han, A. Yagci, & G. Heo 2013: Global Agricultural Drought Monitoring and Forecasting System (GADMFS): a tool to map and analyze agricultural drought. ESIP 2013 Summer Meeting at Chapel Hill, NC.

Pesti. G., B.P. Shrestha, L. Duckstein, & I. Bogardi, 2010: A fuzzy rule-based approach to drought assessment, Vol. 32, 6 (1996), pp. 1741-1747.

Peters., A.J., E.A. Walter-Shea, L. Ji, A. Vina, M. Hayes, and M.D. Svoboda, 2002: Drought Monitoring with NDVI-Based Standardized Vegetation Index, Photogrammertric Engineering & Remote Sensing, Vol. 68, No. 1, Jan. 2002, pp. 71-75

Pinker, R. T., and J. A. Ewing, 1985: Modeling surface solar radiation: Model formulation and validation. J. Climate Appl. Meteor., 24, 389–401.

Pongracz., R., I. Bogardi, & L. Duckstein, 1999, Application of fuzzy rule-based modeling techniques to regional drought, Journal of Hydrology, 224(1999), pp. 100-114.

Price, J.C., 1990, Using spatial context in satellite data to infer regional scale evapotranspiration. IEEE Transactions on Geoscience and Remote Sensing, 28, pp. 940–948.

Prihodko, L., and S. N. Goward, 1997: Estimation of air temperature from remotely sensed surface observations. Remote Sens. Environ., 60, 335–346.

Quiring, S. M., and T. N. Papakryiakou, 2003: An evaluation of agricultural drought indices for the Canadian prairies. Agric. For. Meteor., 118, 49–62.

Raper, J. 2000. Multidimensional Information Science. taylor and Francis, London.

Rechenberg, I., 1965: Cybernetic solution path of an experimental problem, Royal Aircraft Establishment, Translation No. 1122, Ministry of Aviation, Farnborough Hants, UK.

Rigg, D.J., 1985. The role of environment in limiting the adoption of new rice technology in Northeast Thailand. Transs. Inst. Br, Geog. N.S. 10, 481-494.

Rodriguez-Puebla, C., R. T. Pinker, and S. Nigam, 2008: Relationship between downwelling surface shortwave radiative fluxes and sea surface temperature over the tropical Pacific: AMIP II models versus satellite estimates. Ann. Geophys., 26, 785–794.

Rossow, W. B., and R. A. Schiffer, 1999: Advances in understanding clouds from ISCCP. Bull. Amer. Meteor. Soc., 80, 2261–2287.

Rouse, J.W., R.H. Hass, J.A. Schell, & D.W. Deering, 1973: Monitoring vegetation systems in the Great Plains with ERTS, NASA. Goddard Space Flight Center 3d ERTS-1 Symp., Vol. 1, Sect. A, pp 309-317

Sandholt, I., Rasmussen, K. and Andersen, J. 2002. A simple interpretation of the surface temperature /vegetation index space for assessment of surface moisture. Remote Sensing of Environment, 79: 213-224.

SAS Support, http://support.sas.com/publishing/pubcat/chaps/55129.pdf, accessed in 03/2013

Sastri, A.S.R.A.S., Ramakrishna, Y.S. & Rao, B.V. 1981. A new method of classifying agricultural drought. Archiv fur Meterologies Geophysik und Bioklimatologie, ser B.29, pp. 283-287.

Satti, S.R. & Jacobs, J.M. 2004. A GIS-based model to estimate the regionally distributed drought demand. Agricultural Water Management, 66, pp. 1-13.

Sandholt, I., Rasmussen, K. and Anderson, J., 2002, A simple interpretation of the surface temperature/vegetation index space for assessment of the surface moisture status. Remote Sensing of Environment, 79, pp. 213–224.

Schiffer, R. A., and W. B. Rossow, 1985: ISCCP global radiance data set: A new resource for climate research. Bull. Amer. Meteor. Soc., 66, 1498–1505.

Schultz, P. A., and M. S. Halpert, 1995: Global analysis of the relationships among a vegetation index, precipitation and land-surface temperature. Int. J. Remote Sens., 16, 2755–2777.

Schut., P., 2007: OpenGIS web processing service, version 1.0.0, OGC 05-007r7, Open Geospatial Consortium, Inc., p 87.

Seiler, R. A., F. Kogan, and J. Sullivan, 1998: AVHRR-based vegetation and temperature condition indices for drought detection in Argentina. Adv. Space Res., 21, 481–484.

Shakya N. and Yamaguchi Y., 2007. Drought Monitoring Using Vegetation and LST Indices in Nepal and Northeastern India. ACRS 2007 Proceedings in CD-ROM, 12-16 November 2007 Kuala Lumpur, Malaysia. Paper No.285.

Shakya N. and Y. Yamaguchi, 2010: Vegetation, water and thermal stress index for study of drought in Nepal and central northeastern India, International Journal of Remote Sensing, 31:4, 903-912

Shiau, J.T. & Shen, H.W. 2001. Recurrence analysis of hydrological droughts of differing severity. Journal of Water Resource Planning and Management, 127(1), pp. 30-40.

Shukla, J., and Y. Mintz. 1982. "Influence of Land-Surface Evapotranspiration on the Earth's Climate." Science 215: 1498–501.

Sims, D.A. and Gamon, J.A., 2002. Relationships between leaf pigment content and spectral reflectance across a wide range of species, leaf structures and developmental stages. Remote Sensing of Environment, 81, pp. 337-354.

SMEX Website, 2014: https://nsidc.org/data/amsr_validation/soil_moisture, accessed on 01/22/2014

Smith, R. C. G., and B. J. Choudhury, 1991: Analysis of normalized difference and surface temperature observations over southeastern Australia. Int. J. Remote Sens., 12, 2021–2044.

Sobrino, J. A., and N. Raissouni, 2000: Toward remote sensing methods for land cover dynamic monitoring: Application to Morocco. Int. J. Remote Sens., 21, 353–366.

Soulé, P. T., 1990: Spatial patterns of multiple drought types in the contiguous United States: a seasonal comparison: Climate Research, Vol. 1: 13-21

SPSS 15.0 Command Syntax Reference 2006. Chicago Ill: SPSS Inc; 2006.

Steinemann, A., Hayes, M.J. & Cavalcanti, L. 2005. Drought Indicators and triggers. In: Wilhite, D. (ed.) Drought and Water Crises: Science, Technology, and Management Issues. Marcel Dekker, NY.

Stisen, S., I. Sandholt, A. Nørgaard, R. Fensholt, and L. Eklundh, 2007: Estimation of diurnal air temperature using MSG SEVIRI data in West Africa. Remote Sens. Environ., 110, 262–274.

Stooksbury, D. Miskus, & S. Stephens. (2002). The drought monitor. American Meteorological Society, Aug. 2002, pp. 1181-1190.

Stow, D. A., and Coauthors, 2004: Remote sensing of vegetation and land-cover change in Arctic tundra ecosystems. Remote Sens. Environ., 89, 281–308.

Sui, C. H., X. F. Li, M. M. Rienecker, K. M. Lau, I. Laszlo, and R. T. Pinker, 2003: The role of daily surface forcing in the upper ocean over the tropical Pacific: A numerical study. J. Climate, 16, 756–766.

Sun, D., and M. Kafatos, 2007: Note on the NDVI-LST relationship and the use of temperature-related drought indices over North America. Geophys. Res. Lett., 34, L24406, doi:10.1029/2007GL031485.

Svoboda., M., D. LeComte, M. Hayes, R. Heim, K. Gleason, J. Angel, B. Rippey, R. Tinker, M. Palecki, D. Stooksbury, D. Miskus, & S. Stephens, 2002: The drought monitor. American Meteorological Society, Aug. 2002, pp. 1181-1190.

Tadesse, T., B.D. Wardlow, & J.H. Ryu, 2008: Identifying time-lag relationships between vegetation condition and climate to produce vegetation outlook maps and monitor drought, 22nd Conference on Hydrology, held in 2008.

Tannehill, I.R., 1947: Drought and Its Causes and Effects, Princeton University Press, 597 pp.

Tateishi, R., and M. Ebata, 2004: Analysis of phenological change patterns using 1982-2000 Advanced Very High Resolution Radiometer (AVHRR) data. Int. J. Remote Sens., 25, 2287–2300.

Tucker, C. J., 1979: Red and photographic infrared linear combinations for monitoring vegetation. Remote Sens. Environ., 8, 127–150.

Tucker, C. J., 1985: African land-cover classification using satellite data, Science, January 1985, Volume 227, Number 4685, pp. 369-375

Tucker, C.J. & Sellers, P.J. 1986. Satellite remote sensing of primary production. International J. Remote Sensing, 7, pp. 1395-1416.

Tufekcioglu, A., J. W. Raich, T. M. Isenhart, and R. C. Schultz. 1999. “Fine Root Dynamics, Coarse Root Biomass, Root Distribution, and Soil Respiration in a

Multispecies Riparian Buffer in Central Iowa, USA.” Agroforestry Systems 44: 163–74.

Unganai, L. S., and F. N. Kogan, 1998: Southern Africa’s recent droughts from space. Adv. Space Res., 21, 507–511.

USDM Drought Classification (2014), http://droughtmonitor.unl.edu/AboutUs/ClassificationScheme.aspx, last accessed on 01/21/2014

USDM Predictions, 2014: http://www.cpc.ncep.noaa.gov/products/predictions/tools/edb/both.pdf, accessed on 01/21/2014

U. S. Drought Monitor Weekly Report (2012), ftp://ftp.wcc.nrcs.usda.gov/support/drought/dmrpt-20120823.pdf, last accessed on 08/23/2012

Van Wijk, M. T., M. Williams, J. A. Laundre, and G. R. Shaver, 2003: Interannual variability of plant phenology in tussock tundra: Modelling interactions of plant productivity, plant phenology, snowmelt and soil thaw. Global Change Biol., 9, 743–758.

Vretanos., P., 2010: OpenGIS Web Feature Service 2.0 Interface Standard. Version 2.0.0, OGC 09-025r1, Open Geospatial Consortium, Inc., p 253.

Volcani, A., Karnieli. A. and Svoray, T., 2005. The use of remote sensing and GIS for spatio-temporal analysis of the physiological state of a semi-arid forest with respect to drought years. Forest Ecology and Management, 215, pp. 239-250.

W3C Website, http://www.w3schools.com/webservices/ws_intro.asp, last access on 01/23/2014

Walker, M. D., and Coauthors, 2006: Plant community responses to experimental warming across the tundra biome. Proc. Natl. Acad. Sci. USA, 103, 1342–1346.

Wan, Z., P. Wang, and X. Li, 2004: Using MODIS Land Surface Temperature and Normalized Difference Vegetation Index products for monitoring drought in the southern Great Plains, USA. Int. J. Remote Sens., 25, 61–72.

Wang, C., Qia, J. and Marsettb, R. 2004. Soil moisture estimation in a semiarid rangeland using ERS-2 and TM imagery. Remote Sensing of Environment, 90: 178–189.

Wang, L., & J. Qu, 2007: NMDI: A normalized multi-band drought index for monitoring soil and vegetation moisture with satellite remote sensing, Geophysical Research Letters, Vol. 34, Issue 20, Oct. 2007.

Wang, P.,Wen, X., Gong, J. and Song, C., 2001, Vegetation temperature condition index and its application for drought monitoring. Geoscience and Remote Sensing Symposium, IGARSS '01. IEEE 2001 International, 1, pp. 141–143.

Wardlow, B.D., T. Tadesse, J.F. Brown, Y. Gu, and K. Callahan, 2008: The Vegetation Drought Response Index (VegDRI) – Zooming in to a Local Scale to Meet the Needs of the Drought Monitoring Community, Association of American Geographers Annual Meeting, Boston, MA, April 15-19.

Weng, Q. Lu, D. Schubring , J., 2003: Estimation of land surface temperature vegetation abundance relationship for urban heat Island studies. Remote Sensing of Environment (89), Pp 467- 483

Wilhite, D. A., and M. H. Glantz, 1985: Understanding the drought phenomenon: The role of definitions. Water Int., 10, 111–120.

Wilhite, D.A. 1996: A methodology for drought preparedness. Natural Hazards, 13, pp. 229-252.

Wilson, D.J., A.W. Western, R.B. Grayson, A.A. Berg, M.S. Lear, M. Rodell, J.S., Famiglietti, R.S. Woods, and T.A. McMahon, 2003: Spatial distribution of soil moisture over 6 and 30cm depth, Mahurangi river catchment, New Zealand. Journal of Hydrology, 276: 254-274.

Yagci, A., L. Di, & M. Deng, 2013: The Effect of Land Cover Change on Vegetation Greenness-Based Satellite Agricultural Drought Indicators: A Case Study in the Southwest Climate Division of Indiana, U.S.A., 1-22. International Journal of Remote Sensing, 34 (10).

Zhang, B. L., R. T. Pinker, and P. W. Stackhouse, 2007: An empirical orthogonal function iteration approach for obtaining homogeneous radiative fluxes from satellite observations. J. Appl. Meteor. Climatol., 46, 435–444.

BIOGRAPHY

Chunming Peng graduated from Zhejiang University with a B. E. degree in Computer Science and Technology in 2008. She worked as a graduate research assistant in the Center for Spatial Information Science and System (CSISS) in George Mason starting from 2009, and received her M. S. in Geographic and Cartographic Sciences from George Mason University in 2010. Her PhD studies in George Mason University majoring in Earth System and Geoinformation Sciences will be finished by May 2014. Her research interests include agricultural drought, web-based GIS, image processing and software testing.